

**Mediated Electroorganic Oxidations: Applications in Pharmaceutical Building Block
Synthesis and Lignin Valorization**

By

Shannon L. Goes

A dissertation submitted in partial fulfillment of
the requirements for the degree of

Doctor of Philosophy

(Chemistry)

at the

UNIVERSITY OF WISCONSIN–MADISON

2022

Date of final oral examination: 04/29/2022

The dissertation is approved by the following members of the Final Oral Committee:
Shannon S. Stahl, Professor, Chemistry
Ive Hermans, Professor, Chemistry
Kyoung-Shin Choi, Professor, Chemistry
John Ralph, Professor, Biochemistry

© Copyright by Shannon L. Goes 2022

All Rights Reserved

Mediated Electroorganic Oxidations: Applications in Pharmaceutical Building Block Synthesis and Lignin Valorization

By

Shannon L. Goes

Under the supervision of Professor Shannon S. Stahl

At the University of Wisconsin-Madison

Abstract

Electroorganic oxidation reactions are appealing because protons, rather than undesirable stoichiometric chemicals, act as the terminal oxidant. Direct electrochemical oxidation of an organic molecule generates a high-energy radical cation. The high potentials required to produce these species frequently cause decomposition of reagents and/or reactions with ancillary functional groups. Proton-coupled electron-transfer (PCET) mediators are a specialized class of organic molecules that undergo facile electron transfer at an electrode to generate an active oxidant that subsequently removes at least one electron and one proton from substrate. This mediated strategy bypasses the formation of high-energy intermediates, thereby reducing the electrode potentials needed for analogous direct electrolysis reactions.

The first part of this thesis serves as an introduction to electrochemistry and mediated electrosynthesis. In **Chapter 1**, mediated electrosynthesis is broadly described for a general audience. Specific examples from my research are used to showcase the chemoselectivity afforded by PCET electrochemical mediators. In **Chapter 2**, an undergraduate laboratory exercise based on a classic electrochemical reaction, the Shono oxidation, is explained. The experiments in this lab demonstrate that direct electrochemical oxidation of amines is not compatible with electron-rich

functional groups. In **Chapter 3**, the exploration of aminoxyl-mediated $2e^-/H^+$ hydride transfer mechanism and quantification of electrocatalytic rates forms the basis for an undergraduate laboratory exercise.

The second part of this thesis presents a study of mediated electrolysis for enabling organic synthesis. In **Chapter 4**, electrochemical aminoxyl-mediated oxidation of secondary piperidines is employed to generate pharmaceutically-relevant α -cyanopiperidines. Use of an aminoxyl hydride-transfer mediator allows the reactions to proceed at low applied potentials, thereby enabling broad functional group tolerance. In **Chapter 5**, strategies for the oxidation of lignin, a complex polymer found in non-edible biomass, and subsequent depolymerization to valuable aromatic chemicals are summarized. In **Chapter 6**, the stability and oxidative driving force for a series of electrochemical e^-/H^+ hydrogen atom transfer radical mediators are evaluated. The long lifetimes and selectivity for secondary benzylic alcohol oxidation, even in the presence of sugars, indicate that oximes are well-suited to oxidative conversion of heterogeneous biomass. In **Chapter 7**, oxime-mediated oxidation of lignin facilitates the conversion of biomass to high-quality polysaccharides and promising yields of aromatic chemicals. The stability of the electrogenerated radical enables the reaction to be conducted off-electrode using scalable and sustainable electrochemical flow reactor technologies.

Acknowledgements

I extend my first thanks to Professor Shannon Stahl. You are a visionary who has pushed me to achieve more than I ever would have thought possible. From one Shannon to another, thank you for your scientific enthusiasm and guidance when I was a young student learning organic, electro-, and lignin chemistry and for your trust and support as I became an increasingly independent educator and researcher.

Thank you to the colleagues who became my family. You have shared your scientific ideas, holidays, and culture with me, and supported me through the everyday highs and lows of graduate school. Mohammad Rafiee, you have always been an incredible mentor and friend to me. I owe both my saffron tea addiction and love of electrochemistry to you. Alastair Lennox, through regular pow-wows and subgroups you taught me to be a researcher and electroorganic chemist (go team almond!). Jordan Nutting, I'm fortunate and grateful that you have read and edited everything I've ever written in graduate school, guided me through every degree requirement, and made delicious birthday treats for group meetings. Manar Alherech, you have selflessly given many late nights to help me collect NMR's and talk through life. SJ Chen, I learn something new every time we talk, and your unique and honest perspective is the cornerstone of our friendship. Eric Weeda, your thoughtful scientific insight and genuine kindness have made my every day at the WEI better. My gratitude also goes out to Fei Wang, Xing Zhong, Sung-Eun, Suh, Asmaul Hoque, Caitlin Kozack, Spring Knapp, Chris Holland, Jieru Zhu, James Gerken, and everyone that has been part of the Stahl group during my time here.

I am indebted to many people who have directly enabled my work through their skills and expertise. Special thanks to Tracy Drier. You made the days I frequented the glass shop fun and positive, and without your rapid and excellent work there could not have been Organic Electrochemistry Short Course or CHEM 840 labs. Tim Paschkewitz, your technical knowledge,

general enthusiasm, and genuine curiosity made your every visit and email fun and incredibly informative. Nick Hill, your generous and steadfast support, mentorship, and trust enabled me to share my love of electrochemistry through graduate and undergraduate education. My gratitude also goes out to Steve Myers, Heike Hofstetter, Charlie Fry, and Sarah Liu.

Thank you to my committee members Ive Hermans and Kyoung-Shin Choi. Your thoughtful questions during my degree requirement presentations have improved my understanding and depth of scientific knowledge, and I appreciate your unfailing encouragement through the years. And thank you to John Ralph for lending your expertise to my thesis defense committee.

I began my research career in the lab of Professor Wenyu Huang at Iowa State University. Thank you, Professor Huang, for accepting a first-year undergraduate chemistry student into your research lab. You always saw greater potential in me than I did in myself, and only through your direct mentorship and support was I able to achieve authorship on my first paper, accept research awards, and enroll in graduate school at the University of Wisconsin–Madison. Special thanks to Dr. Chaoxian Xiao for his patient guidance, and to Dr. Denny Tesfagaber and Dr. Raghu Maligal-Ganesh.

I am incredibly fortunate to have the love and support of my oldest friends and new friends I've made during my time here. Kim Martinez and Darcie Farrell, even though we no longer live together, the Team has been there for me during all of my biggest adventures (from study abroad and to my first river tubing), and I know that you both will always have my back. Nadarra Stokes, you are the strongest and most caring person I know, and I love you like a sister. Erin O'Donnell, you are so fun and the easiest person to talk to that I've ever met. We've proven that distance is never a barrier to our friendship. Rob Millikin, your honest, thoughtful, and kind perspective make

you wise beyond your years. I treasure our weekly lunches and the ride-or-die bond that was forged during windsurfing. Dan SantaLucia, you are the most open person I've ever met, and every time we talk it brightens my day as I find myself smiling or laugh crying at your silly memes, dad jokes, and epic stories. Paige Pizsel, you are so fun and are always finding new ways to show the ones you love how much you care. You have orchestrated all of my fondest graduate school memories, from decorating desks during birthdays to sleepovers and chocolate souffles. Mikey Ryan, you are incredibly intelligent, kind, and deep. Thank you for macaroons, late night discussions about the universe, and for introducing me to chess boxing.

A profound and loving thank you to my family. I have missed birthdays and holidays, and through it all you have treasured the time we do spend together and given me your support, encouragement, and love. To my Grandpas and Grandmas, you have instilled a value and love of education in me since I was born. Grandma and Grandpa Goes, you have brightened my day with treasured phone calls, holiday treats, birthday songs, and cards all these years. Grandma and Grandpa Stayner, you have shared your love of the lake, books, card games, balloons, and letters with me and now we love them together. To my parents, you have both been there for me my entire life. From staying home with me when I was little to helping me move *many* times as I traveled further from home, you have celebrated all my successes and helped me in every way to realize my dreams. To my brothers Ethan and Trevor, a sister couldn't ask for two more fun and supportive siblings. I tease you because I love you. A big thank you to Great Grandpa and Grandma Breeding, Great Grandpa and Grandma Lotter, Aunt Diane, Aunt Susie and Uncle Josh, Uncle Bob, Uncle Jeff and Aunt Cheryl, Cousins Marc and Lauren, Cousins Courtney and Lindsey, Cousins Jack and Lucy, Aunt Joanne and Uncle Jerry, Aunt Lorna and Uncle Bill, Aunt Kim and Uncle Garry,

Cousins Pat, Tim, and Sarah, Cousins Emma and Jimmy, Cousin Victoria, and the rest of my wonderful extended family. I love you all.

Finally, thank you to my partner, Zach. You sat with me in lab during late nights in lab on some of our earliest dates, and you've continued to support me in so many ways. You make me a better person, and I love you and can't wait to continue building our lives together in Cincinnati. All my love to Gidget, my incredibly cuddly and loving little cat. She has been my constant companion and source of comfort for eight years. And to her new best friend, Moxie.

This thesis would not be possible without everyone listed here. Thank you.

Table of Contents

Abstract	i
Acknowledgements	iii
Table of Contents	vii
List of Schemes	xi
List of Tables	xii
List of Figures	xiv
Abbreviations and Acronyms	xx
Chapter 1: Control is the Goal! Using Electricity and Mediators to Make Molecules	1
Chapter 2: Exploring Electrosynthesis: Bulk Electrolysis and Cyclic Voltammetry Analysis of the Shono Oxidation	12
2.1. Abstract	13
2.2. Introduction	13
2.3. Educational Context	15
2.3.1. Cyclic Voltammetry Analysis	16
2.3.2. Bulk Electrosynthesis	17
2.4. Hazards	18
2.5. Results and Discussion	19
2.6. Assessment	24
2.7. Conclusions	25
2.8. Acknowledgements	25
2.9. References	26
Chapter 3: Deriving the Turnover Frequency of Aminoxyl-Catalyzed Alcohol Oxidation by Chronoamperometry: An Introduction to Organic Electrocatalysis	28
3.1. Abstract	29
3.2. Experimental Overview	33
3.3. Experimental Procedure	35
3.4. Hazards	35
3.5. Results and Discussion	36
3.6. Conclusion	40
3.7. Acknowledgements	41
3.8. References	41
Chapter 4: Electrochemical Aminoxyl-Mediated α-Cyanation of Secondary Piperidines for Pharmaceutical Building Block Diversification	46
4.1. Abstract	47
4.2. Introduction	47
4.3. Results and Discussion	49
4.4. Conclusion	55
4.5. Acknowledgements	56
4.6. Reference	56

Chapter 5: Sequential Oxidation-Depolymerization Strategies for Lignin Conversion to Low Molecular Weight Aromatic Chemicals.....	59
5.1. Abstract.....	60
5.2. Introduction.....	60
5.3. Top-Down vs. Bottom-Up Strategies for Lignin Depolymerization	64
5.3.1. Top-Down Strategies for Efficient Aromatic Monomer Production	64
5.3.2. Bottom-Up Strategy for Mechanistic Insight into Lignin Depolymerization.....	66
5.4. Sequential Oxidation-Cleavage Methods for Lignin Depolymerization	72
5.4.3. Concepts and Initial Discovery of the Alcohol Oxidation-Cleavage Strategy	72
5.4.4. Secondary Alcohol Oxidation.....	76
5.4.5. NHPI	78
5.4.6. Primary Alcohol Oxidation.....	85
5.4.7. Bond Cleavage Methods	86
5.5. Conclusions and Future Outlook	96
5.6. Acknowledgements.....	97
5.7. Reference	97
Chapter 6: Fundamental Studies of N-Oxyl Radicals: Assessment of Stability, Bond Strength, and Time-Delayed Alcohol Oxidation.....	105
6.1. Abstract.....	106
6.2. Introduction.....	106
6.3. Results and Discussion	108
6.3.1. Radical Stability and Bond Dissociation Free Energy Studies	108
6.3.2. Mediated Oxidation of Secondary Benzylic Alcohols.....	114
6.4. Conclusion	116
6.5. Acknowledgments.....	117
6.6. References.....	117
Chapter 7: Electrochemical Oxidative Stabilization in Mild Aqueous Conditions Enhances Lignin Monomer Production During Biomass Depolymerization	120
7.1. Abstract.....	121
7.2. Introduction.....	121
7.3. Results and Discussion	123
7.4. Conclusions.....	128
7.5. Acknowledgements.....	128
7.6. References.....	129
Appendices.....	131
Appendix A: Exploring Electrosynthesis: Bulk Electrolysis and Cyclic Voltammetry Analysis of the Shono Oxidation Supporting Information	132
A.1. Equipment and Hazards	133
A.2. Instructor Notes.....	138
A.3. Student Laboratory Manual Chapter and Assessment Questions	143
A.3.1. Introduction to Organic Electrochemistry and the Electrochemical Shono Oxidation	143
A.4. Optional Addendum to Student Laboratory Manual Chapter and Assessment Questions	161
A.5. Grading Key.....	163

A.6. Alternative Set-Up Addendum to Grading Key.....	170
A.7. Practice Exercise: Yield Calculation from ^1H NMR Using Internal Standard	171
A.8. Links to High-Resolution Lecture and Experimental Videos.....	177
A.9. Spectral Data.....	177
A.10. Computational Methods and Linked Job Output.....	180
A.11. References.....	182
Appendix B: Deriving the Turnover Frequency of Aminoxy-Catalyzed Alcohol Oxidation by Chronoamperometry: An Introduction to Organic Electrocatalysis Supporting Information.....	184
B.1. Introduction.....	185
B.2. Note for Instructors	185
B.3. Safety	187
B.4. Experimental Procedure and making the Stock Solution	187
B.5. Additional Electrochemical Data and the Results by Students.....	188
B.6. Deriving the Diffusion Coefficient of ACT.....	189
B.7. Deriving the Kinetic Information from Voltammetric Results.....	190
B.8. Consumed Charge for Chronoamperometry Experiment	194
B.9. Summary of Assessment.....	195
B.10. Student Handouts	200
B.11. References.....	213
Appendix C: Electrochemical Aminoxy-Mediated α-Cyanation of Secondary Piperidines for Pharmaceutical Building Block Diversification Supporting Information.....	215
C.1. General Experimental Details	216
C.2. Reaction Optimization	218
C.3. Optimized Procedure for the Electrochemical Cyanation of Secondary Amines	219
C.3.1. Bulk Electrolysis.....	219
C.3.2. Work-Up	221
C.3.3. Characterization Data.....	222
C.3.4. Large Scale Reaction	223
C.3.5. ElectraSyn 2.0 Reaction:.....	224
C.3.6. Coupling constant assignments.....	242
C.3.7. Determination of Stereochemistry	244
C.4. Cyanation and Hydrolysis of Secondary Amines	245
C.4.1. Bulk Electrolysis:.....	245
C.4.2. Work-Up	245
C.4.3. Characterization Data.....	246
C.5. Unsuccessful Substrates.....	248
C.6. X-Ray Crystallographic Data.....	249
C.6.1. Data Collection for Compound 3e [PhSO_3^-].....	249
C.6.2. Structure Solution and Refinement.....	249
C.6.3. Crystal Data	250
C.7. Reference	308
Appendix D: Fundamental Studies of N-Oxyl Radicals: Assessment of Stability, Bond Strength, and Time-Delayed Alcohol Oxidation Supporting Information.....	309
D.1. General Information.....	310

D.2. CV of HAT Mediators	311
D.3. pK _a Analysis by NMR	316
D.4. Bulk Electrolysis	321
D.5. References	323
Appendix E: Electrochemical Oxidative Stabilization in Mild Aqueous Conditions Enhances Lignin Monomer Production During Biomass Depolymerization	324
E.1. Chemicals and Materials	325
E.2. Experimental	326
E.2.1. Flow Reaction Set-Up	326
E.2.2. Mild-Acidolysis Fractionation	329
E.2.3. Formic Acid Depolymerization	329
E.2.4. Preliminary Radical Pool Batch Reaction	330
E.3. Analysis	330
E.3.1. 2D Gel-NMR HSQC	330
E.3.2. 2D HSQC	330
E.3.3. ssNMR	331
E.4. References	331

List of Schemes

Scheme 2.1. The Shono oxidation.....	15
Scheme 3.1. Structures and Oxidation Reaction of ACT and TEMPO (a), Anelli–Montonari Oxidation (b), and TEMPO-Catalyzed Electrochemical Alcohol Oxidation (c) with Blue Arrows Showing the Catalytic Turnover	31
Scheme 4.1. Context and Strategy for α -Cyanation of 2° Piperidines	48
Scheme 6.1. NHPI-Mediated Oxidation of Alcohols.....	106
Scheme A.1. a) Chromic acid oxidation of 2-propanol to acetone: b) Redox half-reactions for the overall process.	144
Scheme A.2. Shono electrochemical oxidation of <i>N</i> -Boc-pyrrolidine to the corresponding α -functionalized compound.....	152
Scheme A.3. Overview of the electrochemical Shono oxidation.	152
Scheme B.1. Anelli–Montonari oxidation. B. electrode reaction and structure of ACT and TEMPO, and C. TEMPO catalyzed electrochemical Alcohol oxidation.....	201

List of Tables

Table 1.1. Mediator comparison of required voltage and amount of product for indirect electrochemistry of piperidine	7
Table 3.1. TOF (h^{-1}) of ACT for different concentrations of solketal in the absence and presence of base	40
Table 4.1. Bulk Electrolysis Optimization Data	51
Table 4.2. Substrate Scope for Electrochemical α -Cyanation of 2° Piperidines (A) and Cyanation/Hydrolysis to Generate Pipecolic Acids (B) ^a	55
Table 6.1. Comparative bond dissociation free energies for <i>N</i> -oxyl mediators in H ₂ O.....	111
Table 7.1. Optimization of Oxidative Lignin Stabilization.....	126
Table A.1. Link to Computational Jobs	181
Table B.1. Turnover frequency (TOF) of ACT for oxidation of solketal.	192
Table B.2. Turnover frequency (TOF) of ACT for oxidation of solketal.	193
Table B.3. Turnover frequency (TOF) of ACT for oxidation of solketal.	194
Table B.4. Crystal data and structure refinement for <i>3e</i> [<i>PhSO</i> ₃ ⁻].....	251
Table C.5. Fractional Atomic Coordinates ($\times 10^4$) and Equivalent Isotropic Displacement Parameters ($\text{\AA}^2 \times 10^3$) for <i>3e</i> [<i>PhSO</i> ₃ ⁻]. U_{eq} is defined as 1/3 of of the trace of the orthogonalised U_{IJ} tensor.	253
Table B.6. Anisotropic Displacement Parameters ($\text{\AA}^2 \times 10^3$) for <i>3e</i> [<i>PhSO</i> ₃ ⁻]. The Anisotropic displacement factor exponent takes the form: $-2\pi^2[h^2a^{*2}U_{11}+2hka^*b^*U_{12}+\dots]$	254
Table B.7. Bond Lengths for <i>3e</i> [<i>PhSO</i> ₃].	256
Table B.8. Bond Angles for <i>3e</i> [<i>PhSO</i> ₃ ⁻].	256
Table B.9. Hydrogen Bonds for <i>3e</i> [<i>PhSO</i> ₃].	258
Table B.10. Torsion Angles for <i>3e</i> [<i>PhSO</i> ₃].	258
Table B.11. Hydrogen Atom Coordinates ($\text{\AA} \times 10^4$) and Isotropic Displacement Parameters ($\text{\AA}^2 \times 10^3$) for <i>3e</i> [<i>PhSO</i> ₃].	259
Table B.12. Atomic Occupancy for <i>3e</i> [<i>PhSO</i> ₃].	261
Table B.13. Fractional Atomic Coordinates ($\times 10^4$) and Equivalent Isotropic Displacement Parameters ($\text{\AA}^2 \times 10^3$) for 4a. U_{eq} is defined as 1/3 of of the trace of the orthogonalised U_{IJ} tensor.	266
Table B.14. Anisotropic Displacement Parameters ($\text{\AA}^2 \times 10^3$) for 4a The Anisotropic displacement factor exponent takes the form: $-2\pi^2[h^2a^{*2}U_{11}+2hka^*b^*U_{12}+\dots]$	267
Table B.15. Bond Lengths for 4a.	268
Table B.16. Bond Angles for 4a.....	269
Table B.17. Hydrogen Bonds for 4a.	270
Table B.18. Torsion Angles for 4a.....	270

Table B.19. Hydrogen Atom Coordinates ($\text{\AA}\times 10^4$) and Isotropic Displacement Parameters ($\text{\AA}^2\times 10^3$) for 4a.....	271
--	-----

List of Figures

Figure 1.1. The direct electrochemical removal of an electron (yellow circle) from a target molecule (red square) and indirect removal an electron (yellow circle) and proton (gray circle) using a mediator (blue diamond).	5
Figure 1.2. The indirect electrochemical reaction of lignin and sugar model molecules	10
Figure 2.1. Electrochemical α -methoxylation of <i>N</i> -Boc-pyrrolidine	18
Figure 2.2. Cyclic voltammograms (0.1 V/s) in [NBu ₄][PF ₆] (0.1 M) acetonitrile solution of anisole 1 , piperidine carbamate 2 , anisole piperidine carbamate 3 (5 mM) referenced to Fc/Fc ⁺ .21	
Figure 2.3. Electron transfer - proton transfer - electron transfer (ET-PT-ET) mechanism for electrochemical oxidation of piperidine carbamate 2	21
Figure 2.4. Mechanism of electrochemical α -methoxylation of <i>N</i> -Boc-pyrrolidine	22
Figure 2.5. ¹ H NMR spectrum of the crude Shono reaction mixture (CDCl ₃ , 400 MHz)	24
Figure 3.1. Applied potential waveform (a) and the resulting current-time trace (b) for a chronoamperometric experiment of a general oxidation reaction.	30
Figure 3.2. Cyclic voltammograms (left) and chronoamperograms (right) of 1.0 mM ACT in the absence (red traces, a and c) and presence of 4 mM solketal (blue traces, b and d). Solution conditions: aqueous solution with NaHCO ₃ /Na ₂ CO ₃ electrolyte (0.1/0.1 M, pH 10), scan rate for cyclic voltammetry 10 mV s ⁻¹ , and applied potential for chronoamperometry 0.8 V vs Ag/AgCl.	34
Figure 3.3. Cyclic voltammograms (a) of 1.0 mM ACT at different scan rates; scan rates (mV s ⁻¹) are depicted for each CV. The blank CV (black dashed trace) is the CV of 4 mM solketal substrate in the absence of ACT at a scan rate of 80 mV s ⁻¹ . The plot of anodic and cathodic peak currents versus square root of scan rate (b). Solution conditions: aqueous solution with NaHCO ₃ /Na ₂ CO ₃ electrolyte 0.1/0.1 M, and pH 10.	37
Figure 3.4. Cyclic voltammograms of 1.0 mM ACT in the absence (dotted line) and presence of 9 mM solketal at different scan rates (25–120 mV s ⁻¹) (a) and cyclic voltammograms of 1.0 mM ACT in the presence of various concentrations of solketal (b). Scan rate for dotted trace is 80 mV s ⁻¹ , and for traces in part b, it is 25 mV s ⁻¹ . Solution conditions: aqueous solution with NaHCO ₃ /Na ₂ CO ₃ electrolyte 0.1/0.1 M, and pH 10.	38
Figure 3.5. Chronoamperograms for a blank solution and ACT in the absence and presence of various concentrations of solketal (a) with applied chronoamperometry potential of 0.8 V vs Ag/AgCl. The consumed charges are shown on each chronoamperogram; the consumed charge for the blank solution is 12 μ C (not depicted on its plot). Proposed mechanism for ACT-catalyzed electrochemical solketal oxidation (b).	39
Figure 4.1. CVs (0.1 V/s) in MeCN (5 mL) and NaClO ₄ (0.1 M) of: ABNO (1 mM) (gray trace); 4-phenyl piperidine (2 mM) (green trace); ABNO (1 mM) and 4-phenyl piperidine (2 mM) (red trace).	50
Figure 4.2. Bulk electrolysis in MeCN, TBAPF ₆ (0.1 M), TMSCN (1.5 equiv), and 1a (0.3 mmol) with/without ABNO (10 mol %) and/or MeOH (0.5 equiv). ¹⁶ MB = mass balance.	53
Figure 5.1. Lignin structure (top) and bond strengths (bottom) with typical lignin linkages.	62

Figure 5.2. Top-down and bottom-up strategies for lignin depolymerization.	64
Figure 5.3. (A) Typical reaction conditions to depolymerize lignin or lignosulfonates through (i) nitrobenzene, (ii) copper-based catalyst, or (iii) commercial vanillin production used by Borregaard; (B) proposed mechanism of vanillin formation under alkaline oxidative conditions.	66
Figure 5.4. Metal complex catalysts used for selective bond cleavage of lignin model compounds.	67
Figure 5.5. Yields of aromatic monomer products through selective bond cleavage of β -O-4 model compounds via different metal complex catalysts listed in Figure 5.4	67
Figure 5.6. Sequential oxidation-cleavage strategies (A) selectively oxidize β -O-4 alcohol groups to weaken the C–O ether bond (B) to facilitate subsequent bond cleavage in a separate step.	73
Figure 5.7. (A) Selective primary or secondary alcohol oxidation through various reaction systems; (B) different bond cleavage methods on secondary alcohol oxidized lignin models. ...	74
Figure 5.8. (A) Depolymerization of aspen lignin with formic acid following oxidation; (B) monomer distribution from depolymerization of oxidized aspen lignin.	75
Figure 5.9. Overview of the sequential oxidation-cleavage approaches applied in real lignin. ..	76
Figure 5.10. TEMPO and its derivatives mediated benzylic alcohol oxidation in lignin and its models.	77
Figure 5.11. NHPI mediated benzylic alcohol oxidation in lignin and its models. DDQ = 2,3-dichloro-5,6-dicyano-1,4-benzoquinone.	79
Figure 5.12. DDQ-mediated benzylic alcohol oxidation in lignin and its models.	81
Figure 5.13. Transition metal mediated secondary alcohol oxidation in lignin models using $[\text{Ir}(\text{Cp}^*)\text{L}]$, where L = 2,20 -bipyridine-6,60 -diol.	83
Figure 5.14. Heterogeneous catalyst-mediated secondary alcohol oxidation in lignin model compounds using (A) Pd/C, (B) Pd/ZnIn ₂ S ₄ , and (C) Au/Li-Al LDH.	84
Figure 5.15. Mechanism of TEMPO mediated primary alcohol oxidation of a lignin model compound.	85
Figure 5.16. Different bond cleavage patterns in lignin model with C _α ketone structure.	87
Figure 5.17. Mechanisms of redox-neutral bond cleavage method of primary alcohol oxidized lignin.	88
Figure 5.18. Mechanism of formic acid-mediated redox-neutral bond cleavage method on secondary alcohol oxidized lignin model.	90
Figure 5.19. Baeyer-Villiger bond cleavage for β -O-4 linkages.	92
Figure 5.20. Mechanisms of reductive bond cleavage methods.	94
Figure 6.1. Mediators investigated in this study and typical redox states.	108
Figure 6.2. Cyclic voltammograms of (a) 1 mM HAT mediators (NHPI, NHSI, HOBt, VA, DVA, MAN salt, DAN, and CyAN) in 0.1 M pH 5 acetate buffer at a scan rate of 20 mV/s, and peak current ratio analysis over (b) pH range 3-10.5 and (c) concentration range 1-10 mM.	109

- Figure 6.3.** Normalized currents obtained from rotating disk electrode linear sweep voltammograms of a 10 mM radical solution generated from bulk electrolysis (graphite working electrode, Pt wire counter electrode, 3 M KCl Ag/AgCl reference electrode; 5 mA; 2.1 F/mol) of VA (red), DVA (yellow), DAN (green), MAN salt (blue), and NHPI (black). Glassy carbon working electrode, Pt wire counter electrode, 3 M KCl Ag/AgCl reference electrode; 10000 rpm, 20 mV/s; 1.5 minutes between end of bulk electrolysis and start of data collection. 114
- Figure 6.4.** RDE analysis of reaction of benzyl alcohol substrate with VANO radical provides further support for previously proposed hydrogen atom transfer mechanism. Glassy carbon working electrode, Pt wire counter electrode, 3 M KCl Ag/AgCl reference electrode; 1000 rpm, 20 mV/s; NMR yields against a 1,3,5-trimethoxybenzene internal standard. 115
- Figure 6.5.** Yield data for alcohol oxidation mediated radicals electrochemically generated from VA, DVA, DAN, MAN, and NHPI and mediated by VANO after addition between 0.5 and 120 minutes. 116
- Figure 7.1.** Overview of selective lignin oxidation approaches: (A) condensation or stabilization of lignin. (B) Previous oxidative lignin conversion from biomass approaches and (C) monomers produced from oxidative biomass conversion. (D) This oxidative biomass conversion approach via selective benzylic alcohol oxidation. Biomass icon courtesy of Matthew Wisniewski (Wisconsin Energy Institute). 123
- Figure 7.2.** Overview of electrochemical oxidative stabilization of lignin: schematic of flow reactor and electrochemical half reactions in aqueous solution. 124
- Figure 7.3.** Preliminary data for the oxidative stabilization of lignin in batch and depolymerization to monomers. 128
- Figure A.1.** Electrochemical bulk electrolysis cell used by students. 136
- Figure A.2.** Example of alternative electrochemical bulk electrolysis cell used by instructors during lab development. 137
- Figure A.3.** Power supply used for bulk electrolysis reaction. 142
- Figure A.4.** Balanced redox reaction for the electrochemical oxidation of 2-propanol and reduction of protons. 146
- Figure A.5.** The components of an electrochemical cell. 146
- Figure A.6.** Constant potential (left) and constant current (right) electrolysis traces for an electrochemical oxidation reaction. 149
- Figure A.7.** Cyclic voltammetry potential waveform (input, left) and resulting cyclic voltammogram (right) for a reversible redox couple, $A^{\text{Red}}/A^{\text{Ox}}$, with a half-wave potential of 0.5 V. 150
- Figure A.8.** Substrates to be analyzed by cyclic voltammetry. 153
- Figure A.9.** Image highlights location of “Raw Output” button to access raw output data file for job 648285. 181
- Figure A.10.** Image highlights location of Absolute NMR shifts in data file for job 697487 ... 182
- Figure B.1.** Demonstration of shiny surface of polished glassy carbon (GC) electrode. 187

- Figure B.2.** Four examples of the plotted data (by four individual groups) for post analysis of chronoamperometric responses. The plots show the correlation of current as a function of $t^{-1/2}$ which is supposed to be linear. Solution conditions: 1.0 mM ACT in aqueous solution with $\text{NaHCO}_3/\text{Na}_2\text{CO}_3$ electrolyte (0.1/0.1 M, pH 10). Applied potential for chronoamperometry is 0.8 V vs Ag/AgCl. 189
- Figure B.3.** Chronoamperogram (a) and the plot of current as a function of $t^{-1/2}$ (b) for 1.0 mM ACT in aqueous solution with $\text{NaHCO}_3/\text{Na}_2\text{CO}_3$ (0.1/0.1 M, pH 10). Applied potential for chronoamperometry is 0.8 V vs Ag/AgCl. 190
- Figure B.4.** The plot of anodic and cathodic peak currents versus square root of scan rate. Solution conditions: aqueous solution with $\text{NaHCO}_3/\text{Na}_2\text{CO}_3$ electrolyte 0.1/0.1 M, and pH 10. 190
- Figure B.5.** Plot of the anodic peak current of cyclic voltammograms as a function of square root of concentration of solketal ($C^{-1/2}$). Solution conditions: 1.0 mM ACT in aqueous solution with $\text{NaHCO}_3/\text{Na}_2\text{CO}_3$ electrolyte (0.1/0.1 M, pH 10). 192
- Figure B.6.** Plot of the anodic peak current of cyclic voltammograms as a function of square root of concentration of solketal ($C^{-1/2}$). Solution conditions: 1.0 mM ACT in aqueous solution with $\text{NaHCO}_3/\text{Na}_2\text{CO}_3$ electrolyte (0.1/0.1 M, pH 10). 193
- Figure B.7.** Plot of the anodic peak current of cyclic voltammograms as a function of square root of concentration of solketal ($C^{-1/2}$). Solution conditions: 1.0 mM ACT in aqueous solution with $\text{NaHCO}_3/\text{Na}_2\text{CO}_3$ electrolyte (0.1/0.1 M, pH 10). 194
- Figure B.8.** Demonstration of charge calculation in Excel for the chronoamperogram. 195
- Figure B.9.** Pine Research cell setup for electrochemical analysis. 207
- Figure B.10.** Aftermath software interface for cyclic voltammetry analysis. 208
- Figure B.11.** A CV displayed on Aftermath Software. 208
- Figure B.12.** Polishing the working electrode. 209
- Figure B.13.** Aftermath software interface for chronoamperometric analysis. 210
- Figure B.14.** Determining the oxidation (anodic) and reduction (cathodic) peak current. 211
- Figure C.1.** A molecular drawing of **3e** [PhSO_3^-] shown with 50% probability ellipsoids. All non-ammonium H atoms and minor disorder components are omitted. 251
- Figure C.2.** A molecular drawing of the cation of **3e** [PhSO_3^-] shown with 50% probability ellipsoids. All H atoms are omitted by both disorder components are shown. 251
- Figure C.3.** A molecular drawing of the asymmetric unit of **4a** shown with 50% probability ellipsoids. The H atoms at O3 and O4 pointing toward each other are 50% occupied. 264
- Figure C.4.** A molecular drawing of **4a** shown with 50% probability ellipsoids. Symmetry code: $i\ 1-x, -1-y, 1-z$ 264
- Figure D.1.** Divided bulk electrolysis cell. 311
- Figure D.2.** Example of CV analyzed using Pine Aftermath software. 312
- Figure D.3.** 1 mM VA; 20, 50, or 100mV/s; glassy carbon working electrode, Pt wire counter electrode, 3 M KCl Ag/AgCl reference electrode; 0.1 M buffer: pH 3 (0.1 M sodium citrate/citric

acid), pH 5 (0.1 M sodium acetate/acetic acid, pH 7 (0.1 M monosodium/disodium phosphate), pH 9.5-10.5 (0.1 M carbonic acid/sodium bicarbonate), and pH 1 solution (0.1 M HCl to water).. 312

Figure D.4. 1 mM DVA; 20, 50, or 100mV/s; glassy carbon working electrode, Pt wire counter electrode, 3 M KCl Ag/AgCl reference electrode; 0.1 M buffer: pH 3 (0.1 M sodium citrate/citric acid), pH 5 (0.1 M sodium acetate/acetic acid, pH 7 (0.1 M monosodium/disodium phosphate), pH 9.5-10.5 (0.1 M carbonic acid/sodium bicarbonate), and pH 1 solution (0.1 M HCl to water).. 313

Figure D.5. 1 mM MAN; 20, 50, or 100mV/s; glassy carbon working electrode, Pt wire counter electrode, 3 M KCl Ag/AgCl reference electrode; 0.1 M buffer: pH 3 (0.1 M sodium citrate/citric acid), pH 5 (0.1 M sodium acetate/acetic acid, pH 7 (0.1 M monosodium/disodium phosphate), pH 9.5-10.5 (0.1 M carbonic acid/sodium bicarbonate), and pH 1 solution (0.1 M HCl to water).. 313

Figure D.6. 1 mM CyAN; 20, 50, or 100mV/s; glassy carbon working electrode, Pt wire counter electrode, 3 M KCl Ag/AgCl reference electrode; 0.1 M buffer: pH 3 (0.1 M sodium citrate/citric acid), pH 5 (0.1 M sodium acetate/acetic acid, pH 7 (0.1 M monosodium/disodium phosphate), pH 9.5-10.5 (0.1 M carbonic acid/sodium bicarbonate), and pH 1 solution (0.1 M HCl to water).. 314

Figure D.7. 1 mM NHPI; 20, 50, or 100mV/s; glassy carbon working electrode, Pt wire counter electrode, 3 M KCl Ag/AgCl reference electrode; 0.1 M buffer: pH 3 (0.1 M sodium citrate/citric acid), pH 5 (0.1 M sodium acetate/acetic acid, pH 7 (0.1 M monosodium/disodium phosphate), pH 9.5-10.5 (0.1 M carbonic acid/sodium bicarbonate), and pH 1 solution (0.1 M HCl to water).. 314

Figure D.8. 1 mM NHSI; 20, 50, or 100mV/s; glassy carbon working electrode, Pt wire counter electrode, 3 M KCl Ag/AgCl reference electrode; 0.1 M buffer: pH 3 (0.1 M sodium citrate/citric acid), pH 5 (0.1 M sodium acetate/acetic acid, pH 7 (0.1 M monosodium/disodium phosphate), pH 9.5-10.5 (0.1 M carbonic acid/sodium bicarbonate), and pH 1 solution (0.1 M HCl to water).. 315

Figure D.9. 1 mM HOBt; 20, 50, or 100mV/s; glassy carbon working electrode, Pt wire counter electrode, 3 M KCl Ag/AgCl reference electrode; 0.1 M buffer: pH 3 (0.1 M sodium citrate/citric acid), pH 5 (0.1 M sodium acetate/acetic acid, pH 7 (0.1 M monosodium/disodium phosphate), pH 9.5-10.5 (0.1 M carbonic acid/sodium bicarbonate), and pH 1 solution (0.1 M HCl to water).. 315

Figure D.10. 1 mM HOBT; glassy carbon working electrode, Pt wire counter electrode, 3 M KCl Ag/AgCl reference electrode; 0.1 M buffer: pH 3 (0.1 M sodium citrate/citric acid); pulse height: 100 mV, width: 0.01 s, period: 0.1 s, increment: 10 mV; pre- and post-pulse width: 0.003 s. ... 316

Figure D.11. 1 mM DVA in D₂O titrated from pH 2-10 using DCl or NaOD and analysis in R. 317

Figure D.12. 1 mM MAN in D₂O titrated from pH 2-10 using DCl or NaOD and analysis in R. 318

Figure D.13. 1 mM CyAN in D₂O titrated from pH 2-10 using DCl or NaOD and analysis in R. 319

Figure D.14. 1 mM NHPI in D₂O titrated from pH 2-10 using DCl or NaOD and analysis in R. 320

Figure D.15. 1 mM NHSI in D₂O titrated from pH 2-10 using DCl or NaOD and analysis in R. 321

- Figure D.16.** An example of radical degradation data collected by LSV; 3.0 mm glassy carbon working electrode, Pt wire counter electrode, Ag/AgCl reference electrode; 1000 rpm; 20 mV/s. 322
- Figure D.17.** An example of LSV monitoring during radical pooling (red traces) and after addition of substrate (blue traces). 10 mM VA; 1:1 MeCN: 0.1 M HCl (aq); 20 mV/s; graphite rod (working electrode: generation), carbon fiber microelectrode (working electrode: monitoring), Pt wire counter electrode; Ag/AgCl reference; divided cell. 323
- Figure E.1.** Graphic illustration of the components of the divided flow cell reactor. Interelectrode distance between anode and cathode is 3.5 mm. 327
- Figure E.2.** Flow reaction set up with three flow pumps, two columns, pair of anodic and cathodic reservoirs and two flow cells. 328

Abbreviations and Acronyms

2D HSQC NMR	two-dimensional heteronuclear single-quantum coherence nuclear magnetic resonance
A	amps
ABNO	9-azabicyclo-[3.3.1]nonane <i>N</i> -oxyl
ACT	4-acetamido-TEMPO
BDE	bond dissociation energy
BDFE	bond dissociation free energy
Bpy	2,2'-bipyridine
BtNO	benzotriazole <i>N</i> -oxyl
CA	chronoamperometry
Cu-AHP	copper-catalyzed alkaline hydrogen peroxide
CV	cyclic voltammetry
DAIB	diacetoxyiodo benzene
DDQ	2,3-dichloro-5,6-dicyano-1,4-benzoquinone
DDQH ₂	2,3-dichloro-5,6-dicyano-1,4-dihydroquinone
DIPEA	<i>N,N</i> -diisopropylethylamine
DPA-BP	4,4'-bis(diphenylamino)benzophenone
DPV	differential pulse voltammetry
Dtbbpy	4,4'-di- <i>tert</i> -butyl-2,2'-bipyridyl, 110
$E_{1/2}$	half wave potential
EA	extractive ammonia
ET	single-electron transfer
G	guaiacyl

GPC	gel permeation chromatography
GVL	γ -valerolactone
H	<i>para</i> -hydroxyphenyl
HAT	hydrogen atom transfer
HFIP	hexafluoroisopropanol
LDH	layered double hydroxide
LO	learning objective
MCF	mesoporous cellular silica foam
mV	millivolts
NHC	<i>N</i> -heterocyclic carbene
NHPI	<i>N</i> -hydroxyphthalimide
O ₂	molecular oxygen
OCF	oxidative catalytic fractionation
PINO	phthalimide <i>N</i> -oxyl
POM	polyoxometalates
Ppy	2-phenylpyridine
PT-ET	proton and electron transfer
RCF	reductive catalytic fractionation
S	syringyl
SET	single-electron-transfer
<i>t</i> BuONO	<i>tert</i> -butyl nitrite
<i>t</i> BuOOH	<i>tert</i> -butyl hydroperoxide
TEMPO	2,2,6,6-Tetramethylpiperidin- <i>N</i> -oxyl

TOF	turnover frequency
TON	turnover number
TPPFeCl	meso-tetraphenylporphyrin iron(III) chloride
V	volts
VA	violuric acid
VANO	violuric acid <i>N</i> -oxyl
ΔE	change in cell potential
ΔG	change in free energy
μA	microamps

Chapter 1: Control is the Goal! Using Electricity and Mediators to Make Molecules

This work is an introductory chapter for a general audience.

I wrote this chapter to describe the context and some findings of my doctoral research to my family and friends who are part of a broad, non-specialist audience because I want to share my science with everyone in my life. I would like to thank the Wisconsin Initiative for Science Literacy (WISL) at UW-Madison for providing this platform, and for sponsoring and supporting the creation of this chapter. I am especially grateful to Professor Bassam Shakhashiri, Elizabeth Reynolds, and Cayce Osborne for their valuable feedback and encouragement.

It's hard to imagine a world without electricity; we use it to power everything from smart watches to city lights. We're also familiar with the idea of storing electrical energy in batteries. But did you know that electricity is also used to make the chemicals found in everyday items?! **The field of electrochemistry**, a compound word formed from "electricity" and "chemistry", **uses electrical energy to drive chemical reactions that do not happen spontaneously**. Electricity is the movement of small, negatively charged bits of energy called electrons, and the atoms that make up molecules are made of electrons and central positively charged bits called protons. In **Figure 1.1** the electrons are shown as little yellow circles joined with their best friend, the bigger gray proton circle. The bonds between atoms in a molecule are made of the shared electrons. The yellow electron circles in **Figure 1.1** are also joined with a big red square, which represents all the other atoms and bonds that make up the rest of the molecule.

When you think of chemical reactions, you probably imagine a scientist adding a liquid to another liquid or powder in a glass container. Electrochemical reactions are similar, but they need a little something extra to conduct electricity through liquid. Two pieces of electrically conductive material like metal or graphite are added into the container liquid and chemicals. The ends of the conductive pieces sticking out of the solution are attached to a piece of equipment that modulates the electricity coming out of a typical wall socket to the amount of electrical energy

needed for the reaction. Both pieces of conductive material are needed to conduct an electrochemical reaction, like a battery needs both a positive and negative end, but often the electrochemical reaction of interest is only occurring at one of the pieces and any reactions at the other piece can largely be ignored. **Figure 1.1** shows just the one piece of conductive material as a big gray bar attached to the source of electricity, although we don't actually use lightning.

Electrical energy applied to these conductive pieces can directly add or remove one or more electrons from a target molecule. **Figure 1.1** shows one electron being removed from the red block molecules at the conductive surface. Notice that the proton is not removed with its electron best friend. These "direct" electrochemistry reactions have been around since the 1800's and are performed on large scale by chemical companies in the process of making Nylon, a plastic used in swimsuits and carpets. **The direct transfer of a single electron from most carbon-based molecules incurs a high energetic cost** because electrons and their atomic proton counterparts are happier and more stable moving together as the element hydrogen (one electron and one proton) or the negatively charged version known as a hydride (two electrons and one proton). **Figure 1.1** shows that after direct electrochemical removal of an electron the lonely proton (gray circle) leaves the molecule (red square) quickly afterwards.

The high energetic cost means that a relatively large amount of electrical energy, measured as voltage, is required to remove or add a single electron without its proton friend to or from a molecule. For simple molecules containing few atoms and bonds, like the molecule used for making Nylon, direct electrochemistry works well because it doesn't matter how much energy you use to separate the electron and proton couple. Imagine the electrical energy as a big sledgehammer. Using the sledgehammer to pound one nail into a simple wooden board might be overkill, but it'll work. Now imagine trying to pound just one nail in the center of a board full of

nails using just the sledgehammer and it becomes clear that the high voltage required by direct electrochemistry fails for selective addition or removal of a desired electron from more complex molecules.

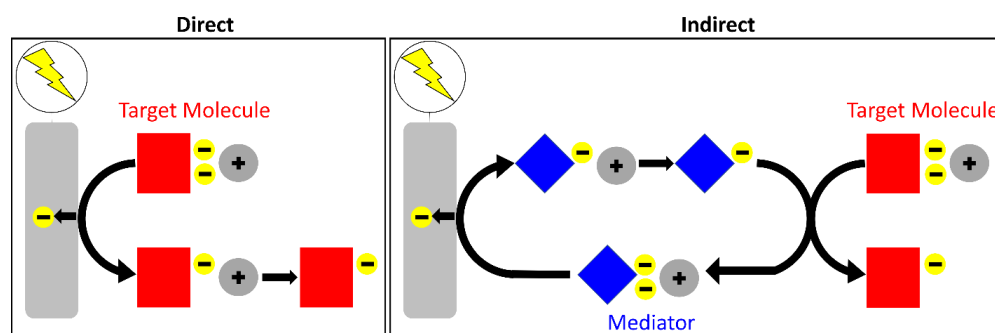
Scientists over the last 40 years worked hard to overcome the limitations of direct electrochemistry and find a toolbox that has a smaller hammer. They searched for, and found, a handful of relatively simple molecules that were able to undergo direct electron transfer at low voltages. This small group of molecules are not themselves valuable as target molecules and cannot be converted into new or valuable chemicals. However, some of these special molecules could *also* transfer one or more electrons and its coupled proton together from interesting target molecules. This subset of specialized molecules is known as proton-coupled electron-transfer mediators and are shown as blue diamonds in **Figure 1.1**.

The use of mediators has been used to develop an entirely new type of electrochemistry! The full process of transferring an electron from the target molecule (red square) to the mediator (blue diamond) and then to the electrical source shown in **Figure 1.1** is aptly named “indirect” or “mediated” electrochemistry. **Figure 1.1** also shows that after direct electrochemistry removes an electron from the mediator (blue square), it transfers an electron and proton from the target molecule (red square) and regenerates the initial form of the mediator. Therefore, the mediator molecule is not used up during the reaction.

Indirect reactions employing proton-coupled electron-transfer mediators can operate at much lower energy than direct electrochemistry, which is like trading that big sledgehammer for a standard claw hammer. The voltage hammer is small and only sufficient to add or remove electrons from the mediator. The mediator is then able to transfer only one set of coupled electrons and protons from the target molecule, even if the target molecule is complex and

contains many types of atoms and bonds. Furthermore, molecules are also kind of like puzzle pieces in that they have a specific shape that fits well with only some parts of other molecules. Both traits enable mediators to be selective in the electrons and protons they remove from complex molecules.

The selectivity of indirect reactions can be used to enable new types of chemical reactions.



Example 1

Figure 1.1. The direct electrochemical removal of an electron (yellow circle) from a target molecule (red square) and indirect removal an electron (yellow circle) and proton (gray circle) using a mediator (blue diamond).

Let's examine an example from my own research. Science is rarely carried out without the collaboration and support of other scientists. I conducted this research under the mentorship of my coworker Alastair Lennox. The research that we completed together showcases the power of electrochemical mediators for making molecules that could be used in the discovery of new drugs.

Pharmaceutical chemists create the large and very complex molecules typically used for drugs by sequentially adding molecules to one small molecule in the same way that small pieces are glued together to build a model airplane. Piperidine is a simple molecule that is often found as part of the larger molecular structure of many commercial drugs. Removing electrons and a proton from piperidine allows another molecule to be attached to piperidine. Since this kind of attachment

to piperidine may need to occur later in the drug building process, the ability to remove electrons from only the piperidine part of a complex molecule is highly desirable and may enable the design of new life-saving drugs.

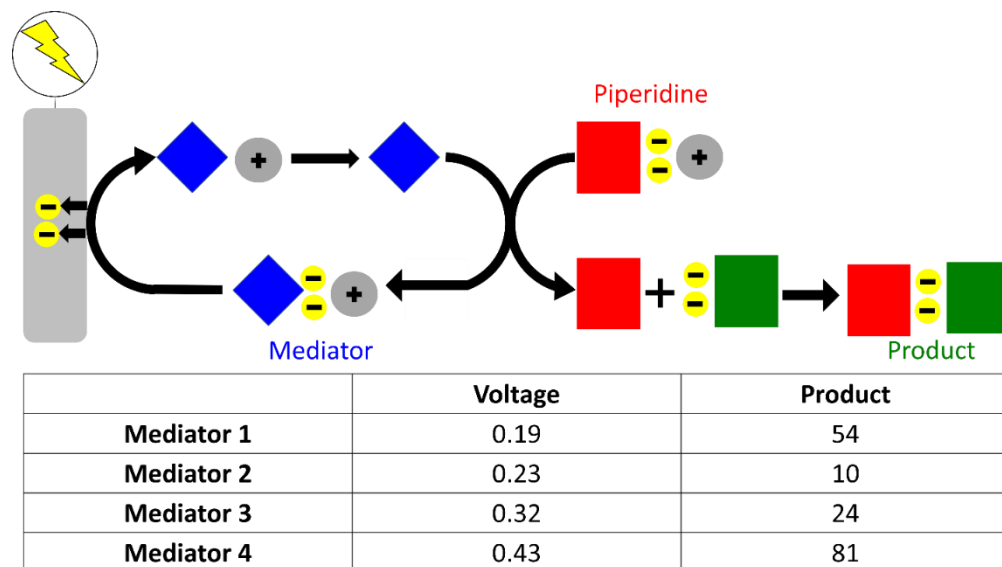
To start this project, the first thing that we did was throw out the sledgehammer. Piperidine undergoes direct electrochemical removal of electrons using approximately 0.85 volts of electrical energy. Other parts of complex drug-like molecules that may be found alongside piperidine could *also* undergo electron transfer at or around this voltage. Using a high voltage sledgehammer to remove electrons from piperidine may affect the other parts of the molecule capable of undergoing electron transfer. Remember all those nails in the board? These other parts may be crucial to how the drug works in the body, so we wanted a way to lower the voltage and facilitate the selective removal of electrons from piperidine in complex molecules.

A mediator seemed like it might be perfect for this job! First, we required a mediator that undergoes direct electrochemical removal of electrons at voltages lower than any part of the target piperidine-containing molecules. We selected four similar mediators with slightly different molecular structures labeled as **1-4** in **Table 1.1** that we suspected, based on work done by other scientists, could undergo direct electrochemical transfer of electrons at low voltages. We added each mediator to some liquid, inserted, the conductive pieces into the liquid, and measured the voltage needed to remove electrons from each of the four mediators. Direct electron transfer occurred between 0.19 and 0.43 volts for all the mediators. The mediator that undergoes direct electron transfer at the lowest voltages (as shown in **Table 1.1**) was the most desirable because any part of a target molecule with a higher energetic requirement for direct electron transfer wouldn't be affected. Basically, the tinier the voltage hammer, the easier it is to hit only the mediator. But, we couldn't just pick a mediator based on voltage. The mediator also must

successfully transfer two electrons and a proton (a hydride) from a simple piperidine-containing molecule.

Unlike voltage, which can be measured directly, the hydride transfer reaction between the mediator and piperidine had to be measured indirectly. Since hydride transfer enables the attachment of another molecule (green square) to piperidine (red square), we simply measured the amount of conjoined product (attached red and green squares) produced from the indirect electrochemical reaction with each mediator in **Table 1.1**. An indirect reaction that converted all the piperidine to the conjoined product (100%) would indicate that the mediator is perfectly successful for indirect transfer from piperidine. Mediators **2** and **3** give only small amounts of product. These mediators have a molecular structure that likely does not fit well with piperidine, like two puzzle pieces that don't match. Mediator **1** results in the formation of less product than mediator **4**, but it also requires much less energy for direct electron transfer.

Table 1.1. Mediator comparison of required voltage and amount of product for indirect electrochemistry of piperidine.



We chose to test mediator **1** for the indirect proton-coupled electron-transfer of more complex piperidine-containing molecules. Many different piperidine-containing molecules were

able to be converted to the desired product, meaning that the only part of the molecule primarily engaging in electron transfer was piperidine! A method for making these products had never been reported before, we published a paper in a scientific journal letting other scientists know that **mediators enable the production of molecules that could be useful for making new drugs.**

Example 2

This example from my research showcases the power of electrochemical mediators for facilitating the production of valuable chemicals from wood.

The part of wood we're most familiar with is the part of wood used to make paper. During the paper making process, the rest of the wood is removed and burned to generate the heat needed for processing more wood into paper. One of these "waste" components is an incredibly complex molecule called lignin, which is made up of many smaller molecules linked together into a long chain. Imagine lignin as a series of blocks each tied together with string. Chemically cutting certain ties between the molecules has been shown by other researchers to produce many valuable molecules that may replace chemicals typically derived from non-renewable fossil fuels.

Unfortunately, the chemical process of separating lignin from the part of wood used for paper damages the lignin linkages and prevents them from being cut, which is akin to taking all the strings and tying the blocks together in one big knot. The removal of two electrons and one proton from lignin could protect the lignin from being damaged during the wood separation process and will facilitate the subsequent chemical severing of the linkages in isolated lignin. However, the part of wood used for paper making can also undergo electron transfer. Once this occurs, it can no longer be used for paper making. Making just the molecules you want, and few or none of the ones you don't, is one of the biggest challenges in chemistry.

Wood is an amalgamation of very complex molecules, and the analysis of such a complex mixture is... complex. Since we knew that we may have to conduct many reactions and analyze the products of those many reactions, we decided to start with reactions using simplified molecules, known as models, that would likely react similarly to the real thing. The simplified lignin model molecule is a type of alcohol, and the simplified lignin model is a sugar. Sugars can also be considered a type of alcohol, but the bonds that form this alcohol are slightly different than the ones in the lignin model.

The mediators from Example 1 undergo electron transfer at low voltages and can transfer two electrons and a proton from a target molecule, so we thought those mediators might be perfect for this reaction too! Looking through some articles published in scientific journals saved us from wasting our time conducting these reactions in the lab. Other researchers had already demonstrated that those mediators will affect both the lignin and the part of wood used for paper.

Instead, the literature indicated that we should look at a proton-coupled electron-transfer mediator that transfers only one electron and one proton. As expected, we found that this mediator also undergoes direct electron transfer at a much lower potential than the direct electrochemical removal of electrons from either of the models. We've successfully exchanged the sledgehammer for the smaller hammer!

We then evaluated the ability of the mediator to remove one electron and one proton from the lignin model molecule. Since two electrons (yellow circles) and two protons (gray circles) must be removed from the alcohol to generate the product (green square), two mediator molecules (blue diamond) are required to transform one model alcohol (red square) to product as shown in **Figure 1.2**. The indirect electrochemical reaction of the mediator with the lignin model alcohol generated product. No product was formed in the indirect electrochemical reaction of the mediator with

the sugar model and all the sugar model was recovered at the end of the reaction. Therefore, the mediator does not transfer a hydrogen atom (one electron and one proton) as shown in **Figure 1.2**.

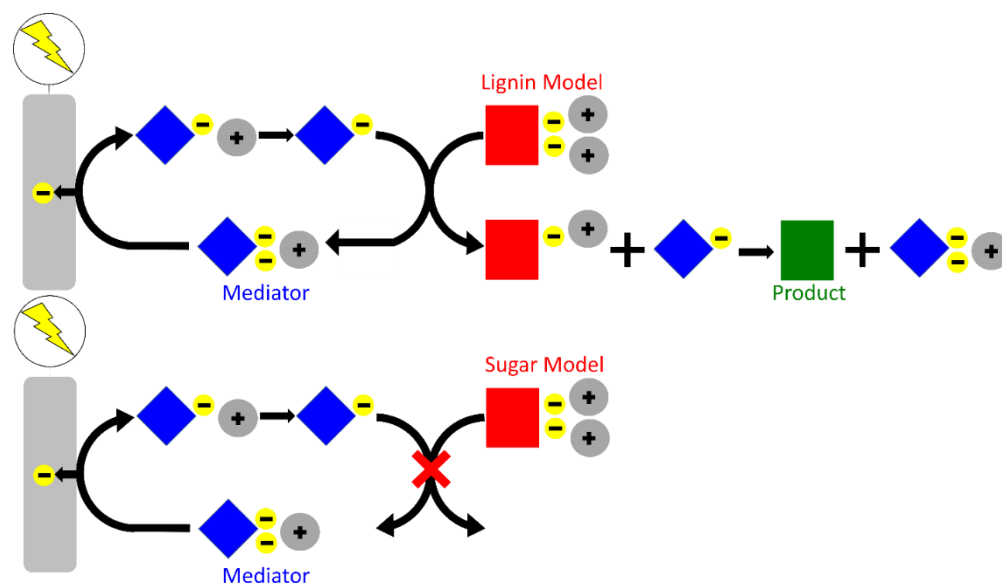


Figure 1.2. The indirect electrochemical reaction of lignin and sugar model molecules.

Encouraged by the reaction of the mediator with the lignin model, and lack of reaction with the sugar, we decided it was time to try the indirect electrochemical reaction with actual wood. The complicated analysis of the reaction products indicated that many of the alcohols in lignin linkages had been converted to the protected form, and no changes were detected in the part of the wood used for paper! **Despite the immense chemical complexity of wood, mediators enabled the transformation of just one part of the many complex molecules in wood.**

Scientists around the world are becoming increasingly interested in the ability of indirect electrochemistry to make new molecules or make known molecules in more efficient or environmentally friendly ways. Although the chemical reactions described in examples 1 and 2 will likely never be used directly in the commercial production of drug molecules or valuable chemicals from wood, future researchers may be able to improve upon these strategies to enable commercial applications. To further that goal, I've helped develop indirect electrochemistry lab

experiments for undergraduate students, graduate students, and industrial scientists. These educational labs will be used for many years at multiple institutions and companies to provide other researchers with the knowledge and skills to develop their own new electrochemical reactions.

Chapter 2: Exploring Electrosynthesis: Bulk Electrolysis and Cyclic Voltammetry Analysis of the Shono Oxidation

Submitted for publication: Shannon L. Goes,* Jordan E. Nutting,* Nicholas J. Hill, Shannon S. Stahl, and Mohammad Rafiee contributed to this work.

*Corresponding authors

2.1. Abstract

As electrochemistry continues to gain broader acceptance and use within the organic chemistry community, it is important that advanced undergraduate students are exposed to fundamental and practical knowledge of electrochemical applications for chemical synthesis. Herein, we describe the development of an undergraduate laboratory experience that introduces synthetic and analytical electrochemistry concepts to an advanced organic chemistry class. Experiments focus on the electrooxidative α -functionalization of carbamates, more generally known as the Shono oxidation, and include cyclic voltammetry analysis of two cyclic carbamates and a constant current bulk electrolysis reaction. The exercise offers students an authentic experience in organic electrochemistry, lays a practical and theoretical foundation for future engagement with concepts in electrochemistry and redox chemistry, and strengthens fundamental organic chemistry skills.

2.2. Introduction

The field of organic electrochemistry has recently received increased attention and undergone a “renaissance” of new methods and technologies.

¹ The organic chemistry community’s newfound interest in electrochemistry builds upon a rich history of using electricity to drive organic reactions. Examples range from Faraday’s electrolysis of acetic acid reported in 1834 to contemporary multi-ton per year syntheses of industrial chemicals.^{2,3} Despite the important role of electrosynthesis and electrochemical techniques in the field of organic chemistry, authentic lab experiments are largely absent from the undergraduate organic chemistry curriculum.^{4,5} In the context of organic electrochemistry’s history and recent resurgence, it would be valuable for undergraduate students to learn about basic electrochemistry concepts and techniques and gain experience working with electrochemical instruments in the laboratory.

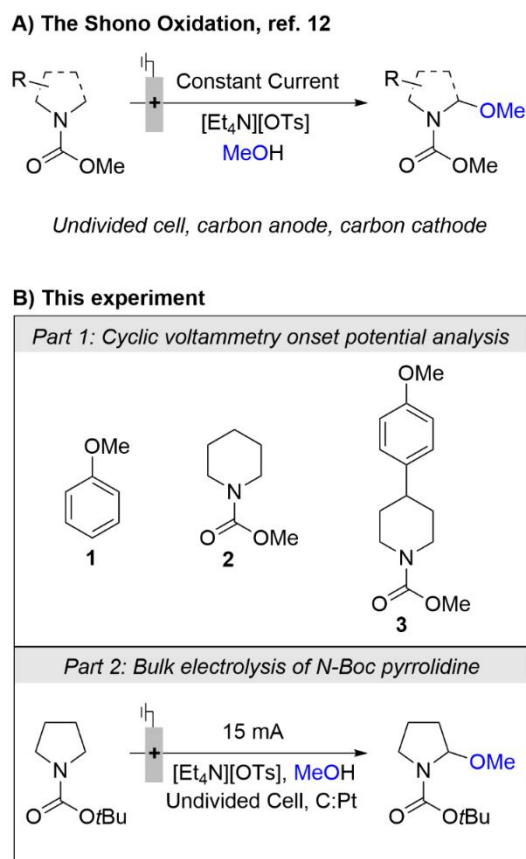
Several publications describe experimental protocols for an undergraduate-level organic electrochemistry laboratory that focus on synthetic applications.⁶⁻¹⁰ Some of these protocols, however, require complex or hazardous equipment, such as divided H-type electrolysis cells or mercury pool electrodes that are impractical for undergraduate lab courses, or use equipment that is not authentic to academic or industrial organic electrosynthesis. Furthermore, few undergraduate organic electrochemistry lab experiences incorporate both the synthetic and analytical applications afforded by electrochemical tools.¹¹ An undergraduate laboratory module that combines bulk electrolysis and analytical electrochemistry experiments, along with analysis of the authentic data, would be a valuable pedagogical experience.

Herein, we report an organic electrochemistry laboratory module for an advanced undergraduate organic chemistry laboratory course. The experiments within the module explore the oxidative α -functionalization of cyclic carbamates, a classic electrosynthesis reaction commonly referred to as the Shono oxidation (**Scheme 2.1A**).¹² This reaction was selected due to its broad use,¹³ functionally simple electrolysis setup,¹⁴ and the relative difficulty in accessing the same reactivity and products with other oxidation strategies.^{15,16} Following an introductory lecture on basic concepts in organic electrochemistry, students gain hands-on experience in performing cyclic voltammetry (CV) experiments where they assess the electrochemical oxidation potentials of two carbamates as potential substrates for the Shono oxidation (**Scheme 2.1B**). Following the CV lab exercise, students perform electrochemical α -methoxylation of *N*-Boc-pyrrolidine and calculate the yield of the reaction by ¹H NMR spectroscopy using an internal standard in a concentrated solution of the crude reaction mixture. Students are asked to complete a written laboratory report that addresses specific questions about the data generated from the CV and bulk electrolysis experiments. The learning objectives (LO) for this project are for students to (a) gain

familiarity with basic electrochemistry concepts and equipment in the context of organic chemistry (LO1), (b) use electroanalytical techniques to inform electrosynthesis methods (LO2), and (c) build on standard organic chemistry laboratory skills (LO3), including determination of reaction yield by analysis of authentic ^1H NMR spectroscopy data.

Course materials, including the instructional manual, assessment questions, yield (%) practice, and a list of necessary equipment, are provided in the Supporting Information. Additional tutorials on electrochemistry theory, techniques, and tools are available in the literature.¹⁷

Scheme 2.1. The Shono oxidation.



2.3. Educational Context

The module described here was introduced to CHEM 346, a semester-long undergraduate course at University of Wisconsin-Madison. In the course, students learn advanced laboratory methods in organic synthesis. Up to 36 senior-level undergraduates (typically chemistry majors)

are enrolled each semester. The students typically meet for two four-hour laboratory sessions per week, and each session begins with a brief instructor-led discussion.¹⁸

Recorded lecture videos and written introductory content in a lab manual are provided to the students before the laboratory exercises. For this module, students are also provided with materials to practice calculating a reaction yield based on ¹H NMR analysis of a crude reaction mixture containing an internal standard. This ungraded practice is designed to prepare students for the percent yield analysis of the Shono oxidation that is included as part of the graded laboratory assessment.¹⁹ Assessment for each exercise is accomplished through a written laboratory report formatted as a journal article that addresses specific aspects of the experimental data.¹⁹

The organic electrochemistry module described here was conducted in the Fall 2020 and 2021 semesters and was introduced approximately halfway through the course. Due to limited in-person instruction during the COVID-19 pandemic, the second part of the 2020 laboratory module was demonstrated with a video recording of the instructors performing the bulk electrolysis reaction, and students were given electronic copies of NMR spectra. Student pairs were assigned a 40-minute in-person session to perform the CV experiments with an instructor. For the 2021 semester, student pairs performed both the bulk electrolysis and CV analysis experiments in-person under the guidance of the course instructors.

2.3.1. Cyclic Voltammetry Analysis

Instructors prepare separate solutions of anisole **1**, piperidine carbamate **2**, anisole piperidine carbamate **3**, and ferrocene in tetrabutylammonium hexafluorophosphate electrolyte solution. The solutions are transferred to individual CV cells, which are placed in a fume hood along with rinsing solutions, electrodes and electrode holder, and an electrode polishing pad. A potentiostat and laptop interface are located next to the fume hood. The complete CV cell setup includes the glass cell, a polymer electrode holder, a glassy carbon disk working electrode (3 mm

diameter), a platinum coil counter electrode, and a Ag/Ag⁺ reference electrode. Instructors set the CV experiment parameters in the potentiostat software to the appropriate scan rate and potential range.¹⁹

Students work in pairs under supervision of a course instructor to obtain cyclic voltammograms of each of the analyte solutions. Students polish the working electrode after each experiment. After all CV data are collected, students polish and clean the electrodes to prepare the experimental set-up for the next pair. Students export the CV data as .csv files and copy the .csv data to a .xlsx template for data analysis.²⁰ The .xlsx template converts the current and potential units from amps (A) and volts (V) to microamps (μA) and millivolts (mV) and references the potentials of the cyclic voltammograms of **1**, **2**, and **3** against the measured half wave potential ($E_{1/2}$) of ferrocene.²¹ Detailed experimental procedures for this CV analysis and the synthesis of **3** are provided in the Supporting Information.

2.3.2. Bulk Electrosynthesis

Instructors prepare undivided electrolysis cells consisting of a 3-dram glass vial, septum cap, a graphite rod working electrode, and a stainless-steel counter electrode. The experimental procedure directs students to add tetraethylammonium *p*-toluene sulfonate and a Teflon-coated stir bar to an undivided electrolysis cell, followed by methanol (5 mL) and *N*-Boc-pyrrolidine (0.25 mmol). Tetraethylammonium *p*-toluene sulfonate is the electrolyte, *N*-Boc-pyrrolidine is the substrate, and methanol serves as both solvent and nucleophile. (**Figure 2.1**). The cell is secured on a stir plate and the stir rate increased until rapid convection is observed. A current of 15 mA is applied for 67 minutes (corresponding to 2.5 Faradays/mol substrate) using a power supply. When the electrolysis is complete, students transfer the solution to a round bottom flask and concentrate using a rotary evaporator. Students add 1,3-5-trimethylbenzene (0.072 mmol) as the internal standard to the crude material and dissolve the mixture in CDCl_3 to prepare a sample for ¹H-NMR

spectroscopic analysis. Detailed experimental procedures for this bulk electrosynthesis and cell fabrication are provided in the Supporting Information.

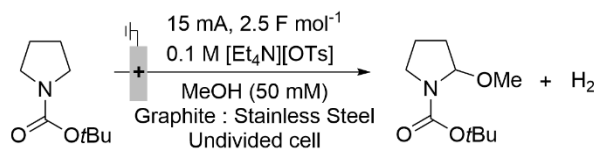


Figure 2.1. Electrochemical α -methoxylation of *N*-Boc-pyrrolidine.

Students are asked in the assessment to use computational methods to predict the chemical shifts of the expected Shono oxidation product to assist their analysis of the ^1H NMR spectrum of the crude reaction solution. Using the WebMO interface, students are asked to optimize the structure of the expected Shono oxidation product in Gaussian 09 using the B3LYP/6-31G(d) level of theory and basis set. The optimization requires approximately 3 hours of computational time. An NMR calculation is then performed on the optimized geometry.¹⁹ Students in the course have experience in computational chemistry and the WebMO interface from pre-requisite courses.²²

2.4. Hazards

Appropriate personal protective equipment, such as disposable gloves, goggles, closed-toe shoes, and a lab coat, must be worn. Students were required to wear face masks during the laboratory exercises as a precaution against transmission of SARS-CoV-2. Procedures must be performed in a fume hood or similarly ventilated workspace. Liquid and solid waste must be disposed into sealed and appropriately labeled containers. The organic solvents and substrates used in these experiments are flammable and should be handled in a well-ventilated fume hood. Chlorinated solvents are carcinogens and skin irritants. Specific safety information for reagents is available in the appropriate SDS. Electrical equipment can provide an electric shock hazard, and instructors should inspect students' experimental setups before an electric current is applied.

2.5. Results and Discussion

Students first watch a pre-recorded lecture video, or attend a live pre-laboratory discussion, and read the introduction of the associated lab chapter.¹⁹ This material includes discussion of:

- Redox reactions, defining reduction and oxidation in terms of electron transfer. A chromium oxide alcohol oxidation is presented as a canonical organic redox reaction.
- Electron transfer at electrode surfaces, emphasizing that redox reactions can occur at electrode surfaces, but that the individual reduction and oxidation steps are separated in space. The relationship between change in free energy (ΔG) and cell potential (ΔE) is also discussed.
- The equipment and reagents required for electrochemical experiments. Definitions of working and counter electrodes are provided, as well as discussion on the role of reference electrodes and electrolyte.
- Common analytical and synthetic electrochemical experiments, including constant current and constant potential electrolyses and cyclic voltammetry. An introductory discussion of why chemically and electrochemically reversible cyclic voltammograms are “duck-shaped” is also provided.
- Historical background for the Shono oxidation, providing information about the development of the reaction and its application in organic chemistry since the 1970s.

The introductory content presents students with sufficient theoretical and practical context to perform and study organic redox reactions in electrochemical experiments.

Following this introduction, students perform electrochemical analysis of anisole **1** and the piperidine carbamates **2** and **3**. The CV experiments are based on a recent study of an aminoxyl-mediated Shono-type oxidation²³ wherein the direct electrochemical oxidation of cyclic carbamates was found to be unsuccessful if the carbamate substrate contains an electron-rich functional group. In the report, CV analysis and bulk electrolysis results suggested that preferential electrochemical oxidation of the electron-rich functional group, rather than the carbamate functional group, leads to unproductive consumption of substrate. Students' CV analyses of **1-3** reproduces the CV analysis in the literature report (**Figure 2.2**). The similar electrochemical oxidation potentials of **1** (1420 mV) and **3** (1280 mV) are both lower than that of the carbamate **2** (1610 mV) and indicate that electrochemical oxidation of **3** likely occurs at the anisole functional group rather than the carbamate. Students are challenged to use their CV analysis and relevant literature²³ to predict how substrates **2** and **3** would react under the bulk electrolysis conditions used for the Shono oxidation. Of the two substrates, only oxidation of **2** generates the necessary iminium intermediate capable of reacting with methoxide to form the Shono product.

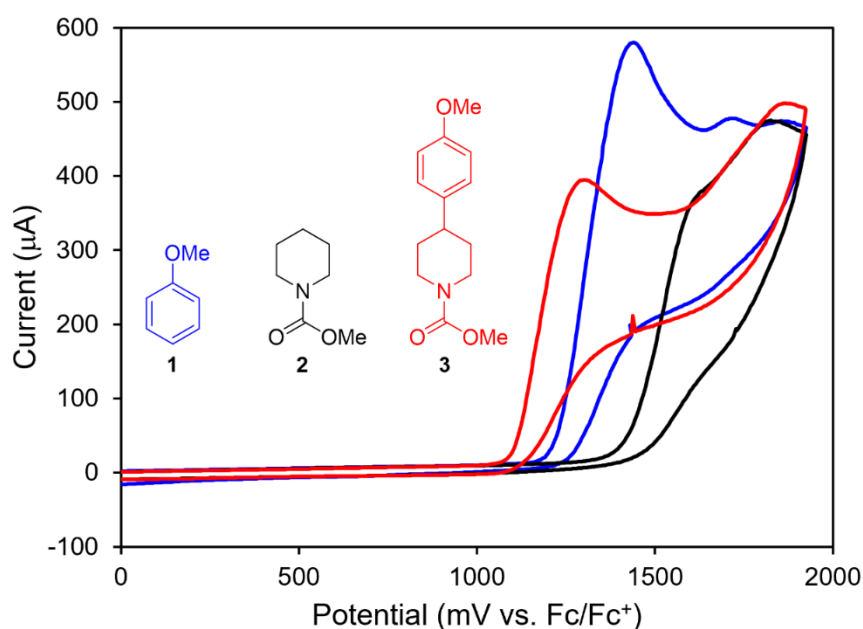


Figure 2.2. Cyclic voltammograms (0.1 V/s) in [NBu₄][PF₆] (0.1 M) acetonitrile solution of anisole **1**, piperidine carbamate **2**, anisole piperidine carbamate **3** (5 mM) referenced to Fc/Fc⁺.

The analysis of the CV data is also intended to give students insight into the mechanism of the Shono oxidation reaction. At the potential needed to initiate single electron transfer from the carbamate substrate, an initial electron transfer (ET) step generates a radical cation that immediately undergoes a second ET and proton transfer (PT) to form an iminium intermediate (**Figure 2.3**). The result is an oxidative CV peak during the forward scan (from 0 V to 1.9 V) corresponding to a chemically irreversible, 2 e⁻ transfer process.²⁴ As the potential is scanned in the reverse direction (from 1.9 V back to 0 V), the radical cation is no longer available to undergo electrochemical reduction at the same potential because it has already reacted to form the iminium cation, and thus no current is observed. The formation and trapping of the iminium intermediate are the basis for the Shono bulk electrolysis reaction.

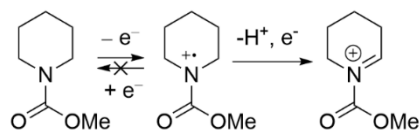


Figure 2.3. Electron transfer - proton transfer - electron transfer (ET-PT-ET) mechanism for electrochemical oxidation of piperidine carbamate **2**.

After CV analysis, students perform a Shono oxidation under constant current bulk electrolysis in an undivided electrolysis cell. The specific reaction is the electrochemical α -methoxylation of *N*-Boc-pyrrolidine. The process begins with electron transfer - proton transfer - electron transfer (ET-PT-ET) of the substrate to form the iminium intermediate, which is then trapped by a methoxide nucleophile to form the product (**Figure 2.4**).^{12,23} Methoxide is produced by reductive generation of H_{2(g)} at the cathode.

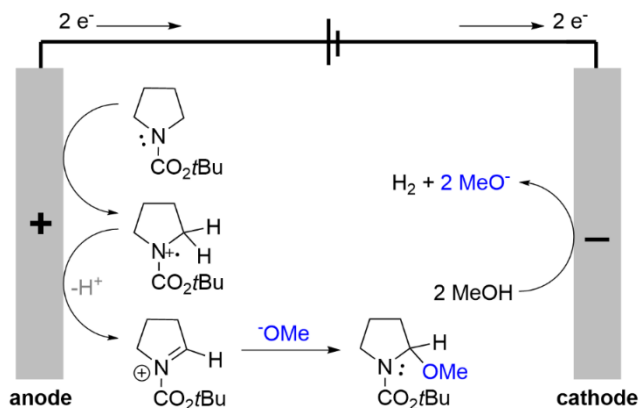


Figure 2.4. Mechanism of electrochemical α -methoxylation of *N*-Boc-pyrrolidine.

The amount of charge passed in the cell during an electrolysis can be used to determine the efficiency with which electrons are used to generate the desired product. A Faraday (F) is the amount of charge carried by one mole of electrons and is equal to 96,485 Coulombs (C). The Shono oxidation is a $2e^-$ reaction. Therefore, a minimum of 2 Faradays per mole of substrate are needed to convert all the substrate to product. The amount of charge passed during a reaction can be determined from the electrolysis current, duration of the electrolysis, and quantity of substrate.¹⁹ In the electrolysis protocol described here, the actual quantity of charge during the electrolysis is 2.5 F per mole of substrate. The excess charge is passed to account for competing electrochemical oxidation of methanol solvent as substrate concentration decreases. The role of electrons as a stoichiometric reagent, including relevant equations, is discussed with students during the pre-lab lecture.

In addition to exposing students to contemporary analytical and synthetic electrochemical techniques, an advantage of this module is that electrolysis can be carried out with inexpensive and readily accessible materials. The electrolysis cell consists of a glass dram vial, a septum cap, graphite and steel rod electrodes, and a Teflon-coated stir bar. At the time of construction, each cell was prepared for less than 2.50 USD per cell, and all the materials required for the set-up, or

direct substitutes, could be purchased online through typical retail outlets. A power source rated to provide $\geq 15\text{mA}$ current can be purchased from most department and hardware stores and typically costs less than 70 USD. The supporting electrolyte (tetraethylammonium *p*-toluene sulfonate) and substrate are inexpensive and commercially available. All other glassware and equipment are standard in an organic chemistry teaching lab. Information about the equipment and setup for the bulk electrolysis reaction can be found in the Supporting Information.

Students analyzed the outcome of their bulk electrolyses by ^1H NMR spectroscopy and were asked to assign all signals in the spectrum arising from the electrolyte, product, and internal standard (**Figure 2.5**). A ^1H NMR spectrum of pure electrolyte is provided to assist with the assignment of the electrolyte peaks. Computational methods are used to assist assignment of signals from the Shono oxidation product. The signals from the aromatic protons of the internal standard (H_g) and an a H-atom of the product (H_a) enable the most accurate integrations for each species (*i.e.*, these signals do not overlap with others) and should be used for calculating yield (%).¹⁹ The average yield for the reaction is 72% (range 36-86%), and no leftover starting material is observed in the ^1H NMR spectrum of the crude reaction mixture. Students may also use the reaction yield and the charge passed during the electrolysis (60 C) to determine the Faradaic efficiency of the reaction,²⁵ but they were not required to do so in the lab assessment.

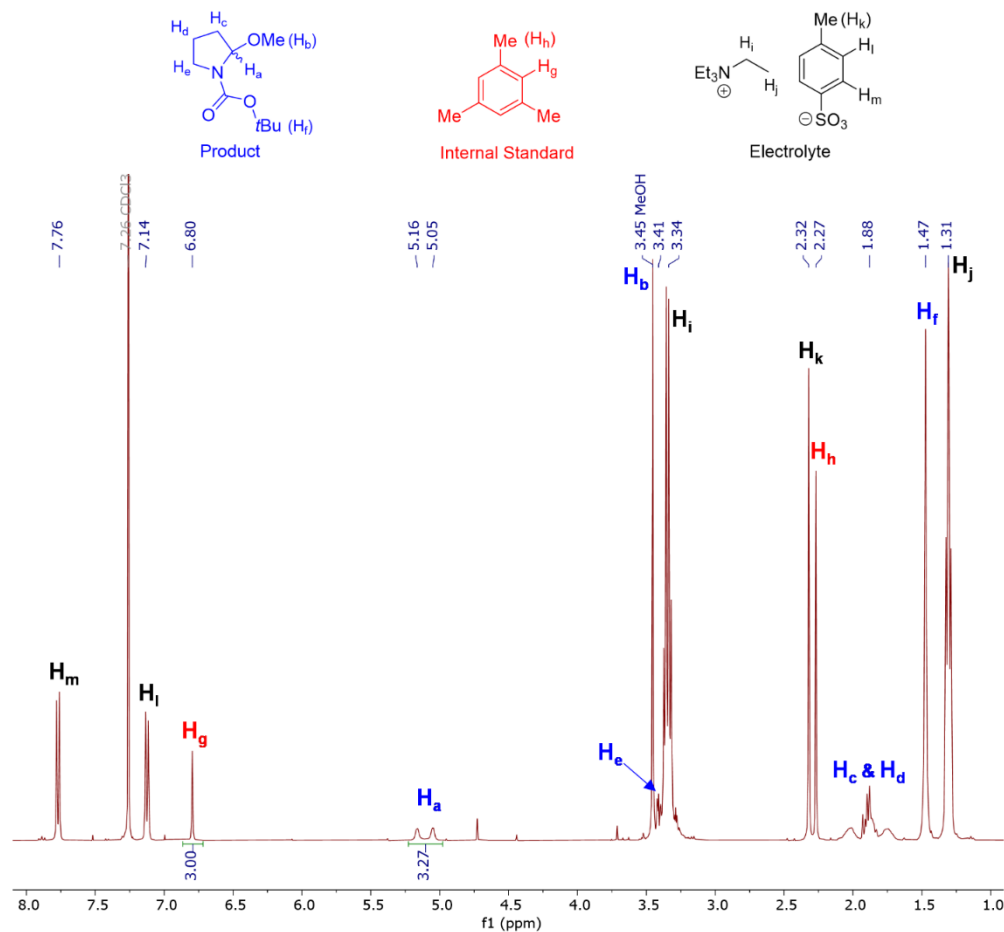


Figure 2.5. ^1H NMR spectrum of the crude Shono reaction mixture (CDCl_3 , 400 MHz).

2.6. Assessment

Conceptual learning objective LO1 was assessed indirectly (not for credit) during the lab session by asking students to identify important pieces of electrochemical equipment and discuss their utility with the lab instructor. Most (92%) students were able to identify the basic features of reversible (ferrocene) and irreversible (substrate) cyclic voltammograms. Key aspects of safe and effective set-up are noted by instructors during the initial CV portion of the lab, including ensuring that electrodes are not touching each other or other conductive materials before beginning an experiment. During the bulk electrolysis session, most students independently performed these safety measures before the set-ups were checked by an instructor. Learning objectives LO2 and LO3 were assessed directly using student reports written in ACS journal style. Students are asked

to analyze the shapes of the reversible and irreversible CV traces they collect for substrates **1-3** and comment on the implications of these data for the effectiveness of a Shono oxidation with these (or similar) substrates. A majority (72%) of students used the cyclic voltammetry data to correctly identify the substrate that is easiest to oxidize, and nearly half (43%) of the students correctly identified the substrate that would lead to a desired Shono product when subjected to bulk electrolysis conditions. Students justified their conclusions based on the CV data and related literature.²³ All students generated the desired α -methoxylated Shono product. Many students correctly assigned the relevant ^1H NMR signals from the product (68%), internal standard (94%), and electrolyte (84%) in the crude mixture, and 75% correctly calculated the yield (%) of their reaction.

2.7. Conclusions

This laboratory exercise introduces organic electrochemistry to advanced undergraduate students. The exercise incorporates electrochemical analysis techniques and synthetic electrolysis, providing students with an authentic and well-rounded learning experience. The flexible in-class, virtual, or hybrid approach is readily adaptable to a variety of class sizes, and the inexpensive synthesis equipment lends itself to adoption at a range of institutions. The written assessment requires students to build upon experiences from previous lab modules and incorporates fundamental organic chemistry analysis skills in an electrochemical context.

2.8. Acknowledgements

We are grateful to the CHEM 346 students for feedback. We thank the attendees and teaching assistants of the first Organic Electrochemistry Short Course Lab, held in Aug. 2019 at the University of Wisconsin-Madison. We thank the UW-Madison Instructional Laboratory Modernization program (NMR instrument) and the National Science Foundation for funding (CHE-0840494: computational chemistry facility; CHE-1048642: NMR facility). The authors

would like to thank the NIH (R35GM134929; SSS), Great Lakes Bioenergy Research Center, U.S. Department of Energy, Office of Science, Office of Biological and Environmental Research (DE-SC0018409 and DEFC02-07ER64494; SLG) for financial support to develop this laboratory experiment at the University of Wisconsin-Madison and the NSF for a predoctoral fellowship to JEN (DGE-1747503).

2.9. References

1. Yan, M.; Kawamata, Y.; Baran, P. S. *Chem. Rev.* **2017**, *117*, 13230–13319.
2. Faraday, M. *Ann. Phys. (Leipzig, Ger.)* **1834**, *109*, 481–520.
3. Cardoso, D. S. P.; Šljukić, B.; Santos, D. M. F.; Sequeira, C. A. C. *Org. Process Res. Dev.* **2017**, *21*, 1213–1226.
4. *New Horizons in Electrochemical Science and Technology*; National Research Council, The National Academies Press: Washington, DC, 1986.
5. The Coe College (Cedar Rapids, IA) Chemistry Department has put together a useful webpage on experiments and background in electrochemical education for undergraduate students. *Electrochemical Education*. <http://www.public.coe.edu/departments/ElectrochemEd/> (accessed 2022-03-11).
6. Iversen, P. E. *J. Chem. Educ.* **1971**, *48*, 136–137.
7. Iversen, P. E. *J. Chem. Educ.* **1974**, *51*, 489–490.
8. Pouliquen, J.; Heintz, M.; Sock, O.; Troupel, M. *J. Chem. Educ.* **1986**, *63*, 1013–1014.
9. Navarro, D. M. d. A. F.; Navarro, M. *J. Chem. Educ.* **2004**, *81*, 1350–1352.
10. Lam, C. H.; Jackson, J. E. *J. Chem. Educ.* **2020**, *97*, 172–177.
11. Ref. 7 is an exception.
12. Shono, T.; Hamaguchi, H.; Matsumura, Y. *J. Am. Chem. Soc.* **1975**, *97*, 4264–4268.
13. Kärkäs, M. D. *Chem. Soc. Rev.* **2018**, *47*, 5786–5865.
14. Jones, A. M.; Banks, C. E. *Beilstein J. Org. Chem.* **2014**, *10*, 3056–3072.
15. Li, C-J. *Acc. Chem. Res.* **2009**, *42*, 335–344.
16. Moriyama, K. *Tetrahedron Lett.* **2017**, *58*, 4655–4662.
17. For general information on electrochemical theory, techniques, and tools, see the following helpful articles: (a) Elgrishi, N.; Rountree, K. J.; McCarthy, B. D.; Rountree, E. S.; Eisenhart, T. T.; Dempsey, J. L. *J. Chem. Educ.* **2018**, *95*, 197–206. (b) Kingston, C.; Palkowitz, M. D.; Takahira, Y.; Vantourout, J. C.; Peters, B. K.; Kawamata, Y.; Baran, P. S. *Acc. Chem. Res.* **2020**, *53*, 72–83. (c) Schotten, C.; Nicholls, T. P.; Bourne, R. A.; Kapur, N.; Nguyen, B. N.;

- Willans, C. E. *Green Chem.* **2020**, *22*, 3358-3375. (d) Rafiee, M.; Mayer, M. N.; Punchihewa, B. T.; Mumau, M. R. *J. Org. Chem.* **2021**, *86*, 15866-15874.
18. For details on the course structure, see Nicastrì, K. A.; Hill, N. J. *J. Chem. Educ.* **2021**, *98*, 2990-2996.
 19. See Supporting Information for more details.
 20. Template provided in Supporting Information.
 21. Gritzner, G.; Kùta, J. *Pure Appl. Chem.* **1984**, *56*, 461– 466.
 22. Esselman, B. J.; Hill, N. J. *J. Chem. Educ.* **2016**, *93*, 932-936.
 23. Wang, F.; Rafiee, M.; Stahl, S. S. *Angew. Chem. Int. Ed.* **2018**, *57*, 6686–6690.
 24. Nutting, J. E.; Gerken, J. B.; Stamoulis, A. G.; Bruns, D. L.; Stahl, S. S. *J. Org. Chem.* **2021**, *86*, 15875-15885.
 25. Bard, A. J.; Faulkner, L. R. *Electrochemical Methods: Fundamentals and Applications*, 2nd ed.; John Wiley & Sons, 2001.

**Chapter 3: Deriving the Turnover Frequency of Aminoxy-Catalyzed Alcohol
Oxidation by Chronoamperometry: An Introduction to Organic
Electrocatalysis**

This work is published: Goes, S. L.; Mayer, M. N.; Nutting, J. E.; Hooper-Burkhardt, L. E.;
Stahl, S. S.; Rafiee, M. R. *J. Chem. Educ.* **2021**, *98*, 600-606.

3.1. Abstract

Organic electrosynthesis is an increasingly popular tool for driving and probing redox reactions. Recent advances in this field often employ an electrocatalyst to enhance the selectivity and efficiency of electrochemical reactions. A laboratory experiment was developed to introduce students to relevant mechanistic techniques in electrochemistry for analysis of electrocatalytic reactions using aminoxyl-catalyzed alcohol oxidation as a case study. This lab activity employs cyclic voltammetry for qualitative assessment of catalytic turnover prior to introducing students to chronoamperometry, an underutilized technique that facilitates quantitative determination of the rate of catalysis. Students identify and rationalize the important features of a reversible electron transfer and a catalytic reaction in a cyclic voltammogram, probe the origin of scan rate effects on these traces, and calculate turnover frequency using a series of chronoamperograms. The method employs safe and readily available reagents: basic aqueous buffer solution, alcohol substrate, and an inexpensive organic aminoxyl catalyst. Student data presented herein were obtained from a course attended by undergraduate students, graduate students, and pharmaceutical chemists.

Electrochemistry is one of the oldest and most fundamental methods to promote and analyze redox reactions.¹ Recent advances in the electrosynthesis of organic compounds demonstrate that electrochemistry is a powerful tool to access unique reactivity and investigate complex mechanisms.²⁻⁸ Investigation of these redox reactions and their coupled chemical reactions can play a valuable role in improving electrochemical reactions and chemical reactions that involve electron transfer and/or redox steps.⁶ Cyclic voltammetry (CV) is the most widely used electrochemical technique for studying electrode processes.⁹⁻¹² The flexible time window and forward and reverse scans of CV make it a powerful technique to study the mechanism of reactions that occur at an electrode surface; however, extracting quantitative information from CV data can be complicated.^{13,14} Chronoamperometry (CA) is another standard electrochemical technique for

understanding electrode reaction processes.¹⁵ Although CA data contain less mechanistic information than CV data, the former can be more straightforward to analyze than CV data to obtain quantitative information from electrochemical processes.¹⁶ CA is comparatively underexplored in instructional electrochemistry curricula and limited to theoretical discussions.¹⁷ The present article outlines laboratory experiments to demonstrate how CA represents a versatile complement to CV for analysis of electrochemical reactions.

In a CA experiment, the electrode potential steps from a potential where no electron transfer occurs (E_{init}) to one at which a faradaic process occurs (E_{app}). The resulting current is monitored as a function of time (**Figure 3.1b**).¹⁸ In the case of an oxidative electrochemical reaction (Error! Reference source not found. **3.1a**), E_{app} is sufficiently more positive than E° (large ΔE is applied) where the rate of electron transfer no longer influences the current.¹⁹ In the case of a reductive reaction, E_{app} would be more negative than E° .

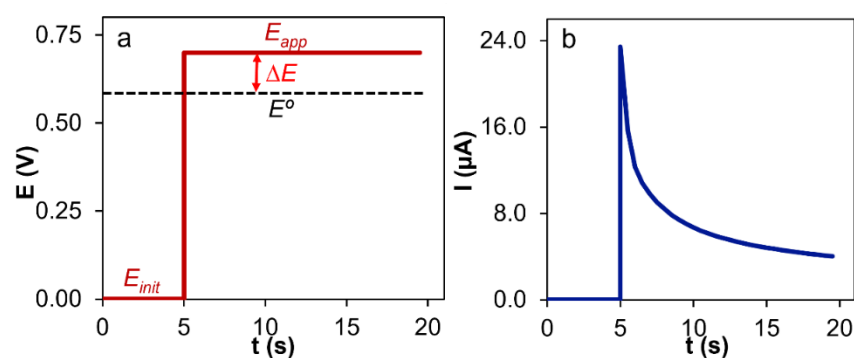


Figure 3.1. Applied potential waveform (a) and the resulting current-time trace (b) for a chronoamperometric experiment of a general oxidation reaction.

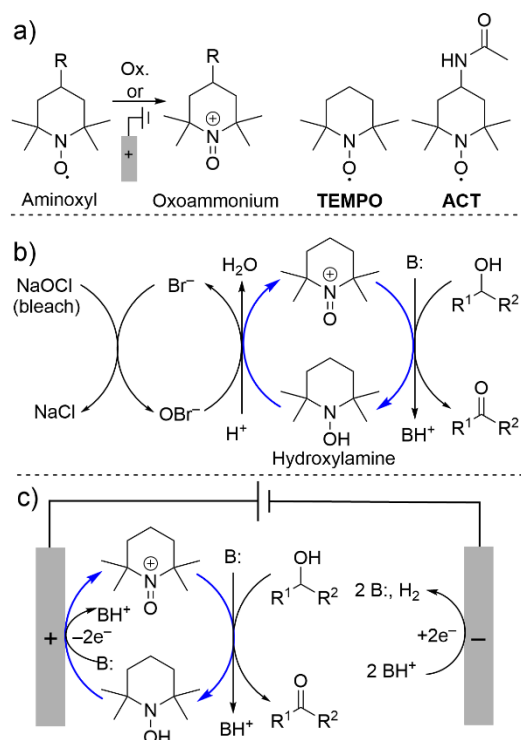
The current is controlled (limited) by the flux of the redox-active species to the electrode (**Figure 3.1b**) or the kinetics of the reaction that (re)generates the redox-active species.^{15,20} Under these limiting conditions, extracting quantitative information from the CA for electrode processes is straightforward. When the current is controlled by diffusion, the diffusion coefficient of the electroactive species can be derived on the basis of the Cottrell equation (eq 1).

$$I = nFA\pi^{-1/2}C_A D_A^{1/2} t^{-1/2} \quad (1)$$

In this equation, I is current (amperes, A), n is the number of electrons transferred in the half reaction, F is the Faraday constant ($96,485 \text{ C mol}^{-1}$), A is the area of the electrode (in cm^2), D_A and C_A are the diffusion coefficient ($\text{cm}^2 \text{ s}^{-1}$) and the initial (bulk) concentration of electroactive species (mol cm^{-3}), and t is time (s).^{15,21} When the current is reaction controlled, quantitative information about the reaction kinetics can be derived by analysis of the amperometric responses. The goal of this experiment is to introduce students to electroorganic chemistry and to teach students how to employ CV for mechanistic investigation of catalysis and CA for quantitative analysis of catalytic turnover rates.

2,2,6,6-Tetramethylpiperidin-N-oxyl (TEMPO) and its derivatives represent a class of organic radicals (**Scheme 3.1a**) known as aminoxyl radicals that find widespread applications as catalysts for the oxidation of organic molecules.²²⁻²⁴ Oxidation of aminoxyl compounds results in formation of the corresponding oxoammonium species (**Scheme 3.1a**), which is the reactive form of the catalysts. Oxoammonium oxidizes the substrate, herein alcohol, and undergoes reduction to hydroxylamine (**Scheme 3.1b**). The turnover of these catalysts may be accomplished by using stoichiometric oxidants such as oxygen or bleach (**Scheme 3.1b**).^{25,26} Aminoxyl radicals undergo facile redox reactions at electrode surfaces (**Scheme 3.1a**).²⁷ Aminoxyl-catalyzed electrochemical oxidation reactions generate hydrogen gas as the sole byproduct of the oxidation reactions and avoid stoichiometric chemical oxidants altogether (**Scheme 3.1c**).²⁷⁻²⁹ Moreover, the electrochemical activity of aminoxyl radicals provides insights into the origin of their reactivity and structure–reactivity correlations.³⁰⁻³³

Scheme 3.1. Structures and oxidation reaction of ACT and TEMPO (a), Anelli–Montonari oxidation (b), and TEMPO-catalyzed electrochemical alcohol oxidation (c) with blue arrows showing the catalytic turnover.



In this report, we describe a study of electrochemical alcohol oxidation catalyzed by 4-AcNH-TEMPO (ACT). This laboratory exercise introduces students to the interdisciplinary concepts of electroorganic chemistry, electrocatalysis, organocatalysis, and kinetic analysis. In contrast to many undergraduate education resources that focus only on examining direct electron transfer to and from inorganic molecules using CV,^{12,34} this experiment teaches students to conduct a mechanistic investigation of an electrocatalytic organic reaction. The experiment is well-suited for upper-level undergraduate laboratory courses, including physical chemistry, organic chemistry, instrumental analysis, and electro chemistry. The procedure has been successfully completed by 16 graduate students and scientists from pharmaceutical companies as part of the “Organic Electrochemistry Short Course”³⁵ lab section held during summer 2019 and by 12 students in the University of Missouri–Kansas City physical chemistry lab during spring 2020.

3.2. Experimental Overview

A variety of aminoxyl radicals, including TEMPO, are capable of catalyzing alcohol oxidation under both chemical and electrochemical conditions. For this laboratory experiment, the catalyst is the low-cost aminoxyl derivative ACT that has been shown to be one of the most effective aminoxyls for electrochemical oxidation of alcohols.³⁰ Sufficiently basic conditions (pH 8–11) are required for fast oxidation of alcohols by oxoammonium. Aqueous carbonate buffer is a suitable reaction medium, and the pH can easily be adjusted by changing the ratio of carbonate/bicarbonate. For this experiment, identical quantities of carbonate and bicarbonate are used, resulting in a pH 10 solution.^{29,30} This electrolyte provides simple and safe reaction conditions that avoid the need for more costly organic electrolytes and bases, making this experiment ideal for educational purposes. The substrate 1,2-isopropylidenglycerol (solketal) is a protected form of glycerol and is soluble in the buffered aqueous solution conditions.^{36,37} The reversible electrode reaction for ACT and its corresponding oxoammonium (ACT⁺) under these experimental conditions results in a well-defined voltammetric signal (**Figure 3.2**, trace a) that may be analyzed by students.³⁸ Electrochemical oxidation of ACT also exhibits an ideal diffusion-controlled chronoamperometric response (**Figure 3.2**, trace c). The substantial changes in voltammetric (**Figure 3.2**, trace b) and chronoamperometric (**Figure 3.2**, trace d) responses of ACT in the presence of solketal match diagnostic criteria for electrocatalytic behavior.¹⁵ We will show that the enhancement of the oxidative CA current and the additional charge during the CA experiment can be used to derive the turnover frequency (TOF)³⁹ of ACT-catalyzed electrochemical oxidation of solketal. The experimental procedure outlined below was readily completed by students within a 3 h laboratory period. All experiments were performed at ambient temperature (ca. 25 °C).

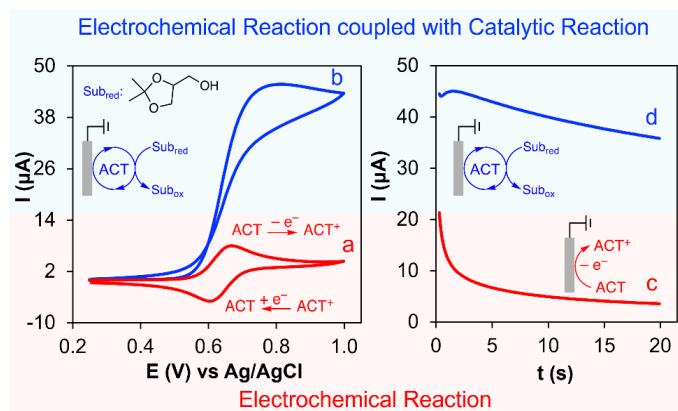


Figure 3.2. Cyclic voltammograms (left) and chronoamperograms (right) of 1.0 mM ACT in the absence (red traces, a and c) and presence of 4 mM solketal (blue traces, b and d). Solution conditions: aqueous solution with $\text{NaHCO}_3/\text{Na}_2\text{CO}_3$ electrolyte (0.1/0.1 M, pH 10), scan rate for cyclic voltammetry 10 mV s^{-1} , and applied potential for chronoamperometry 0.8 V vs Ag/AgCl.

A typical experiment was carried out in the following manner. After making the buffer solutions, the students conducted an initial voltammetric experiment with a solution of ACT. After observation of the oxidation and reduction peaks, the potential range was adjusted for further voltammetric experiments. For the CA experiment, the initial voltage (E_{init} , cf. **Figure 3.1**) should be a value at which no oxidation was observed for the CV experiment, or approximately 200 mV less than oxidation peak potential of ACT. The applied potential to measure the oxidation current (E_{app}) should be 100–150 mV more positive than the oxidation peak potential, which was determined by the students from the initial CV experiment. CV data at various scan rates and CA data were collected for solutions containing ACT in the absence and presence of various concentrations of solketal. The CA experiment and one CV experiment were then conducted with a buffered solution containing only solketal as a “blank” experiment. The same CA and CV experiments were also performed for ACT in the presence of 4 mM of solketal in a NaCl solution, instead of carbonate/bicarbonate buffer, to examine the effect of basic conditions on this catalytic reaction.

3.3. Experimental Procedure

The students were given a 0.2 M stock solution of solketal and were asked to prepare the following additional stock solutions: 10 mL of 20 mM ACT solution, 100 mL of 0.2 M NaHCO₃ solution, 100 mL of 0.2 M Na₂CO₃ solution, and 50 mL of 0.2 M NaCl solution. The required solutions for electrochemical studies were prepared by mixing the required volumes of solketal stock solution, 0.5 mL ACT, 4 mL stock solution of NaHCO₃, and 4 mL stock solution of Na₂CO₃ followed by dilution with deionized water in a 10 mL volumetric flask. To study the effect of base, a separate solution was prepared with unbuffered electrolyte as follows: 0.2 mL stock solution of solketal, 0.5 mL ACT, 8 mL stock solution of NaCl, followed by dilution with deionized water in a 10 mL volumetric flask. The blank solution where no ACT was added was prepared as follows: 0.2 mL stock solution of solketal, 8 mL stock solution of NaCl, followed by dilution with deionized water in a 10 mL volumetric flask. The entire contents of each solution were transferred and analyzed independently in the electrochemical cell. A Pine Wavenow XV 100 Potentio/Galvano-Stat and a Pine Low Volume Three Electrode Cell were used to perform the electrochemical experiments.⁴⁰⁻⁴³ The cell was equipped with a Ag/AgCl (internal solution 3 M KCl) reference electrode, a Pt wire counter electrode, and a glassy carbon disk (2 mm) as the working electrode.⁴⁴⁻⁴⁷ The reference and working electrodes should be placed close together to minimize solution resistance. The working electrode was polished using alumina powder on a polishing pad before each chronoamperometric experiment.⁴⁸

3.4. Hazards

Proper laboratory attire, gloves, and approved safety goggles should be worn in the laboratory at all times. Sodium carbonate, bicarbonate, and solketal can cause eye irritation. Solketal is flammable and should be kept away from heat or open flame. 4-Acetamido-TEMPO

(ACT) has oral toxicity. All chemicals should be handled carefully. Flush eyes or skin with plenty of water for at least 15 min in the case of contact.

3.5. Results and Discussion

We initiated the CV and CA study of ACT in the absence of solketal to examine an electrochemically reversible redox reaction. The CV of ACT shows one anodic peak corresponding to oxidation of ACT to the corresponding oxoammonium (ACT⁺) and a cathodic peak for the reduction of electrogenerated ACT⁺ to ACT (**Figure 3.3a**). The potential difference between the cathodic peak and anodic peaks, also known as the peak to peak separation, is 59 mV, and the anodic to cathodic peak current ratio is near unity. The peak height of both the anodic and cathodic peaks, I_p (A), is best described by the Randles–Ševčík equation (at 25 °C):

$$I_p = 2.69 \times 10^5 n^{3/2} A D_{\text{ACT}}^{1/2} C_{\text{ACT}} \nu^{-1/2} \quad (2)$$

In this equation, n is the number of electrons, A is the electrode surface area (cm²), D_{ACT} is the diffusion coefficient of ACT (cm² s⁻¹), C_{ACT} is the concentration of ACT in the bulk solution (mol cm⁻³), and ν is the scan rate of voltammetric experiment (V s⁻¹).⁴⁹ Plotting the peak currents versus the square root of scan rate (**Figure 3.3b**) shows a linear correlation: evidence of an electron transfer process involving freely diffusing redox species.⁵⁰ These CV features agree with the characteristics of a reversible, one-electron reaction at the electrode. The CA of ACT in the absence of solketal shows that the current–time profile follows the diffusion-controlled correlation described by the Cottrell equation (**Figure 3.3c**).⁵¹

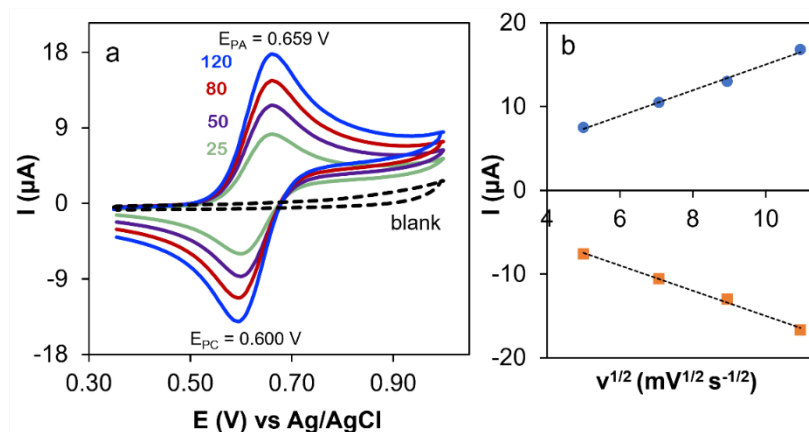


Figure 3.3. Cyclic voltammograms (a) of 1.0 mM ACT at different scan rates; scan rates (mV s^{-1}) are depicted for each CV. The blank CV (black dashed trace) is the CV of 4 mM solketal substrate in the absence of ACT at a scan rate of 80 mV s^{-1} . The plot of anodic and cathodic peak currents versus square root of scan rate (b). Solution conditions: aqueous solution with $\text{NaHCO}_3/\text{Na}_2\text{CO}_3$ electrolyte 0.1/0.1 M, and pH 10.

CVs of ACT in the presence of solketal were then considered to show the characteristics of an electrocatalytic mechanism (**Figure 3.4**). Compared to the CV of ACT alone, two significant differences were observed for the CV of ACT in the presence of solketal. First, the cathodic peak disappears, indicating that ACT^+ reacts with solketal and does not persist as the oxidized form. Therefore, it is not present and able to be reduced at the electrode in the reverse scan. Second, the anodic peak current exhibits an increase in magnitude. This increase indicates that the reduced form of ACT (i.e., the hydroxylamine form, ACTH), generated upon reaction of oxoammonium with substrate, can be oxidized again at the electrode surface on the time scale of the CV scan. It should be noted that solketal does not undergo direct electron transfer within this potential range (Error! Reference source not found. **3a**, black dashed trace). Thus, the enhancement in oxidation current does not arise from direct oxidation of solketal at the electrode. If the reaction between excess solketal and ACT^+ continuously generates ACTH, the CV traces will exhibit a plateau current instead of a peak. Under these conditions, the current is controlled by the kinetics of the reaction between solketal and ACT^+ and is called the reaction-controlled current. The scan rate

shows a minimal influence on the current (**Figure 3.4a**). Instead, these reaction-controlled currents now depend on solketal concentration as demonstrated in **Figure 3.4b**.⁵²

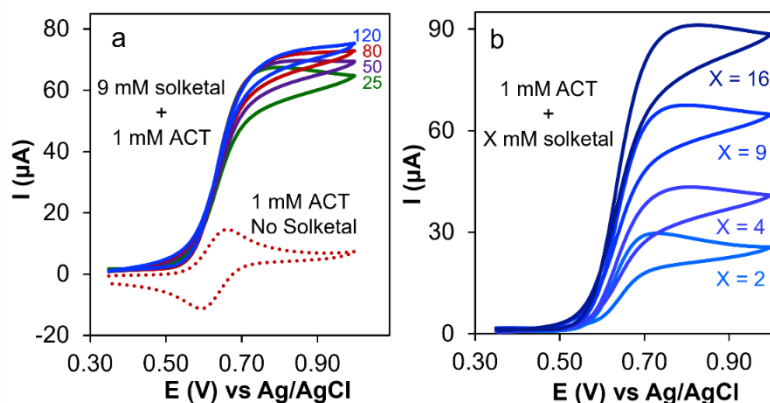


Figure 3.4. Cyclic voltammograms of 1.0 mM ACT in the absence (dotted line) and presence of 9 mM solketal at different scan rates (25–120 mV s^{-1}) (a) and cyclic voltammograms of 1.0 mM ACT in the presence of various concentrations of solketal (b). Scan rate for dotted trace is 80 mV s^{-1} , and for traces in part b, it is 25 mV s^{-1} . Solution conditions: aqueous solution with $\text{NaHCO}_3/\text{Na}_2\text{CO}_3$ electrolyte 0.1/0.1 M, and pH 10.

After collecting information about the electrochemical reaction mechanism using CV, CA analysis was performed for the quantitative analysis of the reaction kinetics. The CAs of ACT in the presence of various concentrations of solketal are shown in Error! Reference source not found.

3.5a. The total consumed charge (Q) for each CA experiment was derived by integrating the current-time trace.⁵³ For the “ACT-only” solution, the consumed charge (Q_A) is related to the number of ACT molecules in the electrode diffusion layer that are oxidized to ACT^+ . In the presence of solketal, ACT^+ reacts with solketal to generate the corresponding carbonyl product and ACTH (**Figure 3.5b**), and the latter is reoxidized at the electrode surface via a two-electron, one-proton oxidation process.⁵⁴

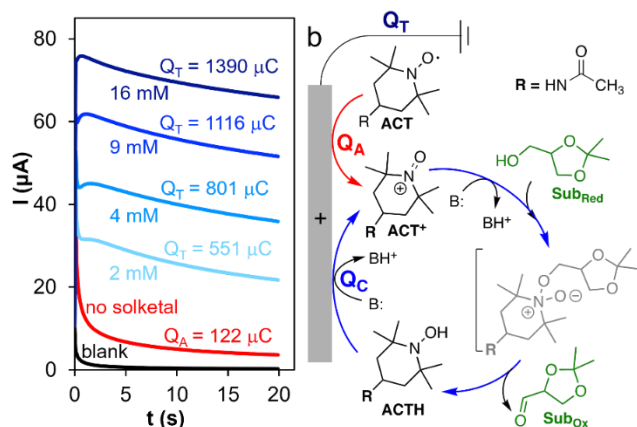


Figure 3.5. Chronoamperograms for a blank solution and ACT in the absence and presence of various concentrations of solketal (a) with applied chronoamperometry potential of 0.8 V vs Ag/AgCl. The consumed charges are shown on each chronoamperogram; the consumed charge for the blank solution is 12 μC (not depicted on its plot). Proposed mechanism for ACT-catalyzed electrochemical solketal oxidation (b).

The total consumed charge (Q_T) contains the initial charge required for ACT oxidation (Q_A) plus the charge consumed as a result of catalytic turnover of ACTH at the electrode surface, Q_C , such that $Q_T = Q_C + Q_A$. The ratio of Q_C to Q_A is proportional to the turnover numbers (TONs) of ACT under these conditions. To precisely determine TOFs, the consumed charged for a blank solution (Q_B) needs to be subtracted from Q_A to account for nonfaradaic charging of the electrode.⁵⁵ Considering the number of electrons corresponding to one turnover ($n = 2$) and the conversion factor of the time unit for turnover frequency (1 h or 3600 s) over the CA experiment time (t), the TOF can be calculated as shown in eq 3:

$$\text{TOF} = \frac{(Q_T - Q_A) \times 3600}{(Q_A - Q_B) \times n \times t} \quad (3)$$

The unit of the resulting TOF value is per hour (h^{-1}). The TOFs derived from the CA experiments in **Figure 3.5a** are shown in **Table 3.1**. The voltammetric and chronoamperometric studies of the reaction under neutral conditions were performed to demonstrate the effect of base on the reaction kinetics. As demonstrated in entry 5 of **Table 3.1**, the catalytic activity of ACT in the absence of

base is negligible.⁵⁶ The presence of base favors formation of the alkoxide adduct between ACT⁺ and solketal and favors the electrochemical oxidation of ACTH.^{30,37}

Table 3.1. TOF (h⁻¹) of ACT for different concentrations of solketal in the absence and presence of base.

Entry	Solketal concentration	TOF (h ⁻¹) ^c
1	2 mM ^a	346
2	4 mM ^a	548
3	9 mM ^a	802
4	16 mM ^a	1024
5	4 mM ^b	36

^a Reaction Conditions: aqueous solution with NaHCO₃/Na₂CO₃ electrolyte 0.1/0.1 M, pH 10, 1.0 mM ACT, applied potential 0.8 V, experiment duration 20 sec.

^b Reaction Conditions: aqueous solution with NaCl electrolyte 0.2 M, pH 6.7, 1.0 mM ACT.

^c "Turnover Frequency", defined as the molecules of solketal converted per molecule of catalyst per hour. The standard deviation of reported TOFs (h⁻¹) for four groups of students were (8-14%).

The CA and CV experiments demonstrated here form the basis for several inquiry laboratories or an undergraduate research project. For example, CV analysis of ACT under a range of basic buffers pH 8–11 visually demonstrates the basicity–reactivity relationship. CA analysis of the reaction between ACT and diverse substrates, such as secondary benzylic alcohols and primary and secondary aliphatic alcohols, is a simple and quantitative way to explore substrate structure-reactivity relationships. Experimenting with electronically/ structurally distinct aminoxyl catalysts, such as commercially available TEMPO or 9-azabicyclo-[3.3.1]nonane N-oxyl (ABNO), allows a research student to begin making connections between catalyst structure and activity.³⁰

3.6. Conclusion

This lab allows students to explore the concepts of chronoamperometry, cyclic voltammetry, and electrocatalysis. The operationally simple experiments give students experience in voltammetric and chronoamperometric analysis of both direct and mediated (catalytic) electron transfer reactions. The emphasis on chronoamperometry provides students with an example of how

a simple electrochemical technique can be used for quantitative analysis of a catalytic reaction and for the derivation of the turnover frequency (TOF). The pedagogically rich protocol reported herein is an example of an interdisciplinary experiment that is well-suited for incorporation into various upper-level undergraduate laboratory courses, including instrumental analysis, physical chemistry, organic chemistry, and electrochemistry.

3.7. Acknowledgements

We are grateful to the attendees and teaching assistants of our first Organic Electrochemistry Short Course, held during Aug 2019 at the University of Wisconsin–Madison, and to the students and teaching assistant of the Chem 437WI (Physical Chemistry Laboratory) laboratory course at University of Missouri–Kansas City (UMKC) for sharing their observations and feedback on this experiment. The authors would like to thank the NIH (R35 GM134929; S.S.S.) for financial support to develop this laboratory experiment at the University of Wisconsin–Madison, the NSF for a predoctoral fellowship to J.E.N. (DGE-1747503), and the Chemistry Department of the UMKC for its support in purchasing equipment and chemicals to run this experiment in the Chem 437WI class. We also thank Pine Research for providing equipment for the Rafiee–Stahl Organic Electrochemistry Short Course lab section (at University of Wisconsin–Madison) and Timothy Paschkewitz and Alex Peroff (Pine Research Instrument) for demonstrating the Aftermath software’s functions that facilitate post-analysis of voltammetric and amperometric results.

3.8. References

1. Yan, M.; Kawamata, Y.; Baran, P. S. *Chem. Rev.* **2017**, *117*, 13230–13319.
2. Remick, A. E. *J. Chem. Educ.* **1956**, *33*, 564–574.
3. Ibanez, J. G.; Singh, M. M.; Pike, R. M.; Szafran, Z. *J. Chem. Educ.* **1997**, *74*, 1149–1450.

4. Manchanayakage, R. Designing and Incorporating Green Chemistry Courses at a Liberal Arts College to Increase Students' Awareness and Interdisciplinary Collaborative Work. *J. Chem. Educ.* **2013**, *90*, 1167–1171.
5. An editorial note for an open access virtual issue focused on electrochemical concepts and their spread into different areas of research and development: Gollas, B. *ChemistryOpen* **2017**, *6*, 299–300.
6. Rubner, I.; Berry, A. J.; Grofe, T.; Oetken, M. *J. Chem. Educ.* **2019**, *96*, 248–255.
7. Sandford, C.; Edwards, M. A.; Klunder, K. J.; Hickey, D. P.; Li, M.; Barman, K.; Sigman, M. S.; White, H. S. and Minter S. D. *Chem. Sci.* **2019**, *10*, 6404–6422.
8. Lam, C. H.; Jackson, J. E. *J. Chem. Educ.* **2020**, *97*, 172–177.
9. For leading reference see: Nicholson, R. S.; Shain, I. *Anal. Chem.* **1964**, *36*, 706–723.
10. Bard, A. J. *J. Chem. Educ.* **2007**, *84*, 644–650.
11. Khalafi, L.; Rafiee, M. Cyclic Voltammetry. In *Encyclopedia of Physical Organic Chemistry*; Wang, Z., Ed.; Wiley: Hoboken, NJ, 2017; Vol. 5, pp 3437–3478.
12. Elgrishi, N.; Rountree, K. J.; McCarthy, B. D.; Rountree, E. S.; Eisenhart, T. T.; Dempsey, J. L. *J. Chem. Educ.* **2018**, *95*, 197–206.
13. To see the example of voltammetric working curves for deriving the quantitative information see ref 9 and the following ref: Andrieux, C. P.; Blocman, C.; Dumas-Bouchiat, J. M.; M'Halla, F.; Savéant, J. M. *J. Electroanal. Chem. Interf. Electrochem.* **1980**, *11*, 19–40.
14. Messersmith, S. J. *J. Chem. Educ.* **2014**, *91*, 1498–1500.
15. Bard, A. J.; Faulkner, L. R. *Electrochemical Methods. Fundamentals and Applications*; John Wiley & Sons, Inc.: New York, 2001.
16. Savéant, J. M.; Vianello, E. *Electrochim. Acta* **1965**, *10*, 905–920.
17. Chronoamperometry is typically only discussed in basic electroanalytical chemistry literature and is less well known by students/scientists from other disciplines. For example, there is only one paper published in *J. Chem. Educ.* on this subject, and it focuses on its mathematical foundations, rather than application to understanding chemical reactions: Ryswyk, H. V. Simulation of Single-Step Chronoamperometry via Spreadsheet. *J. Chem. Educ.* **1991**, *68*, A283–A285.
18. This is the description of a normal or single-step CA experiment, but application of more than one potential step in a CA experiment is also possible. Depending on the number of steps, these experiments are called double step or multi-step CA.
19. The region of interest at which the potential is held is typically one where the electrochemical reaction is complete and the concentration of one of the electroactive species is nearly zero at the electrode surface. For example, the applied potential (E_{app}) should be 120 mV more positive (ΔE) than the redox potential (E°) for the oxidation reaction of interest, and 120 mV

more negative than the redox potential for reduction reactions, to meet the requirement of simplified boundary conditions.

20. Stephens, L. I.; Mauzeroll, J. *J. Chem. Educ.* **2019**, *96*, 2217–2224.
21. See **Section B.6** and **Figure B.3**. Chronoamperogram (a) and the plot of current as a function of $t^{1/2}$ (b) for 1.0 mM ACT in aqueous solution with $\text{NaHCO}_3/\text{Na}_2\text{CO}_3$ (0.1/0.1 M, pH 10). Applied potential for chronoamperometry is 0.8 V vs Ag/AgCl. of the Supporting Information.
22. Sheldon, R. A.; Arends, I. W. C. E. *Adv. Synth. Catal.* **2004**, *346*, 1051–1071.
23. Vogler, T.; Studer, A. *Synthesis* **2008**, *2008*, 1979–1993.
24. Hill, N. J.; Hoover, J. M.; Stahl, S. S. *J. Chem. Educ.* **2013**, *90*, 102–105.
25. Straub T. S. *J. Chem. Educ.* **1991**, *68*, 1048–1049.
26. Bobbitt, J. M.; Brückner, C.; Merbouh, N. In *Organic Reactions*; Wiley: Hoboken, NJ, 2009; pp 103–424.
27. For leading reference see: Semmelhack, M. F.; Chou, C. S.; Cortes, D. A. *J. Am. Chem. Soc.* **1983**, *105*, 4492–4494.
28. For review see: Nutting, J. E.; Rafiee, M.; Stahl, S. S. *Chem. Rev.* **2018**, *118*, 4834–4885.
29. Rafiee, M.; Konz, Z. M.; Graaf, M. D.; Koolman, H. F.; Stahl, S. S. *ACS Catal.* **2018**, *8*, 6738–6744.
30. Rafiee, M.; Miles, K. C.; Stahl, S. S. *J. Am. Chem. Soc.* **2015**, *137*, 14751–14757.
31. Hickey, D. P.; Schiedler, D. A.; Matanovic, I.; Doan, P. V.; Atanassov, P.; Minter, S. D.; Sigman, M. S. *J. Am. Chem. Soc.* **2015**, *137*, 16179–16186.
32. Siu, J. C.; Sauer, G. S.; Saha, A.; Macey, R. L.; Fu, N.; Chauvire, T.; Lancaster, K. M.; Lin, S. *J. Am. Chem. Soc.* **2018**, *140*, 12511–12520.
33. Rafiee, M.; Alherech, M.; Karlen, S. D.; Stahl, S. S. *J. Am. Chem. Soc.* **2019**, *141*, 15266–15276.
34. Toma, H. E.; Araki, K.; Dovidauskas, S. A. *J. Chem. Educ.* **2000**, *77*, 1351–1353.
35. <http://128.104.71.100/content/organic-electrochemistry-short-course>, accessed Jun 30, 2020.
36. Solketal has a chiral center. Our recent study shows that ACT-catalyzed electrochemical oxidation of *S*-solketal to the corresponding carboxylic acid retains the enantiomeric excess of the starting alcohol. Solketal also contains a heterocycle that makes it a challenging substrate for metal catalyzed alcohol oxidation. This aminoxyl-mediated electrochemical method produces the carboxylic acid efficiently. These features make solketal an appealing substrate for students and scientists oriented in organic chemistry. However, a variety of other primary and secondary alcohols can be used as the substrate. For water-insoluble substrates, the mixture of acetonitrile and carbonate buffer results in sufficient solubility for

the substrate. For other possible substrates and the reactions conditions, see the substrate scopes in refs 27, 29, and 37.

37. Rafiee, M.; Karimi, B.; Alizadeh, S. *ChemElectroChem* **2014**, *1*, 455–462.
38. In this paper we use IUPAC convention for representation of cyclic voltammograms. Some of the potentiostats use a different notation called Texas or classical notation. See refs 11 and 12 which describe both conventions.
39. The definition of Turnover Frequency (TOF) is “the number of reactant molecules converted per a time unit (hour, minute or second) per catalyst molecule (for given reaction conditions)”. For more details about the definition of TOF and its related topics please see: Kozuch, S.; Martin J. M. L. *ACS Catal.* **2012**, *2*, 2787–2794.
40. Pine Potentiostat is an example of standard equipment for electrochemical studies. For the Physical Chemistry course at UMKC we purchased only one potentiostat and one group of students worked with the potentiostat each week/section. However, if the cost of the potentiostat represents a barrier, a homemade potentiostat provides a cost-effective option. Examples of the latter are included in refs 41-43. Moreover, lower cost potentiostats are available for educational purposes. One example of an open-source potentiostat is Rodeostat: <https://iorodeo.com/collections/cheapstat-open-source-potentiostat>, accessed September 4, 2020.
41. Meloni, G. N. *J. Chem. Educ.* **2016**, *93*, 1320–1322.
42. Li, Y. C.; Melenbrink, E. L.; Cordonier, G. J.; Boggs, C.; Khan, A.; Isaac, M. K.; Nkhonjera, L. K.; Bahati, D.; Billinge, S. J.; Haile, S. M.; Kreuter, R. A.; Crable, R. M.; Mallouk, T. E. *J. Chem. Educ.* **2018**, *95*, 1658–1661.
43. Glasscott, M. W.; Verber, M. D.; Hall, J. R.; Pendergast, A. D.; McKinney, C. J.; Dick, J. E. *J. Chem. Educ.* **2020**, *97*, 265–270.
44. The three required electrodes are also commercially available from different vendors. The more cost-effective options for educational purpose are homemade electrodes. For examples, see refs 45-47.
45. King, D.; Friend, J.; Kariuki, J. *J. Chem. Educ.* **2010**, *87*, 507–509.
46. Masse R. C.; Gerken J. B. *J. Chem. Educ.* **2015**, *92*, 110–115.
47. Schmidt, B.; King, D.; Kariuki, J. *J. Chem. Educ.* **2018**, *95*, 2076–2080.
48. For details of polishing and other experimental conditions, see the Supporting Information. Based on the observed results, polishing the electrode once is enough to perform all the CV and CA experiments for each solution. Discarding the data for the first experiment conducted after polishing and repeating it without polishing results in more reproducible responses.
49. The voltammetric currents normalized by square root of the scan rate should be identical to a reversible electron transfer at various scan rates. The students were asked to normalize the CV currents and compare them: see Student’s Handout in Supporting Information.

50. The plot of peak current (I_P) as a function of the square root of scan rate should be linear. The slope of the line is proportional to the diffusion coefficient of electroactive species. See Supporting Information, **Section B.6**, and **Figure B.4**. The plot of anodic and cathodic peak currents versus square root of scan rate. Solution conditions: aqueous solution with $\text{NaHCO}_3/\text{Na}_2\text{CO}_3$ electrolyte 0.1/0.1 M, and pH 10.
- ⁵¹51. When the current is diffusion-controlled it should be inversely proportional to $t^{1/2}$. An example of a linear correlation was plotted by students and is shown in **Figure B.2** and **Figure B.3** (Supporting Information). The diffusion coefficient derived from amperometric results, based on the Cottrell equation, is in good agreement with the value derived from voltammetric analysis, See Supporting Information, **Section B.6** and **Figure B.3**.
52. Based on the proposed mechanism, the height of the anodic peak is proportional to the concentration of solketal and the number of catalytic cycles. The slope of the linear plot for the anodic plateau current versus the square root of the solketal concentration is proportional to the rate constant of the chemical reaction between ACT^+ and solketal. See ref 37 and **Figure B.5** and **Figure B.6** (Supporting Information).
53. All the chronoamperometric measurements must be taken in exactly the same timeframe to enable subtraction and division of the consumed charge for different chronoamperograms. To derive the consumed charge for each plot, see **Section B.8** of Supporting Information and the Supporting Information Excel file. The optimal time for a chronoamperometry experiment is 15-20 sec. See ref 15.
54. Taitt, B. J.; Bender, M. T.; Choi, K.-S. *ACS Catal.* **2020**, *10*, 265–275.
55. Since solketal is not electroactive at this potential range (e.g. **Figure 3.3a**), the blank experiment can be a solution consisting only of supporting electrolyte/buffer or may include solketal.
56. Examples of more results by students are presented in **Table B.2** and **Table B.3** of the Supporting Information.

Chapter 4: Electrochemical Aminoxy-Mediated α -Cyanation of Secondary Piperidines for Pharmaceutical Building Block Diversification

This work is published: Lennox, A. J. J.; Goes, S. L.; Webster, M. P.; Koolman, H. F.; Djuric, S. W., Stahl, S. S. *J. Am. Chem. Soc.* **2018**, *140*, 11227-11231.

4.1. Abstract

Secondary piperidines are ideal pharmaceutical building blocks owing to the prevalence of piperidines in commercial drugs. Here, we report an electrochemical method for cyanation of the heterocycle adjacent to nitrogen without requiring protection or substitution of the N–H bond. The reaction utilizes ABNO (9-azabicyclononane N-oxyl) as a catalytic mediator. Electrochemical oxidation of ABNO generates the corresponding oxoammonium species, which promotes dehydrogenation of the 2° piperidine to the cyclic imine, followed by addition of cyanide. The low-potential, mediated electrolysis process is compatible with a wide range of heterocyclic and oxidatively sensitive substituents on the piperidine ring and enables synthesis of unnatural amino acids.

4.2. Introduction

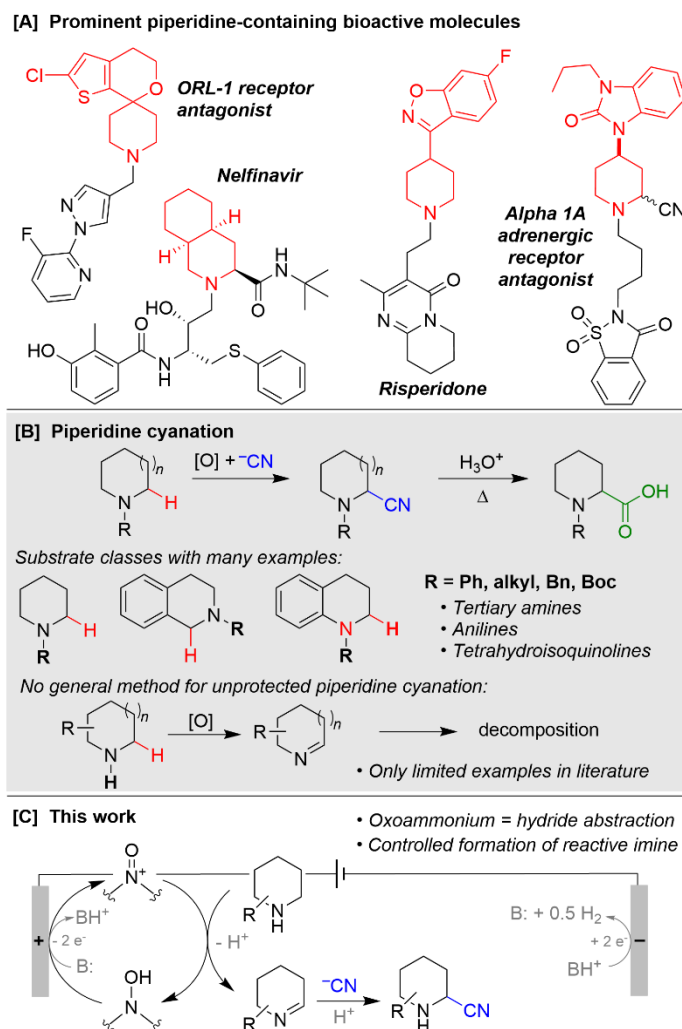
Strategic building blocks are commonly used in drug discovery to create or modify bioactive core structures, and efficient methods for diversification of commercially available building blocks could have broad impact in medicinal chemistry.¹ Piperidines are the most common heterocycle found in FDA-approved drugs² owing to their favorable pharmacokinetic properties that contribute to improved clinical success (**Scheme 4.1A**).³ Secondary piperidines represent ideal targets for chemical modification, and effective methods could greatly expand this pool of available building blocks. Whereas C–H functionalization adjacent to nitrogen in cyclic amines has been the focus of considerable attention,⁴ the vast majority of precedents use N-protected (i.e., N-acyl) or N-aryl/alkyl 3° amine derivatives that are less versatile as pharmaceutical building blocks.^{5,6} Amine protection/deprotection hampers efficient utilization of the former substrates, whereas fixed substitution of the N-aryl/alkyl derivatives limits incorporation of these compounds into more complex structures. Here, we report an electrochemical method for oxidative α -cyanation of diverse 2° piperidines. The method is enabled

by the use of ABNO (9-azabicyclononane N-oxyl) as a catalytic mediator that exhibits broad functional group compatibility.

Nitriles are versatile functional groups that are readily converted into other substituents, including carboxylic acids, amides, ketones and amines, among others.⁷ This versatility underlies the extensive efforts directed toward α -cyanation of piperidine and other amine derivatives (**Scheme 4.1B**).⁸ Synthetically useful precedents, however, are limited to activated substrates (e.g., tetrahydroisoquinolines) and the 3° amine/ amide derivatives noted above. No general methods are available for analogous cyanation of 2° piperidines,⁹ reflecting the susceptibility of cyclic imines to undergo decomposition.^{10,11}

Precedents for electrochemical oxidation of amines typically feature 3° derivatives¹² and/or are initiated by outer sphere single-electron transfer (ET). Subsequent rapid proton and electron transfer (PT–ET) affords an iminium ion.¹³ We recently showed that use of an aminoxyl mediator bypasses this conventional ET–PT–ET sequence by undergoing electrochemical oxidation to an oxoammonium species that promotes direct hydride transfer from the substrate.^{14,15} The aminoxyl-mediated reactions operate at much lower electrode potentials (by >1 V), thereby greatly expanding the functional group compatibility and substrate scope. Here, we demonstrate that analogous principles may be applied to enable efficient α -cyanation of 2° piperidines bearing diverse pharmaceutically relevant substituents (**Scheme 4.1C**).

Scheme 4.1. Context and Strategy for α -Cyanation of 2° Piperidines.



4.3. Results and Discussion

We initiated our studies by investigating the redox behavior of 4-phenylpiperidine **1a** by cyclic voltammetry (CV) in the absence and presence of ABNO (**Figure 4.1**).¹⁶ Substrate **1a** exhibits an irreversible anodic CV feature at 739 mV (**Figure 4.1**, green trace; all potentials are reported relative to Fc/Fc⁺), whereas ABNO, which was selected as a low-potential sterically unhindered aminoxyl mediator,¹⁷ exhibits a reversible CV trace with $E_{1/2} = 195$ mV (**Figure 4.1**, gray trace). CV analysis of a solution containing both **1a** and ABNO reveals a significant increase in the anodic feature at the ABNO redox potential, with a corresponding decrease in the cathodic feature (**Figure 4.1**, red trace). This behavior implicates reaction of ABNO⁺ with the substrate and

electrochemical regeneration of ABNO^+ on the CV time scale (cf. **Scheme 4.1C**). Complete disappearance of the anodic feature corresponding to **1a** under these conditions is consistent with consumption of the substrate from the electrode surface via reaction with ABNO^+ . The large difference between the anodic peak potentials of ABNO and **1a** ($\Delta E_p > 500$ mV; cf. green vs red trace) highlights the lower electrode potential that arises when substrate oxidation proceeds via ABNO-mediated hydride transfer, rather than electrode-initiated electron transfer.¹⁸

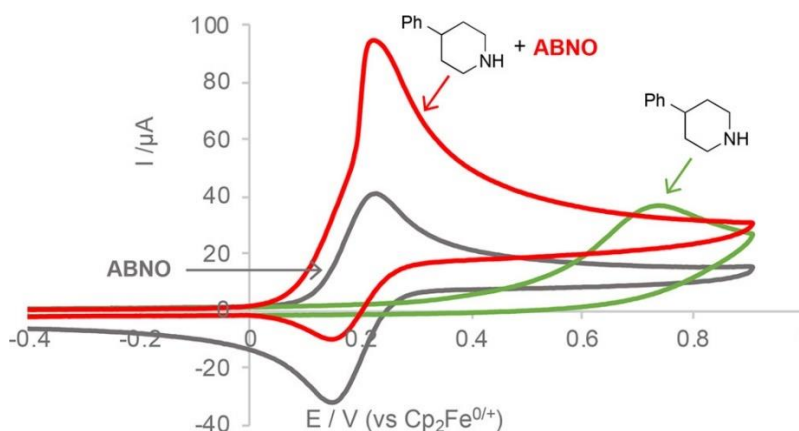
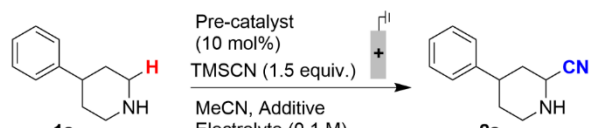


Figure 4.1. CVs (0.1 V/s) in MeCN (5 mL) and NaClO_4 (0.1 M) of: ABNO (1 mM) (gray trace); 4-phenyl piperidine (2 mM) (green trace); ABNO (1 mM) and 4-phenyl piperidine (2 mM) (red trace).

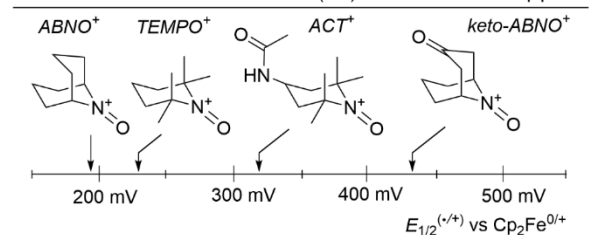
Efforts then shifted to bulk electrolysis studies in order to explore optimal conditions for substrate cyanation. The reactions were conducted under constant-current conditions (1–3 mA) in an undivided cell with a graphite rod working electrode and Pt wire counter electrode. TMSCN was used as an easily handled source of cyanide nucleophile. Initial attempts to perform direct oxidation of the substrate at the electrode (i.e., in the absence of a mediator) resulted in only low yield of the desired product **2a** (19%, **Table 4.1**, entry 1). Inclusion of 10 mol % ABNO in the reaction, under otherwise identical conditions, nearly doubled the yield of **2a** (37%, entry 2). One equivalent of hexafluoroisopropanol (HFIP) was included in the reaction as a proton source to facilitate production of H_2 at the cathode (cf. BH^+ in **Scheme 4.1C**), which also generates an

alkoxide base that can promote proton-coupled oxidation of ABNO-H to ABNO⁺ at the anode (cf. **Scheme 4.1C**).¹⁹ Consistent with this hypothesis, the yield improved considerably upon adding HFIP, 1 equiv; 54% yield, entry 3) as an additive (see below for further discussion).

Table 4.1. Bulk electrolysis optimization data.



Entry	Pre-catalyst	Additive (equiv.)	Current (mA)	Yield/% ^a
1	—	—	1	19
2	ABNO	—	1	37
3	ABNO	HFIP ^b (1)	1	54
4	TEMPO	HFIP (1)	1	10
5	ACT	HFIP (1)	1	24
6	KetoABNO	HFIP (1)	1	81
7	ABNO	HFIP (1)	3	66
8	ABNO	H ₂ O (1)	3	68
9	ABNO	MeOH (1)	3	79
10	ABNO	MeOH (0.5)	3	84
11	ABNO	MeOH (0.5)	3	74 ^c
12	ABNO	MeOH (0.5)	2	74 ^d



ABNO⁺ TEMPO⁺ ACT⁺ keto-ABNO⁺

200 mV 300 mV 400 mV 500 mV

$E_{1/2}^{(+/+)} \text{ vs } \text{Cp}_2\text{Fe}^{0/+}$

Testing of other aminoxyl mediators clearly indicated the importance of steric effects as the primary indicator of mediator effectiveness.²⁰ Specifically, TEMPO and 4-acetamidoTEMPO (ACT) have higher redox potentials than ABNO, but they afforded lower yields of **2a** (entries 4 and 5). KetoABNO exhibited the highest yield, but, as its higher redox potential could interfere with functional-group compatibility, we explored further optimization of the reaction with ABNO as the mediator. Increasing the electrolysis current from 1 to 3 mA led to an increase in yield from 54% to 66% (entries 3 and 7). Further improvement was achieved by replacing HFIP with MeOH as the protic additive and reducing the stoichiometry to 0.5 equiv, ultimately affording 84% yield of **2a** (entries 7–10). To ensure reproducibility, the optimized reaction conditions were directly

implemented in two commercially available bulk electrolysis cells, one from BASi and the ElectroSyn 2.0 unit from IKA, with the former conducted on 1 g scale (entries 11 and 12). Both reactions afforded **2a** in good yield.

Analysis of the constant current electrolysis traces provides valuable insights into the ABNO-mediated reactions (**Figure 4.2**). Under the optimized reaction conditions (red trace), the electrode potential needed to sustain 3 mA current is low (approximately 150–250 mV) and is stable throughout the entire reaction. In the absence of MeOH (blue trace), a low potential is observed only when the charge passed is less than that needed for electrochemical oxidation of ABNO to ABNO⁺. The increase in potential beyond this point (to approximately 600–700 mV) is attributed to the lack of an effective Brønsted base (i.e., no methoxide is available) to support proton-coupled oxidation of ABNOH to ABNO⁺. In the absence of both MeOH and ABNO (green trace), a much higher electrode potential is needed to support the 3 mA current. The initial observed potential is similar to that expected from the CV studies (cf. **Figure 4.1**); however, this potential rises significantly during the reaction, possibly arising from fouling of the electrode by reactive intermediates generated in the direct electrolysis process.²¹ The reaction yield correlates inversely with the potential needed to sustain the reaction, demonstrating the benefit of pairing a mediator with an appropriate proton shuttle in the undivided cell.

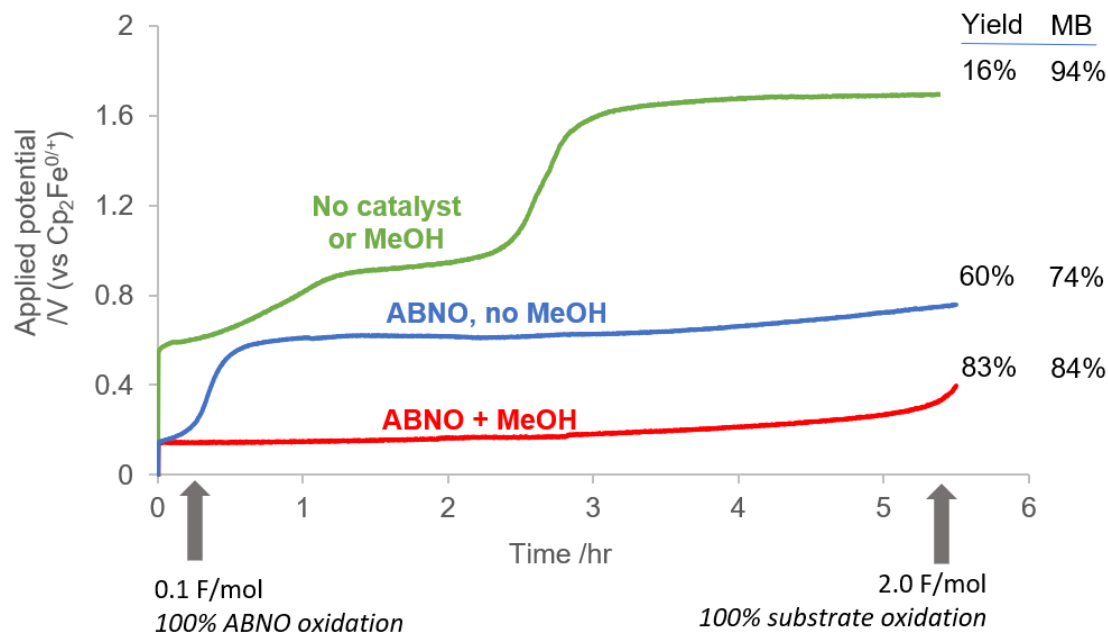


Figure 4.2. Bulk electrolysis in MeCN, TBAPF₆ (0.1 M), TMSCN (1.5 equiv), and **1a** (0.3 mmol) with/without ABNO (10 mol %) and/or MeOH (0.5 equiv).¹⁶ MB = mass balance.

The optimized conditions were then tested on a broad collection of commercially available 2° piperidines (**Table 4.2A**). 4-Substituted piperidines are especially readily available, and good-to-excellent yields of the corresponding α -cyanopiperidines were obtained for substrates bearing a diverse array of functional groups, including aryl, aryl halide, aryl ether, amide, ester, pyridine and related heteroaryl derivatives, and azoles, among other groups (**3a–3r**). The method even tolerates an unprotected 2° alcohol (**3x**), indicating that amine oxidation is favored over the well-established aminoxyl-mediated alcohol oxidation.¹⁵ The products were primarily isolated as the *p*-toluenesulfonic acid salts. Analytically pure electrolyte salt (TBAPF₆) was also recovered from the reaction mixture and reused. High diastereoselectivity, often reflecting only a single diastereomer, is observed in all cases where the substituent is large enough to bias the ring conformation (**3a–3p**, **3s**). The favored anti relationship between the cyano group and substituent was confirmed by NOE measurements and X-ray crystallography. The observed stereochemistry is rationalized by axial attack of cyanide on the intermediate imine and aligns with stereochemical

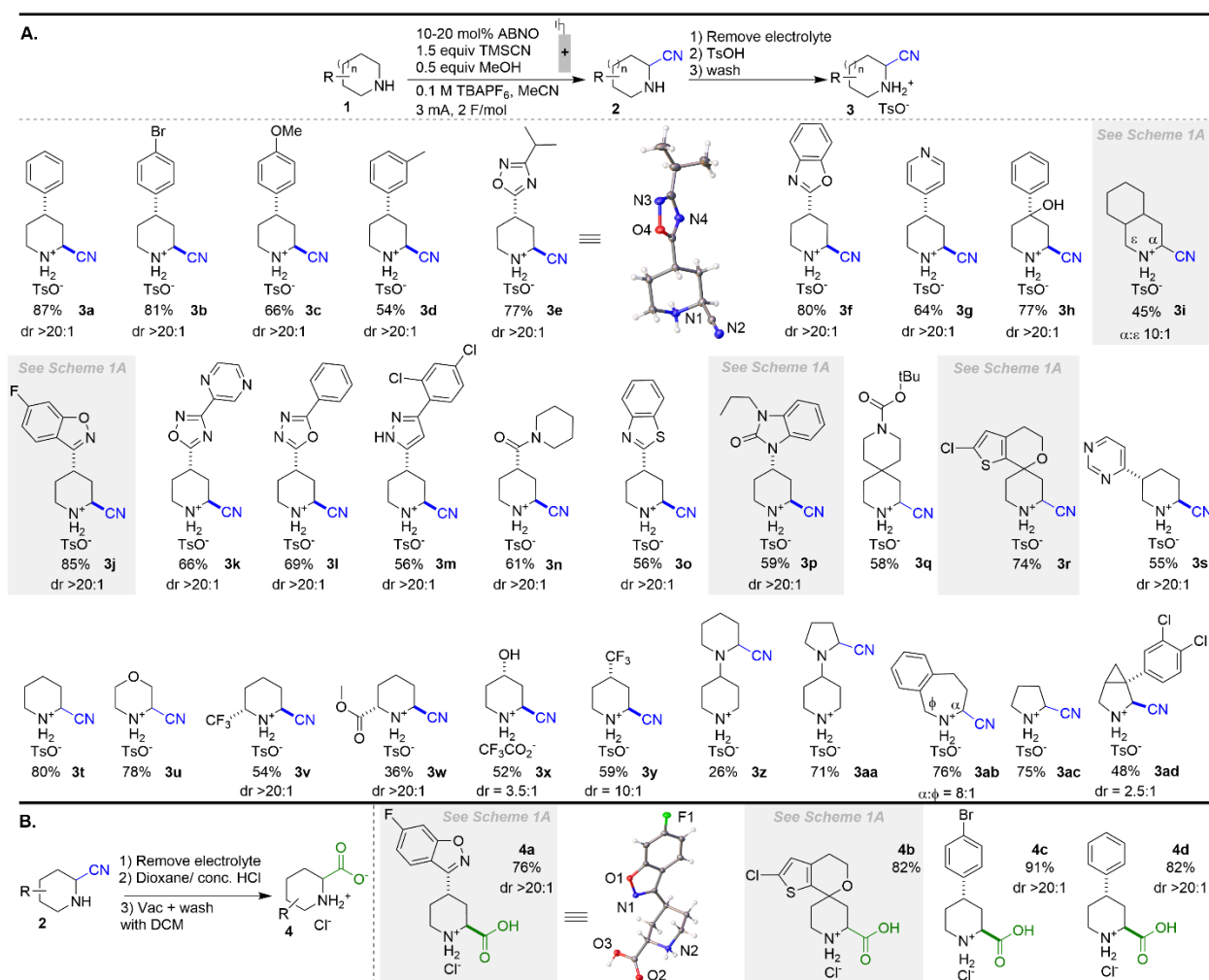
models that have been reported by Houk²² and Cieplak.²³ A mixture is observed in two cases when the substituent is smaller (**3x**, **3y**) and in a bicyclic pyrrolidine substrate (**3ad**). The latter result demonstrates that the method is applicable to heterocycles beyond piperidines, as further exemplified by the reaction of the parent pyrrolidine, (**3ac**), an azepane (**3ab**), and morpholine (**3u**). Piperidine substitution in the 2- and 3- positions leads to highly regioselective cyanation at the less hindered position, suggesting that steric accessibility overrides thermodynamic considerations (**3s**, **3v**, **3w**). This observation is also evident from the selectivity observed with the azepane derivative **3ab**, where the benzylic position is avoided in favor of the more accessible site.

For a substrate containing both an unprotected and a Boc-protected 2° piperidine, cyanation only occurred on the unprotected piperidine ring (**3q**). On the other hand, 2° piperidine substrates bearing 5- or 6-membered cyclic 3° alkylamine substituents undergo preferential cyanation on the alkylamine ring (**3z**, **3aa**), presumably reflecting the enhanced hydricity of the C–H bonds at this site.¹⁶ Ineffective substrates primarily corresponded to substrates that were not soluble in the reaction medium.¹⁶

The relevance of this method for medicinal chemistry is evident from a number of substrates that feature functional groups directly corresponding to active pharmaceuticals and drug candidates in **Scheme 1A**. Examples include risperidone (**3j**),²⁴ two receptor antagonists (**3p** and **3r**)^{25,26} and the HIV drug, Nelfinavir (**3i**).²⁷ Each of the corresponding α -cyanation products was isolated in diastereomeric purity. The low potential and mild conditions that make this method applicable to building block diversification also make it amenable to late-stage functionalization, as revealed by the cyanation of the antidepressant Amitifadine (**3ad**), which proceeded in 48% yield.

The hydrolysis of the nitriles to carboxylic acids provides an efficient means to generate non-natural amino acids. To demonstrate this concept, several cyanation products were subjected directly to hydrolysis conditions, without isolation, to generate the corresponding carboxylic acid derivatives in excellent yields (**4a–d**, **Table 4.2B**).²⁸

Table 4.2. Substrate Scope for Electrochemical α -Cyanation of 2° Piperidines (A) and Cyanation/Hydrolysis to Generate Pipecolic Acids (B)^a.



4.4. Conclusion

In summary, we have developed a highly effective, user-friendly method for electrochemical α -cyanation of 2° piperidines. This class of molecules represents an especially important class of pharmaceutical building blocks. Use of ABNO as a hydride-transfer mediator

allows the reactions to proceed at low electrode potentials, thereby tolerating a broad array of important functional groups. C–H functionalization methods and related reactions of this type that enable direct building block diversification should have considerable utility in medicinal chemistry and drug discovery.

4.5. Acknowledgements

We thank Ilia Guzei and Manar Alherech (UW) for assistance with X-ray crystallography and NMR spectroscopy, respectively, Fei Wang (UW) for preliminary investigations, Damian Hruszkewycz (UW) for synthesis of 1r, and Matthew Graaf (AbbVie) for helpful discussions. We thank IKA for their donation of an ElectraSyn 2.0 apparatus. Financial support for this project was provided by the NIH (R01 GM100143) and AbbVie. Spectroscopic instrumentation was supported by a gift from Paul. J. Bender, NSF (CHE-1048642), and NIH (1S10 OD020022-1).

4.6. Reference

1. (a) Krotko, D.; Chuprina, A.; Shivanyuk, A.; Tolmachev, A. *Chim. Oggi Chem. Today* **2010**, *28*, 16–17. (b) Goldberg, F. W.; Kettle, J. G.; Kogej, T.; Perry, M. W. D.; Tomkinson, N. P. *Drug Discovery Today* **2015**, *20*, 11–17. (c) Blakemore, D. C.; Castro, L.; Churcher, I.; Rees, D. C.; Thomas, A. W.; Wilson, D. M.; Wood, A. *Nat. Chem.* **2018**, *10*, 383–394.
2. Vitaku, E.; Smith, D. T.; Njardarson, J. T. *J. Med. Chem.* **2014**, *57*, 10257–10274.
3. (a) Lovering, F.; Bikker, J.; Humblet, C. *J. Med. Chem.* **2009**, *52*, 6752–6756. (b) Ritchie, T. J.; Macdonald, S. J. F.; Young, R. J.; Pickett, S. D. *Drug Discovery Today* **2011**, *16*, 164–171. (c) Ritchie, T. J.; Macdonald, S. J. F.; Peace, S.; Pickett, S. D.; Luscombe, C. N. *MedChemComm* **2012**, *3*, 1062–1069.
4. Mitchell, E. A.; Peschiulli, A.; Lefevre, N.; Meerpoel, L.; Maes, B. U. W. *Chem. - Eur. J.* **2012**, *18*, 10092–10142.
5. For an important exception, see: Chen, W.; Ma, L.; Paul, A.; Seidel, D. *Nat. Chem.* **2018**, *10*, 165–169.
6. The utility of cyclic secondary amines as building blocks is illustrated in the “SnAP” chemistry developed by Bode and co-workers: Luescher, M. U.; Geoghegan, K.; Nichols, P. L.; Bode, J. W. *Aldrichimica Acta* **2015**, *48*, 43–48.
7. (a) Henry, R. A. *J. Org. Chem.* **1959**, *24*, 1363–1364. (b) Portevin, B.; Benoist, A.; Rémond, G.; Hervé, Y.; Vincent, M.; Lepagnol, J.; De Nanteuil, G. *J. Med. Chem.* **1996**, *39*, 2379–2391. (c) Branch, C. L.; Johnson, C. N.; Stemp, G.; Thewlis, K. U.S. Patent 6,677,354,

- Jan. 13, 2004. (d) Ma, Y.-N.; Yang, X.-J.; Pan, L.; Hou, Z.; Geng, H.-L.; Song, X.-P.; Zhou, L.; Miao, F. *Chem. Pharm. Bull.* **2013**, *61*, 204–211. (e) Cioffi, C. L.; Liu, S.; Wolf, M. A.; Guzzo, P. R.; Sadalapure, K.; Parthasarathy, V.; Loong, D. T. J.; Maeng, J.-H.; Carulli, E.; Fang, X.; Karunakaran, K.; Matta, L.; Choo, S.-H.; Panduga, S.; Buckle, R. N.; Davis, R. N.; Sakwa, S. A.; Gupta, P.; Sargent, B. J.; Moore, N. A.; Luche, M. M.; Carr, G. J.; Khmelnsky, Y. L.; Ismail, J.; Chung, M.; Bai, M.; Leong, W. Y.; Sachdev, N.; Swaminathan, S.; Mhyre, A. J. *J. Med. Chem.* **2016**, *59*, 8473–8494. (f) Blaskovich, M. A. *T. J. Med. Chem.* **2016**, *59*, 10807–10836. (g) Fuentes de Arriba, Á. L.; Lenci, E.; Sonawane, M.; Formery, O.; Dixon, D. J. *Angew. Chem., Int. Ed.* **2017**, *56*, 3655–3659. (h) Jaegli, S.; Schmidt, T.; Oftring, A.; Panchenko, A.; Dahmen, K.; Molt, O. U.S. Patent 9,695,121, Jul. 4, 2017.
8. For leading references, see: (a) Chiba, T.; Takata, Y. *J. Org. Chem.* **1977**, *42*, 2973–2977. (b) Le Gall, E.; Hurvois, J.-P.; Renaud, T.; Moinet, C.; Tallec, A.; Uriac, P.; Sinbandhit, S.; Toupet, L. *Liebigs Ann.* **1997**, *1997*, 2089–2101. (c) Tajima, T.; Nakajima, A. *J. Am. Chem. Soc.* **2008**, *130*, 10496–10497. (d) Han, W.; Ofial, A. R. *Chem. Commun.* **2009**, 5024–5026. (e) Libendi, S. S.; Demizu, Y.; Onomura, O. *Org. Biomol. Chem.* **2009**, *7*, 351–356. (f) Allen, J. M.; Lambert, T. H. *J. Am. Chem. Soc.* **2011**, *133*, 1260–1262. (g) Rueping, M.; Zhu, S.; Koenigs, R. *Chem. Commun.* **2011**, *47*, 12709–12711. (h) Zhang, Y.; Peng, H.; Zhang, M.; Cheng, Y.; Zhu, C. *Chem. Commun.* **2011**, *47*, 2354–2356. (i) Reddy, K. H. V.; Satish, G.; Reddy, V. P.; Kumar, B. S. P. A.; Nageswar, Y. V. D. *RSC Adv.* **2012**, *2*, 11084–11088. (j) Ma, L.; Chen, W.; Seidel, D. *J. Am. Chem. Soc.* **2012**, *134*, 15305–15308. (k) Lin, A.; Peng, H.; Abdukader, A.; Zhu, C. *Eur. J. Org. Chem.* **2013**, *2013*, 7286–7290. (l) Sakai, N.; Mutsuro, A.; Ikeda, R.; Konakahara, T. *Synlett* **2013**, *24*, 1283–1285. (m) Kumar, S.; Kumar, P.; Jain, S. L. *RSC Adv.* **2013**, *3*, 24013–24016. (n) Hoshikawa, T.; Yoshioka, S.; Kamijo, S.; Inoue, M. *Synthesis* **2013**, *45*, 874–887. (o) Yan, C.; Liu, Y.; Wang, Q. *RSC Adv.* **2014**, *4*, 60075–60078. (p) Nauth, A. M.; Otto, N.; Opatz, T. *Adv. Synth. Catal.* **2015**, *357*, 3424–3428. (q) Pacheco, J. C. O.; Lipp, A.; Nauth, A. M.; Acke, F.; Dietz, J.-P.; Opatz, T. *Chem. - Eur. J.* **2016**, *22*, 5409–5415. (r) Wakaki, T.; Sakai, K.; Enomoto, T.; Kondo, M.; Oisaki, K.; Kanai, M.; Masaoka, S. *Chem. - Eur. J.* **2018**, *24*, 8051–8055.
9. For isolated precedents, see: (a) Barton, D. H. R.; Billion, A.; Boivin, J. *Tetrahedron Lett.* **1985**, *26*, 1229–1232. (b) Troyanskii, É. I.; Ioffe, V. A.; Nikishin, G. I. *Russ. Chem. Bull.* **1985**, *34*, 2537–2546. (c) Moriarty, R. M.; Vaid, R. K.; Duncan, M. P.; Ochiai, M.; Inenaga, M.; Nagao, Y. *Tetrahedron Lett.* **1988**, *29*, 6913–6916. (d) Ushakov, D. B.; Gilmore, K.; Kopetzki, D.; McQuade, D. T.; Seeberger, P. H. *Angew. Chem., Int. Ed.* **2014**, *53*, 557–561. (e) Kumar, R.; Gleißner, E. H.; Tiu, E. G. V.; Yamakoshi, Y. *Org. Lett.* **2016**, *18*, 184–187. (f) Shen, H.; Hu, L.; Liu, Q.; Hussain, M. I.; Pan, J.; Huang, M.; Xiong, Y. *Chem. Commun.* **2016**, *52*, 2776–2779.
10. Mitch, C. H. *Tetrahedron Lett.* **1988**, *29*, 6831–6834.
11. Fandrick, D. R.; Hart, C. A.; Okafor, I. S.; Mercadante, M. A.; Sanyal, S.; Masters, J. T.; Sarvestani, M.; Fandrick, K. R.; Stockdill, J. L.; Grinberg, N.; Gonnella, N.; Lee, H.; Senanayake, C. H. *Org. Lett.* **2016**, *18*, 6192–6195.

12. For an example employing a cation-pool strategy for Boc-protected secondary amines, see: Yoshida, J.-I.; Suga, S.; Suzuki, S.; Kinomura, N.; Yamamoto, A.; Fujiwara, K. *J. Am. Chem. Soc.* **1999**, *121*, 9546–9549.
13. This is the pathway proposed for classical Shono oxidations, for example: (a) Shono, T.; Hamaguchi, H.; Matsumura, Y. *J. Am. Chem. Soc.* **1975**, *97*, 4264–4268. (b) Shono, T.; Matsumura, Y.; Tsubata, K. *J. Am. Chem. Soc.* **1981**, *103*, 1172–1176.
14. Wang, F.; Rafiee, M.; Stahl, S. S. *Angew. Chem., Int. Ed.* **2018**, *57*, 6686–6690.
15. For a comprehensive review of aminoxyl-mediated electrochemistry, see: Nutting, J. E.; Rafiee, M.; Stahl, S. S. *Chem. Rev.* **2018**, *118*, 4834–4885.
16. See Supporting Information for details.
17. (a) Rafiee, M.; Miles, K. C.; Stahl, S. S. *J. Am. Chem. Soc.* **2015**, *137*, 14751–14757. (b) Hickey, D. P.; Schiedler, D. A.; Matanovic, I.; Doan, P. V.; Atanassov, P.; Minter, S. D.; Sigman, M. S. *J. Am. Chem. Soc.* **2015**, *137*, 16179–16186.
18. For related observations involving mediated hydrogen-atom transfer versus electron transfer, see: Rafiee, M.; Wang, F.; Hruszkewycz, D. P.; Stahl, S. S. *J. Am. Chem. Soc.* **2018**, *140*, 22–25.
19. Utle, J. H. P.; Nielsen, M. F.; Wyatt, P. B. *Electrogenerated Bases and Nucleophiles. In Organic Electrochemistry; Revised and Expanded; Hammerich, O., Speiser, B., Eds.; CRC Press, 2015.*
20. For previous studies of steric vs electronic effects in aminoxyl-mediated oxidation reactions, see ref 17 and the following: Steves, J. E.; Stahl, S. S. *J. Am. Chem. Soc.* **2013**, *135*, 15742–15745.
21. (a) Andrieux, C. P.; Gonzalez, F.; Savéant, J.-M. *J. Am. Chem. Soc.* **1997**, *119*, 4292–4300. (b) Lennox, A. J. J.; Nutting, J. E.; Stahl, S. S. *Chem. Sci.* **2018**, *9*, 356–361.
22. Caramella, P.; Rondan, N. G.; Paddon-Row, M. N.; Houk, K. N. *J. Am. Chem. Soc.* **1981**, *103*, 2438–2440.
23. Cieplak, A. S. *J. Am. Chem. Soc.* **1981**, *103*, 4540–4552.
24. Colpaert, F. C. *Nat. Rev. Drug Discovery* **2003**, *2*, 315–320.
25. DeBaillie, A. C.; Jones, C. D.; Magnus, N. A.; Mateos, C.; Torrado, A.; Wepsiec, J. P.; Tokala, R.; Raje, P. *Org. Process Res. Dev.* **2015**, *19*, 1568–1575.
26. Evans, B. E.; Ponticello, G. S.; Hoffman, J. M. U.S. Patent 5,952,351, Sep. 14, 1999.
27. Albizati, K. F.; Babu, S.; Birchler, A.; Busse, J. K.; Fugett, M.; Grubbs, A.; Haddach, A.; Pagan, M.; Potts, B.; Remarchuk, T.; Rieger, D.; Rodriguez, R.; Shanley, J.; Szendroi, R.; Tibbetts, T.; Whitten, K.; Borer, B. C. *Tetrahedron Lett.* **2001**, *42*, 6481–6485.
28. ¹H NMR analysis of the cyanation crude mixture showed that near quantitative yields were obtained from the hydrolysis workup and isolation. In two cases, the carboxylic acid product was isolated in higher yield than isolation of the cyanation precursor (cf. **4b** and **4c** vs **3b** and **3j**).

Chapter 5: Sequential Oxidation-Depolymerization Strategies for Lignin Conversion to Low Molecular Weight Aromatic Chemicals

This work is published: Cui, Y.[†]; Goes, S. L.[†]; Stahl, S. S. In *Advances in Inorganic Chemistry: Catalysis in Biomass Conversion*; Ford, P. C., van Eldik, R., Eds.; Academic Press: Cambridge, MA, 2021; Vol. 77, pp 99–136.

[†]These authors contributed equally to this work.

5.1. Abstract

Lignin is the largest source of bio-derived aromatic chemicals, and oxidative conversion of this polymeric material can generate valuable oxygenated aromatic compounds. Oxidative depolymerization of lignosulfonate feedstocks under alkaline conditions is used commercially for vanillin production. Recent studies have led to other oxidation methods that access different aromatic products from lignin in good yields. A particularly effective strategy that accesses some of the highest yields of aromatic monomers to date features a two-step process in which the oxidation of specific alcohol groups in lignin is followed by an oxidative, reductive, or redox-neutral step that cleaves the polymer into aromatic monomers and oligomers. Studies of model compounds have provided crucial mechanistic insights and contributed to the development of effective lignin depolymerization methods. This review provides a general overview of lignin depolymerization methods, followed by a survey of oxidation-depolymerization methods that access oxygenated aromatic monomers in good yields.

5.2. Introduction

Increasing global demand for sustainable alternatives to organic chemicals derived from coal and petroleum is driving efforts to leverage biomass-derived feedstocks. Lignin is a significant component of lignocellulosic biomass and represents an abundant source of functionalized, renewable aromatics that could be used directly as valuable products or transformed into fuels or chemicals. Many tons of lignin are produced as a byproduct of the pulp and paper and biofuel industries that prioritize acquisition of cellulose;¹ however, the majority of this material is burned as low value fuel to provide energy.² Strategies to convert lignin into value-added chemicals could play an important role in supporting the economic viability of future biorefineries.

Lignin is a non-repeating, mostly linear biopolymer created by radical coupling of monolignols, consisting of *p*-hydroxy-3-phenylpropanolderived building blocks.³ Lignin is composed of different quantities of *para*-hydroxyphenyl (H), guaiacyl (G) and syringyl (S) aromatic subunits linked via C–C and C–O bonds comprising β -O-4, α -O-4, β -1, β -5, β - β , and 5-5 units (**Figure 5.1**). Many plant sources contain other aromatic units, such as *p*-hydroxybenzoate, appended to the alcohols in these linker units. The relative abundance of each type of subunit and linkage varies between plant species, and the amount of lignin can vary from 15% to 35% of the overall biomass weight.⁴ Multiple methods have been developed to extract lignin from biomass, including Kraft, enzymatic, organosolv, and mild acidolysis methods,⁵ and each can lead to modifications of the lignin structure that influence subsequent depolymerization. Some methods of lignin depolymerization, such as pyrolysis, use harsh conditions to break many inter-unit linkages and generate a wide array of small-molecule products.⁶ Other depolymerization methods are tailored to cleave specific linkages and lead to a smaller distribution of products. The β -O-4 ether unit is the most common linkage in lignin (40–70 wt%) and is among the most readily cleaved. It contains comparatively weak C–C/C–O bonds with bond dissociation energies (BDE) as low as 67.0 kcal/mol.⁷ The prevalence and reactivity of β -O-4 lignin units have made them a target for many depolymerization strategies and provide a basis for generation of S- and G-derived aromatic products in up to 45–55% (hardwoods) or 20–30% (softwood) monomer yields,^{8,9} often supplemented by *p*-hydroxybenzoate and other aromatic groups appended to the naturally occurring polymer.

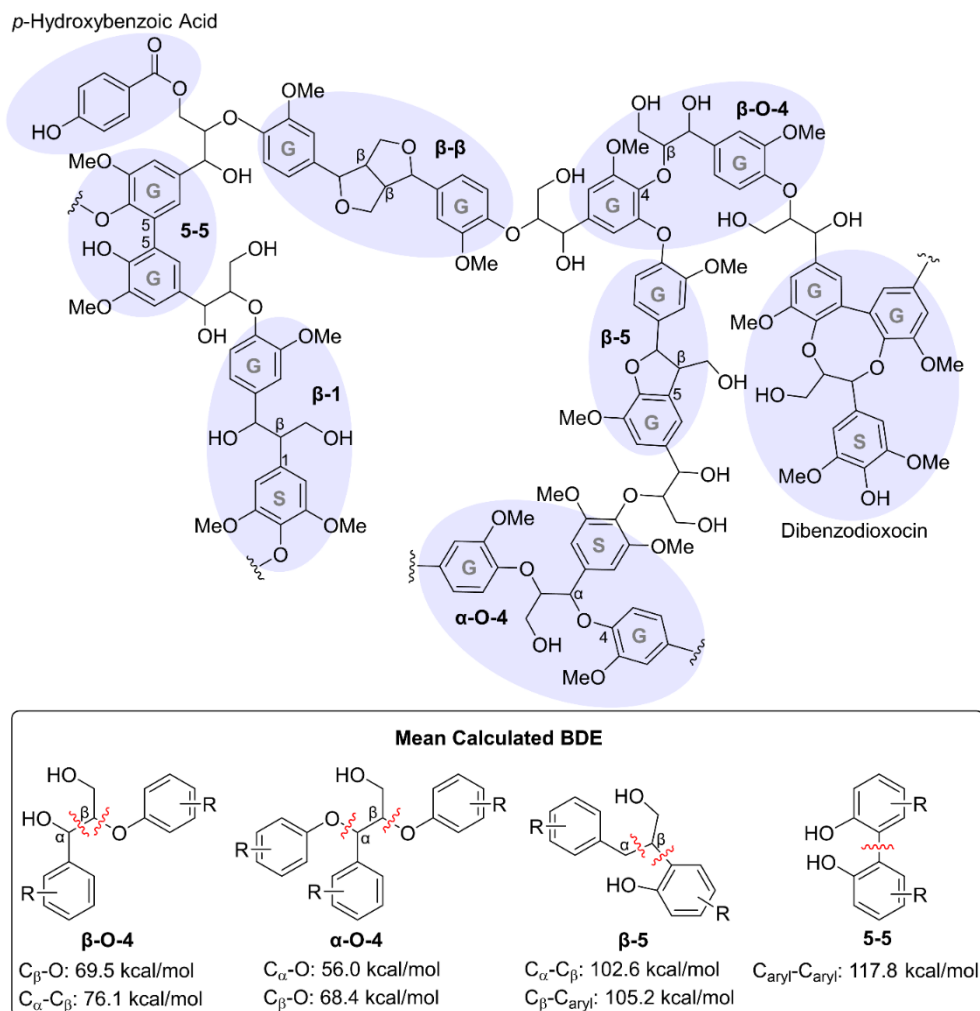


Figure 5.1. Lignin structure (top) and bond strengths (bottom) with typical lignin linkages.

Reduction methods have been the focus of extensive attention for lignin depolymerization. These have been reviewed elsewhere,^{8,10-11} but reductive catalytic fractionation (RCF) methods are particularly noteworthy because they are capable of producing near theoretical yields of aromatics in one step.¹²⁻¹⁸ These methods combine heterogeneous supported metal catalysts with solubilized lignin or raw biomass under elevated temperature (180–250 °C) and H₂ pressure (5–15 MPa). RCF conditions lead to hydrogenation and hydrogenolysis pathways that stabilize reactive lignin intermediates and prevent lignin degradation and condensation in the process of generating propylphenol-derived aromatics.

Oxidative lignin depolymerization strategies are appealing because they provide access to a different set of value-added aromatics relative to those obtained from reduction methods. A prominent example is vanillin, an aromatic aldehyde derived from the G subunit that is widely used in the flavor, fragrance, and cosmetic industries.¹⁹ It has been produced commercially through oxidative lignin depolymerization using copper-based catalysts under strong alkaline conditions.²⁰⁻²²Recent research has focused on identifying new oxidative depolymerization strategies to generate other lignin-derived aromatics.^{23,24} Oxidized aromatics derived from lignin have strategic benefits for microbial funneling of product mixtures into a single value-added chemical, owing to the higher solubility of these precursors in the aqueous growth media.^{25,26} Research into the development of oxidative lignin depolymerization processes has featured two general strategies: top-down and bottom-up (**Figure 5.2**). Top-down strategies directly use raw lignocellulosic biomass or extracted lignin as the feedstock in efforts to develop new depolymerization methods. In contrast, bottom-up strategies start with well-defined model compounds in an effort to identify new catalytic methods and characterize mechanisms of reactions capable of cleaving strategic linkages in lignin, such as β -O-4 units. Successful examples are then tested on authentic lignin samples to assess their efficacy with complex feedstocks. This review provides a brief overview of methods that have been developed for oxidative conversion of lignin and related models into aromatic monomers, followed by an extensive presentation of two-step alcohol oxidation-bond cleavage methods that have proven to be particularly effective for lignin conversion into oxygenated aromatic monomers. These processes correspond to bottom-up strategies originating from systematic studies of reactions with model compounds that were successfully translated to depolymerization of lignin in high yield.²⁷⁻²⁹

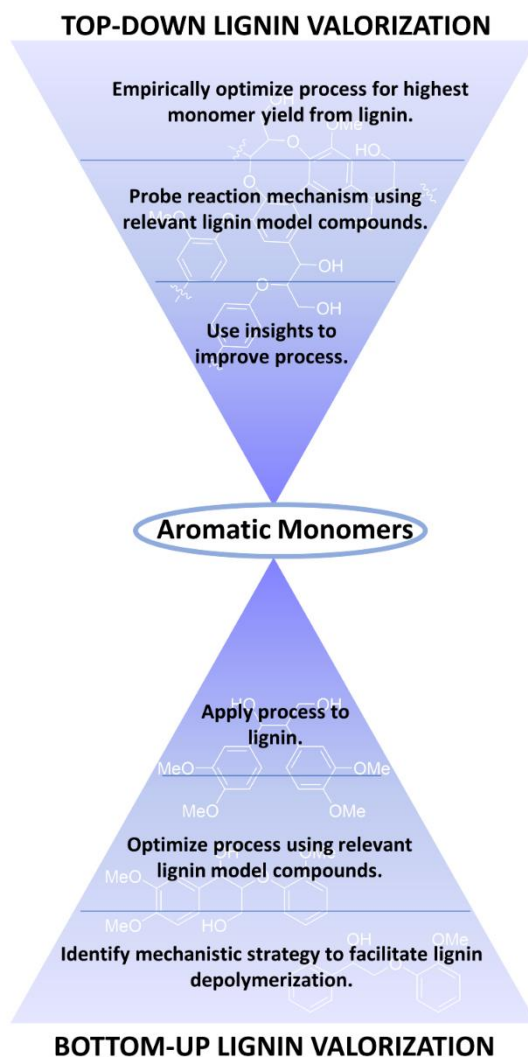


Figure 5.2. Top-down and bottom-up strategies for lignin depolymerization.

5.3. Top-Down vs. Bottom-Up Strategies for Lignin Depolymerization

5.3.1. Top-Down Strategies for Efficient Aromatic Monomer Production

Top-down strategies for lignin depolymerization (

Figure 5.2) empirically optimize methods to obtain monomers from biomass or extracted lignin, frontloading challenges associated with using a complex polymer substrate, such as solubility, source variation, and product analysis. Intermediates generated during reactions with the complex feedstock are difficult to detect or characterize, and thus limit mechanistic insights that could be used to guide process optimization. Nonetheless, top-down approaches provide the

most direct test of the utility of different methods for lignin conversion into aromatic monomers. Top-down strategies have led to several effective oxidative methods to obtain vanillin from lignin. In the 1940s, stoichiometric oxidants under basic conditions were found to convert lignin materials into vanillin (**Figure 5.3A-i/ii**).^{30,31} Mechanistic studies implicate a single-electron-transfer (SET) pathway that generates radicals in alkaline solution, which result in homolytic cleavage of the C α -C β bond of β -O-4 linkages to form the aldehyde product (**Figure 5.3B**).^{5,32-33} As a representative protocol, nitrobenzene (2–4 M NaOH, 160–180 °C, 2–3 h) yields up to 16 wt% vanillin from softwood sulfite lignin as the major product.^{20,34} The cost and toxic by-products of nitrobenzene relegate its use to laboratory scale applications, for example, to quantify the β -O-4 linkages and/or the relative amounts of uncondensed H, G, and S units of various lignin sources.³⁵ CuO was also identified as an effective oxidant, although it was used at rather high loading (up to 600 wt%) and the vanillin is slowly converted to vanillic acid under the oxidizing alkaline conditions.^{22,36}

Molecular oxygen (O₂) is an ideal oxidant, and high yields of vanillin are possible by controlling the O₂ partial pressure, reaction temperature, and reaction pH in the presence of CuSO₄ as a catalyst (**Figure 5.3A-iii**).³⁷ A variation of this method was developed by Borregaard for conversion of lignosulfonates, which provides the basis for commercial production of bio-based vanillin.^{20,22,38} Other variations of this method have been used for direct treatment of raw biomass, enabling direct conversion to low molecular weight chemicals.³⁹⁻⁴¹

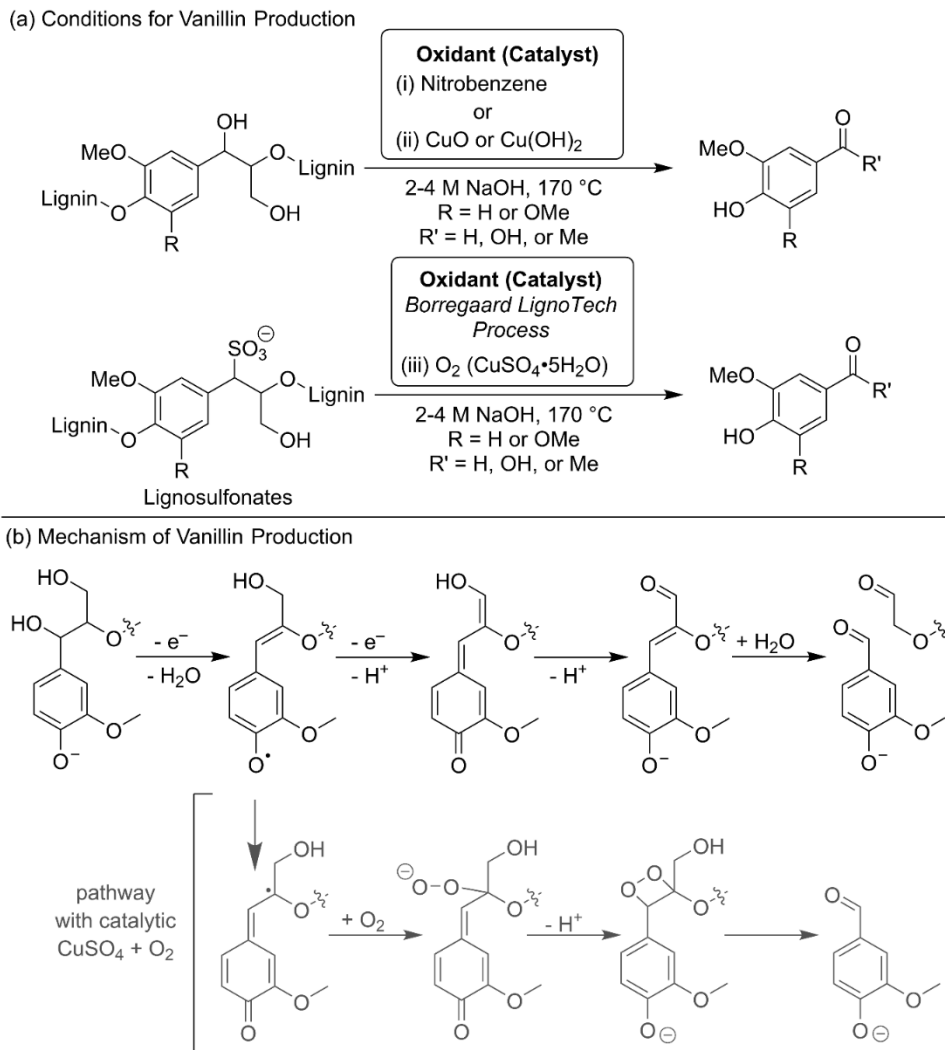


Figure 5.3. (A) Typical reaction conditions to depolymerize lignin or lignosulfonates through (i) nitrobenzene, (ii) copper-based catalyst, or (iii) commercial vanillin production used by Borregaard; (B) proposed mechanism of vanillin formation under alkaline oxidative conditions.

5.3.2. Bottom-Up Strategy for Mechanistic Insight into Lignin Depolymerization

Bottom-up lignin depolymerization (**Figure 5.2**) refers to studies that start with low molecular weight model substrates containing representative fragments of native lignin (e.g., β-O-4 units). These lignin-like models allow for straightforward testing and analysis of chemical reactivity and facilitate mechanistic studies. Numerous homogeneous transition-metal catalysts have been used for selective cleavage of C–C and C–O bonds in β-O-4 model compounds via

oxidative and redox neutral pathways (**Figure 5.4**). As summarized in **Figure 5.5** and elaborated below, a number of these methods generate aromatic monomers in good yield.

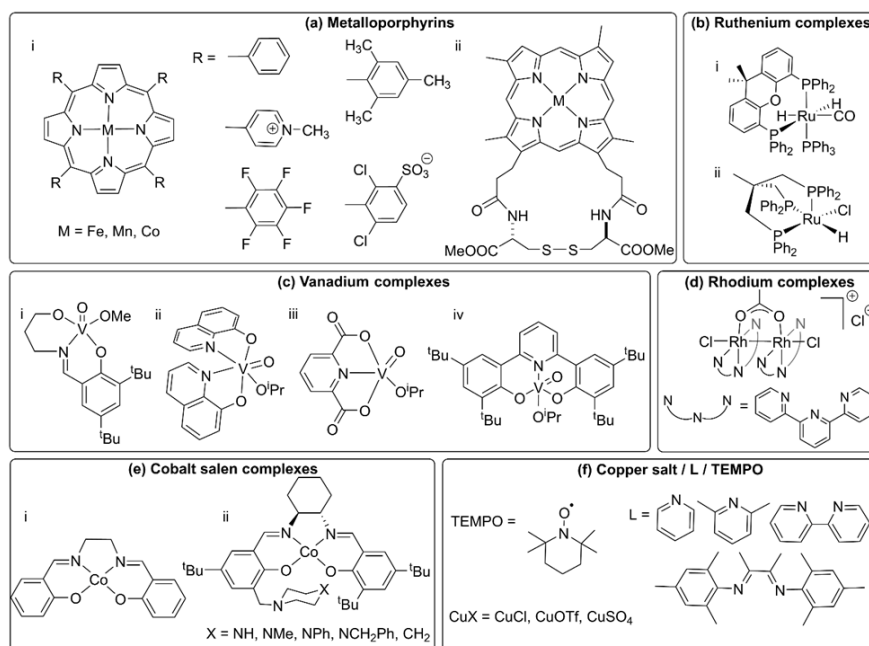


Figure 5.4. Metal complex catalysts used for selective bond cleavage of lignin model compounds.

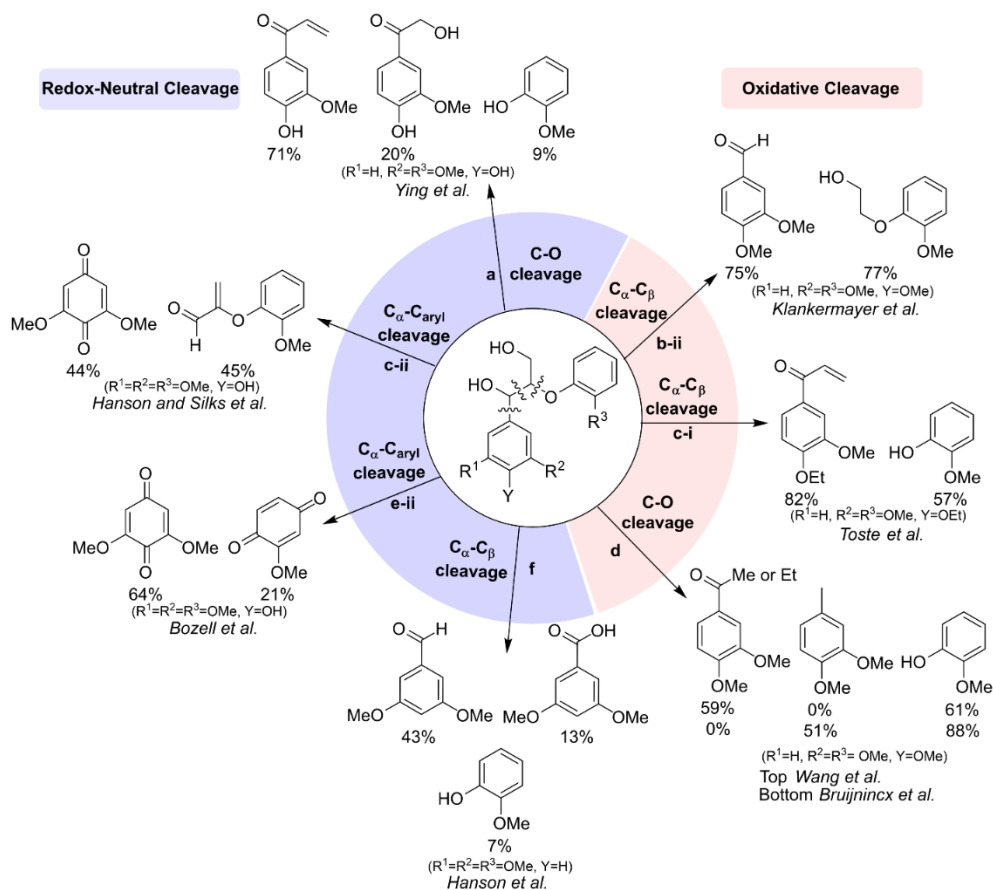


Figure 5.5. Yields of aromatic monomer products through selective bond cleavage of β -O-4 model compounds via different metal complex catalysts listed in **Figure 5.4**.

Naturally occurring enzymes, such as Fe and Mn-based peroxidases, contribute to fungal degradation of lignin,^{42,43} and biomimetic Fe, Mn, and Co porphyrins have been widely tested as synthetic catalysts for lignin and lignin-model degradation (**Figure 5.4A–i**). Various oxidants such as H₂O₂, *tert*-butyl hydroperoxide (*t*BuOOH), and oxone have been used to generate high-valent metal-oxo reactive species.^{23,44} The metal-oxo species are proposed to promote SET from electron-rich phenol and non-phenolic compounds to generate a radical cation that initiates further reaction and degradation of the lignin material. Early studies showed that sterically hindered porphyrins mimic enzyme activity and limit oxidative degradation of the porphyrin scaffold.^{45,46} More recently, Ying and coworkers demonstrated that cobalt-containing deuteroporphyrin derivatives

with tethered disulfide groups (**Figure 5.4A-ii**) depolymerize phenolic lignin models, accessing >90% yield of monomers from C_β-O cleavage monomers with oxone as the oxidant (**Figure 5.5A**).⁴⁷ A lower yield of guaiacol monomer reflects overoxidation of the phenol, resulting in ring cleavage. Subsequent application of this catalyst to various lignin samples generated significant quantities (>30 wt% in several cases) of a lignin oil containing H/G/S-derived aromatics and aliphatic material.

Bergman and Ellman showed that a Ru-based complex, Ru(H)₂(CO) (PPh₃)(xantphos) (Error! Reference source not found. **5.4B-i**) effects C–O bond cleavage in simplified β-O-4 model compounds that lack the -C_γH₂OH functional group.⁴⁸ The catalyst mediates tandem catalytic dehydrogenation/C–O bond cleavage in a redox-neutral process. Incorporation of the C_γH₂OH fragment that is present in lignin, however, blocks dehydrogenation and prevents subsequent C–O bond cleavage.^{49,50} Modified methods from other groups, using KOH addition or acetylation of the γ-hydroxyl group, were able to overcome this problem.^{51,52} A Ru-triphos catalyst system (**Figure 5.4B-ii**) was developed by Klankermayer and coworkers to cleave the C_α–C_β bond in β-O-4 model compounds containing a -C_γH₂OH moiety. The process involves primary alcohol dehydrogenation followed by retro-aldol reaction to achieve C–C bond cleavage (**Figure 5.5B-ii**).⁵³

Oxovanadium catalysts have been used for cleavage of lignin model compounds in both redox-neutral and oxidative methods.⁵⁴ Toste and coworkers used Schiff-base vanadium catalysts (**Figure 5.4C-i**) to generate monomeric enone and guaiacol products from dimeric and trimeric β-O-4 models (**Figure 5.5C-i**). The authors proposed that the reaction is initiated by hydrogen atom transfer (HAT) from the β-O-4 secondary alcohol, followed by subsequent homolysis of the C_β–O bond⁵⁵ When the catalytic oxovanadium system was applied to organosolv grass lignin, a decrease in the lignin polymer molecular weight was observed and selective β-O-4 degradation was

demonstrated by 2D NMR spectroscopy, but less than 3 wt% yield of identified monomers was recovered.⁵⁶ Under similar reaction conditions using V-quinolate catalysts (**Figure 5.4C-ii**), Hanson, Silks, and coworkers propose an oxidative mechanism in which the catalyst promotes SET oxidation of phenolic model compounds to generate a phenoxy radical, followed by subsequent C_{aryl}-C_α bond cleavage (**Figure 5.5C-ii**).⁵⁷ Baker et al. showed that V-quinolate complexes catalyze oxidation of mixed-hardwood organosolv lignin, decreasing the average molecular weight by 77%, although monomer yields were not reported.⁵⁸ Other types of vanadium-based catalysts, (dipic) V^V(O)OiPr (**Figure 5.4C-iii**) and V-bisphenolate (**Figure 5.4C-iv**) are less selective and generate a mixture of C_α-C_β and redox-neutral C_β-O bond cleavage products depending on substrate structure and reaction conditions.^{59,60}

A binuclear Rh complex, reported by Li and Wang (**Figure 5.4D**), was used to cleave a series of lignin model compounds and authentic lignin via hydrogen-transfer methods. Rh-catalyzed dehydrogenation of the benzylic alcohol produces a ketone intermediate that undergoes subsequent C_β-O bond cleavage (110 °C, Ar, NaOH) to afford 61–64% guaiacol and 59–61% methyl- and ethylarene products (Error! Reference source not found. **5.5D**).⁶¹ Almost complete deconstruction of raw basswood powder sample resulted in 26.6 wt% aromatic oil, although monomer yields of only 2.3 wt% (based on the starting raw basswood powder) were generated. Bruijninx and coworkers used Sc(OTf)₃ as a Lewis acid catalyst to promote cleavage of ether bonds. When paired with Rh-catalyzed decarbonylation of aliphatic aldehydes, a Rh/Sc(OTf)₃ catalyst system provided stable aromatic product mixtures. This chemistry led to good yields of methylarenes (51%) and guaiacols (88%) from model compounds and also accessed aromatic monomers from pine (6.8 wt%) and poplar (9.8%) sawdust.⁶²

Cobalt-Schiff base complexes have been studied extensively for phenol oxidation with O₂.^{63,64} Bozell and coworkers have investigated Co(salen) complexes (**Figure 5.4E**) that react with O₂ to form a superoxide adduct that can abstract a hydrogen atom from phenols, generating a phenoxyl radical that can induce cleavage of C_{aryl}-C_α bonds in the lignin models.^{65,66} Catalysts from a family of unsymmetrical Co-Schiff base complexes, each bearing a bulky heterocyclic nitrogen base on the ligand (**Figure 5.4E-ii**), convert phenolic lignin models to benzoquinones in yields up to 64% (**Figure 5.5E-ii**).⁶⁶ When applied to organosolv poplar lignin, however, only small quantities of monomers were obtained due to the low phenolic content of organosolv lignin.

Copper/nitroxyl catalyst systems for aerobic alcohol oxidation⁶⁷ have been investigated with lignin model compounds. Initial studies by Baker, Wu, Hanson and coworkers used 2,2,6,6-tetramethylpiperidine-1-oxyl (TEMPO) as the nitroxyl catalyst in combination with CuCl, pyridine, and O₂ at 100 °C. Limited activity for aerobic oxidative cleavage of simplified lignin models was attributed to instability of the active copper catalyst (**Figure 5.4F**).^{54,59} Use of stoichiometric CuCl/TEMPO with an S/G lignin β-O-4 dimer led to 89% conversion to cleavage products, albeit with only 7–43% yield of monomeric aromatic products (**Figure 5.5F**). A modified Cu/bpy/ TEMPO catalyst system (bpy=2,2'-bipyridine),⁶⁸ investigated by Stahl and coworkers,²⁷ is somewhat more effective and will be revisited below.

This brief survey of catalytic methods is not comprehensive, but it illustrates the types of bottom-up strategies that have been pursued using well-defined model compounds. The attempts to achieve direct conversion of dimeric models into aromatic monomers in a single step has led to mixed success, and oxidative methods derived from these studies have not (yet) led to lignin depolymerization strategies that are competitive with reductive methods or previously known oxidative methods (cf. **Section 5.3.1** and **Figure 5.3**).

5.4. Sequential Oxidation-Cleavage Methods for Lignin Depolymerization

5.4.3. Concepts and Initial Discovery of the Alcohol Oxidation-Cleavage Strategy

Bottom-up approaches to lignin depolymerization necessarily incorporate uncertainty because the model compounds lack the complexity intrinsic to natural biomass or extracted lignin samples. But, studies of relevant model compounds provide a means to access valuable insights that could be applied to biomass conversion. This principle is illustrated by a different bottom-up strategy initiated within the Stahl laboratory in 2011. The central hypothesis in this approach was that selective oxidation of either alcohol within the β -O-4 unit of lignin could facilitate a subsequent cleavage step to generate monomeric aromatic products (**Figure 5.6A**). For example, oxidation of the primary (1°) alcohol would form an aldehyde susceptible to retro-aldol cleavage, while the oxidation of the secondary (2°) benzylic alcohol could be cleaved by various redox and non-redox reaction pathways. Computational studies of lignin suggest that alcohol oxidation weakens the β -O-4 C–O bond by 12–13 kcal/mol, thereby facilitating homolytic cleavage pathways for lignin depolymerization (**Figure 5.6B**).^{7,69-71}

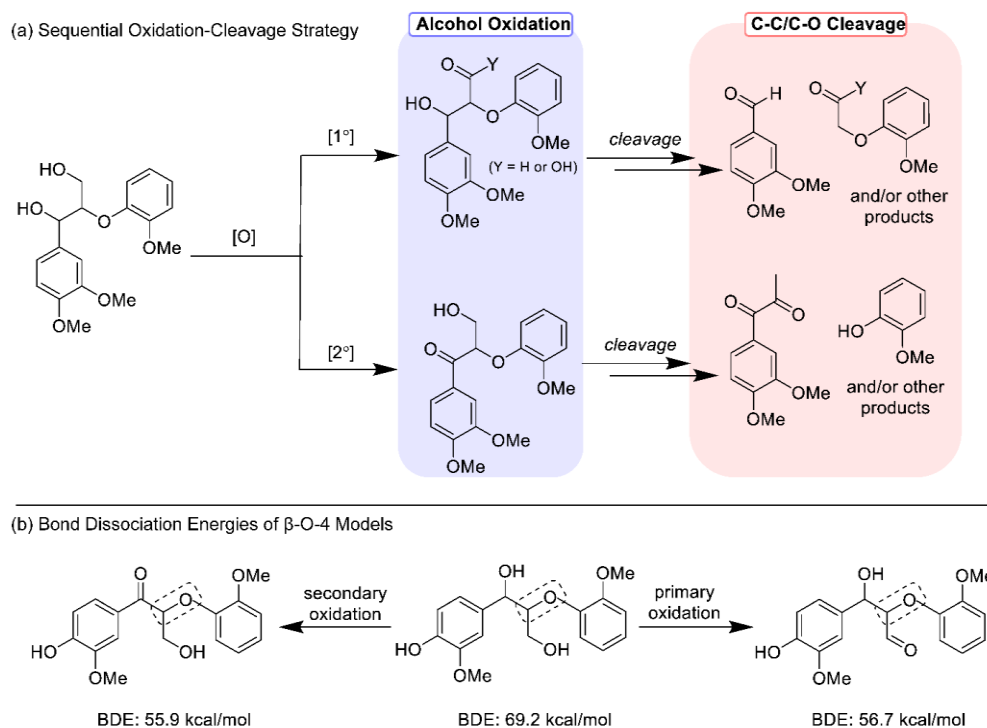


Figure 5.6. Sequential oxidation-cleavage strategies (A) selectively oxidize β -O-4 alcohol groups to weaken the C–O ether bond (B) to facilitate subsequent bond cleavage in a separate step.

Stahl and coworkers tested the reaction of numerous common stoichiometric oxidants and catalytic alcohol oxidation methods with a β -O-4 dimeric model compound, and methods employing nitroxyl catalysts proved to be the most effective (**Figure 5.7A**).²⁷ Nitroxyl catalysts, such as TEMPO and 4-acetamido-TEMPO (ACT), undergo reversible $1 e^-$ electrochemical oxidation to the corresponding oxoammonium and a quasi-reversible $1 e^-/1 H^+$ reduction to hydroxylamines.⁷² The TEMPO radical is generally unreactive with organic species, but various chemical and electrochemical oxidation methods may be used to generate the reactive oxoammonium species from the nitroxyl or hydroxylamine form of the catalyst.⁷³ The oxoammonium, generated in situ or isolated as a salt, mediates hydride transfer oxidation of alcohols. This reactivity is evident in the reaction with stoichiometric Bobbitt's salt, which oxidizes the 2° benzylic alcohol to the corresponding ketone in 97% yield. In contrast, use of TEMPO/bleach (NaOCl) under mildly basic conditions leads to preferential oxidation of the more sterically accessible 1° alcohol, affording the aldehyde product in 49% yield, with only 4% yield of the benzylic ketone. An aerobic CuI /TEMPO catalyst system also shows selectivity for 1° alcohol oxidation, and, while proceeding in only moderate yield, induces retro-aldol reactivity to generate aromatic monomers as the major products. Two other aerobic oxidation methods, employing $(FeNO_3)_3$ /TEMPO and ACT/ HNO_3 /HCl, led to good yields and selectivity for formation of the ketone, with the latter method generating a 94% yield of ketone. The ACT/ HNO_3 /HCl oxidation condition was then tested on poplar lignin extracted using cellulolytic enzyme lignin (CEL), which retains much of the native lignin structure. Analysis of the oxidized lignin by 2D heteronuclear single quantum coherence (HSQC) NMR spectroscopy suggests that

nearly all of the benzylic alcohols adjacent to G and S aromatic units are oxidized in the final lignin material.

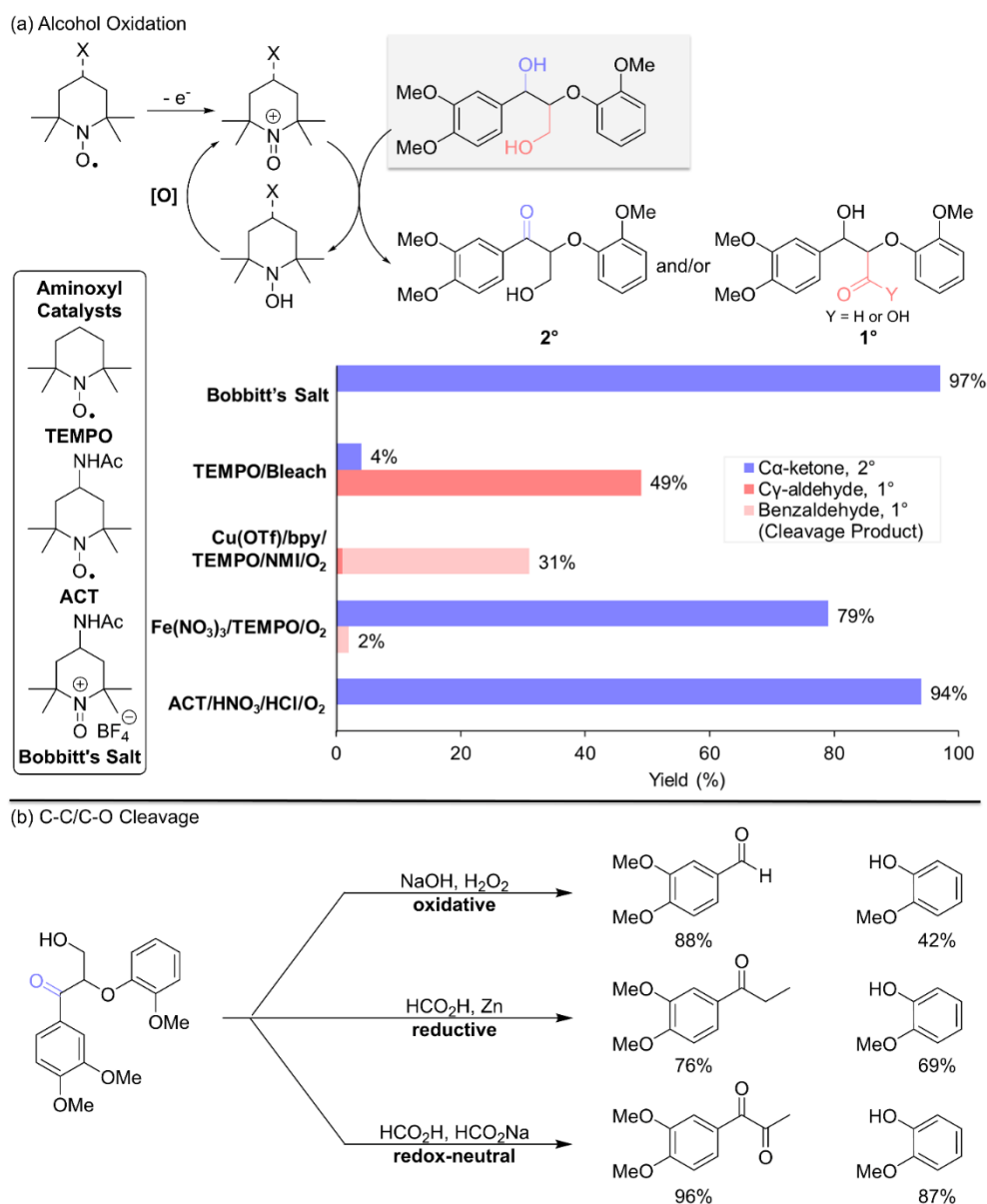


Figure 5.7. (A) Selective primary or secondary alcohol oxidation through various reaction systems; (B) different bond cleavage methods on secondary alcohol oxidized lignin models.

An oxidized β -O-4 model compound bearing a benzylic ketone was shown to undergo cleavage into aromatic monomers under oxidizing, reducing, and redox-neutral conditions (**Figure 5.7B**).^{27,28} Alkaline hydrogen peroxide led to partial degradation of the phenol monomer,²⁷ while

a redox neutral transformation in the presence of aqueous formic acid/formate led to the best results (**Figure 5.7B**).²⁸ Excellent yields of both products were obtained from S-, G-, and H-derived β -O-4 dimer models (89–92% isolated yield of diketone monomer).

ACT/HNO₃/HCl oxidation of poplar CEL, followed by treatment with formic acid/formate, induced lignin depolymerization to afford >60 wt% yield of low molecular weight aromatic compounds, including a 52 wt% yield of characterized aldehyde, carboxylic, and diketone aromatics (**Figure 5.8**).²⁸ These results were later extended to lignin samples obtained from other biomass sources (poplar, maize, and maple) and extracted by different methods, including mild acidolysis,⁷⁴ γ -valerolactone/dilute sulfuric acid (GVL),⁷⁵ extractive ammonia (EA)^{76,77} and copper-catalyzed alkaline hydrogen peroxide (Cu-AHP).⁷⁸ Aromatic yields of 3–42% were obtained when this two-step oxidation-depolymerization sequence was applied to these different lignin samples, with the best yield of aromatics obtained from a poplar sample extracted via mild acidolysis (42%) or Cu-AHP conditions (31%).²⁹

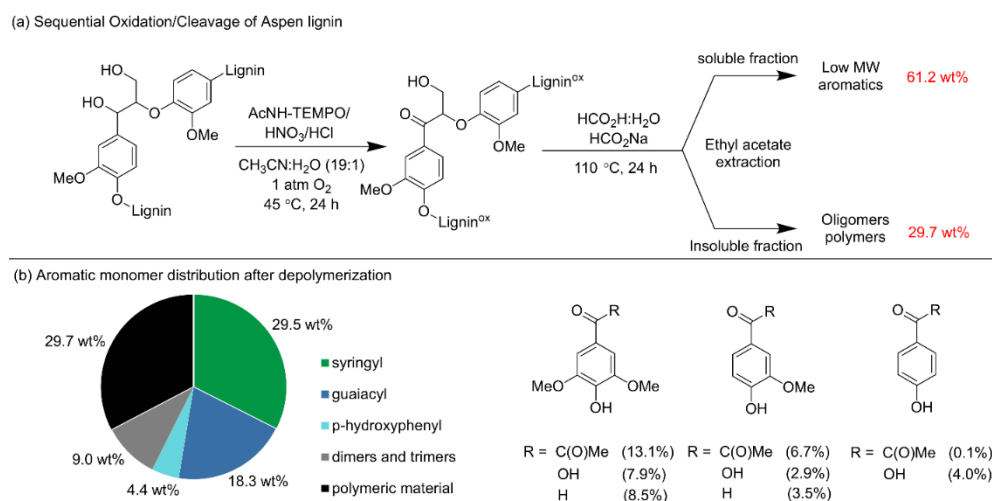


Figure 5.8. (A) Depolymerization of aspen lignin with formic acid following oxidation; (B) monomer distribution from depolymerization of oxidized aspen lignin.

This sequential oxidation-cleavage method demonstrated the best yields of aromatics to date for a lignin depolymerization method originating from a bottom-up strategy. These results

provided a foundation for numerous other studies employing a two-step sequence to access aromatic monomers from lignin. These studies include the development of different alcohol oxidation methods, including those with selectivity for the 2° and 1° positions in β -O-4 units (Sections 5.4.4 and 5.4.6), and different methods for bond cleavage/depolymerization from the oxidized lignin and lignin model compounds (Section 5.4.7). A summary of these various methods is provided in Figure 5.9.

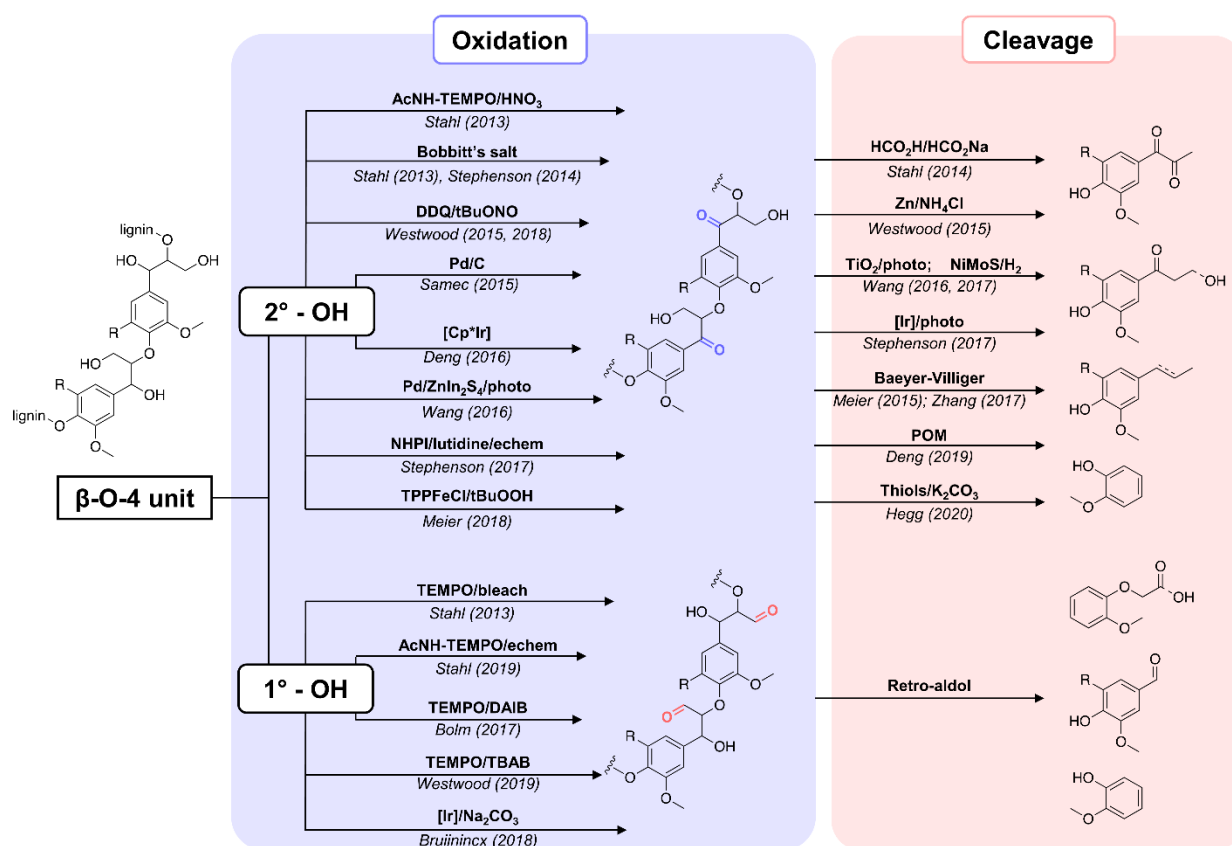


Figure 5.9. Overview of the sequential oxidation-cleavage approaches applied in real lignin.

5.4.4. Secondary Alcohol Oxidation

Oxidation methods that exhibit selective oxidation of 2° alcohols in lignin include those employing TEMPO, *N*-hydroxyphthalimide (NHPI), 2,3-dichloro-5,6-dicyano-1,4-benzoquinone (DDQ), and transition-metal catalyst systems. Some of these oxidants are used in stoichiometric quantities, while others are components of catalyst systems.

5.4.4.1. TEMPO and TEMPO Derivatives

TEMPO derivatives are among the most effective reagents and catalyst systems available for 2° alcohol oxidation in lignin.²⁷ As noted above, Stahl and coworkers showed that stoichiometric Bobbitt's salt and ACT/HNO₃/HCl (O₂, MeCN/H₂O, 45 °C, 20 h) produced up to 97% yields of oxidized lignin model compounds (**Figure 10A and B**).²⁷ Meier et al. obtained similar results, albeit with somewhat lower yields, for similar model compounds using modified catalytic conditions (TEMPO/NaNO₂/HCl/NaCl, O₂, dichloromethane, 19 h).⁷⁹

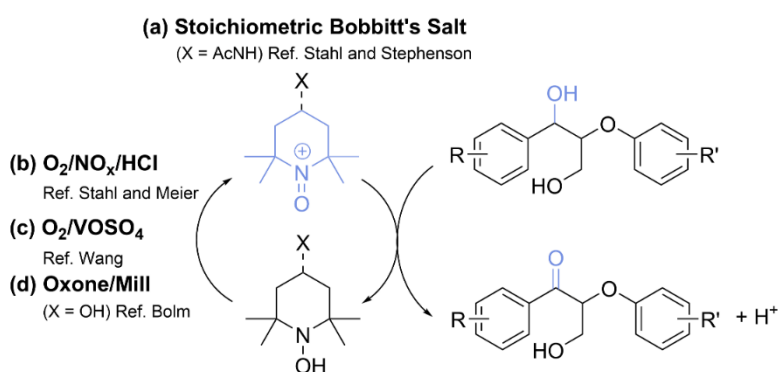


Figure 5.10. TEMPO and its derivatives mediated benzylic alcohol oxidation in lignin and its models.

Wang and coworkers developed an aerobic system using VOSO₄ as a co-catalyst to generate the oxoammonium species (**Figure 10C**), followed by aerobic C–C bond cleavage over a Cu/1,10 phenanthroline (phen) catalyst for production of aromatic acids and phenols. Oxidation of non-phenolic β-O-4 lignin models (20% VOSO₄/TEMPO, 0.4 MPa O₂, MeCN, 90 °C, 6 h) generated the corresponding β-O-4 ketone product in 53% yield, together with a 20% yield of the retro-aldol cleavage product 2-phenoxyacetophenone. When the VOSO₄/TEMPO system was tested on organosolv Alcell lignin, 2D HSQC NMR analysis revealed partial oxidation of the β-O-4 linkages in lignin. Details on the cleavage step are elaborated below (see **Section 5.4.7.2**).⁸⁰

Bolm et al. achieved benzylic oxidation (>94% yield) of non-phenolic β-O-4 lignin model compounds through mechanochemical methods using catalytic amounts of HO-TEMPO/KBr in

the presence of oxone as terminal oxidant (20% HO-TEMPO/KBr, 25 Hz, 90 min) (**Figure 10D**).⁸¹ Dimeric models containing phenols oxidatively cleaved under these conditions, likely reflecting oxone-promoted generation of phenoxy radicals that led to formation of benzoquinone (82–91%) and guaiacol (76–82%) products.

Optimized reaction conditions were applied to organosolv beechwood lignin. Gel permeation chromatography (GPC) analysis and HSQC NMR and IR spectroscopic data supported a high degree of oxidation and some cleavage of β -O-4 linkages of lignin.

Stephenson and coworkers developed a sequential alcohol oxidation-photochemical reductive cleavage method using stoichiometric Bobbitt's salt for the alcohol oxidation step (**Figure 10A**).⁸² Initial efforts to use catalytic ACT/HNO₃/HCl oxidation method²⁷ were not compatible with the subsequent photochemical cleavage step, elaborated below in **Section 5.4.7.3**. Non-phenolic β -O-4 dimers were oxidized, the reaction was filtered, solvent was removed, and the mixture was subjected to depolymerization conditions without further purification. Hegg and coworkers explored a sequential oxidation/depolymerization method with poplar lignin extracted using the Cu-AHP method.⁸³ Although some alcohols are oxidized during the oxidative Cu-AHP extraction process (CuSO₄/bpy, H₂O₂, NaOH, 30 °C), treatment of the extracted lignin with Bobbitt's salt led to an approximately five-fold increase in oxidation at the benzylic position, as revealed by HSQC-NMR spectroscopic analysis. The latter material proved much more susceptible to cleavage by a biomimetic thiol-mediated process than the lignin obtained directly from the Cu-AHP process (see **Section 5.4.7.3** for discussion of the cleavage process).

5.4.5. NHPI

NHPI is the stable precursor to another type of nitroxyl mediator, phthalimide *N*-oxyl (PINO), used in organic oxidation reactions (**Figure 5.11**). Unlike TEMPO, the imidoxyl radical PINO is generated from NHPI in situ. Although it has limited stability in solution, PINO mediates

efficient HAT from weak C–H bonds, such as those in benzylic alcohols.^{72,84} A number of different NHPI oxidation methods have been employed to achieve NHPI/PINO-catalyzed oxidation of lignin and lignin model compounds (**Figure 5.11**).

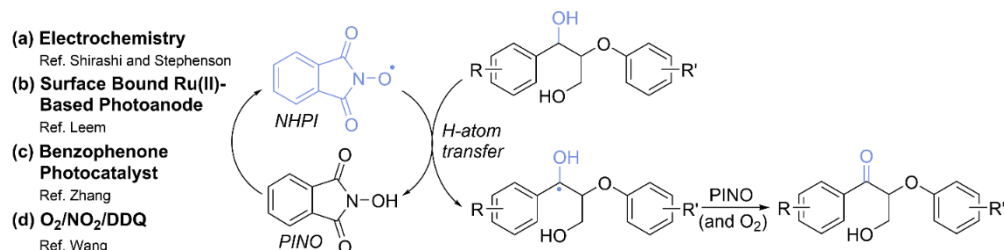


Figure 5.11. NHPI mediated benzylic alcohol oxidation in lignin and its models. DDQ = 2,3-dichloro-5,6-dicyano-1,4-benzoquinone.

Shiraishi and coworkers reported an NHPI-mediated electrochemical oxidation of a non-phenolic β -O-4 dimer into the C $_{\alpha}$ -ketone derivative in excellent yield (93%; conditions: LiClO₄, 2,6-lutidine, MeCN, 0.7 V vs. Ag/Ag⁺) (**Figure 5.11A**).⁸⁵ The lutidine base facilitates electrochemical reoxidation of NHPI to PINO. Stephenson et al. used a similar NHPI/2,6-lutidine electrocatalytic oxidation method,⁸⁶ and showed that inclusion of O₂ in the reaction mixture led to increased yield of the ketone for a series of model compounds. O₂ reacts rapidly with benzylic radicals generated by PINO-mediated HAT, contributing to oxidation at this site.⁸⁷⁻⁸⁹ Analysis of simplified model compounds suggested excellent reactivity and selectivity for benzylic alcohol oxidation; no primary alcohol oxidation was detected. Pine dioxosolv-lignin was subjected to electrochemical NHPI oxidation using a modified acetone:DMSO (98:2) solvent system to solubilize the lignin, and characteristic signals for oxidation of β -O-4 to the C $_{\alpha}$ -ketone were observed by HSQC NMR spectroscopy. This reactivity was paired with a photochemical reduction process to achieve partial depolymerization of the lignin (see **Section 5.4.7.3** for the cleavage step). A photo-electrochemical variant of NHPI-catalyzed alcohol oxidation in lignin and lignin model

compounds was recently developed by Leem et al. using electrode-immobilized Ru^{II}-polypyridyl complexes (**Figure 5.11B**).⁹⁰

Aromatic ketones, such as benzophenone and its derivatives, have been widely used for photochemically initiated HAT, including reactions with weak O–H bonds.^{91,92} Zhang and coworkers utilized donor-substituted aromatic ketones 4,40-bis(diphenylamino)benzophenone (DPA-BP) to generate PINO through chemical photocatalysis (**Figure 5.11C**).⁹³ The DPA-BP/NHPI/O₂ photocatalytic system exhibits good reactivity and selectivity for the aerobic oxidation of phenolic and non-phenolic β -O-4 lignin models. The benzylic ketone products were obtained in excellent isolated yields (81–99%).

Finally, the combination of NHPI, DDQ, and O₂ is a known catalyst system for oxidation of benzylic C–H bonds.⁹⁴ Wang and coworkers supplemented this co-catalyst mixture with a NO_x source to achieve oxidation of benzylic ketones from β -O-4 model compounds in 35–45% yields (**Figure 5.11D**).⁹⁵

5.4.5.1. DDQ

DDQ is a common reagent for dehydrogenation of benzylic alcohols.⁹⁶ Lignin oxidation with stoichiometric or catalytic DDQ has been proposed to be initiated by SET, HAT, or hydride transfer,^{97,98} although the reaction mechanisms have seldom been the focus of specific investigation. Aerobic oxidation of the benzylic alcohol in lignin β -O-4 model compounds was developed by employing NO_x-based co-catalysts (e.g., NaNO₂, *tert*-butyl nitrite (*t*BuONO), HNO₃) to promote re-oxidation of the reduced quinone (2,3-dichloro-5,6-dicyanohydroquinone, DDQH₂).⁹⁹⁻¹⁰¹ Moody et al. reported oxidation of lignin model compounds at ambient temperature using catalytic amounts of DDQ and NaNO₂ or *t*BuONO under visible light irradiation, affording excellent yield (>92%) of the benzylic ketone in β -O-4 model compounds (**Figure 5.12A** and

B).¹⁰² Photoexcitation of DDQ to a long-lived triplet state was proposed to initiate electron transfer from the substrate.¹⁰³

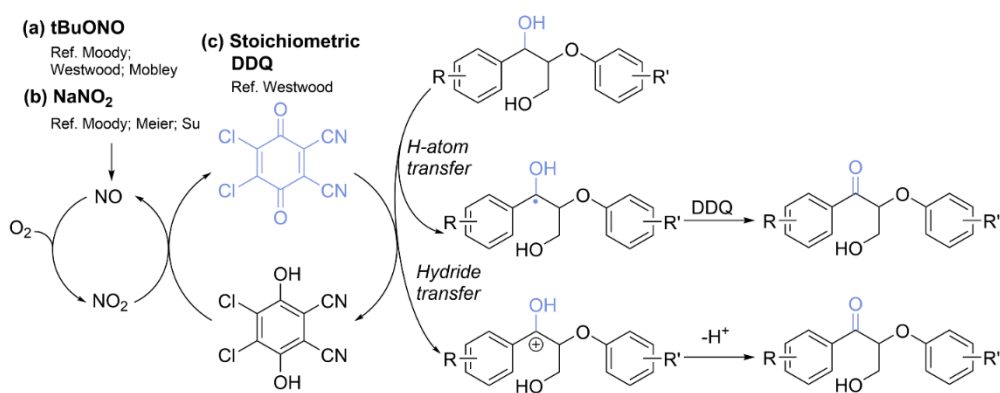


Figure 5.12. DDQ-mediated benzylic alcohol oxidation in lignin and its models.

Westwood et al. applied the DDQ/*t*BuONO catalytic system for the oxidation of simple β -O-4 model compounds and polymeric models at elevated temperature (80 °C) rather than promoting the reaction with light. The reactions produce ketones with high yield and complete selectivity.¹⁰⁴ The optimized catalytic conditions were applied to the oxidation of organosolv birch lignin, and the desired β -O-4 ketone was identified by 2D HSQC NMR spectroscopy. This study was the first to use DDQ in the sequential oxidation/depolymerization of authentic lignin. 6 wt% aromatic monomers were isolated following a Zn-mediated reductive cleavage method, elaborated in **Section 5.4.7.3** below (**Figure 5.12A**). The same group oxidized organosolv beech lignin with varying amounts of stoichiometric DDQ (i.e., no re-oxidation method was employed), and used 2D HSQC NMR analysis to track linkage reactivity with increasing amounts of oxidant (**Figure 5.12C**).¹⁰⁵ This stoichiometric DDQ-based method generated oxidized lignin with six hardwood dioxosolv lignins, including those from beech, oak, maple, hickory, cherry, and birch, and the protocol was validated at 20 g scale. on transfer from the substrate.¹⁰³

DDQ is also capable of oxidizing benzylic ethers.^{98,106} Luterbacher and coworkers have developed an aldehyde-protecting group strategy that enables much higher yields of lignin to be

extracted via acidolysis from various biomass sources.¹⁰⁷ They subsequently showed that the acetal-protected lignin is amenable to stoichiometric or catalytic DDQ-promoted oxidation of the benzylic position to afford the corresponding oxidized lignin.¹⁰⁸ The oxidation method was demonstrated on a series of β -O-4 model compounds and then applied to the oxidation of acetal-protected birch and genetically modified, poplar lignin enriched in syringyl units. A number of subsequent studies have employed stoichiometric DDQ and catalytic DDQ/*t*BuONO or NaNO₂/O₂ catalyst systems to carry out lignin oxidation.^{79,109} Bugg et al. generated oxidized lignin from multiple plant sources using stoichiometric DDQ oxidation and evaluated the monomer yield from a Zn-based depolymerization method.¹¹⁰ The best results were obtained with poplar organosolv lignin, which had the highest β -O-4 content of the investigated lignins. Other examples will be discussed in **Section 5.4.7.2** in connection with depolymerization studies of these materials.

5.4.5.2. Additional Oxidation Methods

Several other metal-catalyzed methods have been evaluated for lignin (model) oxidation. Meier et al. investigated the use of meso-tetraphenylporphyrin iron(III) chloride (TPPFeCl) and *t*BuOOH for catalytic oxidation of benzylic alcohols in lignin model compounds.^{79,111} Ball-milling treatment in KOH and toluene resulted in an increase in the carbonyl content in Kraft lignin, and the mechanochemical processing with TPPFeCl-catalyzed oxidation has a synergistic, positive effect on the depolymerization of lignin. When the TPPFeCl/*t*BuOOH oxidation method was applied to Kraft lignin, 2D HSQC NMR spectra suggested that the β -O-4 benzylic alcohol groups were oxidized, and a Baeyer-Villiger oxidation method was used in a subsequent depolymerization method to generate aromatic monomers (cf. **Section 5.4.7.2**).

Deng, Fu, and coworkers employed Cp*Ir catalysts bearing a cooperative bipyridone ligand to promote dehydrogenation of β -O-4 lignin model compounds (**Figure 5.13**).¹¹² These

reactions promote thermal dehydrogenation of the benzylic alcohols, generating H₂. Good conversions and yields were observed with a series of model compounds.

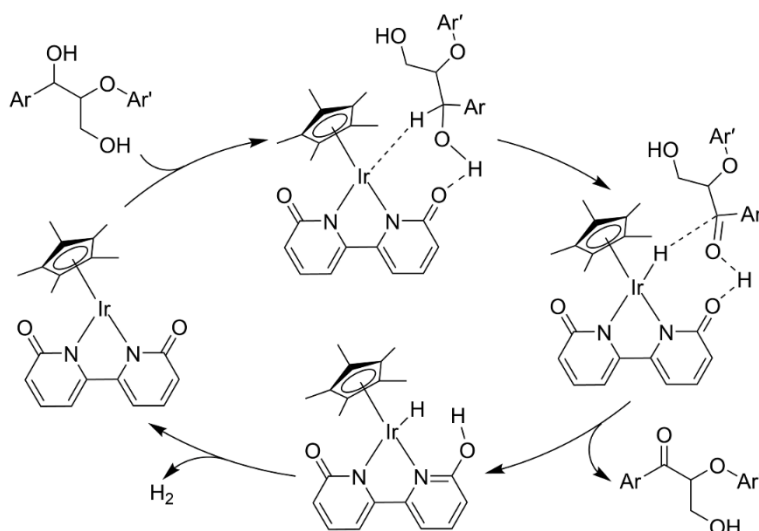


Figure 5.13. Transition metal mediated secondary alcohol oxidation in lignin models using [Ir(Cp*)L], where L = 2,20 -bipyridine-6,60 -diol.

Samec and coworkers demonstrated the selective oxidation of benzylic alcohols in lignin model compounds using carbon supported Pd nanoparticles under mild conditions (**Figure 5.14A**).^{113,114} Use of oxidizing conditions led to benzylic ketone formation without cleavage of C–O or C–C bonds or dehydrogenation of the γ 1° alcohol. Zhang, Wang and coworkers studied cerium oxide-supported Pd catalyst (Pd/CeO₂) for the aerobic oxidation of various model compounds, in addition to a source of organosolv lignin. Low yields of monomers were obtained from the latter process: vanillin (5.2%), guaiacol (0.87%) and 4-hydroxybenzaldehyde (2.4%).¹¹⁵

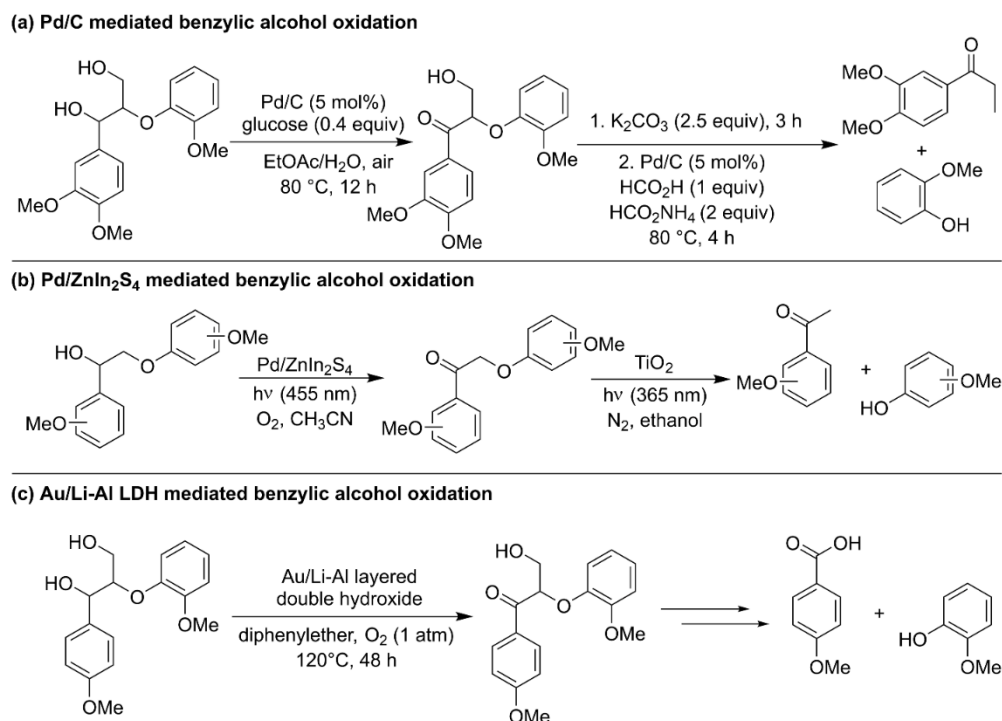


Figure 5.14. Heterogeneous catalyst-mediated secondary alcohol oxidation in lignin model compounds using (A) Pd/C, (B) Pd/ZnIn₂S₄, and (C) Au/Li-Al LDH.

ZnIn₂S₄ is a ternary chalcogenide semiconducting material with a band gap that supports photochemistry with visible light irradiation. Wang et al. found that Pd/ZnIn₂S₄ promoted oxidation of benzylic alcohols with lignin models upon illumination with 455 nm light under ambient conditions (**Figure 5.14B**). This step was paired with TiO₂-mediated photochemical cleavage (365 nm illumination) of the models into aromatic monomers.^{80,116}

Crocker et al. employed the heterogeneous catalyst Au/Li–Al layered double hydroxide (LDH) to catalyze aerobic oxidation of dimeric lignin models with 1 atm O₂ and observed excellent activity for benzylic alcohol oxidation in β-O-4 models (**Figure 5.14C**).¹¹⁷ The high surface area and strong basicity of the Li–Al LDH support facilitated substrate adsorption and reaction on the Au surface. Lignin, one sample sourced from the γ-valerolactone extraction method⁷⁵ and another from the Kraft process, were subjected to aerobic oxidation conditions with this catalyst. Alkaline

hydrolysis of the resulting oxidized lignin materials led to lignin depolymerization, with monomer yields as high as 40% for γ -valerolactone extracted lignin and 10% for Kraft lignin.

5.4.6. Primary Alcohol Oxidation

Under basic conditions, oxoammonium generated from TEMPO or ACT mediates alcohol oxidation by an inner sphere mechanism that favors reaction with sterically unhindered primary alcohols.⁷³ This selectivity was demonstrated by using bleach/TEMPO conditions at pH 9 (cf. **Figure 5.7A**).²⁷ The Cu/TEMPO-catalyzed aerobic oxidation method, which features a different mechanism,¹¹⁸ also shows selectivity for primary alcohol oxidation.²⁷

Bolm et al. reported that the hypervalent iodine reagent diacetoxyiodo benzene (DAIB), in combination with TEMPO, leads to selective oxidation of non-phenolic β -O-4 primary hydroxyl groups to aldehydes in 43% yield (**Figure 5.15A**).¹¹⁹ Stoichiometric DIAB and a TEMPO catalyst were used to oxidize organosolv beech lignin. A reduction of C_7-H_7 signals was revealed by 2D HSQC NMR analysis, corresponding to an increase in carbonyl chemical shifts typical for aldehydes. Depolymerization of this material is presented in **Section 5.4.7.1** below.

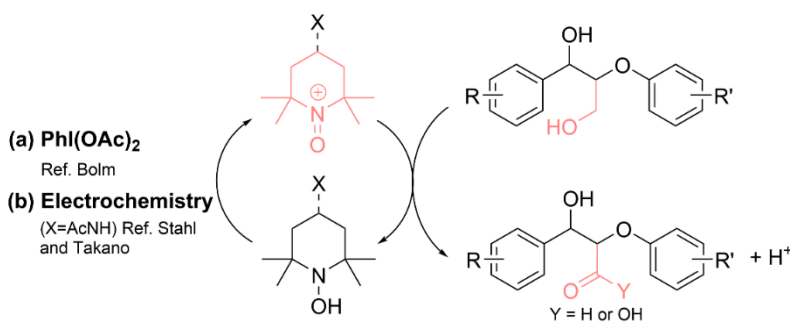


Figure 5.15. Mechanism of TEMPO mediated primary alcohol oxidation of a lignin model compound.

The groups of Takano and Stahl have used electrochemical methods to support TEMPO-catalyzed oxidation of lignin and/or lignin model compounds. Stahl et al. used ACT as the mediator for the oxidation of β -O-4 model substrates lacking free phenols under basic conditions (5% ACT,

pH 10, 70:30 H₂O:MeCN, 0.8 V vs. Ag/AgCl). Higher turnover frequencies were observed for models containing primary alcohols with β -ether fragments, similar to those in the β -O-4 unit in lignin.¹²⁰ A systematic comparison of various 1° and 2° alcohol substrates shows that 1° alcohols are much more reactive under these conditions, and β -O-4 models with both types of alcohols undergo selective oxidation of the primary alcohol to the carboxylic acid in >90% yield (**Figure 5.15B**). Takano and coworkers observed comparable yields and selectivity with similar β -O-4 model compounds under modified conditions 90:10 dioxane:phosphate buffer (pH 7, 20 mol% ACT) conditions.¹²¹ Stahl and coworkers also tested the reactivity of a mild-acidolysis poplar lignin material under their optimized reaction conditions. 2D HSQC NMR spectroscopy showed a decrease in characteristic β -O-4 primary alcohol β - and γ - signals, with no change to the secondary alcohol signals. An acid-base titration of oxidized lignin revealed an approximately 12-fold increase in acidic functionality, attributed to the introduction of carboxylic acid functional groups in the polymer. Some lignin cleavage is observed by GPC during the oxidation step, but the oxidized polymer was also amenable to depolymerization under acidic conditions, as described below (see **Section 5.4.7.1**).

Lancefield, Bruijninx and coworkers reported an efficient catalytic dehydrogenation system using a Cp*Ir-bipyridonate complex (same as that in **Figure 5.13**) in a 1,4-dioxane/water solution at pH 11. This approach exhibited selectivity for primary over secondary alcohol dehydrogenation and led to cleavage of the C $_{\alpha}$ -C $_{\beta}$ bond. This catalytic system was applied to enzyme-extracted lignin and dioxosolv softwood lignins and led to significant reduction in the lignin molecular weight and low yields of mono-aromatic compounds.¹²²

5.4.7. Bond Cleavage Methods

The two-step oxidation/depolymerization strategy allows for systematic optimization of the two steps, whereby selective oxidation of the primary or secondary alcohols in the backbone

may be subjected to different conditions that enable efficient cleavage of the C β -O aryl, C α -C β , or other bonds in the linkers between aromatic units. A variety of methods, including oxidative, reductive, and redox-neutral reactions, have been developed for this second-step in the process (**Figure 16**). Secondary alcohol oxidation has been paired with both redox and non-redox depolymerization methods, while primary alcohol oxidation has been typically paired with redox-neutral processes.

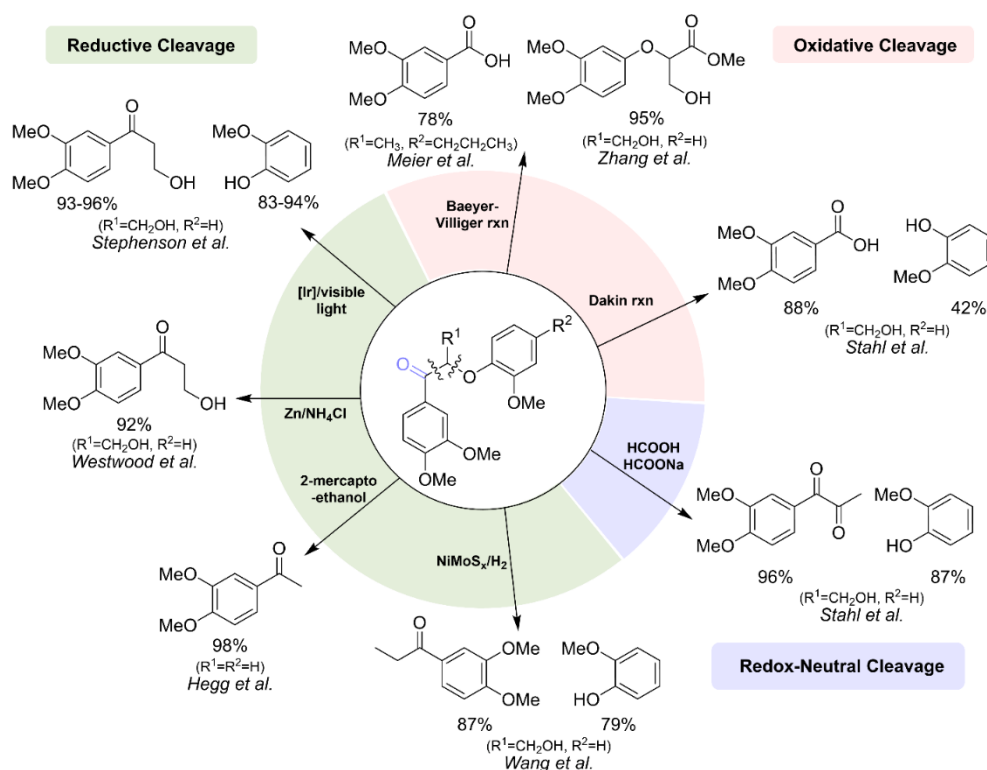


Figure 5.16. Different bond cleavage patterns in lignin model with C α ketone structure.

5.4.7.1. Redox-Neutral Cleavage

A retro-aldol reaction following selective primary alcohol oxidation enables cleavage of the C α -C β bond, resulting in lignin depolymerization.⁵³ In some cases, this reactivity proceeds directly under the oxidative reaction conditions (cf. **Figure 5.7A**), while other cases (emphasized here) feature treatment of the oxidized lignin under modified conditions to promote cleavage. Lignin model compounds with terminal C γ -aldehydes undergo facile retro-aldol under basic

conditions to generate benzylaldehyde and an aryl ether fragment (**Figure 5.17A**). Bolm and coworkers use DL-proline as an organocatalyst to promote this reactivity at ambient temperature, generating veratraldehyde and guaiacol in 70% and 26% yields, respectively.¹¹⁹ Treatment of oxidized organosolv beech lignin (cf. **Section 5.4.6**) led to reduction in the molecular weight of the polymer, consistent with bond cleavage in the backbone.

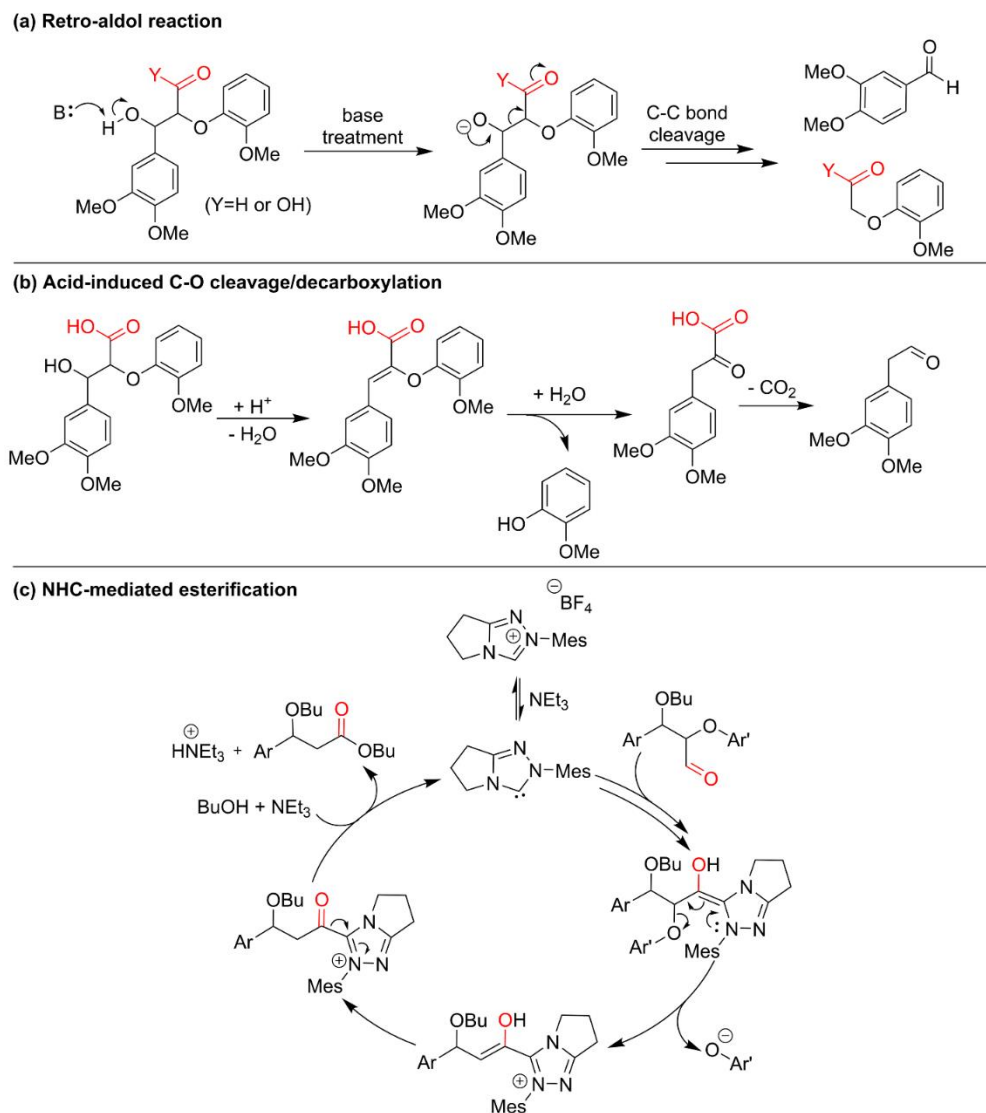


Figure 5.17. Mechanisms of redox-neutral bond cleavage method of primary alcohol oxidized lignin.

Stahl and coworkers explored acidic conditions to promote depolymerization of poplar lignin containing C_γ-carboxylic acids. This approach generated up to 30 wt% yields of monomeric aromatic compounds from an oxidized poplar lignin sample.¹²⁰ Various aqueous acids proved effective (HCl, H₂SO₄, and HCO₂H) for cleavage of the oxidized model compounds, but the highest monomer yields from lignin were obtained with a 9:1 mixture of HCO₂H and H₂O. These products can arise from acid-induced elimination of the benzylic hydroxyl group to afford a vinyl ether that is susceptible to hydrolysis, resulting in generation of Hibbert's ketone-like α-keto-acid and phenol aromatic monomers (**Figure 5.17B**).¹²³ Subsequent decarboxylation of the keto-acid generates the observed aromatic monomer containing an aliphatic aldehyde. The aldehyde is susceptible to subsequent aldol condensation, resulting in the formation of by-products. The latter condensation reactions present major challenges for lignin depolymerization methods that generate aliphatic aldehydes, although strategies to protect the aldehydes and minimize the byproduct formation have been developed.¹²⁴

Westwood and coworkers developed an *N*-heterocyclic carbene (NHC)-mediated internal redox esterification method for depolymerizing oxidized lignin containing C_γ-aldehydes (generated from a modified method of Einhorn et al.)¹²⁵ (**Figure 5.17C**).¹²⁶ Incorporation of butylethers at the C_α position of lignin during the “butanosolv” extraction method supports this process as it prevents the competing retro-aldol reaction. The proposed mechanism involves initial formation of a Breslow-type intermediate from the reaction of the NHC with the C_γ-aldehyde, followed by elimination of the phenolate and formation of the enol intermediate. Tautomerization leads to an acylazolium that reacts with butanol.¹²⁷ The process takes advantage of the inherent structure of the β-aryl ether units present in the butanosolv lignin and delivers novel functionalized aromatic monomers in modest yield (6 wt%).

Redox-neutral processes also support cleavage of lignin oxidized at the 2° benzylic alcohol position (see **Section 5.4.4** for oxidation conditions). Stahl and coworkers showed that aqueous formic acid/formate supports bond cleavage of such structures. In an application with poplar CEL, ACT/HNO₃/HCl oxidation of the lignin followed by HCO₂H/HCO₂Na treatment led to a 52 wt% yield of aromatic monomers. Diketones are the major product of this reaction (cf. **Figure 5.8**), and mechanistic studies supported the mechanism shown in **Figure 5.18**. Acylation of the 1° C_γ-OH group generates a formic ester intermediate that undergoes formate-induced elimination to generate the aryl vinyl ether species. Hydrolysis of the vinyl ether releases the phenol and diketone products (**Figure 5.18**).²⁸ This redox neutral process is noteworthy because it avoids degradation of phenols that can occur under oxidative cleavage conditions. As noted in **Section 5.4.3**, this method was also used successfully in the oxidation/depolymerization of lignin samples from various biomass sources and pretreatment protocols.²⁹

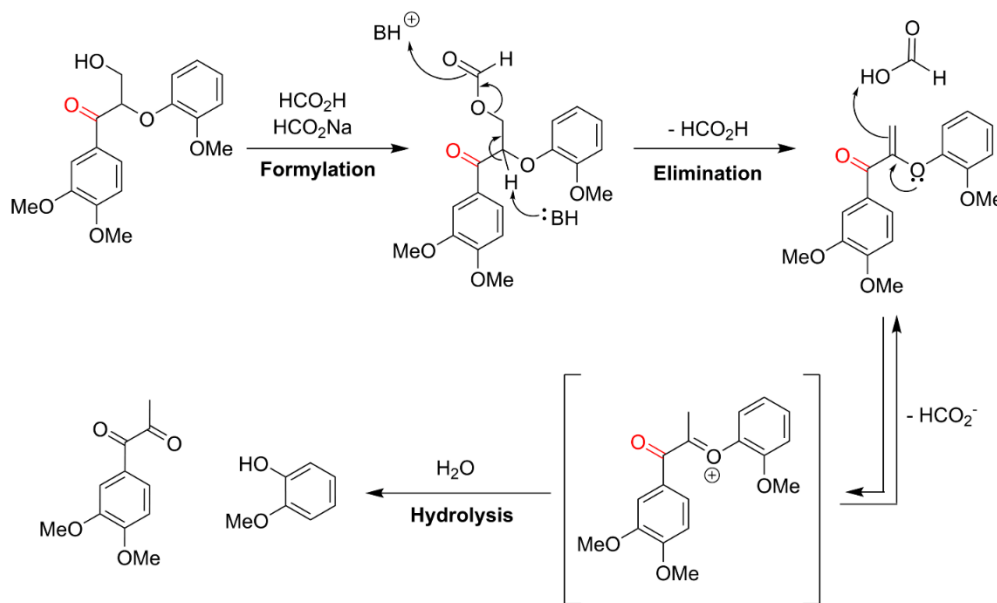


Figure 5.18. Mechanism of formic acid-mediated redox-neutral bond cleavage method on secondary alcohol oxidized lignin model.

The formic acid/formate depolymerization method developed by Stahl et al. has been employed in other two-step oxidation/depolymerization methods to afford aromatic monomers from oxidized lignin with benzylic ketones. Luterbacher and coworkers employed a HCO₂H/HCO₂Na depolymerization step following DDQ-mediated oxidation of their extracted acetal-protected lignin (see **Section 5.4.5.1**).¹⁰⁸ A yield of up to 36% aromatic monomers (diketones, carboxylic acids, and aldehydes) was obtained from propylidene acetal protected birch lignin by using a two-step DDQ oxidation/HCO₂H-HCO₂Na depolymerization sequence. A 52% yield of monomers was obtained with F5H poplar lignin (a genetically modified poplar with high syringyl content). The syringyl propanedione monomer was the major product in both cases, consistent with the mechanism shown in **Figure 5.18**. Mobley and Crocker found that the HCO₂H/HCO₂Na depolymerization process was most effective for conversion of DDQ-oxidized Kraft pine lignin.¹⁰⁹

5.4.7.2. Oxidative Cleavage

Oxidative conditions also support cleavage of oxidized lignin; however, these methods are susceptible to further oxidation and/or oxidative degradation of the monomeric products. This reactivity was noted above in the use of H₂O₂ under basic conditions to cleave benzylic ketone model compounds, resulting in an 88% yield of veratric acid but only 42% yield of guaiacol (**Figure 5.7B**).^{27,65} Baeyer-Villiger oxidation methods provide an alternative strategy for cleavage of the oxidized lignin (models) (**Figure 5.19**). Meier et al. employed in situ generated performic acid to convert benzylic ketones into esters,⁷⁹ and ester hydrolysis resulted in 78% of aromatic acids from models resembling oxidized β-O-4 structures. The corresponding aldehyde and phenol cleavage products were not recovered, likely reflecting their oxidative degradation under the reaction conditions. Oxidized Kraft lignin was subjected to these cleavage conditions (8 eq. H₂O₂, 4 eq. HCOOH, DCE, 50 °C, 24 h), and the resulting aromatic carboxylic acids were esterified in a

work-up step to give a 10 wt% yield of methyl ester products.¹¹¹ Major products included methyl vanillate 7.8 wt% and methyl 5-carbomethoxyvanillate 2.2 wt%. Zhang et al. used modified Baeyer-Villiger conditions, and paired this method with alcoholysis (K_2CO_3 , 45 °C, MeOH) to achieve high yields (>90%) in the cleavage of various model compounds to phenol and methyl benzoate derivatives (**Figure 5.19B**).¹²⁸

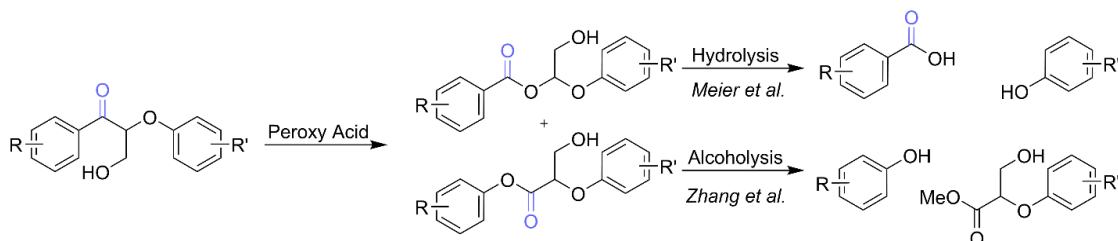


Figure 5.19. Baeyer-Villiger bond cleavage for β -O-4 linkages.

A variety of aerobic cleavage methods have also been explored using organometallic catalysts. Lignin models oxidized to the ketone by Wang et al. were subjected to oxidative cleavage by a variety of Cu salts bearing nitrogen donor ligands.⁸⁰ The $\text{Cu}(\text{OAc})_2/1,10$ -phenanthroline complex led to selective C_α - C_β bond cleavage to form aromatic acids in 92% yield under mild conditions (0.4 MPa O_2 , 150 °C, MeOH, 6 h). Deng et al. employed polyoxometalates (POM) as a regenerable catalyst to depolymerize pre-oxidized dioxosolv lignin. The optimized oxidative conditions (150 °C, 10 bar O_2 , MeOH) used a phosphomolybdic acid ($\text{H}_3\text{PMo}_{12}\text{O}_{40}$) catalyst to generate monomer yields up to 33 wt%. Aromatic monomers account for 19.4 wt% of these products, with other products derived from aromatic ring-opening. Overoxidation also converts low molecular weight depolymerization products to CO , CO_2 , and H_2O .¹²⁹

Su and coworkers reported a mechanochemical approach for selective cleavage of C_β -O bonds and C_α - C_β bonds of lignin β -O-4 ketones via NaOH-promoted oxidation under milling conditions (5 equiv. NaOH, 25 Hz milling, 2 h).¹³⁰ In contrast to other oxidative cleavage methods, the yield of phenol (87–92%) is always 13–22% higher than the yield of the corresponding

aromatic acid. Dioxosolv birch lignin milled with DDQ/NaNO₂ (see **Section 5.4.5.1** for oxidation conditions) led to a 9.1 wt% yield of aromatic monomers. When the lignin was independently oxidized with the DDQ/*t*BuONO conditions of Westwood (see **Section 5.4.5.1** for oxidation conditions),¹⁰⁴ mechanochemical cleavage generated a 15.5 wt% yield of aromatic monomers, with syringate as the major product (7.5 wt%).

5.4.7.3. Reductive Cleavage

Oxidized β -O-4 fragments with the benzylic ketone correspond to O-aryl acyloin derivatives that are susceptible to reductive cleavage. Zinc is an effective reductant in these reactions,¹³¹⁻¹³³ and could initiate single electron transfer or direct two-electron reactivity (**Figure 5.20A**). This reactivity was among those demonstrated by Stahl and coworkers using β -O-4 model compounds in their initial report on two-step oxidation/depolymerization of lignin.²⁸ Westwood and co-workers used Zn/NH₄Cl at 80 °C after DDQ-mediated oxidation of benzylic alcohol in both lignin and model compounds.¹⁰⁴ The approach generates β -hydroxy phenyl ketone products in >80% yield for different types of β -O-4 model compounds, and modest yields of phenolic monomers were also obtained from the oxidation/reductive depolymerization of birch lignin. Deng and Fu et al. used this method for lignin depolymerization following Cp*Ir-catalyzed dehydrogenation of benzyl alcohols in lignin (cf. **Figure 5.13**).¹¹²

Reductive cleavage of oxidized lignin and lignin model compounds also may be achieved via photoredox-initiated SET. Stephenson and coworkers reported that an [Ir(ppy)₂(dtbbpy)]PF₆ photocatalyst (ppy = 2-phenylpyridine, dtbbpy = 4,40-di-tert-butyl-2,20-bipyridyl) under blue LED irradiation could promote C α -O bond cleavage, generating phenols (yield >70%) and β -hydroxyaryl ketones (yield >81%) from oxidized lignin model compounds (**Figure 5.20B**).^{82,86} Bond cleavage is proposed to proceed via fragmentation of the ketone radical anion generated by SET from the photocatalyst. *N,N*-diisopropylethylamine (DIPEA) and formic acid provide a source

of reducing equivalents for the reaction. Modest yields of aromatic monomers were also obtained from a two-step oxidation/photoreductive cleavage sequence when applied to purified dioxosolv pine lignin (2.4 wt% guaiacol and phenyl ketone monomers were recovered) (**Figure 5.20A**).⁸⁶ The latter process was implemented as a batch-to-flow sequence involving electrochemical NHPI-mediated lignin oxidation in batch, followed by photochemically initiated reductive cleavage in flow.⁸⁶ Zhang and coworkers expanded on this work by developing a thiol-functionalized mesoporous cellular silica foam (MCF) with immobilized Ir(ppy)₂(bpy) photocatalyst.¹³⁴ The Ir(ppy)₂(bpy)-MCF material was effective for the reductive cleavage of oxidized lignin β-O-4 model compounds under mild reaction conditions (yield >90%). The photocatalyst could be reused at least six times without a significant drop in performance.

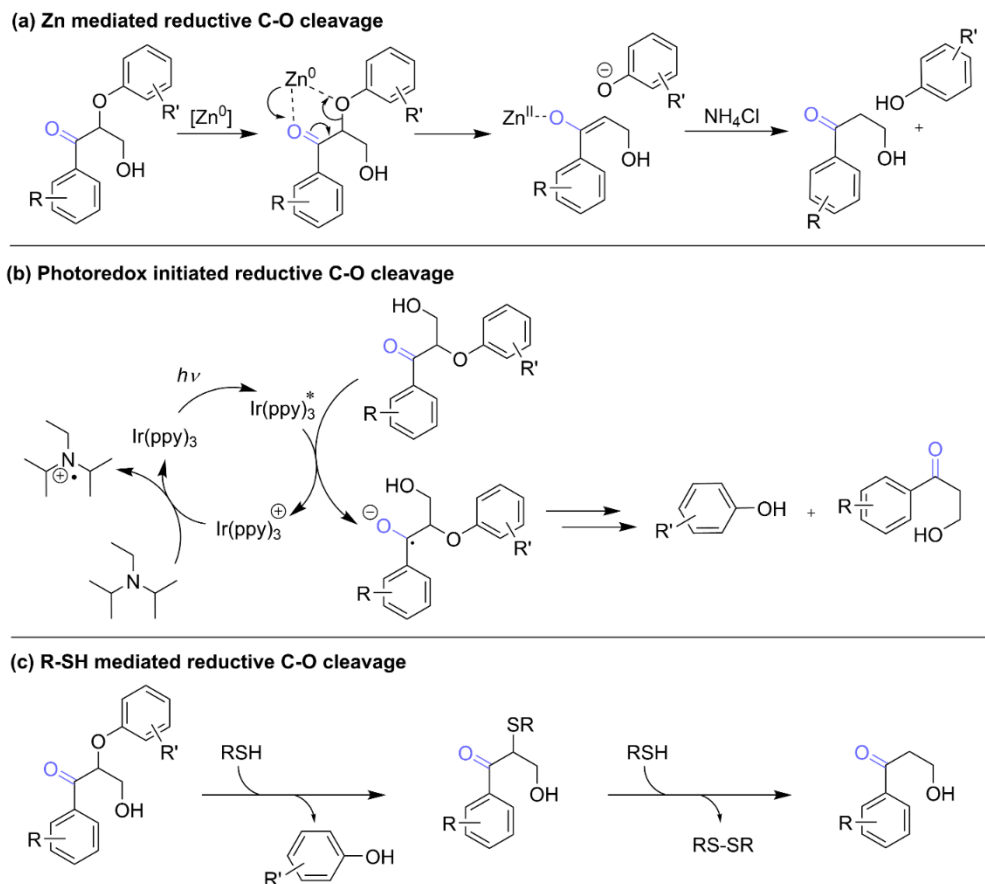


Figure 5.20. Mechanisms of reductive bond cleavage methods.

Wang and coworkers showed that oxidized lignin models are amenable to hydrogenolytic cleavage with a NiMoS_x catalyst. The C_β-OPh bond is cleaved without hydrogenation of the aromatic ring or the C_α ketone to afford phenols and benzylic ketones. The authors propose direct cleavage of the C_β-OPh bond on the NiMoS_x catalyst surface. This process was combined with an initial oxidation step using a NaNO₂/DDQ/NHPI oxidation system to afford a 32% yield of aromatic monomers from birch powder.⁹⁵

Wood-digesting bacteria feature enzymes that use thiol-containing tripeptide glutathione as a redox active cofactor to promote aryl ether cleavage in lignin. Examples include the Lig enzymes E, P, F (etherases) and G (lyase) *Sphingobium* sp. strain SYK 6.^{135,136} In this context, Hegg and coworkers demonstrated complementary chemical reactivity, exploiting the nucleophilic and reductive reactivity of small organic thiols to cleave aryl alkyl ether linkages in oxidized lignin model compounds (**Figure 5.20C**). Organic thiols, such as β-mercaptoethanol and dithiothreitol can promote cleavage in nearly quantitative yields with certain β-O-4 model compounds in acetonitrile containing K₂CO₃ as a basic additive.¹³⁷ They further employed small thiols (such as propanedithiol, 2-mercaptoethanol, and dithiothreitol) to support cleavage of model polymers and oxidized lignin materials bearing the C_α-ketone functionality. Thiol-dependent depolymerization is proposed to proceed via S_N2 attack adjacent to the ketone to release a phenol. The thiol is regenerated by nucleophilic attack of another thiol on the S-atom of the thioether to form a disulfide and ketone. Poplar lignin derived from a Cu-AHP extraction method⁷⁸ was oxidized using Bobbitt's salt (cf. **Figure 5.10**) and then incubated with β-mercaptoethanol. This oxidation/reductive cleavage sequence resulted in approximately 65% reduction of the lignin molecular weight.⁸³

5.5. Conclusions and Future Outlook

Lignin valorization remains a persistent challenge that is complicated by the complex structure of lignin and the difficulty in obtaining high-quality native-like lignin materials from biomass fractionation methods. Nonetheless, new methods for conversion of lignin into low molecular weight aromatic chemicals continue to emerge. The content outlined herein highlights the merits of bottom-up strategies to address this long-standing challenge. Consideration of the fundamental reactivity of individual functional groups prevalent in lignin—1° aliphatic and 2° benzylic alcohols—has enabled the development of sequential oxidation/depolymerization methods that successfully convert lignin into oxygenated aromatic chemicals. These efforts greatly benefitted from fundamental studies of well-defined model compounds that incorporate structural features directly present in lignin, especially those present in the common β -O-4 linkage. The development of selective, high-yielding methods for oxidation of the 1° or 2° alcohol in these compounds sets the stage for systematic development of various bond cleavage pathways that are enabled by the initial oxidation step. Insights gained from the well-defined model compounds were then translated into successful lignin depolymerization methods employing similar two-step methods. This approach has been used with a diverse array of lignin materials derived from different biomass plant sources, albeit favoring hardwoods, and different pretreatment/lignin-extraction methods. An appealing feature of this sequential depolymerization strategy is the ability to optimize each step independently, allowing the overall process to be optimized more effectively for individual feedstocks to maximize the yield of aromatic monomers.

Future work will benefit from studies focused on cleaving a broader array of linkages, as the majority of studies to date have focused on the alcohol containing β -O-4 unit. Although the β -O-4 fragment is prevalent in lignin, the development of methods capable of cleaving other linkages could greatly improve the monomer yield.

Another future priority will be the development of improved methods for direct oxidative catalytic fractionation (OCF) of biomass,^{40, 138, 139} resembling existing methods for RCF.^{12–18} Essentially all processes for lignin extraction damage the native lignin, generating recalcitrant subunits that limit the yields of aromatics that may be obtained from lignin. For example, under acidic conditions commonly used for lignin extraction, protonation of the benzylic alcohol in the β -O-4 unit can lead to the loss of water and formation of a benzyl cation that can cross-link the lignin polymer (i.e., via Friedel-Crafts alkylation). This reactivity converts a β -O-4 fragment, which is amenable to cleavage, into a new fragment that blocks depolymerization. OCF methods that oxidize the benzylic alcohol while lignin is still integrated within the biomass could provide a means to “protect” the lignin, while generating a material that is more amenable to depolymerization once the lignin is separated from the sugar. This concept and related approaches take Sequential oxidation-depolymerization strategies¹³¹ inspiration from the two-step oxidation/depolymerization studies outlined herein and could provide the basis for cost-effective valorization of whole biomass.

5.6. Acknowledgements

The lignin-based research in our laboratory and preparation of this article was supported in part by the Great Lakes Bioenergy Research Center, U.S. Department of Energy, Office of Science, Office of Biological and Environmental Research under Award Numbers DE-SC0018409 and DE-FC02-07ER64494 and in part by the U.S. Department of Energy, Office of Energy Efficiency & Renewable Energy under Contract No. DEEE0008148.

5.7. Reference

1. Ragauskas, A. J.; Beckham, G. T.; Biddy, M. J.; Chandra, R.; Chen, F.; Davis, M. F.; Davison, B. H.; Dixon, R. A.; Gilna, P.; Keller, M. *Science* **2014**, *344*.

2. Rinaldi, R.; Jastrzebski, R.; Clough, M. T.; Ralph, J.; Kennema, M.; Bruijninx, P. C.; Weckhuysen, B. M. *Angew. Chem. Int.* **2016**, *55*, 8164-8215.
3. Boerjan, W.; Ralph, J.; Baucher, M. *Annu. Rev. Plant Biol.* **2003**, *54*, 519-546.
4. Vanholme, R.; Morreel, K.; Ralph, J.; Boerjan, W. *Curr. Opin. Plant Biol.* **2008**, *11*, 278-285.
5. Schutyser, W.; Renders, a. T.; Van den Bosch, S.; Koelewijn, S.-F.; Beckham, G.; Sels, B. F. *Chem. Soc. Rev.* **2018**, *47*, 852-908.
6. Mu, W.; Ben, H.; Ragauskas, A.; Deng, Y. *Bioenergy Res.* **2013**, *6*, 1183-1204.
7. Parthasarathi, R.; Romero, R. A.; Redondo, A.; Gnanakaran, S. *J. Phys. Chem. Lett.* **2011**, *2*, 2660-2666.
8. Galkin, M. V.; Samec, J. S. *ChemSusChem* **2016**, *9*, 1544-1558.
9. Phongpreecha, T.; Hool, N. C.; Stoklosa, R. J.; Klett, A. S.; Foster, C. E.; Bhalla, A.; Holmes, D.; Thies, M. C.; Hodge, D. B. *Green Chem.* **2017**, *19*, 5131-5143.
10. Renders, T.; Van den Bossche, G.; Vangeel, T.; Van Aelst, K.; Sels, B. *Curr. Opin. Biotechnol.* **2019**, *56*, 193-201.
11. Cheng, C.; Shen, D.; Gu, S.; Luo, K. H. *Catal. Sci. Technol.* **2018**, *8*, 6275-6296.
12. Yan, N.; Zhao, C.; Dyson, P. J.; Wang, C.; Liu, L. T.; Kou, Y. *ChemSusChem* **2008**, *1*, 626-629.
13. Ferrini, P.; Rinaldi, R. *Angew. Chem. Int.* **2014**, *126*, 8778-8783.
14. Parsell, T.; Yohe, S.; Degenstein, J.; Jarrell, T.; Klein, I.; Gencer, E.; Hewetson, B.; Hurt, M.; Im Kim, J.; Choudhari, H.; Saha, B.; Meilan, R.; Mosier, N.; Ribeiro, R.; Deglass, W. N.; Chapple, C.; Kenttämaaam H. I.; Agrawal, R.; Abu-Omar, M. M. *Green Chem.* **2015**, *17*, 1492-1499.
15. Abu-Omar, M. M.; Barta, K.; Beckham, G. T.; Luterbacher, J.; Ralph, J.; Rinaldi, R.; Roman-Leshkov, Y.; Samec, J.; Sels, B.; Wang, F. *Energy Environ. Sci.* **2020**.
16. Schutyser, W.; Van den Bosch, S.; Dijkmans, J.; Turner, S.; Meledina, M.; Van Tendeloo, G.; Debecker, D. P.; Sels, B. F. *ChemSusChem* **2015**, *8*, 1805-1818.
17. Anderson, E. M.; Katahira, R.; Reed, M.; Resch, M. G.; Karp, E. M.; Beckham, G. T.; Román-Leshkov, Y. *ACS Sustain. Chem. Eng.* **2016**, *4*, 6940-6950.
18. Zhai, Y.; Li, C.; Xu, G.; Ma, Y.; Liu, X.; Zhang, Y. *Green Chem.* **2017**, *19*, 1895-1903.
19. Walton, N. J.; Mayer, M. J.; Narbad, A. *Phytochemistry* **2003**, *63*, 505-515.
20. Evju, H. US Patent 4151207A, **1979**.
21. Pinto, P. C. R.; Da Silva, E. A. B.; Rodrigues, A. E. In *Biomass Conversion*, Springer: Berlin, **2012**, pp. 381-420.
22. Fache, M.; Boutevin, B.; Caillol, S. *ACS Sustain. Chem. Eng.* **2016**, *4*, 35-46.

23. Ma, R.; Xu, Y.; Zhang, X. *ChemSusChem* **2015**, *8*, 24-51.
24. Yu, X.; Wei, Z.; Lu, Z.; Pei, H.; Wang, H. *Bioresour. Technol.* **2019**, *291*, 121885.
25. Beckham, G. T.; Johnson, C. W.; Karp, E. M.; Salvachúa, D.; Vardon, D. R. *Curr. Opin. Biotechnol.* **2016**, *42*, 40-53.
26. Perez, J. M.; Kontur, W. S.; Alherech, M.; Coplien, J.; Karlen, S. D.; Stahl, S. S.; Donohue, T. J.; Noguera, D. R. *Green Chem.* **2019**, *21*, 1340-1350.
27. Rahimi, A.; Azarpira, A.; Kim, H.; Ralph, J.; Stahl, S. S. *J. Am. Chem. Soc.* **2013**, *135*, 6415-6418.
28. Rahimi, A.; Ulbrich, A.; Coon, J. J.; Stahl, S. S. *Nature* **2014**, *515*, 249-252.
29. Das, A.; Rahimi, A.; Ulbrich, A.; Alherech, M.; Motagamwala, A. H.; Bhalla, A.; Da Costa Sousa, L.; Balan, V.; Dumesic, J. A.; Hegg, E. L. *ACS Sustain. Chem. Eng.* **2018**, *6*, 3367-3374.
30. Creighton, R.; McCarthy, J. L.; Hibbert, H. *J. Am. Chem. Soc.* **1941**, *63*, 3049-3052.
31. Pearl, I. A. *J. Am. Chem. Soc.* **1942**, *64*, 1429-1431.
32. Schultz, T. P.; Templeton, M. C. *Holzforschung* **1986**, *40*, 93-97.
33. Tarabanko, V. E.; Tarabanko, N. *Int. J. Mol. Sci.* **2017**, *18*, 2421-2449.
34. Chen, C.-L. In *Methods in lignin chemistry*, Springer: Berlin, **1992**, pp. 301-321.
35. Villar, J.; Caperos, A.; García-Ochoa, F. *J. Wood Chem. Technol.* **1997**, *17*, 259-285.
36. Gierer, J. *Wood Sci. Technol.* **1986**, *19*, 289-312.
37. Tarabanko, V.; Fomova, N.; Kuznetsov, B.; Ivanchenko, N.; Kudryashev, A. *React. Kinet. Catal. Lett.* **1995**, *55*, 161-170.
38. Bjørsvik, H.-R.; Minisci, F. Fine chemicals from liginosulfonates. *Org. Process Res. Dev.* **1999**, *3*, 330-340.
39. Klinke, H. B.; Ahring, B. K.; Schmidt, A. S.; Thomsen, A. B. *Bioresour. Technol.* **2002**, *82*, 15-26.
40. Schutyser, W.; Kruger, J. S.; Robinson, A. M.; Katahira, R.; Brandner, D. G.; Cleveland, N. S.; Mittal, A.; Peterson, D. J.; Meilan, R.; Román-Leshkov, Y.; Beckham, G. T. *Green Chem.* **2018**, *20*, 3828-3844.
41. Kuznetsov, B.; Sudakova, I.; Garyntseva, N.; Tarabanko, V.; Yatsenkova, O.; Djakovitch, L.; Rataboul, F. *Catal. Today* **2020**, *in press*.
42. Hatakka, A. *FEMS Microbiol. Rev.* **1994**, *13*, 125-135.
43. Eggert, C.; Temp, U.; Dean, J. F.; Eriksson, K.-E. L. *Febs Lett.* **1996**, *391*, 144-148.
44. Lange, H.; Decina, S.; Crestini, C. *Eur. Polym. J.* **2013**, *49*, 1151-1173.
45. Artaud, I.; Ben-Aziza, K.; Mansuy, D. *J. Org. Chem.* **1993**, *58*, 3373-3380.

46. Dolphin, D.; Traylor, T. G.; Xie, L. Y. *Acc. Chem. Res.* **1997**, *30*, 251-259.
47. Zhu, C.; Ding, W.; Shen, T.; Tang, C.; Sun, C.; Xu, S.; Chen, Y.; Wu, J.; Ying, H. *ChemSusChem* **2015**, *8*, 1768-1778.
48. Nichols, J. M.; Bishop, L. M.; Bergman, R. G.; Ellman, J. A. *J. Am. Chem. Soc.* **2010**, *132*, 12554-12555.
49. Wu, A.; Patrick, B. O.; Chung, E.; James, B. R. *Dalton Trans.* **2012**, *41*, 11093-11106.
50. Chmely, S. C.; Kim, S.; Ciesielski, P. N.; Jiménez-Osés, G.; Paton, R. S.; Beckham, G. T. *ACS Catal.* **2013**, *3*, 963-974.
51. Huo, W.; Li, W.; Zhang, M.; Fan, W.; Chang, H. M.; Jameel, H. *Catal. Lett.* **2014**, *144*, 1159-1163.
52. Wu, A.; Lauzon, J. M.; James, B. R. *Catal. Lett.* **2015**, *145*, 511-518.
53. vom Stein, T.; den Hartog, T.; Buendia, J.; Stoychev, S.; Mottweiler, J.; Bolm, C.; Klankermayer, J.; Leitner, W. *Angew. Chem. Int.* **2015**, *127*, 5957-5961.
54. Hanson, S. K.; Baker, R. T. *Acc. Chem. Res.* **2015**, *48*, 2037-2048.
55. Son, S.; Toste, F. D. *Angew. Chem. Int.* **2010**, *49*, 3791-3794.
56. Chan, J. M.; Bauer, S.; Sorek, H.; Sreekumar, S.; Wang, K.; Toste, F. D. *ACS Catal.* **2013**, *3*, 1369-1377.
57. Hanson, S. K.; Wu, R.; Silks, L. A. P. *Angew. Chem. Int.* **2012**, *124*, 3466-3469.
58. Díaz-Urrutia, C.; Chen, W.-C.; Crites, C.-O.; Daccache, J.; Korobkov, I.; Baker, R. T. *RSC Adv.* **2015**, *5*, 70502-70511.
59. Sedai, B.; Diaz-Urrutia, C.; Baker, R. T.; Wu, R.; Silks, L. P.; Hanson, S. K. *ACS Catal.* **2011**, *1*, 794-804.
60. Zhang, G.; Scott, B. L.; Wu, R.; Silks, L. P.; Hanson, S. K. *Inorg. Chem.* **2012**, *51*, 7354-7361.
61. Liu, Y.; Li, C.; Miao, W.; Tang, W.; Xue, D.; Li, C.; Zhang, B.; Xiao, J.; Wang, A.; Zhang, T. *ACS Catal.* **2019**, *9*, 4441-4447.
62. Jastrzebski, R.; Constant, S.; Lancefield, C. S.; Westwood, N. J.; Weckhuysen, B. M.; Bruijninx, P. C. A. *ChemSusChem*, **2016**, *9*, 2074-2079.
63. Basolo, F.; Hoffman, B. M.; Ibers, J. A. *Acc. Chem. Res.* **1975**, *8*, 384-392.
64. Zombeck, A.; Drago, R. S.; Corden, B. B.; Gaul, J. H. *J. Am. Chem. Soc.* **1981**, *103*, 7580-7585.
65. Bozell, J. J.; Hames, B. R.; Dimmel, D. R. *J. Org. Chem.* **1995**, *60*, 2398-2404.
66. Biannic, B.; Bozell, J. J. *Org. Lett.* **2013**, *15*, 2730-2733.
67. Ryland, B. L.; Stahl, S. S. *Angew. Chem. Int.* **2014**, *53*, 8824-8838.

68. Hoover, J. M.; Stahl, S. S. *J. Am. Chem. Soc.* **2011**, *133*, 16901-16910.
69. Cho, D. W.; Parthasarathi, R.; Pimentel, A. S.; Maestas, G. D.; Park, H. J.; Yoon, U. C.; Dunaway-Mariano, D.; Gnanakaran, S.; Langan, P.; Mariano, P. S. *J. Org. Chem.* **2010**, *75*, 6549-6562.
70. Elder, T. *Holzforschung* **2010**, *64*, 435-440.
71. Kim, S.; Chmely, S. C.; Nimlos, M. R.; Bomble, Y. J.; Foust, T. D.; Paton, R. S.; Beckham, G. T. *J. Phys. Chem. Lett.* **2011**, *2*, 2846-2852.
72. Nutting, J. E.; Rafiee, M.; Stahl, S. S. *Chem. Rev.* **2018**, *118*, 4834-4885.
73. Bobbitt, J. M.; Brückner, C.; Merbouh, N. *Org. React.* **2009**, *74*, 103-424.
74. Hibino, T.; Shibata, D.; Ito, T.; Tsuchiya, D.; Higuchi, T.; Pollet, B.; Lapierre, C. *Phytochemistry* **1994**, *37*, 445-448.
75. Luterbacher, J. S.; Rand, J. M.; Alonso, D. M.; Han, J.; Youngquist, J. T.; Maravelias, C. T.; Pfleger, B. F.; Dumesic, J. A. *Science* **2014**, *343*, 277-280.
76. da Costa Sousa, L.; Foston, M.; Bokade, V.; Azarpira, A.; Lu, F.; Ragauskas, A. J.; Ralph, J.; Dale, B.; Balan, V. *Green Chem.* **2016**, *18*, 4205-4215.
77. da Costa Sousa, L.; Jin, M.; Chundawat, S. P. S.; Bokade, V.; Tang, X.; Azarpira, A.; Lu, F.; Avci, U.; Humpula, J.; Uppugundla, N.; Gunawan, C.; Pattathil, S.; Cheh, A. M.; Kothari, N.; Kumar, R.; Ralph, J.; Hahn, M. G.; Wyman, C. E.; Singh, S.; Simmons, B. A.; Dale, B. E.; Balan, V. *Energy Environ. Sci.* **2016**, *9*, 1215-1223.
78. Bhalla, A.; Bansal, N.; Stoklosa, R. J.; Fountain, M.; Ralph, J.; Hodge, D. B.; Hegg, E. L. *Biotechnol. Biofuels* **2016**, *9*, 34, 1-10.
79. Patil, N. D.; Yao, S. G.; Meier, M. S.; Mobley, J. K.; Crocker, M. *Org. Biomol. Chem.* **2015**, *13*, 3243-3254.
80. Wang, M.; Lu, J.; Zhang, X.; Li, L.; Li, H.; Luo, N.; Wang, F. *ACS Catal.* **2016**, *6*, 6086-6090.
81. Dabral, S.; Wotruba, H.; Hernández, J. G.; Bolm, C. *ACS Sustain. Chem. Eng.* **2018**, *6*, 3242-3254.
82. Nguyen, J. D.; Matsuura, B. S.; Stephenson, C. R. *J. Am. Chem. Soc.* **2014**, *136*, 1218-1221.
83. Klinger, G. E.; Zhou, Y.; Foote, J. A.; Wester, A. M.; Cui, Y.; Alherech, M.; Stahl, S. S.; Jackson, J. E.; Hegg, E. L. *ChemSusChem* **2020**, *13*, 4394-4399.
84. Sheldon, R. A.; Arends, I. W. *Adv. Synth. Catal.* **2004**, *346*, 1051-1071.
85. Shiraishi, T.; Takano, T.; Kamitakahara, H.; Nakatsubo, F. *Holzforschung* **2012**, *66*, 311-315.
86. Bosque, I.; Magallanes, G.; Rigoulet, M.; Kärkäs, M. D.; Stephenson, C. R. *ACS Cent. Sci.* **2017**, *3*, 621-628.
87. Masui, M.; Hosomi, K.; Tsuchida, K.; Ozaki, S. *Chem. Pharm. Bull.* **1985**, *33*, 4798-4802.

88. Masui, M.; Hara, S.; Ozaki, S. *Chem. Pharm. Bull.* **1986**, *34*, 975-979.
89. Hruszkewycz, D. P.; Miles, K. C.; Thiel, O. R.; Stahl, S. S. *Chem. Sci.* **2017**, *8*, 1282-1287.
90. Li, S.; Li, Z.-J.; Yu, H.; Sytu, M. R.; Wang, Y.; Beerli, D.; Zheng, W.; Sherman, B. D.; Yoo, C. G.; Leem, G. *ACS Energy Lett.* **2020**, *5*, 777-784.
91. Leigh, W. J.; Lathioor, E. C.; St. Pierre, M. J. *J. Am. Chem. Soc.* **1996**, *118*, 12339-12348.
92. Galian, R. E.; Litwinienko, G.; Pérez-Prieto, J.; Ingold, K. U. *J. Am. Chem. Soc.* **2007**, *129*, 9280-9281.
93. Luo, J.; Zhang, J. *J. Org. Chem.* **2016**, *81*, 9131-9137.
94. Recuperero, F.; Punta, C. *Chem. Rev.* **2007**, *107*, 3800-3842.
95. Zhang, C.; Li, H.; Lu, J.; Zhang, X.; MacArthur, K. E.; Heggen, M.; Wang, F. *ACS Catal.* **2017**, *7*, 3419-3429.
96. Walker, D.; Hiebert, J. D. *Chem. Rev.* **1967**, *67*, 153-195.
97. Wurche F.; Sicking W.; Sustmann R.; Klärner F.-G.; Rüchardt C. *Chem. Eur. J.* **2004**, *10*, 2707-2721.
98. Wendlandt, A. E.; Stahl, S. S. *Angew. Chem. Int.* **2015**, *54*, 14638-14658.
99. Shen, Z.; Dai, J.; Xiong, J.; He, X.; Mo, W.; Hu, B.; Sun, N.; Hu, X. *Adv. Synth. Catal.* **2011**, *353*, 3031-3038.
100. Wang, L.; Li, J.; Yang, H.; Lv, Y.; Gao, S. *J. Org. Chem.* **2012**, *77*, 790-794.
101. Katsina, T.; Clavier, L.; Giffard, J.-F.; Macedo Portela da Silva, N.; Fournier, J.; Tamion, R.; Copin, C.; Arseniyadis, S.; Jean, A. *Org. Process Res. Dev.* **2020**, *24*, 856-860.
102. Walsh, K.; Sneddon, H. F.; Moody, C. J. *Org. Lett.* **2014**, *16*, 5224-5227.
103. Ohkubo, K.; Fujimoto, A.; Fukuzumi, S. *J. Am. Chem. Soc.* **2013**, *135*, 5368-5371.
104. Lancefield, C. S.; Ojo, O. S.; Tran, F.; Westwood, N. J. *Angew. Chem. Int.* **2015**, *127*, 260-264.
105. Guo, H.; Miles-Barrett, D. M.; Neal, A. R.; Zhang, T.; Li, C.; Westwood, N. J. *Chem. Sci.* **2018**, *9*, 702-711.
106. Lee-Ruff, E.; Ablenas, F. *Can. J. Chem.* **1989**, *67*, 699-702.
107. Shuai, L.; Amiri, M. T.; Questell-Santiago, Y. M.; Héroguel, F.; Li, Y.; Kim, H.; Meilan, R.; Chapple, C.; Ralph, J.; Luterbacher, J. S. *Science* **2016**, *354*, 329-333.
108. Lan, W.; de Bueren, J. B.; Luterbacher, J. S. *Angew. Chem. Int.* **2019**, *58*, 2649-2654.
109. Song, Y.; Motagamwala, A. H.; Karlen, S. D.; Dumesic, J. A.; Ralph, J.; Mobley, J. K.; Crocker, M. *Green Chem.* **2019**, *21*, 3940-3947.

110. Lancefield, C. S.; Rashid, G. M.; Bouxin, F.; Wasak, A.; Tu, W.-C.; Hallett, J.; Zein, S.; Rodríguez, J.; Jackson, S. D.; Westwood, N. J.; Bugg, D. T. *ACS Sustain. Chem. Eng.* **2016**, *4*, 6921-6930.
111. Yao, S. G.; Mobley, J. K.; Ralph, J.; Crocker, M.; Parkin, S.; Selegue, J. P.; Meier, M. S. *ACS Sustain. Chem. Eng.* **2018**, *6*, 5990-5998.
112. Zhu, R.; Wang, B.; Cui, M.; Deng, J.; Li, X.; Ma, Y.; Fu, Y. *Green Chem.* **2016**, *18*, 2029-2036.
113. Dawange, M.; Galkin, M. V.; Samec, J. S. *ChemCatChem* **2015**, *7*, 401-404.
114. Galkin, M. V.; Sawadjoon, S.; Rohde, V.; Dawange, M.; Samec, J. S. *ChemCatChem* **2014**, *6*, 179-184.
115. Deng, W.; Zhang, H.; Wu, X.; Li, R.; Zhang, Q.; Wang, Y. *Green Chem.* **2015**, *17*, 5009-5018.
116. Chen, Z.; Xu, J.; Ren, Z.; He, Y.; Xiao, G. *J. Solid State Chem.* **2013**, *205*, 134-141.
117. Song, Y.; Mobley, J. K.; Motagamwala, A. H.; Isaacs, M.; Dumesic, J. A.; Ralph, J.; Lee, A. F.; Wilson, K.; Crocker, M. *Chem Sci.* **2018**, *9*, 8127-8133.
118. Ryland, B. L.; McCann, S. D.; Brunold, T. C.; Stahl, S. S. *J. Am. Chem. Soc.* **2014**, *136*, 12166-12173.
119. Dabral, S.; Hernández, J. G.; Kamer, P. C.; Bolm, C. *ChemSusChem* **2017**, *10*, 2707-2713.
120. Rafiee, M.; Alherech, M.; Karlen, S. D.; Stahl, S. S. *J. Am. Chem. Soc.* **2019**, *141*, 15266-15276.
121. Sannami, Y.; Kamitakahara, H.; Takano, T. *Holzforchung* **2017**, *71*, 109-117.
122. Lancefield, C. S.; Teunissen, L. W.; Weckhuysen, B. M.; Bruijninx, P. C. *Green Chem.* **2018**, *20*, 3214-3221.
123. Miles-Barrett, D. M.; Neal, A. R.; Hand, C.; Montgomery, J. R.; Panovic, I.; Ojo, O. S.; Lancefield, C. S.; Cordes, D. B.; Slawin, A. M.; Lebl, T.; Westwood, N. J. *Org. Biomol. Chem.* **2016**, *14*, 10023-10030.
124. Deuss, P. J.; Scott, M.; Tran, F.; Westwood, N. J.; de Vries, J. G.; Barta, K. *J. Am. Chem. Soc.* **2015**, *137*, 7456-7467.
125. Einhorn, J.; Einhorn, C.; Ratajczak, F.; Pierre, J.-L. *J. Org. Chem.* **1996**, *61*, 7452-7454.
126. Xiao, G.; Lancefield, C.; Westwood, N. J. *ChemCatChem* **2019**, *11*, 3182-3186.
127. Ling, K. B.; Smith, A. D. *Chem. Commun.* **2011**, *47*, 373-375.
128. Wang, Y.; Wang, Q.; He, J.; Zhang, Y. *Green Chem.* **2017**, *19*, 3135-3141.
129. Yang, W.; Du, X.; Liu, W.; Tricker, A. W.; Dai, H.; Deng, Y. *Energy Fuels* **2019**, *33*, 6483-6490.
130. Sun, C.; Zheng, L.; Xu, W.; Dushkin, A.V.; and Su, W. *Green Chem.* **2020**, *22*, 3489-3494.

131. Yanagita, M.; Yamakawa, K. *J. Org. Chem.* **1959**, *24*, 903-909.
132. Ibuka, T.; Hayashi, K.; Minakata, H.; Inubushi, Y. *Tetrahedron Lett.* **1979**, *2*, 159-160.
133. Yao, Z.; Ye, D.; Liu, H.; Chen, K.; Jiang, H. *Synth. Commun.* **2007**, *37*, 149-156.
134. Hao, Z.; Li, S.; Sun, J.; Li, S.; Zhang, F. *Appl. Catal. B* **2018**, *237*, 366-372.
135. Pereira, J. H.; Heins, R. A.; Gall, D. L.; McAndrew, R. P.; Deng, K.; Holland, K. C.; Donohue, T. J.; Noguera, D. R.; Simmons, B. A.; Sale, K. L.; Ralph, J.; Adams, P. D. *J. Biol. Chem.* **2016**, *291*, 10228-10238.
136. Kamimura, N.; Takahashi, K.; Mori, K.; Araki, T.; Fujita, M.; Higuchi, Y.; Masai, E. *Appl. Environ. Microbiol.* **2017**, *9*, 679-705.
137. Klinger, G. E.; Zhou, Y.; Hao, P.; Robbins, J.; Aquilina, J. M.; Jackson, J. E.; Hegg, E. L. *ChemSusChem* **2019**, *12*, 4775-4779.
138. Zhu, Y.; Liao, Y.; Lv, W.; Liu, J.; Song, X.; Chen, L.; Wang, C.; Sels, B. F.; Ma, L. *ACS Sustain. Chem. Eng.* **2020**, *8*, 2361-2374.
139. Vangeel, T.; Schutyser, W.; Renders, T.; Sels, B. F. In *Lignin Chemistry*, Springer: Cham, **2020**; pp. 53-68.

Chapter 6: Fundamental Studies of *N*-Oxyl Radicals: Assessment of Stability, Bond Strength, and Time-Delayed Alcohol Oxidation

This work was performed with Mohammad Rafiee and Shannon S. Stahl.

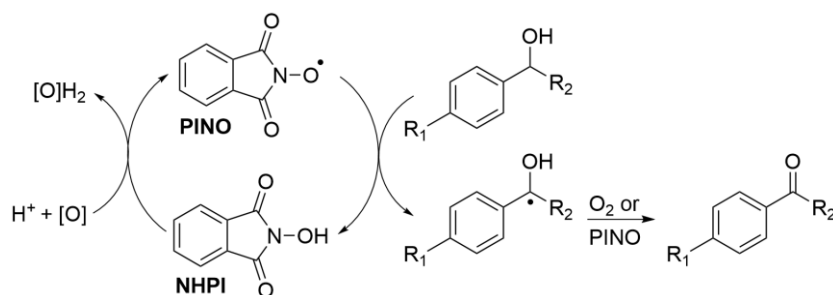
6.1. Abstract

Electrochemical studies of the pH, concentration, and time-dependent degradation and O–H bond strength and were conducted using a variety of *N*-oxyl radicals mediators, including five oximes. The relationship between stability and oxidative driving force is assessed. Stable oxime mediator violuric acid (VA) enables further probing into the alcohol oxidation mechanism and demonstrates utility for time-delayed addition of alcohol substrate to stoichiometric electrochemically generated radical.

6.2. Introduction

N-oxyl radicals represent a special class of stabilized organic radicals that are privileged catalysts and mediators for selective alcohol oxidation reactions.^{1,2} Among the most popular members of this class of radicals, phthalimide *N*-oxyl (PINO) radical can rapidly abstract weak C–H bonds like those found in secondary benzylic alcohols (**Scheme 6.1**). PINO, generated in situ from *N*-hydroxyphthalimide (NHPI), has proven effective for chemical and electrochemical oxidation of secondary aliphatic and benzylic alcohols and diols.³ Basic conditions are typically favored in these reactions to promote rates of catalyst regeneration and hydrogen atom transfer (HAT), despite facilitating base-catalyzed decomposition of the radical.^{4,5}

Scheme 6.1. NHPI-mediated oxidation of alcohols.



The conditions required for high turnover of NHPI limit the use of NHPI for specialized applications involving insoluble secondary alcohol substrates.⁶ Lignin is a polymeric component of biomass and contains a secondary benzylic alcohol as part of the primary linkage between units.

NHPI-mediated oxidation of soluble, isolated lignin facilitates depolymerization to high yields of aromatic monomers.⁷ However, the oxidation of lignin in whole cell biomass, which is insoluble under desirable mild, aqueous conditions, relies on diffusion of the mediator into the substrate. Much of the work in this area, particularly for the oxidative delignification of biomass, is devoted to exploring other *N*-oxyl radical mediators.⁸⁹¹⁰¹¹¹²¹³¹⁴¹⁵¹⁶¹⁷

Aminoxyl benzotriazole *N*-oxyl (BtNO) and iminoxyl violuric acid *N*-oxyl (VANO) radicals have emerged as attractive mediators for HAT from insoluble substrates containing benzylic secondary alcohol functionalities.¹⁸ The latter belongs to a class of persistent σ -radicals. Radical lifetimes on the order of hours or even days are reported for sterically hindered iminoxyl radicals under various conditions.¹⁹²⁰²¹ Fundamental studies of *N*-oxyl mediated secondary benzylic alcohol oxidation reveal that VANO exhibits the slowest rates of alcohol oxidation in comparison to imidoxyl mediators.²² Thermodynamic data collected for these and other *N*-oxyl radicals collected under different experimental conditions cannot be compared directly,²³ and few fundamental studies of water soluble iminoxyls other than VANO exist.¹⁹

The tunable oxidation potential and well-defined surface of glassy carbon electrodes used for electrochemical generation of *N*-oxyl radicals are well-suited for standardized fundamental analysis of radical stability. Electrochemically determined redox potentials can also be used for accurate measurements of mediator O-H bond strength.²⁴ For HAT mediators, this is a measure of the thermodynamic driving force for HAT. Further, on/off control of electrochemical radical generation enables independent analysis of the radical and subsequent chemical steps.

Herein, we use cyclic voltammetry (CV) to analyze the pH and concentration dependent stability and bond dissociation free energy (BDFE) of radicals generated from a selection of imidoxyl, aminoxyl, and iminoxyl mediators (**Figure 6.1**). Stable oxime mediator violuric acid

(VA) enables further probing into the alcohol oxidation mechanism and enables time-delayed addition of alcohol substrate to stoichiometric electrochemically generated radical. This type of “oxidant pool” reaction is traditionally used for the electrochemical synthesis of stable hypervalent iodine reagents²⁵ and the generation of oxoammonium using bleach.²⁶ Addition of alcohol substrate to VANO generated up to 2 h prior to substrate addition yields ketone products in excess of 75%.

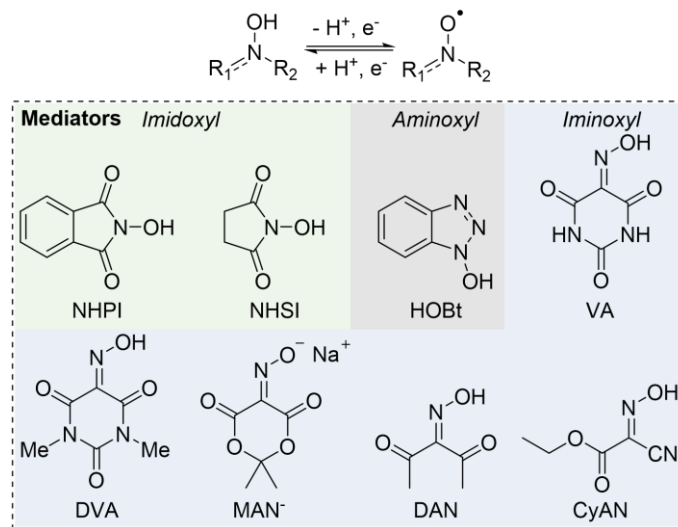


Figure 6.1. Mediators investigated in this study and typical redox states.

6.3. Results and Discussion

6.3.1. Radical Stability and Bond Dissociation Free Energy Studies

Cyclic voltammograms of iminoxyls VA, DVA, MAN, DAN, and CyAN and imidoxyls NHPI and NHSI reveal pH-dependent redox features for the electrochemical oxidation of mediators (Med-H) to *N*-oxyl radical (Med[•]) and, in some cases, the reduction of electrogenerated Med[•] to Med-H at the electrode surface (**Figure 6.2a**). By varying the identity of the buffering electrolyte, it is possible to maintain well-buffered conditions across a wide pH range while performing CV experiments.

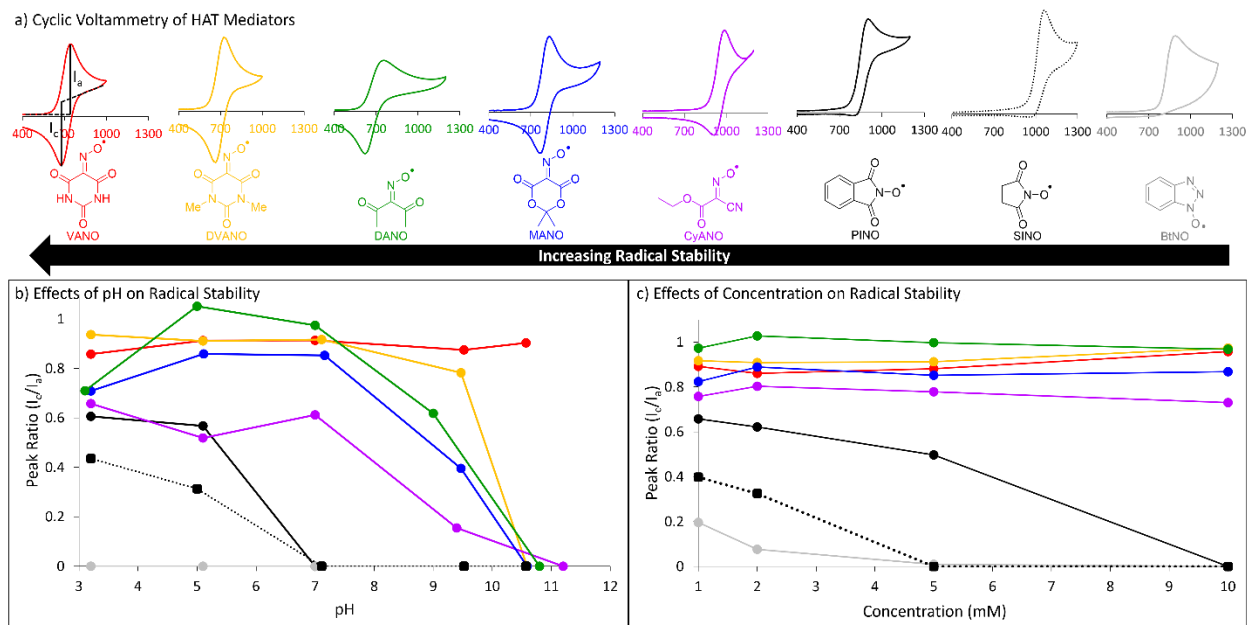


Figure 6.2. Cyclic voltammograms of (a) 1 mM HAT mediators (NHPI, NHSI, HOBt, VA, DVA, MAN salt, DAN, and CyAN) in 0.1 M pH 5 acetate buffer at a scan rate of 20 mV/s, and peak current ratio analysis over (b) pH range 3-10.5 and (c) concentration range 1-10 mM.

The ratio of the magnitude of the anodic to cathodic CV current (I_c/I_a) is an indication of the chemical stability of the electrogenerated radicals. As the potential is scanned forward at a set rate towards more positive potentials, the Med-H is oxidized to Med \cdot . During the reverse scan towards more negative potentials, the radical generated during the reverse scan is reduced at the electrode surface. Radicals that have undergone a chemical reaction to form a new species cannot be reduced at the same potential during the reverse scan, leading to a classic electrochemical-chemical wave. The extent of chemical degradation is dependent on the scan rate. Reversible to quasi-reversible CV's ($I_c/I_a > 0.7$) demonstrate relatively high Med \cdot stability and quasi-irreversible or irreversible CVs ($I_c/I_a < 0.2$) indicate poor radical stability on the CV timescale.

Base catalyzed decomposition of the PINO radical to electrochemically inactive dimer and trimer molecules has been reported in the literature,^{27,28} and explains a general decrease in imidoxyl radical stability with increasing pH (**Figure 6.2b**). At pH 7, imidoxyl mediators become

irreversible while all tested iminoxyls maintain some radical stability on the CV timescale (20 mV/s) until pH 10.5. The pH-dependent stability of iminoxyl mediators does not correlate to the pK_a of the mediator (cf. **Table 6.1**), unlike the imidoxyls.²⁸ The stability of VA is pH independent. The CV data for NHPI, VA, and DVA are consistent with the pH-dependent CV features reported under similar buffer-aqueous conditions.^{19,27,29}

The CV shape for DAN at pH 3-5 indicates an acidic chemical step may precede the first electrochemical step. At these pH, I_c/I_a should not be considered an accurate measure of radical stability.³⁰

The CVs for DVA, MAN, CyAN, NHPI, NHSI, and DAN (only pH 5-7) indicate a shift within error of the 59 mV per pH unit intrinsic to HAT processes. VA has three reported pK_a s corresponding to the O-H and two N-H bonds in the molecule. Without further collection of data at pHs below the first reported pK_a at 4.5, a trend of 59 mV per pH unit could not be established. Above the mediator pK_a , the Med^+/Med^- redox potential is pH insensitive, as would be expected from a process that does not produce or consume protons (SI).

To simulate stability measurements of mediators under typical 5-10 mM concentrations (10 mol%) used for alcohol oxidation reactions with NHPI,³¹ additional CVs were collected at pH 5 for 2, 5, and 10 mM mediator (**Figure 6.2c**). Imidoxyl mediators NHSI and NHPI show complete irreversibility at 5 mM and 10 mM respectively, and iminoxyl mediators show little to no decrease in stability with increasing mediator concentration.

The presence of both relevant oxidation and reduction peaks at low pH for all mediators except HOBt allows for the estimation of a thermodynamically significant midpoint potential. Midpoint potentials used for DAN at pH 5 and 7 give rise to the same calculated BDFE (within 0.1 kcal/mol). In the case of HOBt, which does not exhibit a $Med^+/Med-H$ reduction at any

potential, differential pulse voltammetry (DPV) was used to determine the midpoint potential (SI). These potentials were used to determine the bond dissociation free energy of the mediator O-H bonds.

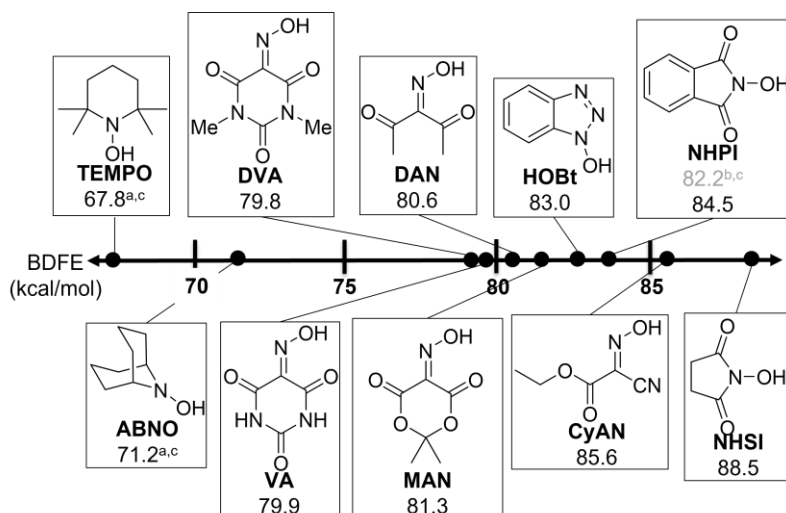
Using the equation for the determination of the bond dissociation free energy (eq 1),²⁴

$$\text{BDFE (Med-H)} = 23.06(E_{\text{pH Med-H/Med}^*}) + 1.37(\text{pH}) + 52.8 \text{ kcal/mol} \quad (1)$$

the relative O-H bond strength of each mediator can be determined from the pH-dependent Med-H/Med* redox potential versus NHE in a buffered aqueous solution of known pH. Midpoint potentials are an average of three repeat values. The pK_a for each mediator was determined by NMR spectroscopy, except for VA and DAN, and is within the pK_a range determined voltammetrically (SI). A correction factor of 52.8 kcal/mol for the E°(H⁺/H*) in aqueous solvent is applied.²⁴ Relative uncertainties for this data are ≤ 0.3 kcal/mol and absolute uncertainties are approximated as ± 1 kcal/mol (SI).

Calculated BDFE data and the paired stability data illustrate a generally inverse relationship between the thermodynamic driving force for HAT and radical stability. All cyclic iminoxyls and DAN have BDFE's in the range of 83-85 kcal/mol (**Table 6.1**, Entries 1-3 and 5). Imidoxyls and HOBt exhibit higher BDFE's and correspondingly lower pH- and concentration-dependent radical stability (**Table 6.1**, Entries 6-8). Interestingly, the iminoxyl CyAN has a comparable BDFE to NHPI (**Table 6.1**, Entry 4), but shows greater radical stability in CV studies. Reliable and comparable literature values for well-known *N*-oxyls 2,2,6,6-tetramethylpiperidine-*N*-oxyl (TEMPO)/TEMPOH and the related 9-azabicyclo[3.3.1]nonane-*N*-oxyl (ABNO)/ABNOH derivative have been included for reference.³²

Table 6.1. Comparative bond dissociation free energies for *N*-oxyl mediators in H₂O.



Entry	Mediator	$E^{1/2}$ (mV v. NHE); pH	pK_{a1}	BDFE (kcal/mol)
1	VA	988; 3.2	3.8 ^d	80.0
2	DVA	981; 3.2	5.29	79.8
3	MAN	1044; 3.2	4.65	81.3
4	CyAN	1231; 3.2	4.94	85.6
5	DAN	924; 5	7-9 ^e	80.6
6	NHPI	1066; 5.1	6.85	84.5
7	NHSI	1245; 5	6.15	88.5
8	HOBt	1124; 3.1	4.63	83.0

^aStahl, S. S. *et al. J. Org. Chem.*, **2018**, *83*, 7323-7330. ^bMayer, J. M. *et al. Chem. Rev.* **2010**, *110*, 6961-7001. ^cCorrected using $C_G = 52.8$ kcal/mol. ^d pK_a reported by Kim, H-C., Mickel, M., and Hampp in *N. Chem. Phys. Lett.* **2003**, *371*, 410-416. ^e pK_a range determined voltametrically.

HOBt represents the only exception to the general BDFE v. radical stability trend, exhibiting a lower BDFE and lower radical stability as compared to CyAN, NHPI, and NHSI. Benzotriazole N-oxyl (BtNO) decomposition, presumably to benzotriazole, has been reported to be faster in the presence of H-bond donors.³³ Quasi-reversible CVs of HOBt have been recorded at scan rates of 2 V/s, and a half-life of 110 s in MeCN was reported by Galli and coworkers, indicating a rapid radical decay on typical CV timescale.³⁴

Electrochemical radical generation and subsequent radical decay were measured under relevant bulk electrolysis conditions for lignin-first biomass oxidation. Using constant current electrolysis, a 10 mM mediator solution in mixed 1:1 pH 1 aq.: MeCN was oxidized at 5 mA for

2.1 F/mol and the electrochemical generation of radical was monitored by microelectrode linear sweep voltammetry (LSV) (SI). The mediator solution was transferred to a rotating disk electrode (RDE) cell, and the decay in current arising from the reduction of radical concentration was measured beginning at 1.5 min after the end of bulk electrolysis. The measured current is proportional to the concentration of the radical and fixed at 1 for the initial point of data collection. Measurable quantities of NHSI, HOBt, and CyAN could not be generated using this method, reflecting general trends of instability observed by CV for mediators with high BDFE.

Normalized current plots of time-dependent radical decay further illustrate the instability of PINO as compared to iminoxyl radicals and support the stability trends observed in the CV studies (**Figure 6.3**). VA and the closely related DVA both show long radical lifetimes as compared to PINO. Although CV and half-life¹⁹ measurements at high pH in aqueous solution show a decrease in DVANO stability as compared to VA, both studies demonstrate DVANO is more stable under highly acidic conditions. A slow initial decay phase, followed by a faster rate of decay indicates a complicated degradation mechanism. DANO degradation may be controlled by the formation of head-to-tail dimers, as is observed with other linear oximes.²⁰ MAN exhibits only slightly better stability than PINO.

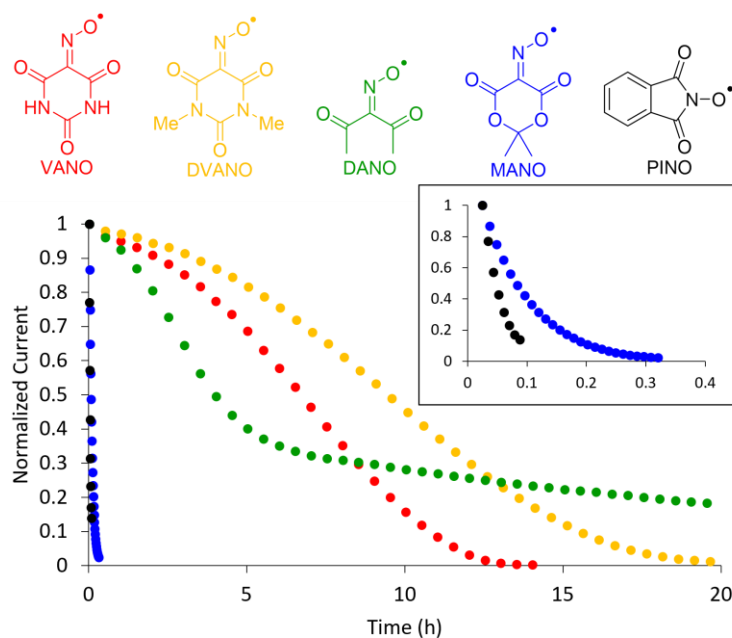


Figure 6.3. Normalized currents obtained from rotating disk electrode linear sweep voltammograms of a 10 mM radical solution generated from bulk electrolysis (graphite working electrode, Pt wire counter electrode, 3 M KCl Ag/AgCl reference electrode; 5 mA; 2.1 F/mol) of VA (red), DVA (yellow), DAN (green), MAN salt (blue), and NHPI (black). Glassy carbon working electrode, Pt wire counter electrode, 3 M KCl Ag/AgCl reference electrode; 10000 rpm, 20 mV/s; 1.5 minutes between end of bulk electrolysis and start of data collection.

6.3.2. Mediated Oxidation of Secondary Benzylic Alcohols

The high stability of VANO under acidic conditions allows for near-stoichiometric electrochemical generation of radical in situ, which opens new avenues for probing the proposed sequential HAT steps for mediated alcohol oxidation. The KIE, Hammett correlations, and oxidized products of probe substrates in an HOBt, NHPI, or VA mediated O_2 /laccase system were consistent with rate-limiting HAT from alcohol.¹⁸ Subsequent cleavage of the O-H bond from the radical intermediate may also be radical-mediated, but this step has not yet been probed directly for HAT mediators.^{12,35} To exclude any mechanistic role of oxygen (**Figure 6.4**), a N_2 purged solution containing 2 equivalents of VA was electrolyzed at 5 mA in N_2 atmosphere. The VANO solution was added to 4-methoxy- α -methylbenzyl alcohol substrate **1** in N_2 atmosphere. The mixed solvent facilitated solubility of substrate and mediator, resulting in 80% yield of carbonyl product **2**. The

yield for a reaction performed in air is the same (85%). When one equivalent of VA substrate is oxidized and allowed to react with one equivalent of alcohol substrate in air, 44% yield, slightly less than theoretical yield, was achieved, demonstrating that VANO mediates both HAT steps even in the presence of O₂.

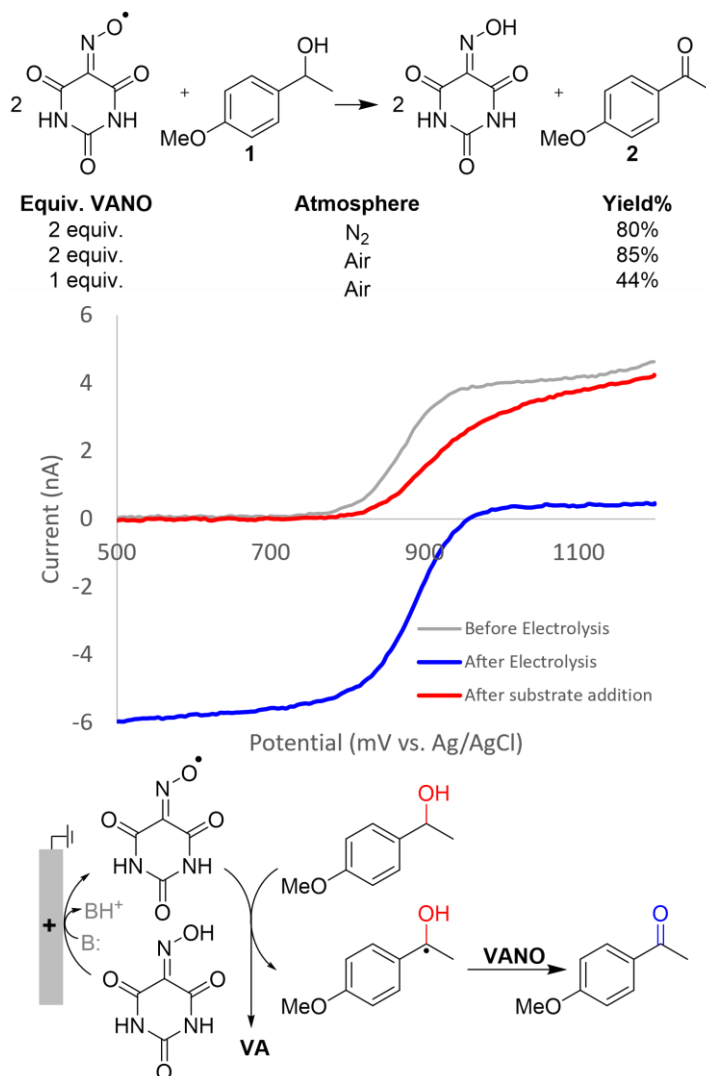


Figure 6.4. RDE analysis of reaction of benzyl alcohol substrate with VANO radical provides further support for previously proposed hydrogen atom transfer mechanism. Glassy carbon working electrode, Pt wire counter electrode, 3 M KCl Ag/AgCl reference electrode; 1000 rpm, 20 mV/s; NMR yields against a 1,3,5-trimethoxybenzene internal standard.

The inverse relationship between radical stability and driving force for HAT of the examined radical mediators both affect the activity for alcohol oxidation. NHPI-mediated

oxidation of **1** resulted in < 5% ketone product due to low concentration of electrogenerated radical and rapid radical decomposition during the 1.5-minute gap between electrolysis and addition (**Figure 6.5a**). DAN and MAN produced similar results. Conversely, VA and DVA achieved high yields of 85% and 85% yield respectively. To further probe the effect of radical stability on alcohol oxidation to simulate extended diffusion into a biomass substrate, the gap between electrolysis and addition to substrate **1** was either shortened to 0.5 minute or extended to 5, 10, 30, 60, or 120 minutes (**Figure 6.5b**). Yields dropped ~ 13% over 2 h, which closely follows to the ~ 10% decay in radical concentration observed over 2 h (see **Figure 6.3**).

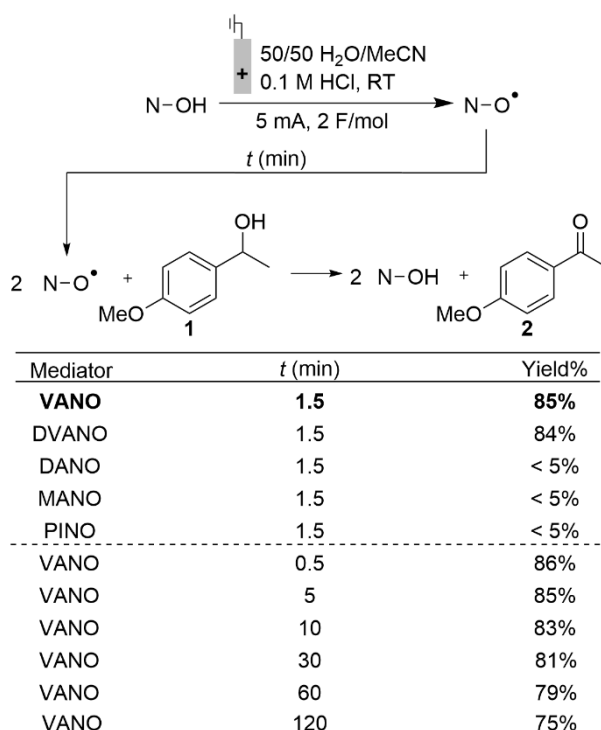


Figure 6.5. Yield data for alcohol oxidation mediated radicals electrochemically generated from VA, DVA, DAN, MAN, and NHPI and mediated by VANO after addition between 0.5 and 120 minutes.

6.4. Conclusion

Herein, we have evaluated the stability, O-H bond strengths, and activity towards simple alcohol oxidation of eight mediators, including five oximes. The results establish comparable

metrics of stability and bond dissociation energy and illustrate a general inverse trend between radical mediator stability and driving force for HAT. The participation of HAT mediator VA in each bond making/breaking step of alcohol oxidation is demonstrated for the first time here, which may contribute to the stronger correlation between off-electrode alcohol oxidation yields and mediator stability (as opposed to BDFE). Future studies will employ VA for the oxidative pretreatment of lignin in biomass to facilitate the production of bio-derived aromatics.

6.5. Acknowledgments

SSS conceived the project in collaboration with SLG, who performed the experimental work and led primary data interpretation and analysis. MR collected some preliminary data. We thank James Gerken and Eric Weeda (UW-M) for helpful discussion. Financial support for this project was provided by the Great Lakes Bioenergy Research Center, U.S. Department of Energy, Office of Science, Office of Biological and Environmental Research, under Award Numbers DE-SC0018409 and DEFC02-07ER64494. The NMR facilities were supported by the NIH (S10 OD012245), by a generous gift from Paul J. and Margaret M. Bender, and by the University of Wisconsin-Madison UW2020 program.

6.6. References

1. Sheldon, R. A.; Arends, I. W. C. E. 2004, 346, 1051–1071.
2. Nutting, J. E.; Rafiee, M.; Stahl, S. S. *Chem. Rev.* **2018**, *118*, 4834–4885.
3. Recupero, F.; Punta, C. *Chem. Rev.* **2007**, *107*, 3800-3842.
4. Ueda, C.; Noyama, M.; Ohmori, H.; Masui, M. *Chem. Pharm. Bull.* **1987**, *35*, 1372–1377.
5. Yang, C.; Farmer, L. A.; Pratt, D. A.; Maldonado, S.; Stephenson, C. R. J. *J. Am. Chem. Soc.* **2021**, *143*, 10324-10332.
6. Galli, C.; Gentili, P.; Lanzalunga, O. *Angew. Chem. Int. Ed.* **2008**, *47*, 4790-4796.
7. Cui, Y.; Goes, S. L.; Stahl, S. S. Sequential Oxidation – Depolymerization Strategies for Lignin Conversion to Low Molecular Weight Aromatic Chemicals. In *Advances in Inorganic Chemistry: Catalysis in Biomass Conversion*; Ford, P. C., van Eldik, R., Eds.; Academic Press: Cambridge, MA, 2021; Vol. 77, pp 99–136.

8. Bourbonnais, R.; Paice, M. G.; Freiermuth, B.; Bodie, E.; Borneman, S. *Appl. Environ. Microbiol.* **1997**, *63*, 4627-4632.
9. Kim, H-C.; Mickel, M.; Bartling, S.; Hampp, N. *Electrochim. Acta.* **2001**, *47*, 799-805.
10. Mickel, M.; Kim, H-C.; Noll, S.; Hampp, N. *J. Electrochem. Soc.* **2003**, *150*, E595-E600.
11. Barreca, A. M.; Sjögren, B.; Fabbrini, M.; Galli, C.; Gentili, P. *Biocatal. Biotransform.* **2004**, *22*, 105-112.
12. Rochefort, D.; Leech, D.; Bourbonnais, R. *Green Chem.* **2004**, *6*, 14-24.
13. Galli, C.; Gentili, P. *J. Phys. Org. Chem.* **2004**, *17*, 973-977.
14. Arzola, K. G.; Arévalo, M. C.; Falcón, M. A. *Electrochim. Acta* **2009**, *54*, 2621-2629.
15. Kong, F.; Wang, S.; Fu, S.; Zhang, H. *Adv. Mater. Res.* **2010**, *113-116*, 2067-2071.
16. Du, X.; Gellerstedt, G.; Rencoret, J.; Del Río, J. C.; Martínez, A. T.; Gutiérrez, A. *Biomacromolecules* **2013**, *14*, 3073-3080.
17. Zhong, Y.; Kong, F.; Wang, S.; Chen, H. *Appl. Mech. Mater.* **2014**, *496-500*, 179-182.
18. Baiocco, P.; Barreca, A. M.; Fabbrini, M.; Galli, C.; Gentili, P. *Org. Biomol. Chem.* **2003**, *1*, 191-197.
19. Kim, H-C.; Mickel, M.; Hampp, N. *Chem. Phys. Lett.* **2003**, *371*, 410-416.
20. Ingold, K. U. The Only Stable Organic Sigma Radicals: Di-tert-Alkyliminoxyls. In *Stable Radicals: Fundamentals and Applied Aspects of Odd-Electron Compounds.*; John Wiley & Sons, 2010; pp 231-244.
21. Krylov, I. G.; Paveliev, S. A.; Budnikov, A. S.; Terent'ev A. O. *Beilstein J. Org. Chem.* **2020**, *16*, 1234-1276.
22. Kushch, O. V.; Hordieieva, I. O.; Kompanets, M. O.; Zosenko, O. O.; Opeida, I. A.; Shendrik, A. N. *J. Org. Chem.* **2021**, *86*, 3792-3799.
23. Kushch, O.; Hordieieva, I.; Novikova, K.; Litvinov, Y.; Kompanets, M.; Shendrik, A.; Opeida, I. Kinetics of N-Oxyl Radicals' Decay. *J. Org. Chem.* **2020**, *85*, 7112-7124.
24. Agarwal, R. G.; Coste, S. C.; Groff, B. D.; Heuer, A. M.; Noh, H.; Parada, G. A.; Wise, C. F.; Nichols, E. M.; Warrne, J. J.; Mayer, J. M. *Chem. Rev.* **2022**, *122*, 1-49.
25. Francke, R. *Curr. Opin. Electrochem.* **2021**, *28*, 100719-100724.
26. Bobbitt, J. M.; Brückner, C.; Merbouh, N. Oxoammonium- and Nitroxide-Catalyzed Oxidations of Alcohols. In *Organic Reactions*; Wiley: Hoboken, NJ, 2009; pp 103-424.
27. Rafiee, M.; Karimi, B.; Alizadeh, S. *ChemElectroChem* **2014**, *1*, 455-462.
28. Yang, C.; Farmer, L. A.; Pratt, D. A.; Maldonado, S.; Stephenson, C. R. J. *J. Am. Chem. Soc.* **2021**, *143*, 10324-10332.
29. Krikstopaitis, K.; Kulys, J. *Electrochem. Commun.* **2000**, *2*, 119-123.

30. The $> 1 I_c/I_a$ ratio of DAN at pH 3 and 5 and CV shape are characteristic of a coupled reversible chemical step, likely deprotonation, followed by a reversible electron transfer. As the pH/scan rate increases, the equilibrium constant for the chemical step becomes large enough for the reaction to be considered irreversible and the CV becomes reversible.
31. Bosque, I.; Magallanes, G.; Rigoulet, M.; Kärkäs, M. D.; Stephenson, C. R. J. *ACS Cent. Sci.* **2017**, *3*, 621-628.
32. Gerken, J. B.; Pang, Y. Q.; Lauber, M. B.; Stahl, S. S. *J. Org. Chem.* **2018**, *83*, 7323-7330.
33. Bourbonnais, R.; Leech, D; Paice, M. G. *Biochim. Biophys. Acta* **1998**, *3*, 381-390.
34. Galli, C.; Gentili, P.; Lanzalunga, O.; Lucarini, M.; Pedulli, G. F. *Chem. Commun.* **2004**, 2356-2357.
35. Shirashi, T.; Takano, T.; Kamitakahara, H.; Nakatsubo, F. *Holzforschung*, **2012**, *66*, 311-315.

Chapter 7: Electrochemical Oxidative Stabilization in Mild Aqueous Conditions Enhances Lignin Monomer Production During Biomass Depolymerization

This work was performed with Chris Holland, Eric, P. Weeda, Rashi Bhatnagar, Suraj Omolabake, Thatcher W. Root, and Shannon S. Stahl.

7.1. Abstract

Lignocellulosic fractionation conditions are commonly used to isolate polysaccharides from lignin, but they often lead to modification of benzylic alcohols in the lignin backbone and degradation of lignin. Oxidative pretreatment of biomass could stabilize the benzyl alcohols, preventing degradation during fractionation and promote lignin depolymerization to oxygenated aromatics. Herein, we demonstrate an oxidative lignin stabilization method using an electrochemical mediator, violuric acid (VA), under mild conditions to enable selective off-electrode oxidation of lignin in heterogeneous biomass. This active stabilization process is a promising strategy for generating high yields of oxygenated aromatic monomers, and preliminary data results in 15.6 wt% yield of monomers from lignin. The oxygenated aromatics derived from this process have appealing features for use in polymer synthesis and/or biological funneling to value-added products, and preliminary results indicate polysaccharides are not modified during oxidative stabilization.

7.2. Introduction

Lignocellulosic biomass is an abundant and sustainable biochemical feedstock comprised of polysaccharides and a structurally complex biopolymer known as lignin.¹ As the most abundant and least recalcitrant biomass component, polysaccharide production remains a cornerstone of biomass conversion efforts in the pulp and paper and bioethanol industries.² However, lignin represents the largest natural source of renewable aromatic chemicals and 15 to 30 weight percent (wt %) of the non-edible biomass.³ Lignin valorization is, therefore, crucial to economic viability of biorefineries.⁴⁻⁷ Growing interest in complete valorization of biomass has translated to few marketable processes owing to the lack of compatible lignin depolymerization and polysaccharide upgrading methods.⁸⁻¹⁰ Conventional fractionation of lignin and polysaccharides results in crosslinking, the formation of recalcitrant C-C bonds that prevent the depolymerization of lignin

into aromatic monomers.⁷ Benzyl alcohols present in the lignin backbone can undergo facile generation of carbocation intermediates under acidic conditions or the formation of quinone methide and/or epoxides under alkaline conditions, leading to lignin degradation (**Figure 7.1A**).

The oxidative pretreatment of biomass is a lignin-first, active alcohol stabilization strategy¹¹ to prevent lignin degradation during fractionation and facilitate depolymerization of lignin to oxygenated aromatics. The chemical functionalization of the benzyl alcohol via acetal formation during fractionation has been shown to improve yields of oxygenated monomers produced after subsequent oxidation and depolymerization steps.^{12,13} Oxidative of the benzyl alcohol in the prevalent β -O-4 linkage similarly stabilizes this reactive site, preventing crosslinking during lignin extraction (**Figure 7.1A**).¹⁴ Furthermore, selective oxidation of undamaged alcohols performed on isolated lignin (**Figure 7.1B**) has been shown to weaken the ether linkages in the polymer backbone towards subsequent oxidative, reductive, or redox-neutral cleavage to oxygenated monomers (**Figure 7.1C**).¹⁵ An oxidative pretreatment strategy prepares the lignin for both downstream fractionation and depolymerization by providing the advantages of alcohol stabilization and ether C-O bond weakening in one step (**Figure 7.1D**). In comparison to oxidative catalytic fractionation methods designed to oxidize, fractionate, and depolymerize in one step, an electrochemical pretreatment strategy allows each unit process to be optimized independently. Thus, the benefits of oxidation can be obtained using milder temperatures, pressures, and solvents^{16,17} that are more desirable for economically viable biorefinery processes.¹⁸

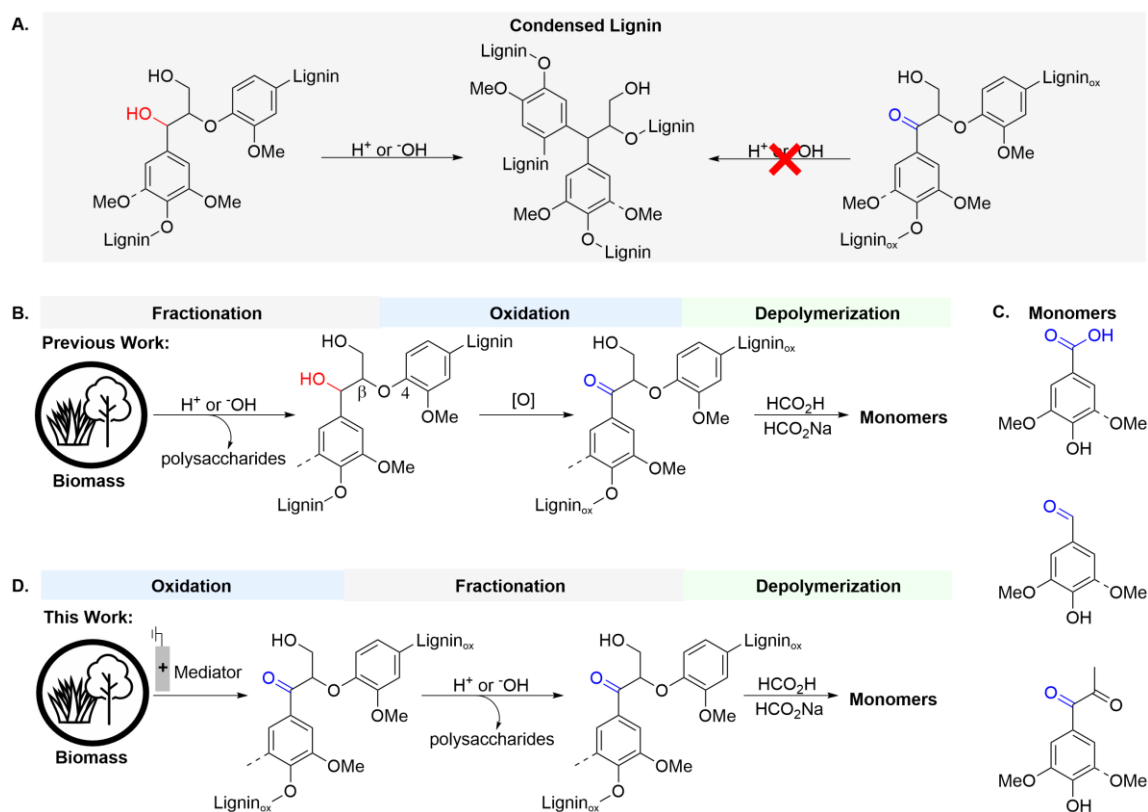


Figure 7.1. Overview of selective lignin oxidation approaches: (A) condensation or stabilization of lignin. (B) Previous oxidative lignin conversion from biomass approaches and (C) monomers produced from oxidative biomass conversion. (D) This oxidative biomass conversion approach via selective benzylic alcohol oxidation. Biomass icon courtesy of Matthew Wisniewski (Wisconsin Energy Institute).

7.3. Results and Discussion

Inspired by these mediated electrochemical oxidation methods, we initiated the present study to explore the prospects of active oxidative stabilization of lignin for enhanced monomer production. Electrochemistry is a sustainable and scalable method for oxidations and can be operated under aqueous conditions in flow. Direct electrochemical oxidation of lignin suffers from electrode fouling due to the polymerization of oxidized phenolic groups on the electrode surface.¹⁹ Instead, an organic molecule known as an electrochemical mediator can mediate the transfer of electrons between the electrode and a packed bed reactor filled with heterogeneous biomass (**Figure 7.2**). Violuric acid (VA) is a mediator known to undergo facile electrochemical oxidation

at an electrode to produce a stable radical (VANO), which is well suited to oxidation of heterogeneous alcohols. The long radical lifetime enables VANO generation at the electrode, travel to the reactor, and diffusion into the heterogeneous substrate. VANO transfers a hydrogen atom (HAT) from the secondary benzylic alcohol to form the corresponding carbon centered radical and regenerate VA. Oxidation by a second equivalent of VANO forms the ketone.

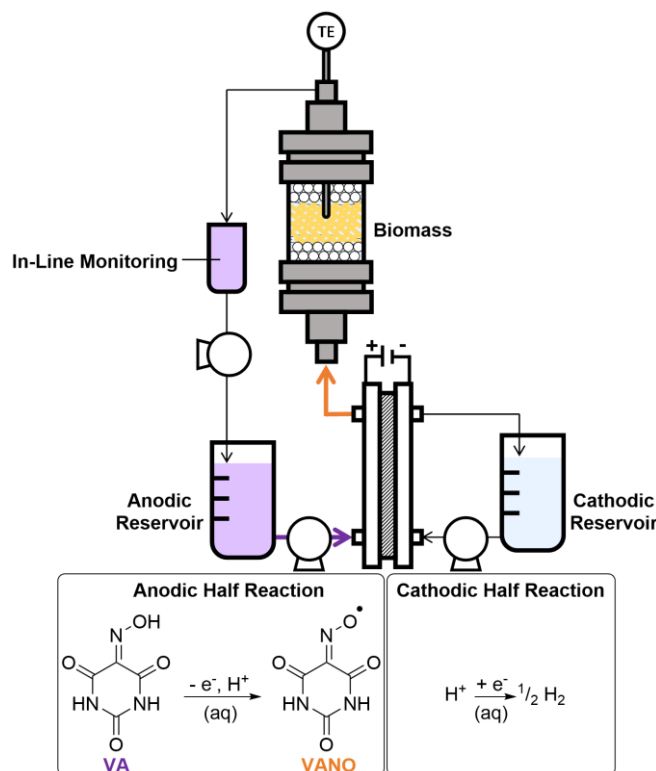


Figure 7.2. Overview of electrochemical oxidative stabilization of lignin: schematic of flow reactor and electrochemical half reactions in aqueous solution.

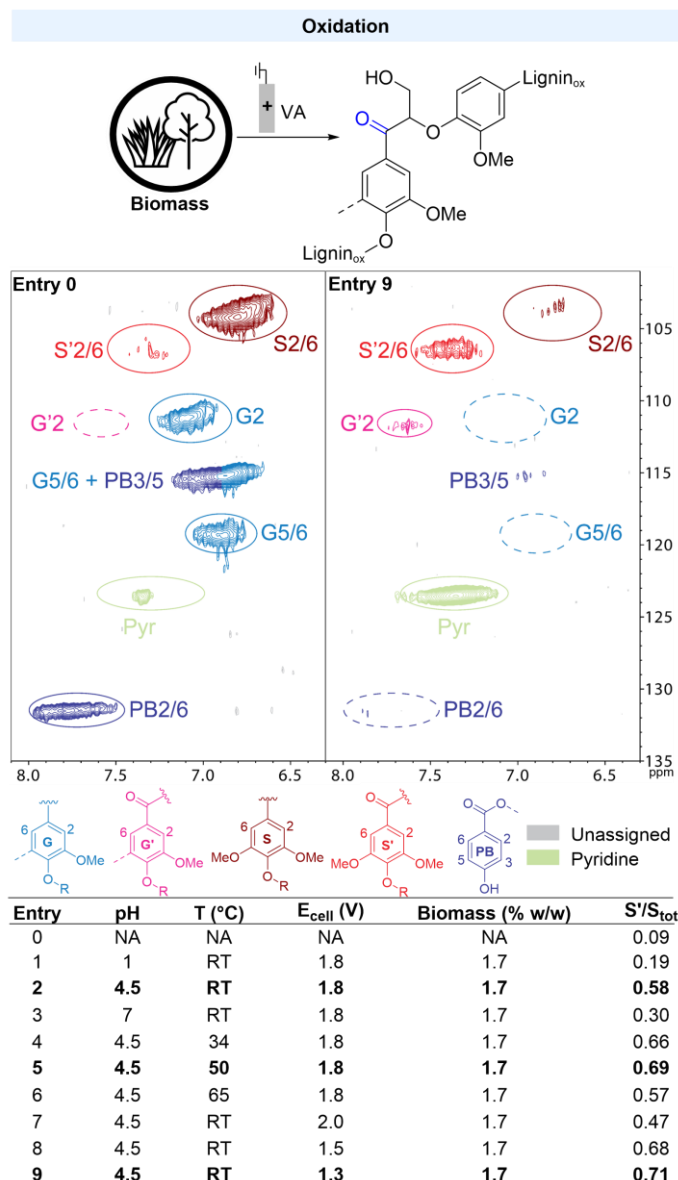
The effect of the oxidative pretreatment can be observed by two-dimensional heteronuclear single-quantum coherence nuclear magnetic resonance (2D HSQC NMR) spectra of whole cell biomass (**Table 7.1**).²⁰ In comparison to untreated washed poplar biomass, biomass treated under the oxidative conditions shows distinct structural changes. Diagnostic peaks for the oxidation of S- and G-derived benzylic ketones, as well as the loss of native S- and G- peaks, are observed in the aromatic region of oxidatively treated biomass. The extent of oxidation has been

reported as the ratio between the integrations of the peak arising from the oxidized S subunit (S²/6) and all S peaks (S²/6 and S²/3). Integrations are determined relative to the integrations of signals arising from methoxy groups on lignin which are not expected to vary between samples of the same wood source or treatment conditions. Relating peak integration to the concentration of chemical groups in a sample without account for different relaxation between different parts of the biopolymer results in a comparative, rather than quantitative, measurement of sample oxidation.²¹

We examined NE-19 poplar (*Populus nigra charkowiensis* × *P. nigra caudina*) wood (particle size, 0.35-0.84 mm; moisture content, 5.6%) under a variety of oxidative pretreatment conditions (**Table 7.1**). The reactions were conducted in recirculating flow using a divided cell (membrane, Nafion; anode, graphite; cathode, stainless steel). Testing of acidic and neutral buffer conditions clearly indicated the importance of maintaining the solution pH around the pK_a of the VANO (3.8)(**Table 7.1**, Entry 2). Decreasing the solution pH to 1 (**Table 7.1**, Entry 1), although expected to increase the radical lifetime, primarily promotes degradation of the benzyl alcohol. This degradation can be observed indirectly as a general decrease in S_{tot}. Unfortunately, attractive neutral pH conditions did not work well (**Table 7.1**, Entry 3). Attempts to increase the rate of VANO HAT by elevating the temperature of the packed bed reactor were successful, revealing an interpolated maximum at 43-45°C (**Table 7.1**, Entries 4-6). Further improvements were achieved by reducing the cell voltage (**Table 7.1**, Entries 7-9). Mediator degradation, measured by electrochemical analysis at the reactor outlet (working; carbon fiber microelectrode; counter; Pt wire; reference; Ag/AgCl), decreases as the applied potential decreases. Similar results can be achieved using 1 mA current. We speculate that low voltages or current may prevent build-up of radical in the anodic reservoir, thus reducing proposed higher-order degradation pathways, or prevent the overoxidation of VANO. These optimized conditions are very similar to the ones used

by Hampf and coworkers for the electrochemical VA-mediated oxidative delignification of Kraft softwood pulp (pH 4, 50°C, 1.7 or 5 V, 200-400 g pulp).²²

Table 7.1. Optimization of oxidative lignin stabilization.



The partial or full loss of signals arising from pendant *p*-hydroxybenzoate (PHBA) groups is observed all examined oxidative treatment conditions (**Table 1**). Cleavage of the pendant PHBA esters on lignin has been previously observed under acidic conditions.²³ We were unable to recover these monomers upon extraction of the mediator solution post-treatment.

Following oxidative pretreatment, the oxidized lignin will be extracted from the polysaccharides using mild-acidolysis or mild base and subjected to redox-neutral formic acid/sodium formate depolymerization.^{7,24,25} The oxygenated lignin derived products, such as those shown in **Figure 7.1**, represent appealing feedstocks for microbial conversion and biological funneling or as protein inhibitors.²⁶⁻²⁸ Preliminary work was conducted under unoptimized oxidative treatment conditions in a pooled-radical batch set-up, followed by direct depolymerization of oxidized biomass, resulted in 15.6 wt% oxygenated monomers from biomass (**Figure 7.3**). The primary products from this early work are carboxylic acids and diketones derived from the S and G lignin subunits. Compared to the wt% monomer yields obtained by other three-step pretreatment, oxidation, and hydrolysis processes¹⁷ (mild acidolysis, 6.2; CuAHP, 9.8; GVL, 12.9; and propionaldehyde protection/acidolysis, 31), the 15.6 wt% of monomers obtained under even unoptimized conditions is very promising.

Analysis of the polysaccharide residue and overall mass balance for this full process will also be conducted. We expect the polysaccharides to be retained during oxidative pre-treatment owing to the excellent selectivity of VANO for secondary alcohols in the presence of dextrose. Solid state analysis of biomass obtained from preliminary, unoptimized oxidative treatment demonstrated that the sugars were not degraded during the treatment process.

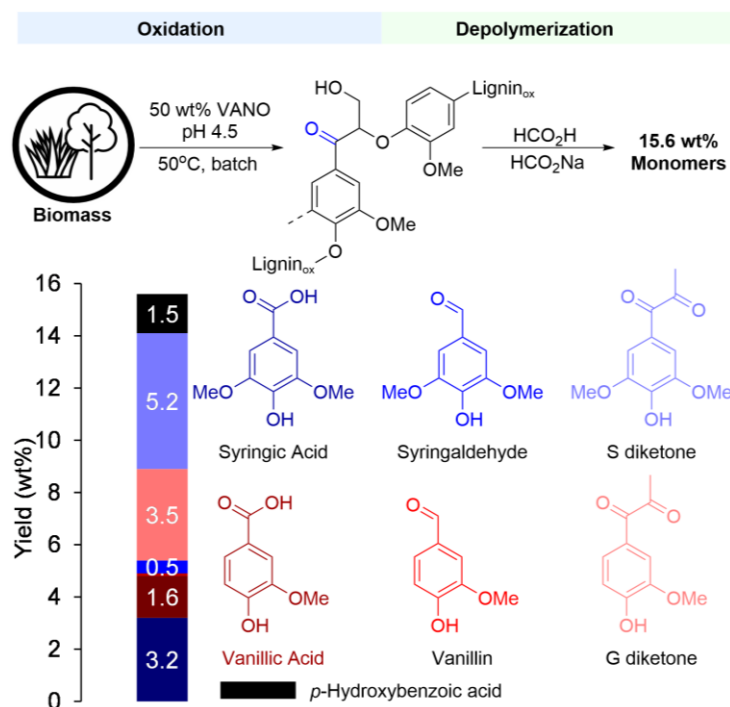


Figure 7.3. Preliminary data for the oxidative stabilization of lignin in batch and depolymerization to monomers.

7.4. Conclusions

These results suggest that electrochemical oxidative stabilization of is a promising route to valuable aromatic chemicals. We expect process can be used to generate valuable bifunctional oxygenated aromatic monomers from lignin in parallel with high-quality polysaccharide solids amenable to further upgrading under mild conditions. Further work will demonstrate the maximum yields of attainable monomers and provide a full characterization of polysaccharides and mass balance.

7.5. Acknowledgements

SSS conceived the project in collaboration with SLG, who performed the experimental work and led primary data interpretation and analysis. CH assisted with reactor design. EPW and SO synthesized compounds used for monomer analysis, and EPW collected calibration data used for monomer analysis and assisted in manuscript preparation. RB assisted with collecting

optimization data. We thank Sarah Liu for NMR data collection and Manar Alherech for helpful discussion. Financial support for this project was provided by the Great Lakes Bioenergy Research Center, U.S. Department of Energy, Office of Science, Office of Biological and Environmental Research, under Award Numbers DE-SC0018409 and DEFC02-07ER64494.

7.6. References

1. Zakzeski, J.; Bruijninx, P. C. A.; Jongerius, A. L.; Weckhuysen, B. *MChem. Rev.* **2010**, *110*, 3552–3599.
2. Chirat, C.; Lachenal, D.; Dufresne, A. *Cellulose Chem. Technol.* **2010**, *44*, 59-64.
3. Ralph, J.; Lundquist, K.; Brunow, G.; Lu, F.; Kim, H.; Schatz, P. F.; Marita, J. M.; Hatfield, M. D.; Ralph, S. A.; Christensen, J. H.; Boerjan, W. **2004**, *3*, 29-60.
4. Ragauskas, A. J.; Beckham, G. T.; Biddy, M. J.; Chandra, R.; Chen, F.; Davis, M. F.; Davison, B. H.; Dixon, R. A.; Gilna, P.; Keller, M.; Langan, P.; Naskar, A. K.; Saddler, J. N.; Tschaplinski, T. J.; Tuskan, G. A.; Wyman, C. E. *Science* **2014**, *344*, 1246843.
5. Li, C.; Zhao, X.; Wang, A.; Huber, G. W.; Zhang, T. *Chem. Rev.* **2015**, *115*, 11559–11624.
6. Sun, Z.; Fridrich, B.; de Santi, A.; Elangovan, S.; Barta, K. *Chem. Rev.* **2018**, *118*, 614–678.
7. Schutyser, W.; Renders, T.; Van den Bosch, S.; Koelewijn, S.-F.; Beckham, G. T.; Sels, B. F. *Chem. Soc. Rev.* **2018**, *47*, 852–908.
8. Evju, H. Process for Preparation of 3-Methoxy-4-Hydroxybenzaldehyde. US Patent 4151207A; 1979.
9. Lora, J. *Industrial Commercial Lignins: Sources, Properties and Applications. In Monomers, Polymers and Composites from Renewable Resources*; Belgacem, M. N., Gandini, A., Eds.; Elsevier Science, 2008; Vol. 1, pp 225–241.
10. Abu-Omar, M. M.; Coller, D. H.; Klein, I. M. Extraction of Natural Ferulate and Coumarate from Biomass. US Patent 20200181060A1; 2021.
11. Renders, T.; Van den Bosch, S.; Koelewijn, S-F. Schutyser, W.; Sels, B. F. *Energy Environ. Sci.* **2017**, *10*, 1551-1557.
12. Shuai, L.; Amiri, M. T.; Questell-Santiago, Y. M.; Héroguel, F.; Li, Y.; Kim, H.; Meilan, R.; Chapple, C.; Ralph, J.; Luterbacher, J. S. *Science* **2016**, *354*, 329–333.
13. Lan, W.; Bahaghel de Buren, J.; Luterbacher, J. S. Highly Selective Oxidation and Depolymerization of α,γ -Diol-Protected Lignin. *Angew. Chem. Int. Ed.* **2019**, *58*, 2649-2654.
14. Questell-Santiago, Y. M.; Galkin, M. V.; Barta, K.; Luterbacher, J. S. *Nature Rev. Chem.* **2020**, *4*, 311–330.

15. Cui, Y.; Goes, S. L.; Stahl, S. S. Sequential Oxidation – Depolymerization Strategies for Lignin Conversion to Low Molecular Weight Aromatic Chemicals. In *Advances in Inorganic Chemistry: Catalysis in Biomass Conversion*; Ford, P. C., van Eldik, R., Eds.; Academic Press: Cambridge, MA, 2021; Vol. 77, pp 99–136.
16. Du, X.; Tricker, A. W.; Yang, W.; Katahira, R.; Liu, W.; Kwok, T. T.; Gogoi, P.; Deng, Y. *ACS Sustainable Chem. Eng.* **2020**, *9*, 7719-7727.
17. Luo, H.; Weeda, E. P.; Alherech, M.; Anson, C. W.; Karlen, S. D.; Cui, Y.; Foster, C. E.; Stahl, S. S. *J. Am. Chem. Soc.* **2021**, *143*, 15462-15470.
18. Bartling, A. W.; Stone, M. L.; Hanes, R. J.; Bhatt, A.; Zhang, Y.; Bidy, M. J.; Davis, R.; Kruger, J. S.; Thornburg, N. E.; Luterbacher, J. S.; Rinaldi, R.; Samec, J. S. M.; Sels, B. F.; Román-Leshkov, Y.; Beckham, G. T. *Energy Environ. Sci.* **2021**, *14*, 4147-4168.
19. Du, X.; Zhang, H.; Sullivan, K. P.; Gogoi, P.; Deng, Y. *ChemSusChem* **2020**, *13*, 4318-4343.
20. Kim, H.; Ralph, J. *RSC Adv.* **2014**, *4*, 7549-7560.
21. Amiri, M. T.; Bertella, S.; Questell-Santiago, Y. M.; Luterbacher, J. S. *Chem. Sci.* **2019**, *10*, 8135-8142.
22. Mickel, M.; Kim, H.-C.; Noll, S.; Hampp, N. *J. Electrochem. Soc.* **2003**, *150*, E595-E600.
23. Sani, I. M.; Iqbal, S.; Chan, K. W.; Ismail, M. *Molecules* **2012**, *17*, 7584-7594.
24. Hibino, T.; Shibata, D.; Ito, T.; Tsuchiya, D.; Higuchi, T.; Pollet, B.; Lapierre, C. *Aralia Cordata. Phytochemistry* **1994**, *37*, 445–448.
25. Rahimi, A.; Ulbrich, A.; Coon, J. J.; Stahl, S. S. *Nature* **2014**, *515*, 249–252
26. Wadkins, R. M.; Hyatt, J. L.; Wei, X.; Yoon, K. J. P.; Wierdl, M.; Edwards, C. C.; Morton, C. L.; Obenauer, J. C.; Damodaran, K.; Beroza, P. Danks, M. K.; Potter, P. M. *J. Med. Chem.* **2005**, *48*, 2906-2915.
27. Beckham, G. T.; Johnson, C. W.; Karp, E. M.; Salvachua, D.; Vardon, D. R. *Curr. Opin. Biotechnol.* **2016**, *42*, 40–53.
28. Linz, A. M.; Ma, Y.; Perez, J. M.; Myers, K. S.; Kontur, W. S.; Noguera, D. R.; Donohue, T. J. *Appl. Environ. Microbiol.* **2021**, *87*, E01742-21.

Appendices

**Appendix A: Exploring Electrosynthesis: Bulk Electrolysis and Cyclic
Voltammetry Analysis of the Shono Oxidation Supporting Information**

A.1. Equipment and Hazards

Reagents

Anisole (CAS 100-66-3), acetonitrile (CAS 75-05-8), silver nitrate (CAS 7761-88-8), *N*-Boc-pyrrolidine (97%, CAS 86953-79-9), tetraethylammonium *p*-toluenesulfonate ([NEt₄][*p*-TsOH])(CAS 733-44-8), 1,3,5-trimethylbenzene (CAS 108-67-8), and deuterated chloroform (CAS 865-49-6) were purchased from Millipore Sigma. Tetrabutylammonium hexafluorophosphate (CAS 3109-63-5) was purchased from Millipore Sigma or Chem-Impex Int'l Inc. Piperidine-1-carboxylic acid methyl ester (98%, CAS 1796-27-6) was purchased from Combi-blocks. Ferrocene was purchased from Chem-Impex Int'l Inc. 4-anisylpiperidine-1-carboxylic acid methyl ester (CAS 1789303-60-1) was prepared by F. Wang via the reaction of 4-(4-Methoxyphenyl)piperidine hydrochloride (CAS 6748-48-7) with methyl chloroformate (CAS 79-22-1).¹ All electrochemical experiments were performed under ambient conditions and no effort was made to exclude moisture or air.

Equipment

Cyclic Voltammetry

Potentiostat. A source of electrons capable of recording a cyclic voltammogram (CV) using a 3-electrode cell set-up including a non-aqueous reference electrode (see below). Electrochemical CV experiments in this lab were conducted using a WaveNow® potentiostat from Pine Research Instrumentation, Inc.

Computer Interface. A separate or integrated apparatus linked to the potentiostat that allows the user to set experiment parameters and record data. Electrochemical CV experiments in this lab were controlled and monitored using Pine Research Instrumentation, Inc. Aftermath Data OrganizerSoftware® and a Dell. Inc. laptop.

Cell. A vessel for holding the reaction solution and the three electrodes. The CV experiments in this lab were collected using a cell (MF-1208) and cell cap (MF-3849) from BASi.

Glassy Carbon Disk Electrode. The working electrode for performing the reaction of interest with a well-defined surface area. The CV experiments in this lab were collected using a 3.0 mm diameter glassy carbon disk electrode (MF-2012) from BASi.

Counter Electrode. The counter electrode used to balance the reaction occurring at the working electrode. The CV experiments in this lab were collected using a homemade platinum wire counter electrode fabricated by the department glassblower. A similar platinum wire counter electrode can also be purchased from BASi (MW-1033). Stainless steel is also an acceptable alternative to Pt wire for these experiments.

Non-Aqueous Reference Electrode. The glass tube with a porous frit filled with a solution containing solvent, electrolyte, and AgNO_3 (10 mM) and cap with silver wire. The electrolyte and solvent should be the same as used in the analysis solution. The Ag/Ag^+ redox couple of the reference electrode is used to measure the potential at the working electrode. The CV experiments in this lab were collected using a non-aqueous reference electrode (MF-2602) reference electrode from BASi. The porous frit can be ceramic or CoralPor®. Although aqueous Ag/AgCl reference electrodes can sometimes be used for CV experiments conducted in non-aqueous solution, they are not recommended for recording accurate redox potentials.

Electrode Polishing Materials. A pad and abrasive suspension used for restoring a clean and uniform working electrode surface. The working electrode in this lab was polished using 0.05 μm alumina (CF-1050) and velvet polishing pads (MF-1040) from BASi. The polishing suspension was applied to the fabric pads attached to the underside of glass plates or petri dishes.

Bulk Electrolysis

Power Supply. A source of electrons capable of applying 15 mA. Electrochemical bulk electrolysis experiments were conducted using a Dr. Meter 30 V/5 A DC bench power supply

(B00O8DJ8QC) from Amazon. A potentiostat capable of running a 15 mA bulk electrolysis or chronopotentiometry experiment is an acceptable alternative.

Cell. A vessel for holding the reaction solution and two electrodes. The bulk electrolysis experiment in this lab was conducted in a 3-dram vial (71000-176) from VWR and with a SURE-LINK™ septa (CG-4910-16) cap from Chemglass Life Sciences.

Carbon Electrode. A large surface area carbon electrode for performing the reaction of interest. The bulk electrolysis experiment in this lab was conducted using a 0.125" diameter fine-extruded graphite rod (NC001295) from the Graphite Store (www.graphitestore.com). Reticulated vitreous carbon (RVC) is an acceptable alternative to graphite. Graphite rods containing a binder or with a diameter much smaller than 0.125" should be tested under the reaction conditions before use.

Counter Electrode. The electrode used to balance the reaction at the working electrode. The bulk electrolysis experiment in this lab was conducted using a 0.045" diameter stainless-steel rod cathode (59801589) from MSC. Platinum and carbon are acceptable alternatives to stainless steel.

Magnetic Stir Bar. A source of convection in the cell. The bulk electrolysis experiment in this lab was conducted with a 10 mm PTFE-coated stir bar.

Bulk Electrolysis Cell Preparation

The cell was assembled by breaking the graphite rod into approximately 3" pieces and cutting the stainless-steel rod into approximately 4" pieces. Using the stainless-steel rod or a needle, the septa in the cap was punctured and the graphite rod was inserted through the cap. The stainless-steel rod was inserted through the cap approximately 3/16" away from the graphite rod. The stir bar was added to the vial and the cap-electrode assembly was attached. The height of the electrodes was adjusted until the end was 1-2 mm above the stir bar. The cap was removed and

graphite rod was wrapped, beginning near the underside of the cap, with PTFE tape. The tape on the graphite rod was overlapped until the tape pushed against the stainless-steel, making the electrodes parallel to one other. Then the tape was wrapped once or twice around both electrodes near the underside of the cap to secure them together and maintain the interelectrode distance at approximately 3/16" (**Figure A.1**). The PTFE tape was not in contact with or immersed in solution during the reaction.



Figure A.1. Electrochemical bulk electrolysis cell used by students.

An alternative electrochemical synthesis cell was constructed and used during a pilot version of the lab. The alternative cell employs a non-aqueous reference electrode and Pt wire counter electrode

(**Figure A.2**)



). The use of a reference electrode means that this set-up must be used with a potentiostat rather than a power source.



Figure A.2. Example of alternative electrochemical bulk electrolysis cell used by instructors during lab development.

Hazards

Appropriate personal protective equipment, including disposable gloves, goggles, closed-toe shoes, and a lab coat, must be worn. Procedures must be performed in a fume hood or similarly ventilated workspace. Liquid and solid waste must be disposed into sealed and appropriately labeled containers. Safety information for all reagents is available via the appropriate SDS. Electrical equipment can represent an electric shock hazard. Instructors should take care when setting the power supply current limit and inspect students' experimental setups before an electric current is applied.

A.2. Instructor Notes

Materials Provided to Students

Reaction Video. Narrated video recording of instructors performing the Shono bulk electrolysis reaction using an alternative set-up: potentiostat as the source of electrons, homemade glass cell, graphite rod working electrode, Pt wire as the counter electrode, and non-aqueous Ag/Ag^+ reference electrode.

Laboratory Manual Chapter and Assessment Questions. An introductory discussion of electrochemical concepts and techniques, standard equipment, and an overview of the Shono reaction, instructions for performing the CV and bulk experiments, and assessment questions to be addressed in a formal laboratory report.

Lecture Video. Video recording of a short (~15 minutes) presentation that discusses important concepts from the introductory content of the *Laboratory Manual Chapter* and provides additional information on the Shono reaction.

Lecture Slides. The slides used for the *Lecture Video* presentation.

Optional Background Reading. Literature for additional information related to organic electrosynthesis and electrochemical techniques.

Safety Data Sheets. Basic properties and hazard information for each chemical used during the lab.

Excel Template for CV Data. A .xlsx file for analyzing CV data.

Stock CV Data. Unprocessed example student CV data.

Stock ^1H NMR Spectrum. Unprocessed example student ^1H NMR data of the crude Shono oxidation reaction mixture using 1,3,5-trimethylbenzene as internal standard.

Yield (%) Practice. An overview of reaction conditions for mediated electrochemical alcohol oxidation and procedure for calculating yield (%) from ^1H NMR data of crude reaction mixture using an internal standard, unprocessed ^1H NMR data, and answer key for calculation of yield (%).

Setting up the CV Experiment

Two identical experiment stations were prepared in separate instructional lab hoods. Four Solutions of 5 mM anisole (1), 5 mM piperidine-1-carboxylic acid methyl ester (2), 5 mM 4-anisylpiperidine-1-carboxylic acid methyl ester (3), and 1 mM ferrocene in acetonitrile were prepared for each station. All the solutions included 0.1 M $[\text{NBu}_4][\text{PF}_6]$ as supporting electrolyte. The solutions were prepared on the day of the lab exercise and stored in four separate cyclic voltammetry cells sealed with parafilm. After students analyzed one of these solutions using cyclic voltammetry, the cell was resealed with parafilm and was used by the subsequent groups.

Two reference electrodes were prepared for the experiment. At least 24 hours before the laboratory experiment, the electrodes were placed in a solution of 0.1 M $[\text{NBu}_4][\text{PF}_6]$ in CH_3CN . The day of the experiment, a solution of 10 mM AgNO_3 and 0.1 M $[\text{NBu}_4][\text{PF}_6]$ in CH_3CN was prepared and was used to fill the reference electrode.

During setup, the instructor should collect cyclic voltammograms of one of the substrate solutions and a “blank” solution (0.1 M $[\text{NBu}_4][\text{PF}_6]$ in CH_3CN). This allows the instructor to ensure that all the equipment is functioning properly, check that the cyclic voltammogram potential windows specified in the laboratory manual are sufficient, and identify any peaks in the potential window that are unrelated to substrate oxidation. Variance in the potential of the prepared

reference electrode may require the instructor to adjust the potential window for the CV scans and to communicate that change to students. If there is enough time allotted for the experiment, the instructor can skip that step and instead help the students adjust the potential window themselves by increasing or decreasing the switching (also known as vertex) potential, shown as E_2 in **Figure A.7**, as needed. Ideally the solvent and electrolyte will not provide any significant current in the selected potential window. However, redox-active contaminants in the electrolyte/solvent or the selection of a potential window that overlaps with potentials for solvent oxidation may result in observable peaks. Provide the CV trace of the blank solution to students for use in interpreting their data during the assessment and briefly discuss the source of these background peaks as the students analyze the substrate solutions during the lab.

Polishing electrodes for the CV experiment

During the pre-laboratory discussion or after the student pairs collected their first cyclic voltammogram, the instructor demonstrated how to clean and polish the glassy carbon disk working electrode.² A velvet-textured polishing pad was wetted with DI water and a few drops of alumina slurry. The glassy carbon disk electrode was first rinsed with acetone followed by DI water. Then, holding the electrode so that the disk is parallel to the polishing pad, the disk is pushed gently onto the pad and swept over the pad in a figure-eight motion. After several seconds of polishing, the carbon disk electrode is rinsed with DI water, acetone, and then allowed to dry under air (or a stream of compressed air, if available). Additional alumina slurry does not need to be added before every polish, and a few more drops of alumina slurry should only be added to the pad if the polished electrode does not become shiny after polishing.

After the demonstration, students are allowed to polish the electrode. The instructor should monitor their technique and correct any errors (*e.g.*, attempting to polish the brass connector at the top of the glassy carbon electrode). Only the glassy carbon disk electrode needs to be

polished. The reference electrode and platinum coil should be rinsed with acetone and allowed to air dry between cyclic voltammetry experiments. The clean reference electrode should not be allowed to dry for longer than a few minutes before it is immersed in the reaction or electrolyte soaking solution.

Setting the current limit for the bulk electrolysis

Before using the green POWER button to turn on the power supply, make sure that the button labelled STOP/OUT is set to the STOP position to prevent current from flowing once the unit is powered (**Figure A.3**). Press the POWER button. Ensure that the digital display reads 0.00 A and 0.00 V are being applied. Connect the red and black leads together. Ensure that the leads are not in contact with a person or other conductive material. Depress the STOP/OUT button to the OUT position to start the flow of electricity through the leads. Use the coarse and fine voltage knobs to increase the voltage to maximum. Use the coarse and fine current knobs to decrease the current to 0 A. Use the fine current knob to increase the current to 15 mA. The C.C. light (constant current) should be lit. Depress the STOP/OUT button to the STOP position and wait until the digital display reads 0.00 A and 0.00 V are being applied. Disconnect the red and black leads from each other. Any subsequent adjustment of the current knobs will adjust the set current.

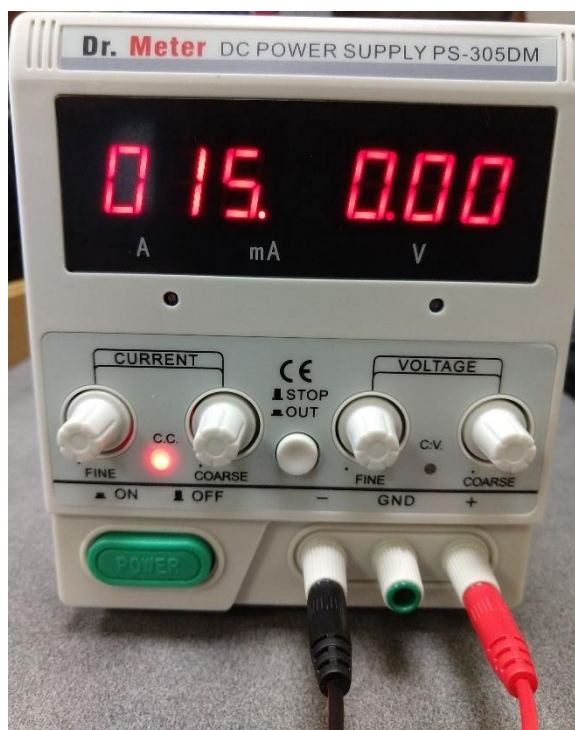


Figure A.3. Power supply used for bulk electrolysis reaction.

Notes on running bulk electrolysis

It is important to ensure that the working electrode and lead are not in contact with the counter electrode or lead. During the instructor's check of the student electrolysis set-ups, use small pieces of rubber or other non-conductive, non-flammable material to prevent the electrodes or leads from creating a short circuit if necessary.

The α -methoxylated *N*-Boc-pyrrolidine Shono product can undergo hydrolysis reaction or an elimination reaction in the crude reaction mixture. Therefore, it is recommended that the bulk electrolysis reaction mixture is worked-up and submitted for ^1H NMR analysis on the same day as the bulk electrolysis occurs.

It is important that the mesitylene NMR standard is added to the crude reaction residue after the methanol has been removed from the crude reaction mixture. In some instances, it was

observed that adding mesitylene prior to the solvent removal step led to unreasonably high NMR yields, indicating likely loss of mesitylene during solvent removal with a rotary evaporator.

Notes on recording video

The bulk electrolysis oxidation of *N*-Boc-pyrrolidine in methanol was conducted in the alternative synthesis cell while an instructor was wearing a chest-mounted GoPro video recorder. Background noise from the fume hood was significant, and it is recommended that audio is recorded later as a voiceover while editing the video.

A.3. Student Laboratory Manual Chapter and Assessment Questions

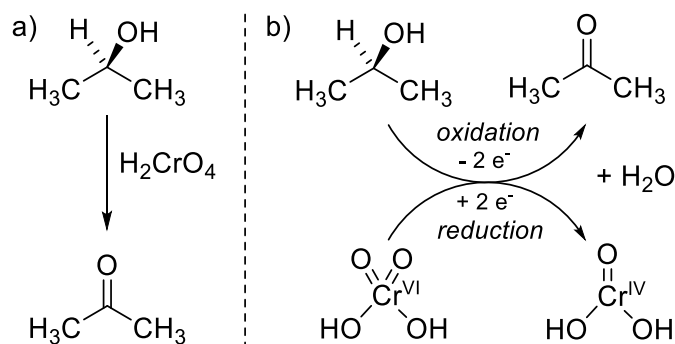
A.3.1. Introduction to Organic Electrochemistry and the Electrochemical Shono Oxidation Introduction

Electrochemistry is a powerful method to study and drive redox reactions *i.e.* reactions in which a chemical species gains or loses one or more electrons. Though electrochemistry is most typically applied in inorganic and analytical chemistry, it is also a valuable technique for organic chemists. The first recorded electrochemical organic reaction was performed in the late 1830s when chemist Michael Faraday electrolyzed acetic acid to form ethane and CO₂. Since then, electrochemical synthesis of organic compounds has been used in widespread applications, from synthesis of fine chemicals and pharmaceuticals to the multi-ton scale preparation of adiponitrile, a precursor to Nylon-66. Over the past five years, organic electrochemistry has experienced a renaissance and is garnering broad interest within the organic chemistry community.³⁻⁶ Renewed academic and industrial focus on electrochemistry is due, in part, to recent innovations in reactivity, selectivity, and energy efficiency. Ongoing efforts to educate organic chemists about electrochemical techniques and make equipment for electroorganic synthesis more accessible and standardized have also contributed to increased interest.

Reduction and Oxidation Reactions

Reduction and oxidation reactions are processes in which a substrate gains or loses one or more electrons, respectively. Consider, for example the two-electron oxidation of 2-propanol to acetone using chromic acid (**Scheme A.1**).

Scheme A.1. a) Chromic acid oxidation of 2-propanol to acetone: b) Redox half-reactions for the overall process.



In this reaction the alcohol is oxidized to the corresponding ketone via a chromate ester, losing two protons and two electrons in the process. Every oxidation reaction is balanced by a corresponding reduction process; that is, oxidation of one substrate must be coupled to reduction of another substrate in solution so that there is no net change in the number of electrons in the reaction. In this case, the chromium species is reduced from Cr(VI) to Cr(IV) by the electrons given up from the alcohol. Cr(VI) and Cr(IV) are a redox couple, an oxidized (reduced) species and its corresponding reduced (oxidized) form, respectively. All reduction and oxidation reactions must be paired in this way; thus, the overall process is referred to as a redox reaction and involves two or more redox couples.

Electrochemical Electron Transfer

The same principles of electron transfer apply to an electrochemical organic redox reaction, but with two key differences. The first is that electron transfer takes place at a conductive surface (an electrode) at which an electric potential is applied, rather than between molecules in

the bulk solution. The second difference is that the reduction and oxidation reactions occur at two different electrodes and are thus separated in space rather than between molecules in close contact.

The driving force for electron transfer from the species in solution to the conductive electrode is controlled by the voltage applied to the electrode. When the energy of the electrode is lower than the energy of the highest occupied molecular orbital (HOMO) of a species in solution, it is thermodynamically favorable for the electron to be transferred from the HOMO to the electrode, which results in the species being oxidized. Conversely, when the voltage applied at the electrode is lower than the energy of the lowest occupied molecular orbital (LUMO) of the species, it becomes favorable for the LUMO to gain an electron, which results in the species being reduced. The energy required to oxidize or reduce a molecule is described by the following equation:

$$\Delta G = - nF\Delta E \quad (1)$$

where the change in free energy (ΔG) is related to the number of electrons required to oxidize or reduce the species (n) and the cell potential (ΔE) with units of voltage (voltage = joule/coulomb). Faraday's constant ($F = 96,485 \text{ C/mol}$) is a unit conversion factor equal to the total electric charge carried by one mole of electrons.

The above describes the process of electron transfer at a single electrode. Every electrochemical cell, however, has two electrodes, one where the oxidation reaction occurs (the anode) and another where the corresponding reduction reaction occurs (the cathode). A schematic of an electrochemical redox process is shown in **Figure A.4**, using the conversion of 2-propanol to acetone as an example (see **Scheme A.1**). Oxidation of the alcohol to the corresponding ketone takes place at the anode, and protons in solutions are reduced to hydrogen at the cathode.

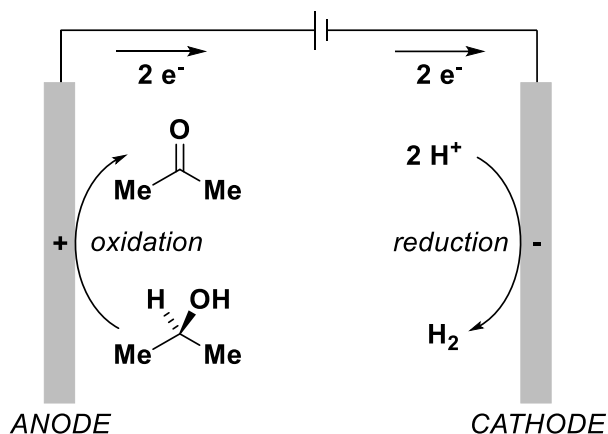


Figure A.4. Balanced redox reaction for the electrochemical oxidation of 2-propanol and reduction of protons.

Electrochemical Equipment

As alluded to above, specific items of equipment are required to run an electrochemical reaction. The main items are a source of electrons, a series of electrodes, and an electrolysis cell (**Figure A.5**). The electrolysis cell is the vessel in which an electrochemical reaction is performed and can range from a simple round bottom flask to the more complex apparatus as seen in the lab video.

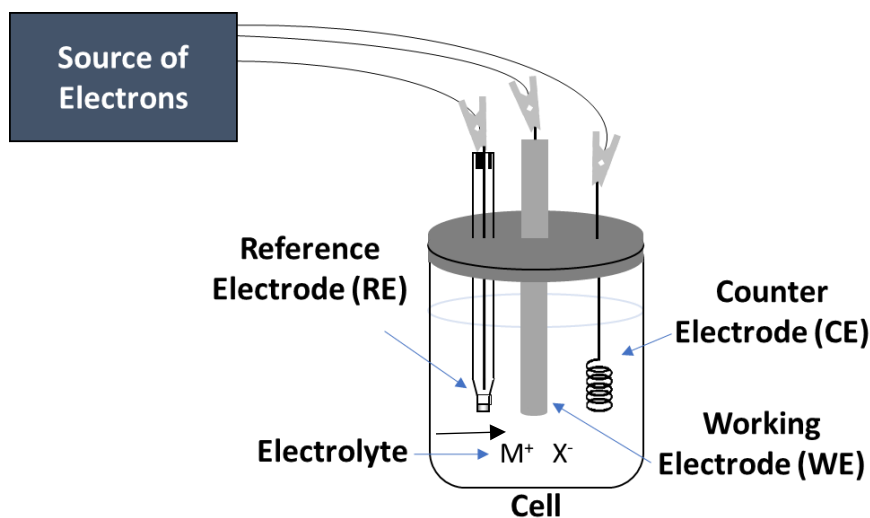


Figure A.5. The components of an electrochemical cell.

The source of electrons provides the electrical energy needed to drive electron transfer at the electrode surfaces. A potentiostat allows the application of variable (rather than fixed) potentials or currents to an electrochemical cell. Modern potentiostats interface with a computer, thus enabling control of various experimental parameters, the design of new electrochemistry experiments, and recording of experiment data. A potentiostat is required for many analytical electrochemistry experiments and can be used to drive bulk electrolysis reactions. A power source, like a simple battery, is a source of electrons that does not allow variation of the potential of the electrochemical cell. Power sources are used for bulk electrolysis reactions but cannot be used for most analytical experiments.

Electrodes are where electron transfer occurs during an electrochemical reaction. The terms anode and cathode refer to which half of a redox reaction is occurring at a given electrode. Additional terms used by electrochemists are working electrode (WE) and counter electrode (CE). The redox reaction of interest occurs at the WE (it can either be a reduction or oxidation reaction) and the balancing redox reaction takes place at the CE. For example, during the oxidation of 2-propanol to acetone (**Figure A.4**), the anode is the WE and the cathode is the CE. The working and counter electrodes are usually constructed from carbon (graphite, cloth, fibers, felt, glassy) or platinum, although other materials can be used.

All electrochemical experiments require an electrolyte, which is an ionic species (such as NaCl or Bu₄NPF₆) dissolved in the reaction solvent. The electrolyte allows charged species (protons, radical cations, etc.) to migrate within the electrolysis cell.

Only the relative potential between two electrodes can be known in an electrochemical experiment. The relative potential between a WE and CE can be highly variable and depends not only on the reaction occurring at each electrode but also on non-chemical parameters (e.g. physical

distance between the electrodes, surface area of the electrodes, etc.). Unless these variables are carefully controlled, the cell potential for a given electrochemical reaction can vary between nominally identical experimental setups, thus making the experiment difficult to reproduce with precision and accuracy. Inclusion of a reference electrode (RE) allows the potential of the WE to either be measured or fixed relative to a standard redox couple. A typical redox couple used in reference electrodes is Ag^0/Ag^1 , typically consisting of a silver wire immersed in a solution of silver(1) ions (AgNO_3 for nonaqueous solutions; AgCl for aqueous solutions) in an electrolyte solution. The RE has a porous glass tip to minimize leaking of the solution in the electrochemical cell into the RE (which could impact the potential of the Ag^0/Ag^1 couple), but also allows some ion exchange to balance any charge that is passed at the RE.

Common Electrochemical Experiments

All electrochemical experiments involve manipulation of potential or current and time. Potential and current are dependent variables, thus many electrochemical experiments involve application of a specific potential to an electrolysis cell via a potentiostat and monitoring how the current varies over time (or *vice versa*).

Constant Potential Electrolysis

In an electrochemical reaction performed at a constant potential (**Figure A.6**, left), the potential at the WE is fixed and the current is allowed to vary. An RE must be used in this process because it provides a fixed value by which the potential at the WE can be maintained during the reaction. As the substrate is consumed by reaction at the WE, less material is available as the reaction proceeds and thus the monitored current decreases over time.

Constant Current Electrolysis

In an electrochemical reaction performed at a constant current (**Figure A.6**, right), the current that is maintained at the WE is set by the experimenter. The potential at the WE adjusts to

match the potential of the most easily oxidized (or reduced) substrate in the electrolysis solution. The substrate is consumed by reaction at the WE, thus less substrate is available to undergo reaction at the WE. To maintain the set current, the potential at the WE increases over time.

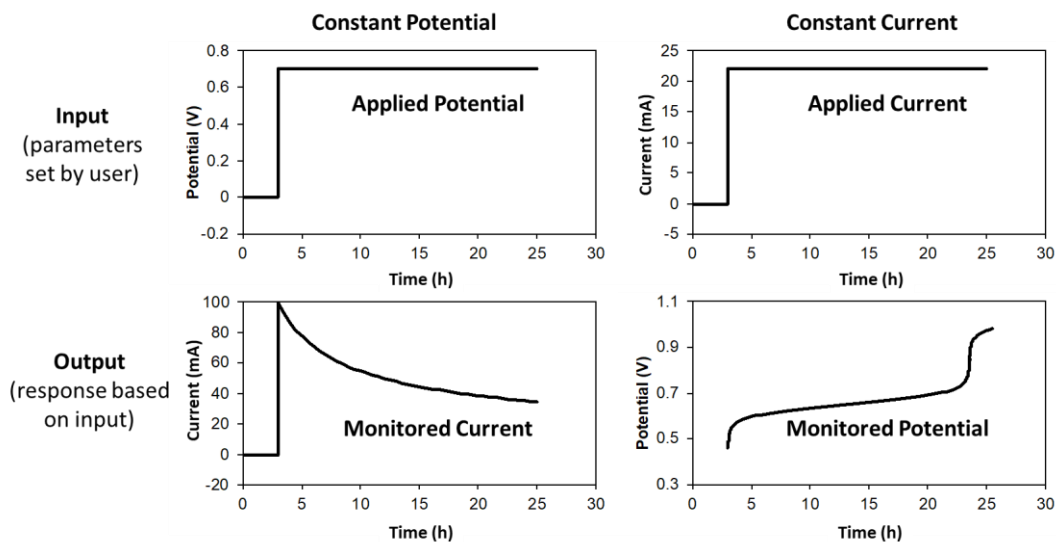


Figure A.6. Constant potential (left) and constant current (right) electrolysis traces for an electrochemical oxidation reaction.

Cyclic Voltammetry

Cyclic voltammetry is an analytical electrochemistry technique.⁷ In this process, the potential at the WE is scanned from a starting potential (E_1) to another potential (E_2) and back to the original potential ($E_3 = E_1$) (see **Figure A.7**, left). The current at the WE is monitored during the scan as a function of potential (see **Figure A.7**, right). A non-zero current indicates that electron transfer occurred at the corresponding potentials.

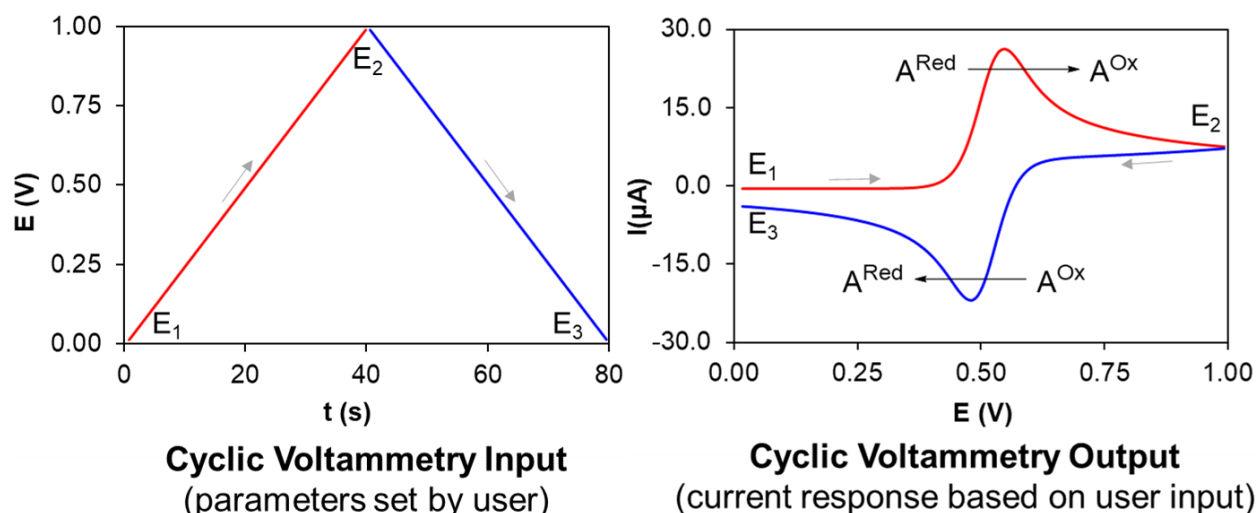


Figure A.7. Cyclic voltammetry potential waveform (input, left) and resulting cyclic voltammogram (right) for a reversible redox couple, $A^{\text{Red}}/A^{\text{Ox}}$, with a half-wave potential of 0.5 V.

In the cyclic voltammogram (CV) shown in **Figure A.7**, the shape of the current-potential curve provides information about the electrochemical reactions occurring at the WE. As the potential is scanned in the positive direction from E_1 to E_2 (red line), the current starts to increase to a positive value at approx. 0.45 V and reaches the highest current at approx. 0.55 V (also known as the oxidative peak potential). This change in current indicates that a molecule is being oxidized at the WE. When the potential is switched and scans toward the negative direction from E_2 to E_3 (blue line), the current decreases to a negative value. The potential corresponding to the most negative current in this peak is the reductive peak potential. The oxidized species that was generated at the WE during the first half of the experiment is now being reduced at the WE.

Cyclic voltammograms that exhibit a symmetrical “duck-shaped” waveform are typical of redox processes where the electrochemically generated species are stable (or are not consumed in further reactions) and can be reduced during the return scan. In contrast, the shape of the CV is not symmetrical if the oxidized species generated during the forward scan either decomposes under

the experimental conditions or reacts to form a new species that cannot be reduced during the returning scan.

A common misconception is that the chemical reactions happening during CV experiments can change the concentration of substrates in the bulk solution being analyzed. However, a WE with a relatively small surface area (*i.e.* less than 7 mm²) is used during these experiments. Using a WE with such a small surface area prevents any change in the concentration of substrates in the bulk solution (in a bulk electrolysis experiment where the goal is to transform substrate to useful quantities of product, WE surface areas are typically $\gg 1$ cm²).

The mathematics of the kinetic and thermodynamic processes that govern the shape of CVs were established by Irving Shain and his student Richard Nicholson in the 1960s.⁸ At the time, Shain was a professor of chemistry at UW-Madison and later served as Chancellor of the University. The Shain Tower of the chemistry building is named in his honor.

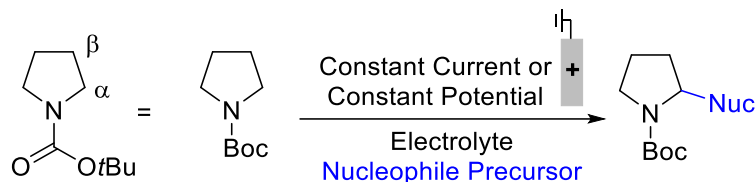
Shono oxidation

Cyclic voltammetry and bulk electrolysis are both useful techniques for designing and executing electrochemical synthesis reactions. As an analytical technique, cyclic voltammetry can be used to characterize the electrochemical behavior of molecules, determine the mechanism of chemical and electrochemical reactions, monitor species generated during chemical or electrochemical reactions, or determine kinetic parameters like the rate of electrocatalytic reactions. As synthesis techniques, constant current and constant potential bulk electrolysis provide controlled methods to drive electron transfer needed to achieve a redox reaction.

The Shono oxidation is a synthetic electrochemical method for the functionalization of carbamate compounds (**Scheme A.2**). It was first reported by Tatsuya Shono at Kyoto University in 1975.⁹ In this reaction, a carbamate is electrochemically oxidized at the anode to an iminium intermediate which is trapped by a nucleophile that is generated *in situ* by reduction of a precursor

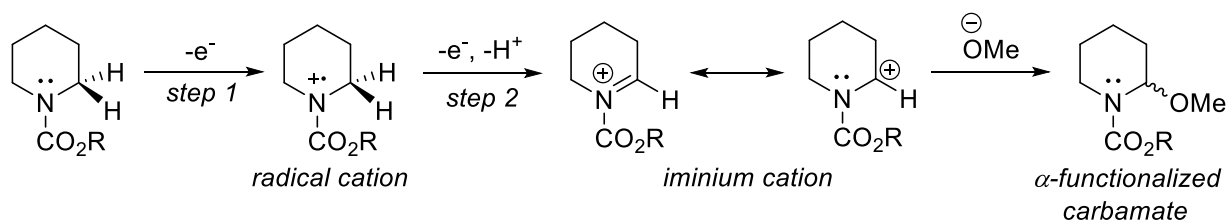
at the cathode. The Shono reaction has been used in total synthesis and for the generation of metabolites.

Scheme A.2. Shono electrochemical oxidation of *N*-Boc-pyrrolidine to the corresponding α -functionalized compound.



The electrochemical oxidation of the carbamate substrate proceeds in two steps (**Scheme A.3**). In the first step, the carbamate undergoes a one-electron oxidation at the anode to generate the corresponding radical cation. A second (easier) oxidation and a deprotonation at the α -position yields an electrophilic iminium cation intermediate. In the original Shono oxidation reaction, methoxide anion was generated from the methanol electrolyte/solvent and served as the nucleophile to react with the iminium cation and generate the corresponding α -methoxylated carbamate product.

Scheme A.3. Overview of the electrochemical Shono oxidation.



Various non-electrochemical methods for the oxidative α -functionalization of carbamates have been reported, however they generally require strong oxidants or are limited in carbamate scope (*i.e.* the α -methylene group must also be benzylic).^{10,11} Likewise, the α -functionalization of unprotected 2° amines (such as piperidine and morpholine) is challenging.¹²

The Shono oxidation is an example of a synthetic electrochemical reaction that is widely used due to its versatility and robustness. Though the process is generally applied to form α -methoxylated carbamates, the methoxy group is relatively labile and can be readily replaced with other nucleophiles in the presence of a Lewis or Brønsted acid, expanding the product scope.¹³ Furthermore, the reaction can be performed in the absence of a nucleophile at low temperatures to form a “pool” of the reactive iminium intermediate, which can then be trapped by addition of a nucleophile to the reaction solution after the electrolysis.¹⁴ The reaction can work with cyclic carbamates of a range of ring sizes and with acyclic carbamates.

Summary and Goals

The purpose of this project is to introduce students to common electrochemistry techniques in the context of the Shono oxidation.

The initial part of the project will use cyclic voltammetry to measure the oxidation potentials of anisole (1), piperidine-1-carboxylic acid methyl ester (2) and 4-anisylpiperidine-1-carboxylic acid methyl ester (3) as potential substrates for a Shono oxidation (**Figure A.8**). The pedagogical goals include a) learning how to perform a cyclic voltammetry experiment, b) interpretation of CV data, and c) using CV data to inform electrosynthesis methods.

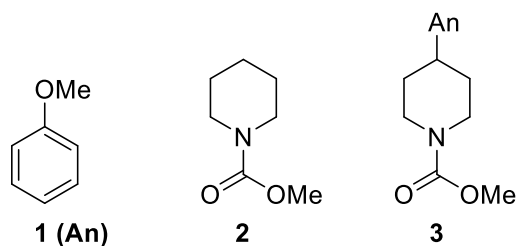


Figure A.8. Substrates to be analyzed by cyclic voltammetry

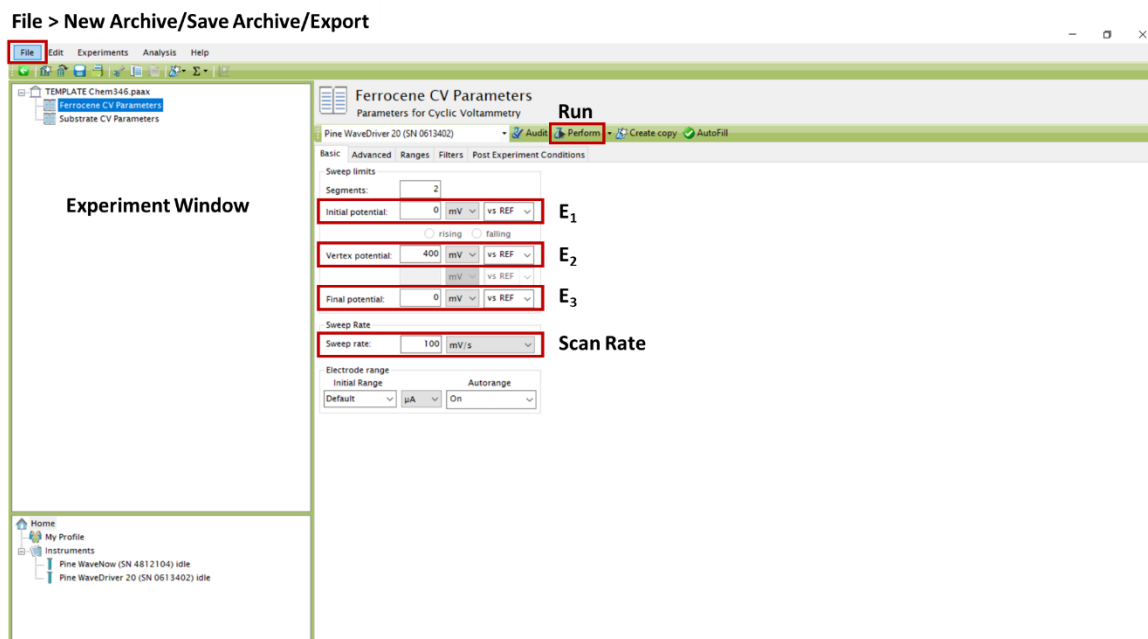
The second part, observed in the video posted on the course website, involves a Shono oxidation of *N*-Boc pyrrolidine to the corresponding α -methoxy compound using constant current

electrolysis. The pedagogical goals include a) learning how to perform an electroanalysis reaction, b) determination of the redox reactions occurring in the electrolysis cell, and c) interpretation of ^1H NMR data to determine the yield (%) of a reaction.

Experimental Procedure

Part 1- Cyclic voltammetry

To the electrolysis cell containing the reference ferrocene solution (1 mM ferrocene, 100 mM tetrabutylammonium hexafluorophosphate in 10 mL MeCN), insert a glassy carbon working electrode and a platinum wire coil counter electrode through the cap into the solution (5-10 cm from cell bottom). The working electrode should be placed in the center hole of the cap. Remove the Ag/Ag^+ reference electrode from the storage solution, rinse the tip with acetone, let the acetone on the RE evaporate, and insert the reference electrode into the reference solution. Attach the red/orange lead to the working electrode, the green lead to the counter electrode, and the white lead to the reference electrode.



Using the Aftermath software, click “File > New Archive” at the top of the software window. An archive named “Archive [date]” will appear. Right click on this archive, select “Save Archive As...”, and save the archive on the desktop with the name “Last name, Chem346”. In the Aftermath experiment window, drag the “Ferrocene CV Parameters” experiment under the “TEMPLATE Chem346” archive into your archive. The parameters should already be set to perform a cyclic voltametric study over the potential range -200 – 400 mV (vs. Ag/Ag⁺) at a sweep rate of 100 mV/s. *After having a TA check your experimental setup*, click “Perform”. Once the experiment is finished, a new experiment will appear underneath “CV Parameters” called “CV Experiment (#)”. Right click on “CV Experiment (#)” and select “Rename” in the pop-up window. Name the experiment “Last name, Ferrocene”.

Remove the leads from the electrodes. Remove the counter and reference electrodes from solution, rinse the electrodes with acetone, let the acetone on the RE evaporate, and insert the electrodes into the electrolysis cell containing the solution of substrate 1 (5 mM anisole, 100 mM tetrabutylammonium hexafluorophosphate in 10 mL MeCN). Remove the working electrode from solution. Rinse the working electrode first with acetone and then deionized water. Your TA will demonstrate how to polish the electrode. After polishing, rinse the electrode with DI water, followed by acetone, and insert it into the anisole solution after the electrode is dry.

In the Aftermath software program, drag the “Substrate CV Parameters” experiment under the “TEMPLATE Chem346” archive into your archive. The parameters should already be set to perform a cyclic voltametric study over the potential range 0.0 – 2.0 V (vs Ag/Ag⁺) at a sweep rate of 100 mV/s. Collect a CV of anisole (compound 1, **Figure A.8**) and name the experiment “Last name, Anisole”.

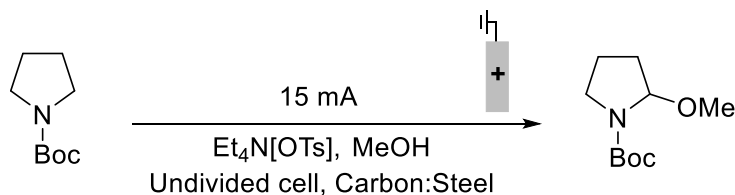
After collecting the CV of 1, rinse/polish the electrodes. Collect and save CVs of solutions containing substrates 2 and 3 (both 5 mM in substrate and 100 mM tetrabutylammonium hexafluorophosphate in 10 mL, MeCN) (**Figure A.8**).

Once all four CVs have been obtained, rinse all three electrodes, replace the reference electrode in the storage solution, and polish and rinse the working electrode. Set these electrodes aside for the next group.

At the top of the Aftermath software window, click “File > Save Archive”. Then click “File > Export”. Check the box next to your archive and click “Export.” Click “Browse” and select the “Desktop” and click “Open”. Click “Export”. This process should save the data to a folder called “Last name, Chem346” on the Desktop in a format that can be opened in Microsoft Excel.

Open the exported folder and double-click on the subfolder containing CV data for ferrocene. Open the “Voltammogram” folder and open the “Current vs Potential” Excel file. On the desktop, click the Excel titled “TEMPLATE Chem346” Excel. Click on the “Ferrocene” tab at the bottom of the Excel. Copy and paste the data from “Current vs Potential” into the highlighted section. Close the “Current vs Potential” Excel file. In the “TEMPLATE Chem346” Excel file, click the “Substrates” tab. Transfer the data from anisole, *N*-Boc-piperidine, and *N*-Boc-4-(4-methoxyphenyl)piperidine to the “TEMPLATE Chem346” Excel. Save the Excel file on the Desktop as “Last name, Chem 346”. Your Excel file should contain a plot of the three CVs and a list of the oxidation peak potentials, all referenced to Fc/Fc⁺ (the ferrocene/ferrocenium couple).

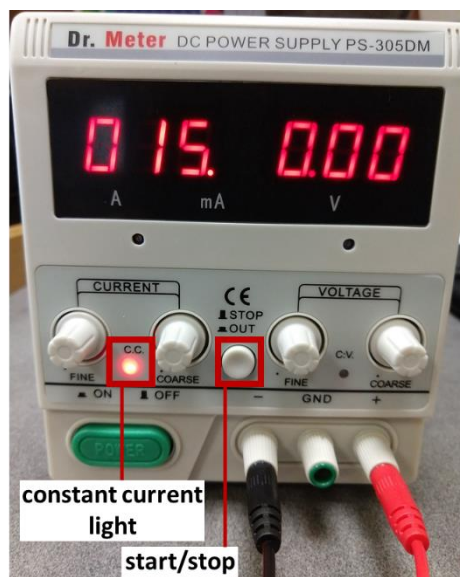
Part 2 - Shono oxidation of N-Boc pyrrolidine



To an undivided electrolysis cell, add tetraethylammonium *p*-toluene sulfonate (150.7 mg, 0.5 mmol, 0.1 M) and a Teflon-coated stir bar. Bring the cell and top to the hood and add methanol (5 mL). Using a micropipette, add *N*-Boc-pyrrolidine (44 μ L, 0.25 mmol, 0.05 M). Before removing the cell from the hood, screw the lid containing the graphite rod working electrode and stainless-steel counter electrode onto the cell.



Secure the cell on the stir plate and increase the stir rate until good convection is observed. Attach the red lead to the working electrode and the black lead to the counter electrode, making sure that the metal leads are not touching each other. *After having a TA check your experimental setup*, depress the start/stop button in the center of the potentiostat and set a timer for 67 min (2.5 F/mol) or note the time when the reaction is started. The power supply should read 15 mA and the constant current light should be red within a few seconds of starting the reaction. When the reaction is finished, push the stop/start button at the center of the power supply to stop the reaction.



When the electrolysis is complete, transfer the electrolysis solution to a round bottom flask, rinsing the cell and electrodes with methanol. Remove the solvent *in vacuo* using a rotary evaporator. Using a micropipette, add 10 μL 1,3-5-trimethylbenzene (0.072 mmol) to the crude material, dissolve the sample in CDCl_3 and obtain a $^1\text{H-NMR}$ spectrum.

Report requirements

Present your report, data, and spectra according to ACS journal style.

Abstract (5 pts)

Summarize the key findings of the CV study and Shono oxidation in a brief abstract (it might be prudent to write this section after you have completed the data analysis).

Introduction (15 pts)

Briefly outline the goal(s) of this study in terms of the chemistry and analysis taking place. (5 pts).

Literature analysis (10 pts)

Read the paper *Angew. Chem. Int. Ed.* 2018, 57, 6686 and briefly outline *i*) a major limitation of the Shono oxidation that impacts substrate scope and *ii*) results discussed in the paper that overcome this limitation. Cite the paper in the ACS style.

Experimental (15 pts total)

Rewrite the Shono oxidation experimental procedure in past tense and include the exact masses, volumes, etc. you used in the lab (5 pts). Include an appropriate reaction scheme and summary of the ^1H NMR (10 pts) of the crude product.

Results & Discussion (60 pts total)

Use this section to present your experimental and theoretical data and outline the overall meaning of the results/data. (5 pts) Tables are useful for showing multiple data sets simultaneously. The following subsections should be included (they do not need a separate heading; instead they should be woven into the narrative).

Data analysis (30 pts)

Show the individual cyclic voltammograms of anisole (**1**), piperidine-1-carboxylic acid methyl ester (**2**), and 4-anisylpiperidine-1-carboxylic acid methyl ester (**3**) on a single, labeled CV plot. Reference the potential axis (x-axis) to the ferrocene CV data. Indicate the peak potential of each CV. (10 pts)

Compare the shape of the CVs of substrates **1-3** to the CV of ferrocene. What do the differences (if any) indicate? Briefly discuss possible reasons for this difference (the Angew. Chem. paper cited above may be useful for this question) (10 pts)

Use the CV data to rank compounds **1-3** in order of ease of electrochemical oxidation. Based on this ordering, briefly explain which of the two piperidine-based substrates would be best suited for a Shono oxidation. (10 pts)

WebMO (10 pts)

Optimize the structure of the Shono oxidation product (B3LYP/6-31G(d), C1 symmetry, ~3 hr to optimize) and perform an NMR calculation on the optimized structure. Be sure that the Boc group is in the *syn* conformation (see NMR assignment key). Show the experimental and

B3LYP-predicted ^1H NMR shifts in a single table (use the average of the individual shifts for any H atoms you expect to be equivalent). The results of this calculation will be useful during your analysis of the ^1H NMR spectrum of the crude product. Include an image of the Shono product next to the NMR table and include the six-digit WebMO job number for each calculation at the end of the assignment.

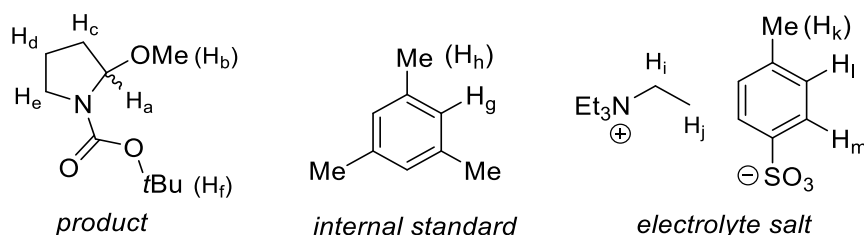
NMR (15 pts)

Use the B3LYP ^1H NMR chemical shift estimates to assign all signals in the experimental ^1H NMR spectrum of the Shono oxidation product mixture (CDCl_3) according to the key below. Note that some signals may overlap, in which case label the composite signal using the appropriate ^1H labels. Use the signals from the internal standard and product to calculate the yield (%) of the Shono oxidation reaction. Show all work for the yield (%) calculation.

In addition to data for the crude product, ^1H NMR spectra (CDCl_3) of the *N*-Boc pyrrolidine substrate and the $[\text{Et}_4\text{N}][\text{OTs}]$ electrolyte are available on the course website. Interpretation of these spectra is not required for credit but will assist in the assignment of each signal in the ^1H NMR spectrum of the crude Shono reaction product.

Assignment key for ^1H NMR spectrum

Use the key shown below to assign all signals in the ^1H NMR data of the Shono oxidation product.



Note that the *N*-Boc group can rotate about the axis of the N-C(O) bond. In solution, the conformational isomers (rotamers) of *N*-Boc pyrrolidine are in equilibrium, therefore H_a experiences different chemical environments that depend on this equilibrium

Conclusion (5 pts total)

Use this section to summarize the outcome of the study. (5 pts) The following subsection should be included (it does not need a separate heading; instead it should be woven into the narrative).

A.4. Optional Addendum to Student Laboratory Manual Chapter and Assessment Questions

When employing bulk electrolysis techniques, electrochemists commonly report the amount of charge passed in the cell during the electrolysis. The Faraday constant (96,485 Coulombs/mol e⁻) represents the amount of charge (C) in one mole of electrons and can be used to relate the charge passed during an electrolysis to the moles of electrons transferred during the electrolysis. In electrolysis reactions, electrons are transferred in stoichiometric quantities. In the Shono oxidation (as in most organic redox reactions), transfer of two moles of electrons per mole of the carbamate substrate are required. The moles of electrons transferred during a reaction per moles of substrate added to the cell is also referred to as the Faraday's per mole (F/mol). The amount of charge passed during a reaction can be described by:

$$\text{Current (amp, A)} \times \text{Time (second, s)} = \text{Charge (coulomb, C)} \quad (2)$$

The quantity of electrons transferred during a reaction can be determined from the total charge applied during the reaction:

$$e^- \text{ (mol)} = \frac{\text{Total Charge (C)}}{96785 \text{ (C mol}^{-1} \text{e}^-)} \quad (3)$$

In “Experimental Procedure (Part 2 – Shono Oxidation of N-Boc pyrrolidine)”



Increase the stir rate until good convection is observed. Connect the potentiostat leads to the electrolysis cell electrodes, taking care to make sure the correct leads are connected to the correct electrodes and that the leads are not contacting any other conductive materials. Standard connections for all Pine potentiostats are described below:

Red: working, anode (here: graphite rod)

White: reference (here: Ag/Ag⁺ electrode)

Green: counter, cathode (here: Pt wire)

Black: ground (attach to a clamp or other convenient conducting material)

After having a TA check your experimental setup, open the AfterMath program. Open the “Shono Oxidation” archive. The archive will contain the conditions for a bulk electrolysis experiment and will either be set up for a constant current experiment (15 mA) or a constant potential (1.5 V) experiment. The parameters have been set to stop the electrolysis once 60 Coulombs have been passed.

In “Report Requirement (Data Analysis)” (p. 20)

Calculate the moles of electrons passed in the Shono oxidation. Show all work for the calculation and report the answer with three significant figures. How does this compare to the theoretical quantity of electrons required for the reaction? What do the differences (if any) indicate? Briefly discuss possible reasons for this difference. (10 pts)

A.5. Grading Key**Abstract (5 pts)**

Summarize the key findings of the CV study and Shono oxidation in a brief abstract (it might be prudent to write this section after you have completed the data analysis).

Grade 5, 3, 1, or 0 pts for a coherent summary of the CV data including: the best Shono oxidation substrate for bulk electrolysis based on CV analysis and the outcome of the Shono bulk electrolysis reaction (product, yield (%)).

Introduction (15 pts)

Briefly outline the goal(s) of this study in terms of the chemistry and analysis taking place. (5 pts).

Grade 5, 3, 1, or 0 pts based on a coherent summary of lab goals.

Literature analysis (10 pts)

Read the paper *Angew. Chem. Int. Ed.* 2018, 57, 6686 and briefly outline *i*) a major limitation of the Shono oxidation that impacts substrate scope, and *ii*) results discussed in the paper that overcome this limitation. Cite the paper in the ACS style. (10 pts)

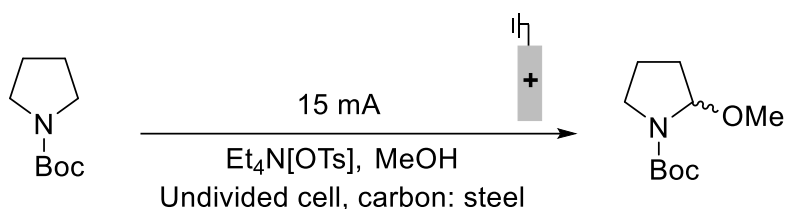
Wang, F.; Rafiee, M.; Stahl, S. S. Electrochemical Functional-Group-Tolerant Shono-type Oxidation of Cyclic Carbamates Enabled by Aminoxyl Mediators. *Angew. Chem. Int. Ed.* 2018, 57, 6686-6690. 2 pts fully correct citation

A major limitation of a typical Shono oxidation is the low compatibility of functional groups on the carbamate (2 pts). This is because the high electrode potentials required to initiate direct electrochemical oxidation of the substrate (1 pt) can lead to decomposition/undesired reactivity (1 pt).

The results described in the ACIE paper show that use of an aminoxyl radical lowers the potential at which the oxidation takes place (2 pts). The aminoxyl radical acts as a hydride-transfer mediator (1 pt) to generate the required iminium cation at lower applied potentials (1 pt) than are required for direct oxidation of the substrate in the classical Shono oxidation.

Experimental (15 pts total)

Rewrite the Shono oxidation experimental procedure in past tense and include the exact masses, volumes, etc. you used in the lab (5 pts). Include an appropriate reaction scheme and summary of the ^1H NMR (10 pts) of the crude product.



To an undivided electrolysis cell was added tetraethylammonium *p*-toluene sulfonate (xx mg, xx mmol) and a Teflon-coated stir bar. Methanol (~5 mL) was added, followed by *N*-Boc-pyrrolidine (44 μL , 0.25 mmol, 0.05 M). The graphite working electrode and stainless-steel counter electrode were added to the cell and the reaction mixture stirred rapidly. The electrodes were activated, and the reaction stirred for 67 min (2.5 F/mol). After this time, the mixture was transferred to a round bottom flask and the solvent removed *in vacuo*. To the residue was added 1,3,5-trimethylbenzene (10 μL , 0.072 mmol), and the mixture dissolved in CDCl_3 .

^1H NMR (d, ppm): 5.10 (m, 1H), 3.45 (s, 3H), 3.41 (m, 2H), 2.09-1.66 (m, 4H), 1.47 (s, 9H).

5 pts scheme (3, 1, or 0 pts)

5 pts coherent and correct procedure (3, 1, or 0 pts)

5 pts NMR data (3, 1, or 0 pts)

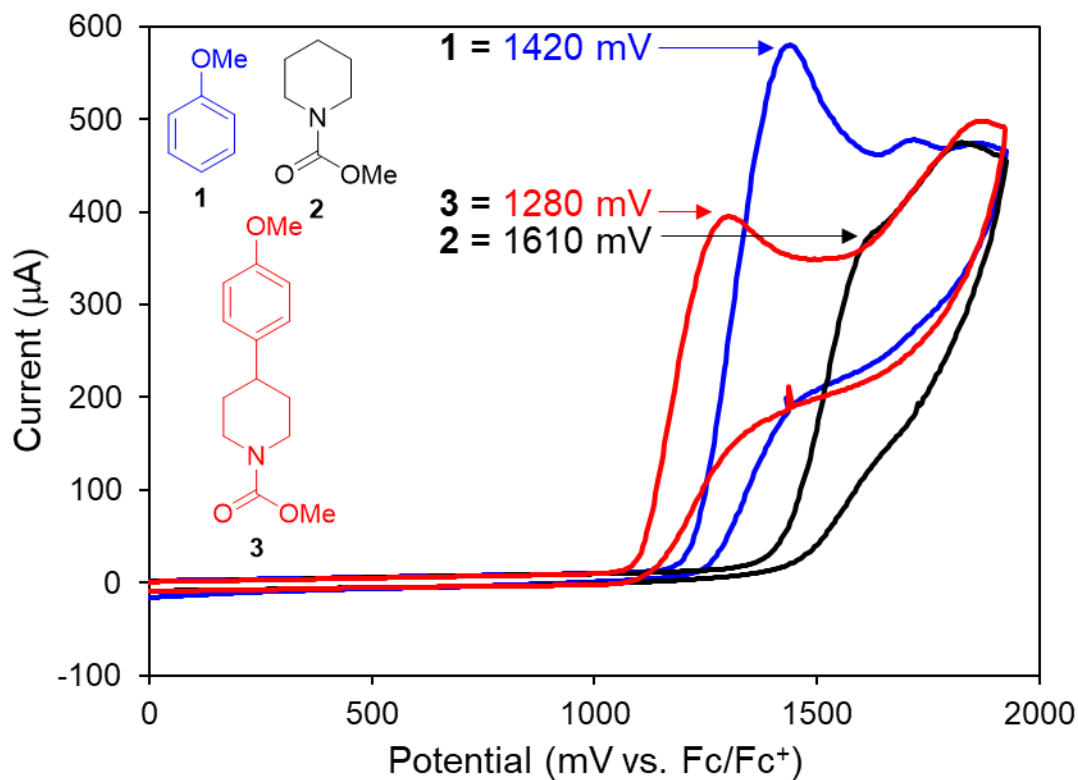
Results & Discussion (60 pts total)

Use this section to present your experimental and theoretical data, and outline the overall meaning of the results/data. (5 pts) Tables are useful for showing multiple data sets simultaneously. The following subsections should be included (they do not need a separate heading; instead they should be weaved into the narrative).

Grade 5, 3, 1, or 0 pts based on coherent summary of the data.

Data analysis (30 pts)

Show the individual cyclic voltammograms of anisole (1), piperidine-1-carboxylic acid methyl ester (2), and 4-anisylpiperidine-1-carboxylic acid methyl ester (3) on a single, labelled CV plot. Reference the potential axis (x -axis) to the ferrocene CV data. Indicate the peak potential of each CV. (10 pts)



4 pts single correct labeled plots showing CVs of all three substrates

Approximate peak potential values are as follows (all vs. Fc):

Anisole (1) = 1420 mV

Piperidine-1-carboxylic acid methyl ester (2) = 1610 mV

4-Anisylpiperidine-1-carboxylic acid methyl ester (3) = 1280 mV

2 pts per reasonably close value (± 0.5 V) (6 pt total)

Compare the shape of the CVs of substrates 1-3 to the CV of ferrocene. What do the differences (if any) indicate? Briefly discuss possible reasons for this difference (the *Angew Chem* paper cited above may be useful for this question) (10 pts)

Ferrocene exhibits a reversible CV that is “duck-shaped” (2 pts). This duck shape indicates that the ferrocene/ferrocenium (Fc/Fc^+) redox couple is reversible (2 pts), that ferrocenium is stable

under these conditions on the time scale of the CV experiment, and that the kinetics of electron transfer at the electrode surface are relatively fast.

The CVs of the organic substrates are irreversible (4 pts). A likely cause is the formation of either an aryl- or carbamate-based radical cation or iminium cation (1 pt) at the electrode surface results in a secondary reaction(s) so that the radical cation or iminium cation is not present at the electrode surface to be electrochemically reduced (1 pt). They can also back this statement up with information about how well the Shono oxidation of compounds 2 and 3 proceed based on the *Angew. Chem. Int. Ed.* article.

Use the CV data to rank compounds 1-3 in order of ease of electrochemical oxidation. Based on this ordering, briefly explain which of the two piperidine-based substrates would be best suited for a Shono oxidation. (10 pts)

4-Anisylpiperidine-1-carboxylic acid methyl ester (3) is easiest to oxidize/has the lowest oxidation potential/requires the least positive electrode potential to undergo oxidative electron transfer, followed by anisole (1), then piperidine-1-carboxylic acid methyl ester (2).

2 pts each correct ordering (6 pts total)

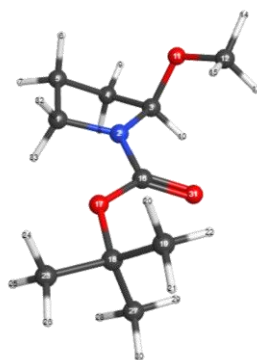
Compound 2 is better suited to the Shono oxidation than compound 3 (2 pts) because it does not have an incompatible functional group (1 pt). If the reaction were run with compound 3, electron transfer would likely occur at the aryl group/an aryl radical cation would be generated.

(1 pt). (4 pts total)

WebMO (10 pts)

Optimize the structure of the Shono oxidation product (B3LYP/6-31G(d), C1 symmetry, ~3 hr to optimize) and perform an NMR calculation on the optimized structure. Be sure that the Boc group is in the *syn* conformation (see NMR assignment key). Show the experimental and B3LYP-predicted ^1H NMR shifts in a single table (use the average of the individual shifts for any H atoms

you expect to be equivalent). The results of this calculation will be useful during your analysis of the ^1H NMR spectrum of the crude product. Include an image of the Shono product next to the NMR table and include the six-digit WebMO job number for each calculation at the end of the assignment.



Atom	Calc. NMR shift	Exp. NMR shift
H _a	5.10	5.11
H _b	$(3.27+3.30+3.44)/3 = 3.34$	3.45
H _c	$(1.56+1.80)/2 = 1.68$	~1.66 – 2.1
H _d	$(2.24+1.58)/2 = 1.91$	~1.66-2.1
H _e	$(3.31+3.19)/2 = 3.25$	~3.41
H _f	$[(1.25)+(1.62)+(1.57)]/3 = 1.48$	1.47

1 pt coherent table

1 pt WebMO image of product

8 pts all correct calculated signals

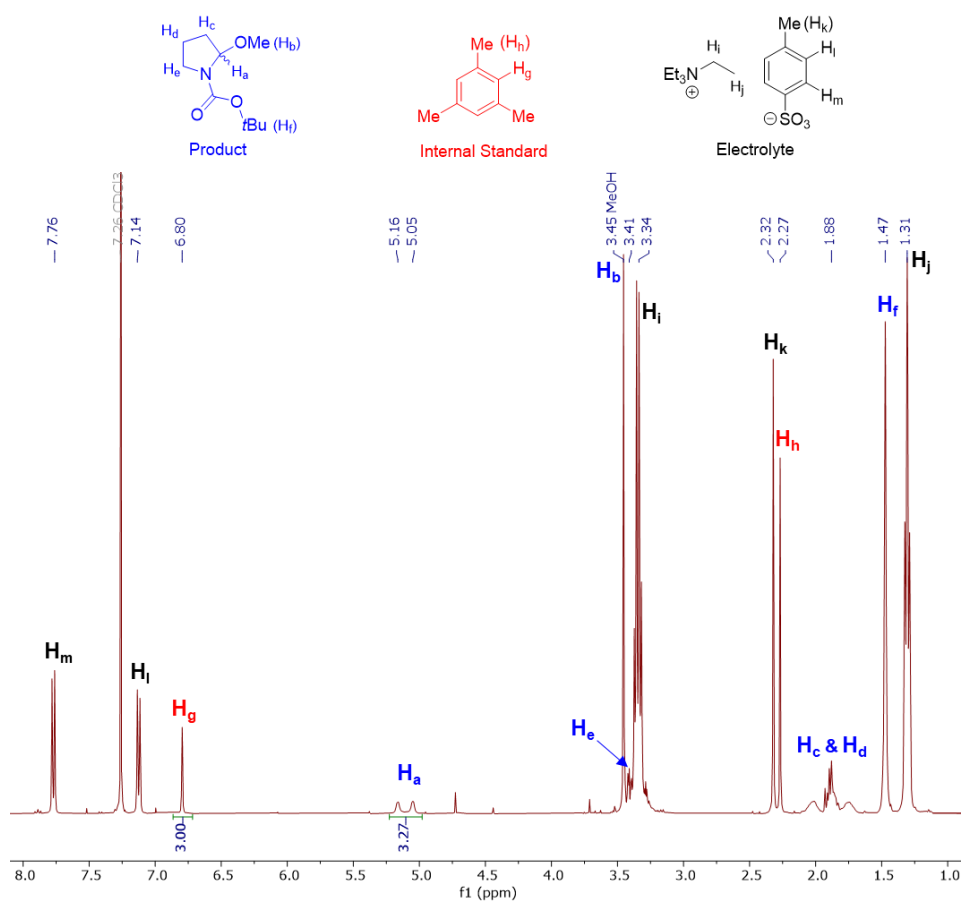
(6 pts one error/omission)

NMR (15 pts)

Use the B3LYP ^1H NMR chemical shift estimates to assign all signals in the experimental ^1H NMR spectrum of the Shono oxidation product mixture (CDCl_3) according to the key below. Note that some signals may overlap, in which case label the composite signal using the appropriate ^1H

labels. Use the signals from the internal standard and product to calculate the %yield of the Shono oxidation reaction. Show all work for the yield (%) calculation.

In addition to data for the crude product, ^1H NMR spectra (CDCl_3) of the *N*-Boc pyrrolidine substrate and the $[\text{Et}_4\text{N}][\text{OTs}]$ electrolyte are available on Canvas. Interpretation of these spectra is not required for credit but will assist in the assignment of each signal in the ^1H NMR spectrum of the crude Shono reaction product.



10 pts all correct assignments

(8 pts one error/omission)

(6 pts two errors/omissions)

(4 pts > two omissions)

$$\text{Product (mmol)} = 0.072 \text{ (mmol)} \times \frac{\frac{\text{Ha Integration}}{1}}{\frac{\text{Hg Integration}}{3}}$$

$$\text{Yield (\%)} = \frac{\text{Product (mmol)}}{0.25 \text{ (mmol)}} \times 100$$

5 pts correct yield (%) calculation

(3 pts if yield is approximately correctly but the calculation incorporates odd signals (H_f or H_h))

(1 pt for incorrect yield calculation)

Conclusion (15 pts total)

Use this section to summarize the outcome of the study. (5 pts) The following subsection should be included (it does not need a separate heading; instead it should be weaved into the narrative).

Grade 5, 3, 1, or 0 pts based on coherent summary of the findings.

A.6. Alternative Set-Up Addendum to Grading Key

In “Report Requirement”

Data Analysis (10 pts)

Calculate the moles of electrons passed in the Shono oxidation. Show all work for the calculation and report the answer with three significant figures. How does this compare to the theoretical quantity of electrons required for the reaction? What do the differences (if any) indicate? Briefly discuss possible reasons for this difference. (10 pts)

$$2.49 \text{ F/mol} = \frac{60 \text{ C}}{96485 \text{ C/mol} \times 0.00025 \text{ mol}}$$

5 pts total

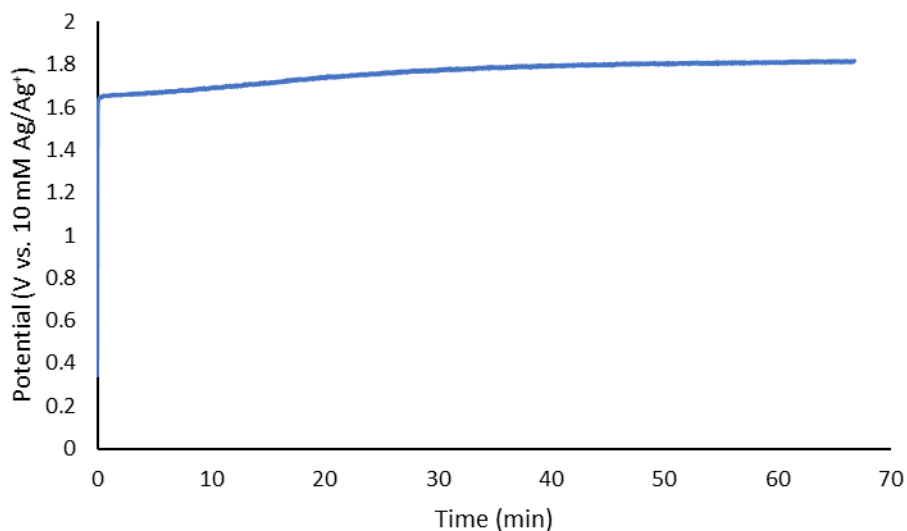
(no units = 2 pts)

(-1 wrong sig figs)

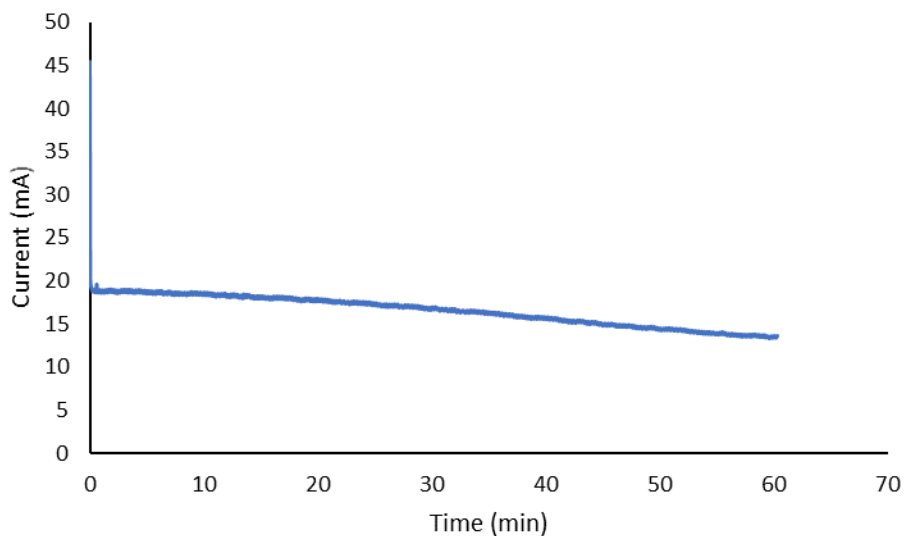
The Shono reaction is a 2e⁻ oxidation reaction, so 2 F/mol is theoretically required to convert all substrate to product (1 pt). 2.5 F/mol is passed in the cell during the reaction, indicating that at

least 0.5 F/mol are not involved in product formation (1 pt). The electrochemical side-reaction is likely oxidation of the MeOH solvent (3 pt). They can include bulk electrolysis traces to support their conclusions.

Constant Current Bulk Electrolysis (15 min)



Constant Potential Bulk Electrolysis (1.5 V)



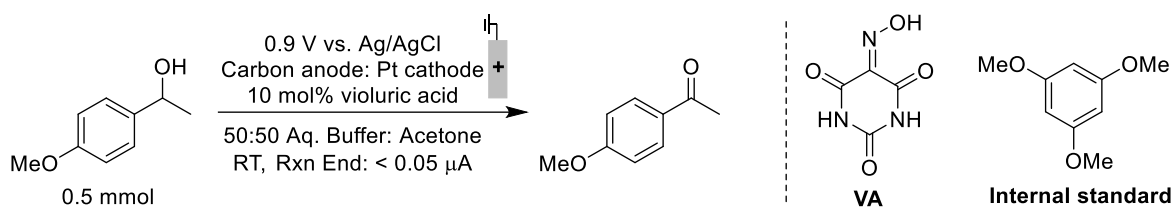
A.7. Practice Exercise: Yield Calculation from ¹H NMR Using Internal Standard

CHEM 346 How to Calculate % Yield Using ¹H NMR Data

NOT FOR CREDIT

The following exercise is a guide on how to use $^1\text{H-NMR}$ data to calculate the yield (%) of product in a crude sample of reaction mixture. The electrochemical alcohol oxidation reaction featured here uses violuric acid (VA) as an electrochemical mediator (catalyst) to convert 4-methoxy- α -methylbenzyl alcohol to 4'-methoxyacetophenone. The aromatic compound 1,3,5-trimethoxybenzene is the internal standard.

Use the procedure below and the $^1\text{H NMR}$ data file posted on the course website to calculate the yield (%) of 4'-methoxyacetophenone in the crude reaction mixture.



Procedure

To an undivided electrolysis cell, add a Teflon stir bar, a solution of 4-methoxy- α -methylbenzyl alcohol (75.7 mg, 0.5 mmol) in 10 mL 1:1 acetone:0.1 M sodium acetate/acetic acid buffer, and VA (8.76 mg, 0.05 mmol). Insert a graphite rod working electrode, a platinum wire coil counter electrode, and a Ag/AgCl reference electrode into the solution. Apply a constant potential of 0.9 V until the current is less than 0.05 μA . When the electrolysis is complete, add 1,3,5-trimethoxybenzene (16.5 mg) to the reaction solution, dissolve an aliquot of the reaction solution in CD_3CN and obtain a $^1\text{H-NMR}$ spectrum.

Notes

Integration of the signal(s) from the internal standard and product are used to determine the ratio of standard and product. The amount of product (mmol) is calculated by using this ratio and the known amount of added standard according to the equivalent equations shown below.

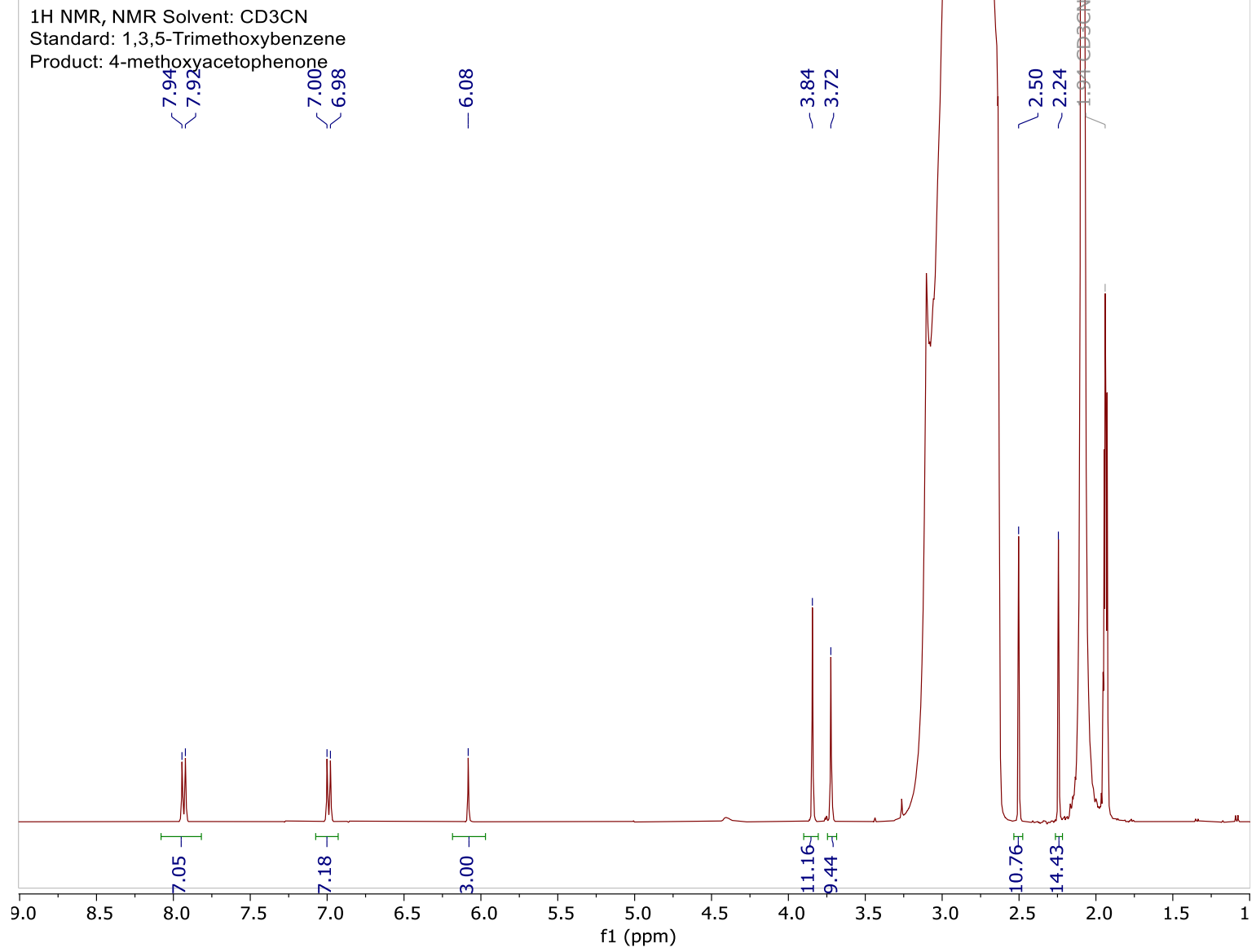
$$\text{Product (mmol)} = \text{Standard (mmol)} \times \frac{\text{Product integration}}{\text{\# H atoms}} \times \frac{\text{\# H atoms}}{\text{Standard integration}}$$

$$\text{Product (mmol)} = \text{Standard (mmol)} \times \frac{\frac{\text{Product integration}}{\# \text{ H atoms}}}{\frac{\text{Standard integration}}{\# \text{ H atoms}}}$$

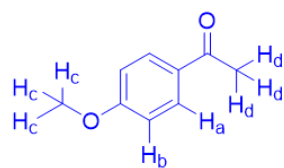
The percent yield is the ratio between the amount of product (mmol) and starting material (mmol) converted to a percentage

The reaction solvent was not evaporated before preparing the NMR sample so large signals from water and acetone are present in the spectrum.

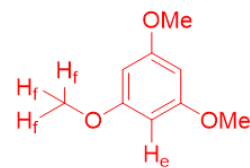
The signal from residual CH₃CN in CD₃CN (the NMR solvent) appears at 1.94 ppm
¹H NMR (400 MHz, CD₃CN):



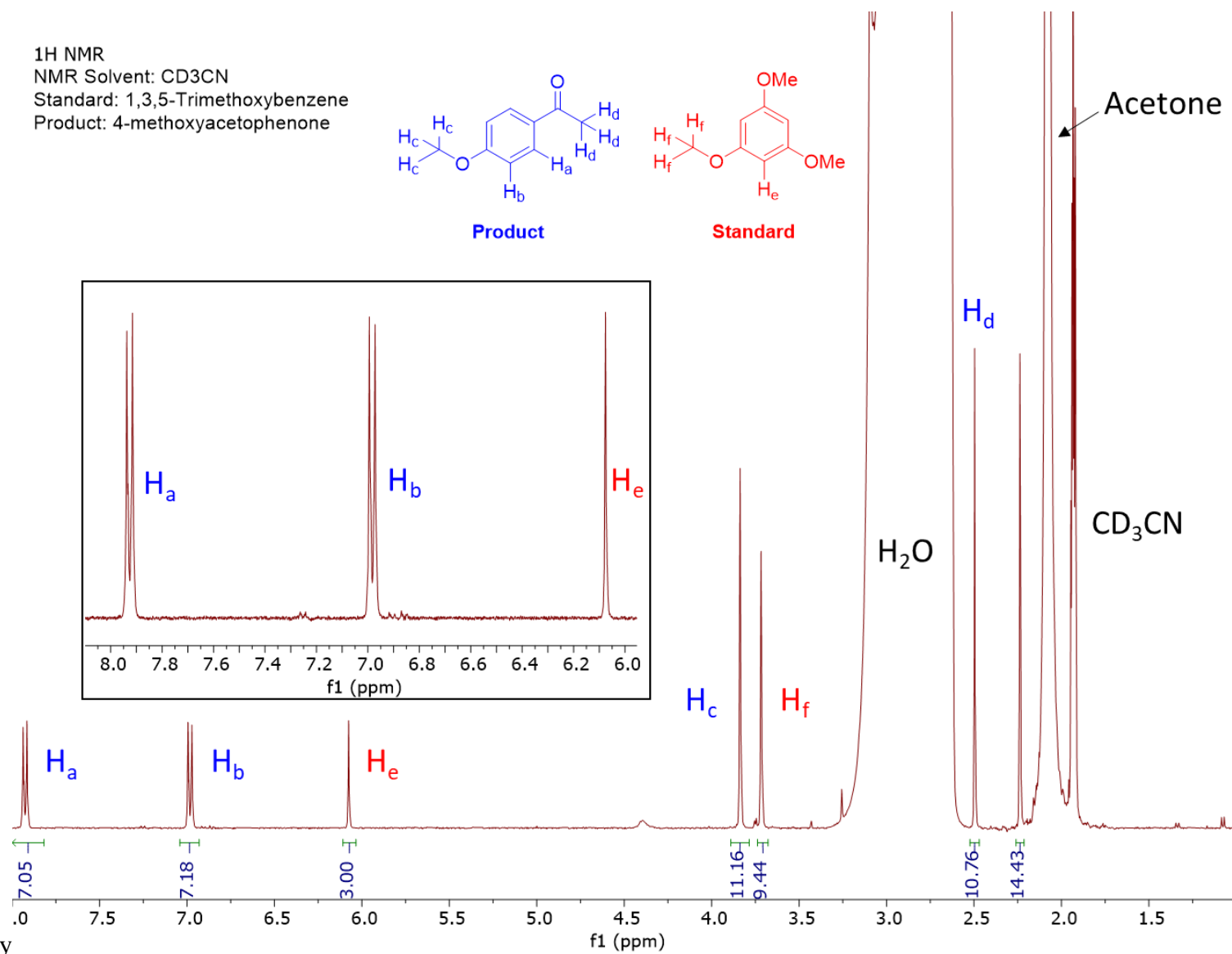
¹H NMR
NMR Solvent: CD₃CN
Standard: 1,3,5-Trimethoxybenzene
Product: 4-methoxyacetophenone



Product



Standard



Answer key

Signal H_e is from the standard and has a clear baseline. Signal H_e has an integration of 3.00 corresponding to three equivalent H-atoms on the aromatic ring. Product signals H_a and H_b also have a clear baseline and are close to standard signal H_e . These two product signals correspond to the two pairs of equivalent protons on the aromatic ring, with integration value of 7.05 and 7.18, respectively.

The integration and corresponding number of hydrogen atoms can be used to determine the ratio between the standard and product. The amount of product can be calculated using this ratio and the known amount of added standard. Using signals H_b and H_e :

$$\text{Standard (mmol)} = \frac{\text{mass standard (mg)}}{\text{molar mass standard (mg/mmol)}} = \frac{16.5 \text{ mg}}{168.19 \text{ mg/mmol}} = 0.0981 \text{ mmol}$$

$$\text{Product (mmol)} = \text{Standard (mmol)} \times \frac{\text{Product integration}}{\# \text{ H atoms}} \times \frac{\# \text{ H atoms}}{\text{Standard integration}}$$

$$\text{Product (mmol)} = 0.0981 \text{ mmol} \times \frac{7.18}{2} \times \frac{3}{3.00} = 0.352 \text{ mmol}$$

Alternately,

$$\text{Product (mmol)} = \text{Standard (mmol)} \times \frac{\frac{\text{Product integration}}{\# \text{ H atoms}}}{\frac{\text{Standard integration}}{\# \text{ H atoms}}}$$

$$\text{Product (mmol)} = 0.0981 \text{ (mmol)} \times \frac{\frac{7.18}{2}}{\frac{3.00}{3}} = 0.352 \text{ mmol}$$

The percent yield is the ratio between the amount of product (in mmol) and substrate (in mmol) converted to a percentage.

$$\text{Yield (\%)} = \frac{\text{Product (mmol)}}{\text{Substrate (mmol)}} \times 100$$

$$\text{Yield (\%)} = \frac{0.352 \text{ mmol Product}}{0.50 \text{ mmol Substrate}} \times 100 = 70.4\%$$

Signal H_a is also valid to use in the calculation, and the %yield would be slightly different.

$$\text{Product (mmol)} = 0.0981 \text{ mmol} \times \frac{7.05}{2} \times \frac{3}{3.00} = 0.346 \text{ mmol}$$

$$\text{Yield (\%)} = \frac{0.346 \text{ mmol Product}}{0.50 \text{ mmol Substrate}} \times 100 = 69.2\%$$

A.8. Links to High-Resolution Lecture and Experimental Videos

Below are links to high-resolution video files of prelab lectures and experimental procedures relevant to Shono oxidation laboratory exercises. The videos were recorded in September 2020 in preparation for an on-line or hybrid version of the CHEM 346 laboratory course. The links are embedded in UW-Madison's Kaltura media space. The raw video files (mp4) and lecture slides are available from the author upon request

Lecture:

https://mediaspace.wisc.edu/media/CHEM%20346%20Cyclic%20Voltammetry%20and%20Electro%20synthesis.mp4/I_30d2zz95

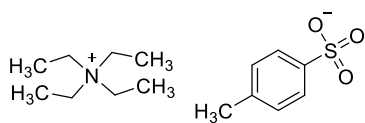
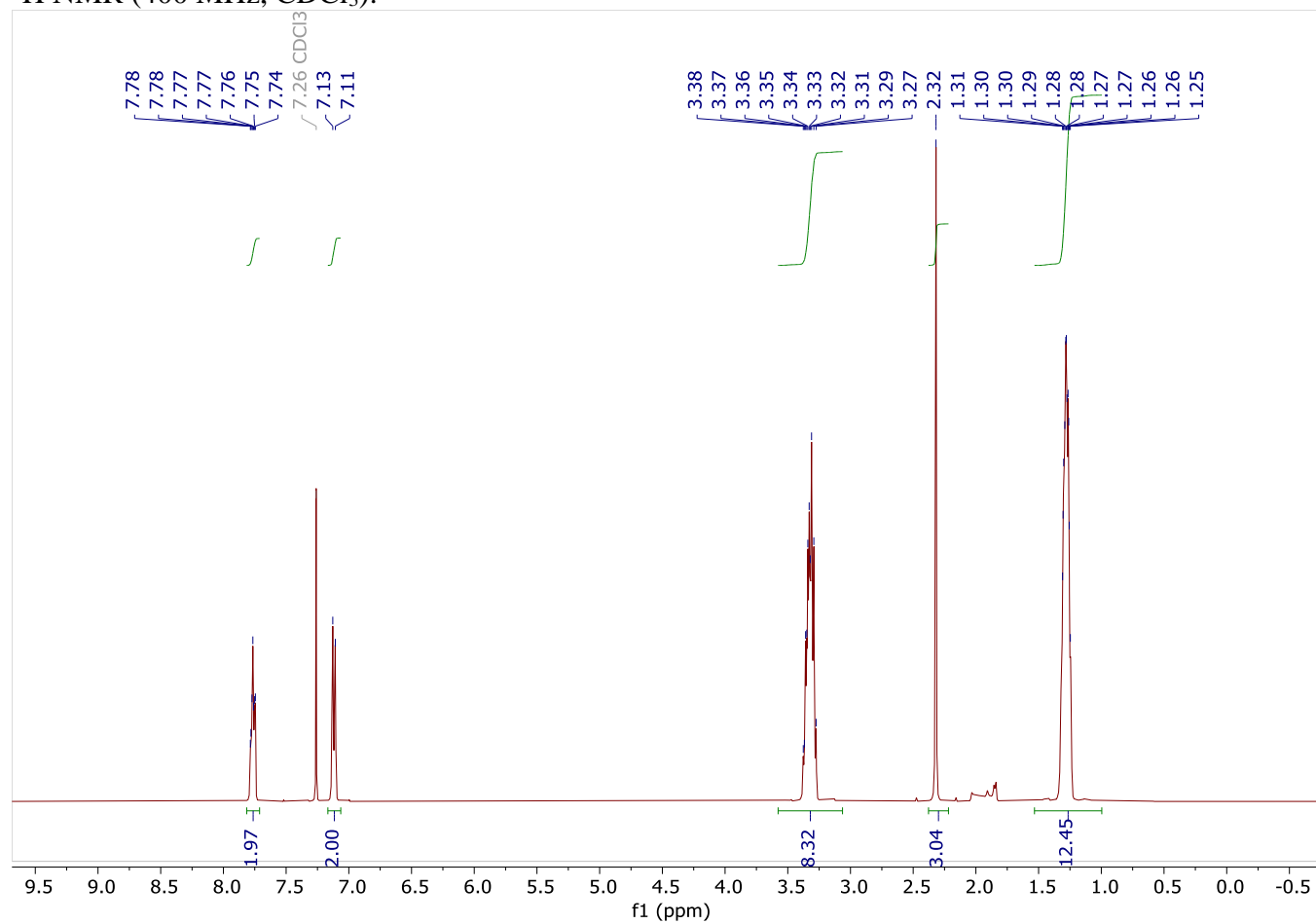
Shono Oxidation Bulk Electrolysis:

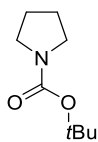
https://mediaspace.wisc.edu/media/CHEM+346+Electrochemical+Shono+Oxidation/I_4x54un0

b

A.9. Spectral Data

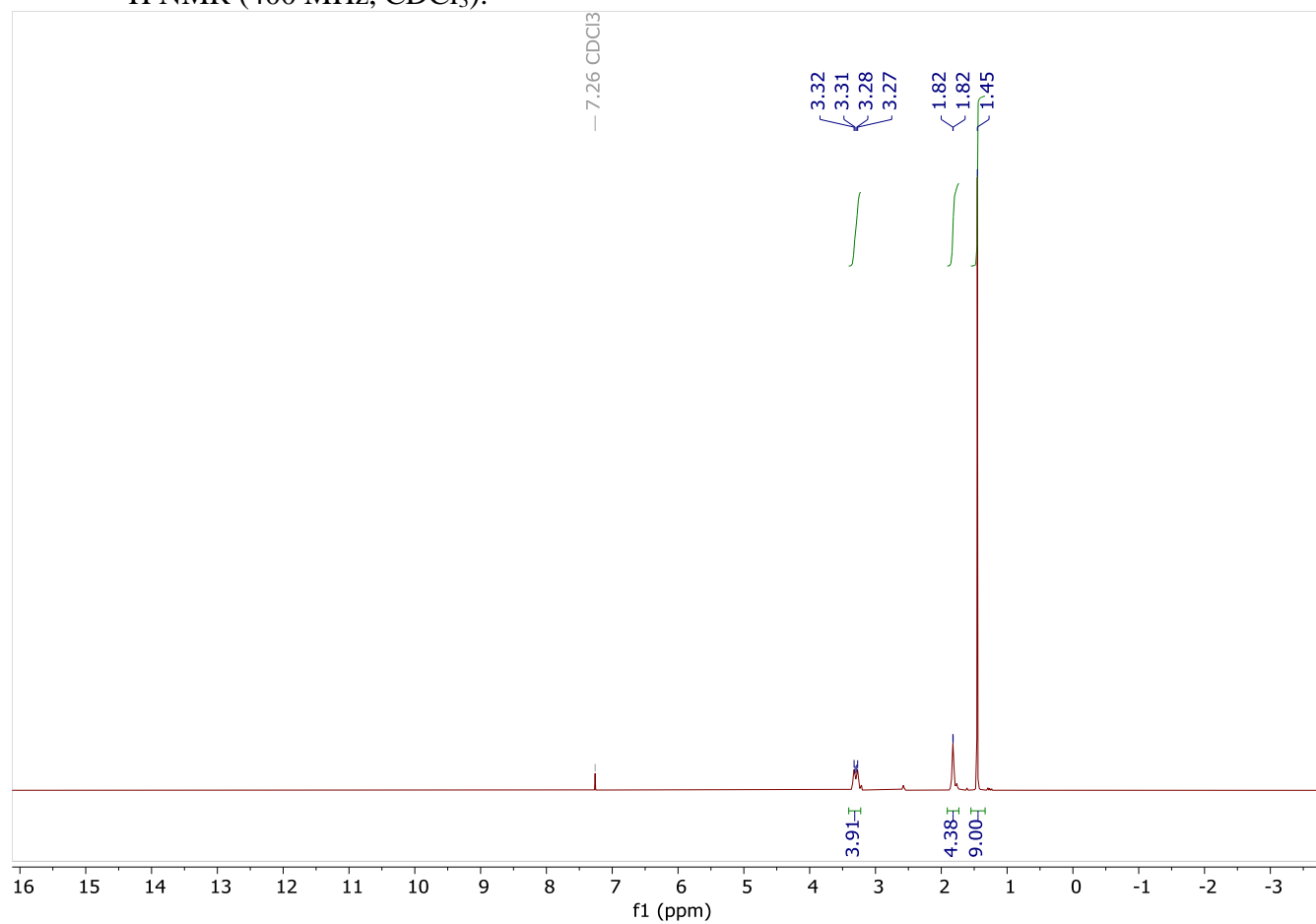
^1H NMR data were obtained on a Bruker SampleJet instrument (1H 400 MHz) in CDCl_3 solution. All NMR data were processed using the MestReNova program. Chemical shift values are reported in parts per million (ppm) relative to CHCl_3 ($\delta = 7.26$ ppm) in CDCl_3 .

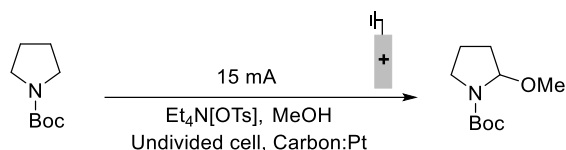
Tetraethylammonium *p*-toluenesulfonate ([NEt₄][*p*-TsOH])¹H NMR (400 MHz, CDCl₃):



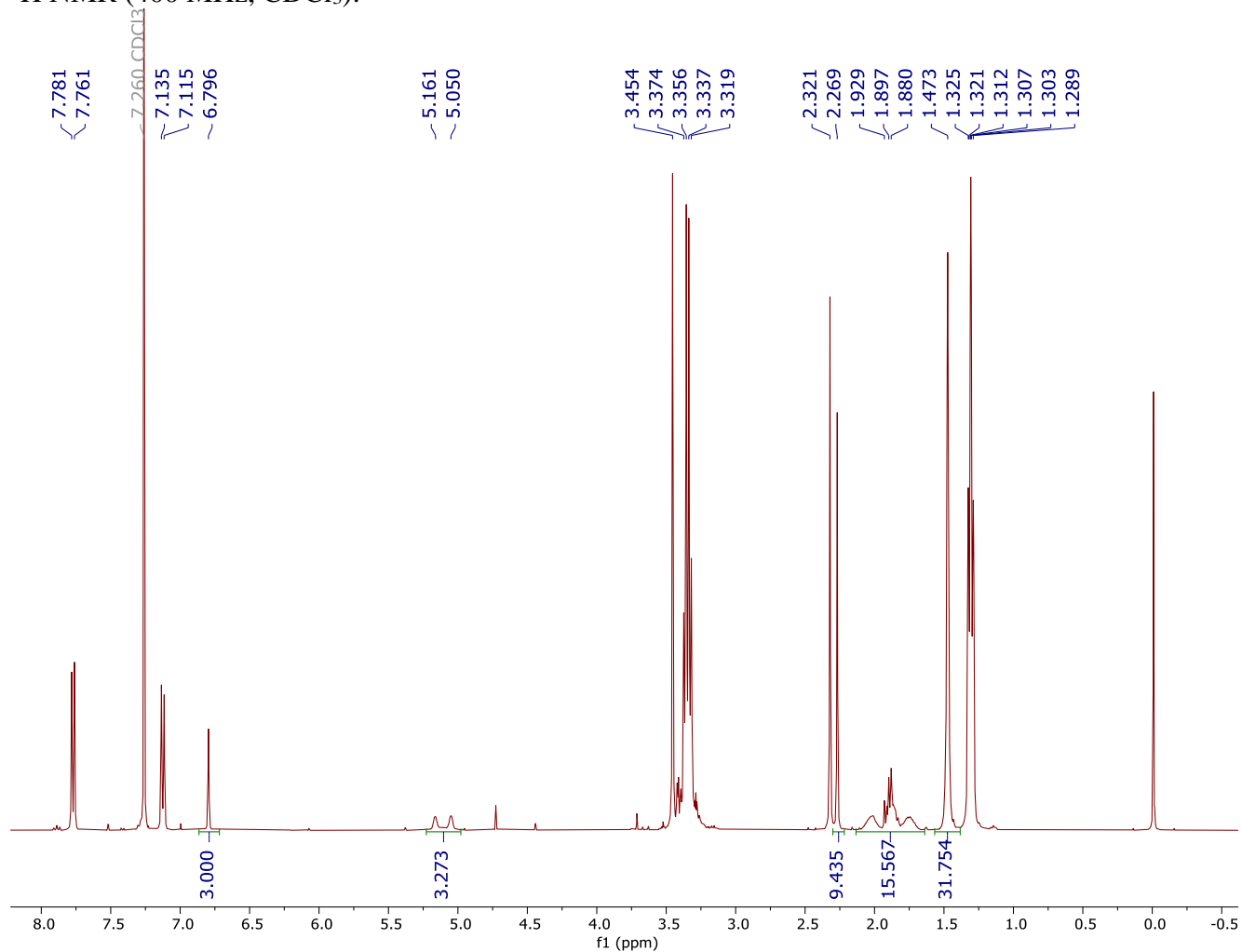
N-Boc-pyrrolidine

^1H NMR (400 MHz, CDCl_3):





Crude reaction mixture with 1,3,5-trimethylbenzene as internal standard
¹H NMR (400 MHz, CDCl₃):



A.10. Computational Methods and Linked Job Output

All calculations were performed in Gaussian 16¹⁵ using WebMO¹⁶ as the user interface at the B3LYP level of theory and 6-31G(d) basis set.

All computational data are available via an HTML-export from WebMO to allow students and instructors direct access to the data. These data are provided as a series of direct links viewable in a web browser (right click on the job number in **Table A.1** and select “Open Hyperlink”).

The raw output file from the calculation is available by clicking the “Raw Output” button in the HTML linked file (see example in **Figure A.9**). The raw output files for each job are also available within a separate zip file (“Raw WebMO Output Files”) in the supporting information.

Table A.1. Link to computational jobs.

Job Number	Job Name
648285	Shono Product (R)-Syn
697487	Shono Product (R)-Syn (NMR) ^a

^aCalculated NMR chemical shifts are located by scrolling into the Calculated Quantities field in the linked output. Isotropic chemical shifts should be used (see **Figure A.10**).

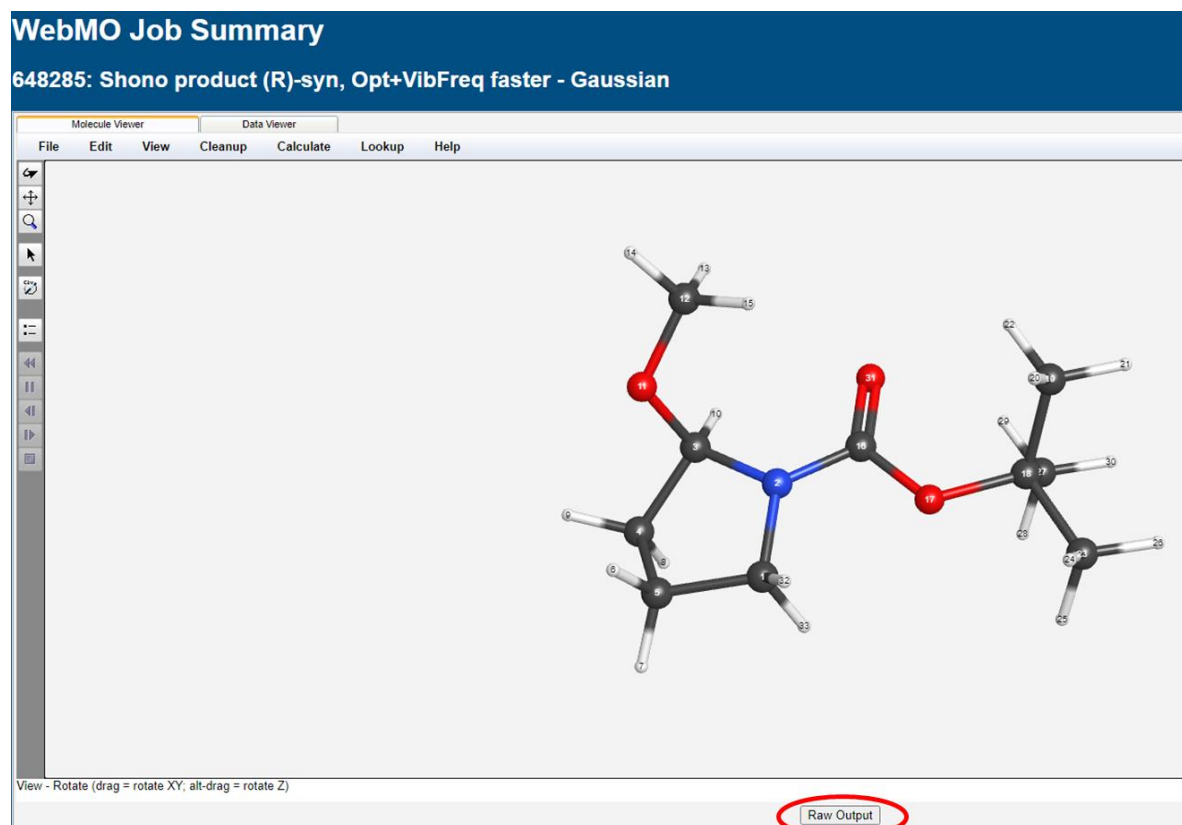


Figure A.9. Image highlights location of “Raw Output” button to access raw output data file for job 648285

Calculated Quantities

Collapse all

Overview

Quantity	Value
Route	#N B3LYP/6-31G(d) NMR Geom=Connectivity
Stoichiometry	C ₁₀ H ₁₀ NO ₃
Symmetry	C1
Basis	6-31G(d)
RB3LYP Energy	-672.955684392 Hartree
Dipole Moment	2.0570 Debye
Server	batch (710954)
CPU time	652.3 sec

Rotational Constants

Constant	Frequency (GHz)	Frequency (cm ⁻¹)
a	1.2278397	0.04095632386
b	0.4159141	0.01387340104
c	0.3574558	0.01192344205

Absolute NMR Shifts

Atom Symbc	Isotropic	Anisotropy
1 C*	46.7136	39.9635
2 N	141.3326	105.5016
3 C*	87.4764	33.9909
4 C*	34.2129	24.7096
5 C*	25.7041	20.9815
6 H*	2.2354	8.7066
7 H*	1.5806	10.1070
8 H*	1.5594	8.6611
9 H*	1.8023	9.1931
10 H*	5.1024	3.1047
11 O	266.5274	87.9925
12 C*	54.4368	68.8867

Figure A.10. Image highlights location of Absolute NMR shifts in data file for job 697487

A.11. References

1. Wang, F.; Rafiee, M.; Stahl, S. S. *Angew. Chem. Int. Ed.* **2018**, *57*, 6686-6690.
2. Elgrishi, N.; Rountree, K. J.; McCarthy, B. D.; Rountree, E. S.; Eisenhart, T. T.; Dempsey, J. L. *J. Chem. Educ.* **2018**, *95*, 197-206.
3. Yan, M.; Kawamata, Y.; Baran, P. S. *Chem. Rev.* **2017**, *117*, 13230-13319.
4. Horn, E. J.; Rosen, B. R.; Baran, P. S. *ACS Cent. Sci.* **2016**, *2*, 302-308.
5. Little, R. D. *J. Org. Chem.* **2020**, *85*, 13375-13390.

6. Schotten, C.; Nicholls, T. P.; Bourne, R. A.; Kapur, N.; Nguyen, B. N.; Willans, C. E. *Green Chem.* **2020**, *22*, 3558-3375.
7. For more information on cyclic voltammetry, see Reference 2. Elgrishi, N.; Rountree, K. J.; McCarthy, B. D.; Rountree, E. S.; Eisenhart, T. T.; Dempsey, J. L. *J. Chem. Educ.* **2018**, *95*, 197-206.
8. Nicholson, R. S.; Shain, I. *Anal. Chem.* **1964**, *36*, 706-723.
9. Shono, T.; Hamaguchi, H.; Matsumura, Y. *J. Am. Chem. Soc.* **1975**, *97*, 4264-4268.
10. Murahashi, S-I.; Naota, T.; Kawabata, T.; Saito, T.; Kumobayashi, H.; Akutagawa, S. *J. Am. Chem. Soc.* **1990**, *112*, 7820-7822.
11. Moriyama, K. *Tetrahedron Lett.* **2017**, *58*, 4655-4662.
12. Lennox, A. J. J.; Goes, S. L.; Webster, M. P.; Koolman, H. F.; Djuric, S. W.; Stahl, S. S. *J. Am. Chem. Soc.* **2018**, *140*, 11227-11231.
13. Frankowski, K. J.; Liu, R.; Milligan, G. L.; Moeller, K. D.; Aubé, J. *Angew. Chem. Int. Ed.* **2015**, *54*, 10555-10558.
14. Yoshida, J-I.; Shimizu, A.; Hayashi, R. *Chem. Rev.* **2018**, *118*, 4702-4730.
15. Frisch, M. J.; Trucks, G. W.; Schlegel, H. B.; Scuseria, G. E.; Robb, M. A.; Cheeseman, J. R.; Scalmani, G.; Barone, V.; Petersson, G. A.; Nakatsuji, H.; Li, X.; Caricato, M.; Marenich, A. V.; Bloino, J.; Janesko, B. G.; Gomperts, R.; Mennucci, B.; Hratchian, H. P.; Ortiz, J. V.; Izmaylov, A. F.; Sonnenberg, J. L.; Williams; Ding, F.; Lipparini, F.; Egidi, F.; Goings, J.; Peng, B.; Petrone, A.; Henderson, T.; Ranasinghe, D.; Zakrzewski, V. G.; Gao, J.; Rega, N.; Zheng, G.; Liang, W.; Hada, M.; Ehara, M.; Toyota, K.; Fukuda, R.; Hasegawa, J.; Ishida, M.; Nakajima, T.; Honda, Y.; Kitao, O.; Nakai, H.; Vreven, T.; Throssell, K.; Montgomery Jr., J. A.; Peralta, J. E.; Ogliaro, F.; Bearpark, M. J.; Heyd, J. J.; Brothers, E. N.; Kudin, K. N.; Staroverov, V. N.; Keith, T. A.; Kobayashi, R.; Normand, J.; Raghavachari, K.; Rendell, A. P.; Burant, J. C.; Iyengar, S. S.; Tomasi, J.; Cossi, M.; Millam, J. M.; Klene, M.; Adamo, C.; Cammi, R.; Ochterski, J. W.; Martin, R. L.; Morokuma, K.; Farkas, O.; Foresman, J. B.; Fox, D. J. *Gaussian 16 Rev. C.01*, Wallingford, CT, 2016.
16. Schmidt, J. R.; Polik, W. F. *WebMO Enterprise, 20.1.012e*; WebMO, LLC.: Holland, MI, USA, 2020.

**Appendix B: Deriving the Turnover Frequency of Aminoxyl-Catalyzed
Alcohol Oxidation by Chronoamperometry: An Introduction to Organic
Electrocatalysis Supporting Information**

B.1. Introduction

Oxidation reactions of alcohols are among the most important and widely used functional group transformation reactions in organic chemistry. Cyclic voltammetry (CV) and chronoamperometry (CA) are useful techniques in electrochemistry which give qualitative and quantitative information for electron transfer reactions. In this laboratory experiment, electrochemical oxidation of solketal, as the alcohol substrate, catalyzed by 4-acetamido-TEMPO, is explored using CA and CV techniques. The description of the CV and CA techniques and catalyzed electrochemical oxidation of alcohols can be found in the included student handout (Section B.9).

B.2. Note for Instructors

Chemical reagents

- 4-Acetamido-2,2,6,6-tetramethylpiperidine 1-Oxyl Free Radical (ACT), CAS 14691-89-5, 98.0+%, TCI America, was purchased from Fisher Scientific. LD50 for ACT is unknown but it has reported 2000mg kg⁻¹ for its derivative, TEMPO.
- Sodium Bicarbonate (Powder/Certified ACS), CAS# 497-19-8, Fisher Chemical, was purchased from Fisher Scientific.
- Sodium Carbonate Anhydrous (Powder/Certified ACS), Fisher Chemical, CAS# 144-55-8, was purchased from Fisher Scientific.
- Solketal, (1,2-Isopropylidenglycerol) 97%, Alfa Aesar™, CAS# 100-79-8, was purchased from Fisher Scientific.
- Alumina Powder Gamma, Type DX, 0.05 μm Particles, was purchased from Fisher Scientific.
- Deionized water was used for making the solutions

Apparatus and labware

- Pine Wavenow XV 100 Potentiostat
- Mettler Toledo Precision Balance (readability of 1 milligram)
- Six – eight 10 mL volumetric flasks,
- Volumetric pipettes
- Pine glass low volume electrochemical cell with Electrode holder
- Pine glassy carbon working electrode, 3 mm diam., with o-ring
- Pine Pt wire counter electrode, with o-ring
- Pine 3M KCl Ag/AgCl reference electrode, with o-ring

The o-rings were used to adjust the height of immersed electrode in the solution and avoid contact with bottom of cell.

- Metal alligator clamps
- BASi Electrochemical Polishing pad
- Water wash bottle
- Rinse beaker and waste container

Other Notes

Pine equipment was utilized for this laboratory experiment. The potentiostat is controlled by a PC laptop with Windows OS using Aftermath software. However, it is not necessary to have a Pine Potentiostat, and any other potentiostat works for this experiment. The three required electrodes are also commercially available from different vendors. The guide for using the software and analyzing the data is described on the Pine website (the link and instructions are listed in the students' handout). Aftermath has a function that calculates the consumed charge for each CA experiment. Two kinds of data analysis can be employed for this experiment. Students utilized Aftermath Software for data analysis in our lab sections. However, this is not necessary and if this

software is not accessible, data can be extracted to Excel for further analysis, see **section B.8.** and the Supporting Information Excel file.

The alumina powder, Gamma, Type DX, 0.05 μm Particles, was mixed with DI water to make the polishing slurry. The shape of the catalytic CVs may appear slightly different when using other forms of alumina or other polishing slurries. The surface of glassy carbon disk when its polished should be shiny as shown in **Figure B.1.**



Figure B.1. Demonstration of shiny surface of polished glassy carbon (GC) electrode

B.3. Safety

Proper laboratory attire should be worn in the laboratory at all times, including gloves, close-toed shoes, and approved safety goggles. Specific precautions for chemicals in this experiment are mentioned in the hazards section and should be referenced; students should also be aware of how to properly dispose of chemical waste.

B.4. Experimental Procedure and making the Stock Solution

- To prepare 10 mL 20 mM stock solution of ACT, the students were given solid ACT, and in a typical experiment they weighed 0.041 g of ACT to be dissolved in DI water.
- To prepare 100 mL 0.2 M NaHCO_3 stock solution, the students were given solid NaHCO_3 , and in a typical experiment they weighed 1.68 g of NaHCO_3 to be dissolved in DI water.
- To prepare 100 mL 0.2 M Na_2CO_3 stock solution, the students were given solid Na_2CO_3 , and in a typical experiment they weighed 2.12 g of Na_2CO_3 to be dissolved in DI water.

The students were given 10 mL 0.2 M stock solution of solketal, and this solution was prepared by dissolution of 0.248 g of solketal in 100 mL DI water. *Aqueous solution of solketal is not stable and should be prepared daily.*

The preparation of the other required solutions for the experiments can be found in detail within the **student handout**.

B.5. Additional Electrochemical Data and the Results by Students

The practical time for a chronoamperogram is ten to twenty seconds under "Cottrell conditions". During the first few second(s) of experiments, non-faradaic current, potentiostatic limitations, and limitations in the recording device can make it difficult to identify the faradaic current precisely. For the measurements longer than twenty seconds, convective disruption of the diffusion layer may occur due to the buildup of density gradients and stray vibrations.

The chronoamperogram of ACT in the absence of solketal, where the current-time profile follows the diffusion-controlled correlation, is described by the Cottrell equation

$$I = nFA\pi^{-1/2}C_{ACT}D_{ACT}^{1/2}t^{-1/2} \quad (\text{eqn. 1S})$$

where I is current (A), n is the number of electrons transferred in the half reaction, F is Faraday's Constant ($96,485 \text{ C mol}^{-1}$), A is the area of the electrode, D_{ACT} is the diffusion coefficient of ACT ($\text{cm}^2 \text{ s}^{-1}$), C_{ACT} is the initial (bulk) concentration of ACT (mol cm^{-3}), and t is time (s). This form of the equation is specific to planar diffusion at an inlaid disk electrode. Current is plotted as a function of $t^{-1/2}$. Examples of linear correlation as plotted by students are shown in **Figure B.2**. Deviation from the linear trend is observed occasionally (*e.g.* **Figure B.2d**) and is mostly due to variations in polishing. Discarding the data for first experiment conducted after polishing and repeating it without polishing results in more reproducible responses.

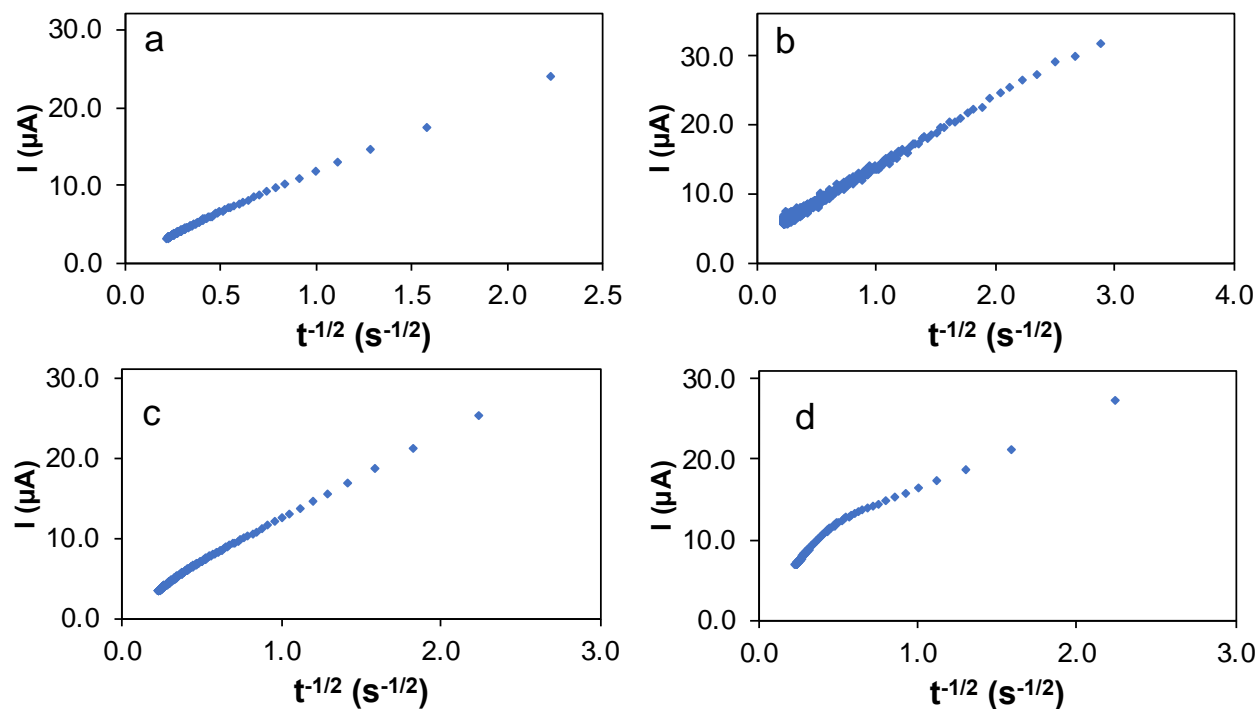


Figure B.2. Four examples of the plotted data (by four individual groups) for post analysis of chronoamperometric responses. The plots show the correlation of current as a function of $t^{-1/2}$ which is supposed to be linear. Solution conditions: 1.0 mM ACT in aqueous solution with $\text{NaHCO}_3/\text{Na}_2\text{CO}_3$ electrolyte (0.1/0.1 M, pH 10). Applied potential for chronoamperometry is 0.8 V vs Ag/AgCl.

B.6. Deriving the Diffusion Coefficient of ACT

Based on Equation 1S, under Cottrell conditions, plotting I (current) vs. $t^{-1/2}$ should give a linear plot (see **Figure B.3**) where the slope gives the diffusion coefficient (D) of ACT. In practice, the Cottrell equation simplifies to $I = kD^{1/2}t^{-1/2}$, where k is the collection of constants for a given system (n , F , A , C and $\pi^{-1/2}$). Then, the value of D can be derived from the slope of the line. **Figure B.3** shows the chronoamperogram of ACT and its linear version as a function of $t^{-1/2}$. The current for the time between 1.6 to 20 s was used (blue plots in **Figure B.3**) and the first 1.4 s (shown in red) was eliminated. The derived D value for ACT was $6.69 \times 10^{-6} \text{ cm}^2 \text{ s}^{-1}$.

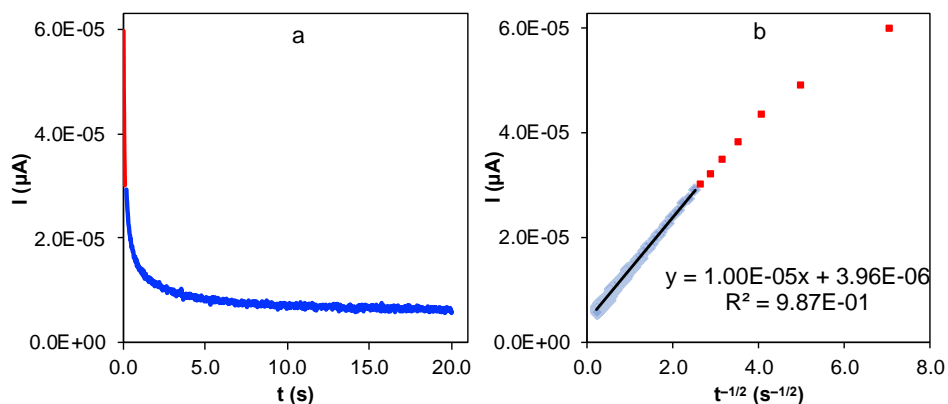


Figure B.3. Chronoamperogram (a) and the plot of current as a function of $t^{-1/2}$ (b) for 1.0 mM ACT in aqueous solution with $\text{NaHCO}_3/\text{Na}_2\text{CO}_3$ (0.1/0.1 M, pH 10). Applied potential for chronoamperometry is 0.8 V vs Ag/AgCl.

The value of D can also be derived from the current vs square root of scan rate plot, **Figure B.4**. In practice, this plot is described by the Randles-Ševčík equation, $I_p = kD^{1/2}\nu^{1/2}$ where ν is scan rate (V s^{-1}) and D ($\text{cm}^2 \text{s}^{-1}$) is the diffusion coefficient, the value of D can be derived from the slope of the line. The derived value of D for ACT was $6.85 \times 10^{-6} \text{ cm}^2 \text{ s}^{-1}$, in agreement with value derived by analysis of chronoamperometric plots.

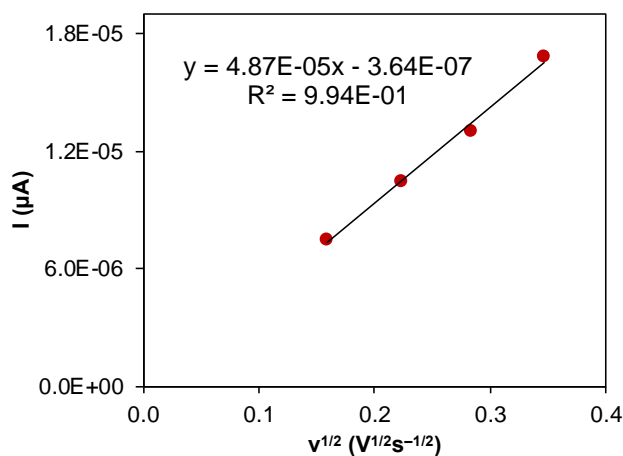


Figure B.4. The plot of anodic and cathodic peak currents versus square root of scan rate. Solution conditions: aqueous solution with $\text{NaHCO}_3/\text{Na}_2\text{CO}_3$ electrolyte 0.1/0.1 M, and pH 10.

B.7. Deriving the Kinetic Information from Voltammetric Results

Deriving kinetic information from a voltammetric experiment is also possible. But, scan rate dependence/independence of voltammetric responses in the absence and presence of substrate makes it difficult to simply derive the turnover frequency (TOF) by measuring the ratio of consumed charges of the voltammograms. The voltammetric currents for an electrocatalyst are diffusion-controlled in the absence of substrate but independent of scan rate in the presence of substrate. One option to derive the kinetic information by cyclic voltammetry is to plot the catalytic peak current in the presence of various concentrations of substrate as a function of the square root of substrate concentration (**Figure B.6** and **Figure B.7**). In circumstances where the anodic peak current is limited by the kinetics of the catalytic reaction, there is a linear correlation between the square root of substrate concentration and catalytic current as described by Eqn. 2S

$$I_{cat} = nFAC_{ACT}(D_{solketal}k_{obs}C_{soletal})^{1/2} \quad (\text{eqn. 2S})$$

where I_{cat} is the anodic catalytic current, C_{ACT} and $C_{solketal}$ are the bulk concentrations of ACT and solketal (mol cm^{-3}), and n , F and A represent the number of transferred electrons in a catalytic cycle, the Faraday constant, and the electrode surface area, respectively. $D_{solketal}$ denotes the diffusion coefficient of solketal ($\text{cm}^2 \text{s}^{-1}$).¹²³ This linear trend can be used to prove that the peak current is controlled by the reaction kinetics. The slopes can be used to compare catalytic activities under different conditions and for different substrates or catalysts.³

Examples of the quantitative results by students are represented here. **Figure B.7** is an example of an experiment and data analysis that produced unexpected trends. The students in this group concluded that volumetric flasks were marked and analyzed in wrong order. Careful labeling of the solution is crucial for getting accurate results.

Table B.1. Turnover frequency (TOF) of ACT for oxidation of solketal.

Solketal concentration (mM)	Turnover Frequency (h^{-1})
2 mM	346
4 mM	548
9 mM	802
16 mM	1024

Reaction Conditions: aqueous solution with $\text{NaHCO}_3/\text{Na}_2\text{CO}_3$ electrolyte 0.1/0.1 M, pH 10, 1.0 mM ACT.

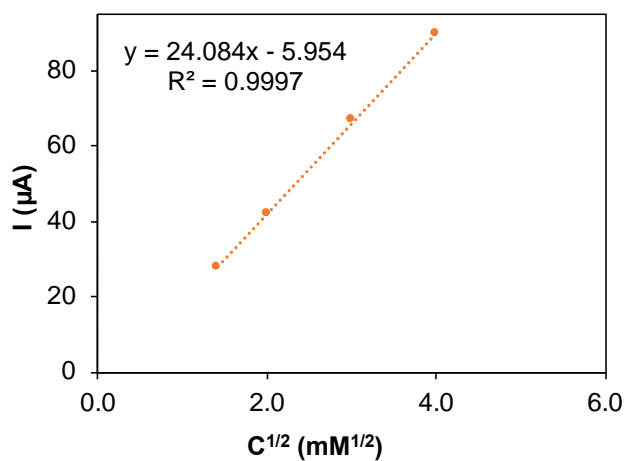
**Figure B.5.** Plot of the anodic peak current of cyclic voltammograms as a function of square root of concentration of solketal ($C^{1/2}$). Solution conditions: 1.0 mM ACT in aqueous solution with $\text{NaHCO}_3/\text{Na}_2\text{CO}_3$ electrolyte (0.1/0.1 M, pH 10).

Table B.2. Turnover frequency (TOF) of ACT for oxidation of solketal.

Solketal concentration (mM)	Turnover Frequency (h^{-1})
2 mM	345
4 mM	359
9 mM	694
16 mM	879

Reaction Conditions: aqueous solution with $\text{NaHCO}_3/\text{Na}_2\text{CO}_3$ electrolyte 0.1/0.1 M, pH 10, 1.0 mM ACT.

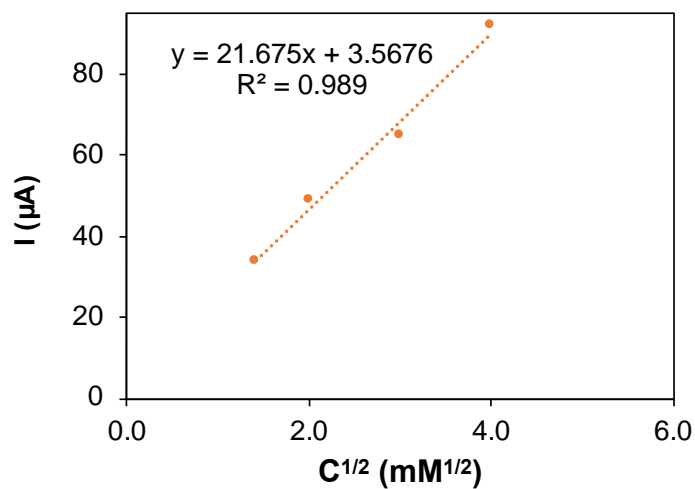
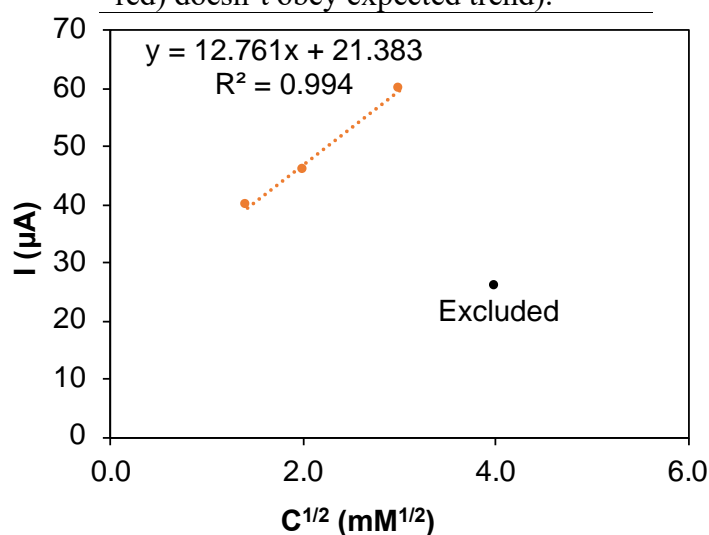
**Figure B.6.** Plot of the anodic peak current of cyclic voltammograms as a function of square root of concentration of solketal ($C^{-1/2}$). Solution conditions: 1.0 mM ACT in aqueous solution with $\text{NaHCO}_3/\text{Na}_2\text{CO}_3$ electrolyte (0.1/0.1 M, pH 10).

Table B.3. Turnover frequency (TOF) of ACT for oxidation of solketal.

Solketal concentration (mM)	Turnover Frequency (h^{-1})
2 mM	543
4 mM	618
9 mM	658
16 mM	262

Reaction Conditions: aqueous solution with $\text{NaHCO}_3/\text{Na}_2\text{CO}_3$ electrolyte 0.1/0.1 M, pH 10, 1.0 mM ACT. The data presented for 16 mM (in red) doesn't obey expected trend).

**Figure B.7.** Plot of the anodic peak current of cyclic voltammograms as a function of square root of concentration of solketal ($C^{-1/2}$). Solution conditions: 1.0 mM ACT in aqueous solution with $\text{NaHCO}_3/\text{Na}_2\text{CO}_3$ electrolyte (0.1/0.1 M, pH 10).**B.8. Consumed Charge for Chronoamperometry Experiment**

The consumed charge for each data point of the chronoamperogram equals the current at each time interval (**Figure B.8**, cell C3). For example, cell B3 in **Figure B.8** is multiplied by corresponding time interval (i.e. the difference between the recorded times depicted in A3 and A4). The summation of these consumed charge is the total amount charge for each chronoamperogram (**Figure B.8**, cell D3). See the Excel file in Supporting Information.

	A	B	C	D
1			The amount of electric charge (in coulomb) is calculated by multiplying the current at each point (in ampere) by the time interval (in second)	
2	Time (s)	Current (A)	Charge for Each Sampling Point (C.)	Total Consumed Charge (C.)
3	0	0.000010621	=B3*(A4-A3)	=SUM(C3:C201)
4	0.1	0.000034237	3.4237E-06	
5	0.2	0.00002547	0.000002547	
6	0.3	0.0000213	0.00000213	
7	0.4	0.000018717	1.8717E-06	
8	0.5	0.000017007	1.7007E-06	
9	0.6	0.000015693	1.5693E-06	
10	0.7	0.00001467	0.000001467	
11	0.8	0.000013861	1.3861E-06	

Figure B.8. Demonstration of charge calculation in Excel for the chronoamperogram.

B.9. Summary of Assessment

This assessment was done at University of Missouri-Kansas City (UMKC) for Physical Chemistry Laboratory Course. The Following questions were the basis for assessment. Students included answers to these questions in their laboratory reports. We did not ask students to derive the diffusion coefficient (D) by analysis of voltammetric and chronoamperometric data. At the suggestion of reviewers, discussion of deriving the value of D from chronoamperometric and voltammetric results were added.

The summary of the assessment results is in *italicized Arial font*:

1. Obtain the following graphs for the ACT-only voltammetric data:
 - a) CV curves (overlaid over one another) at the four scan rates.
 - b) Plot ACT Peak Current vs scan rate.
 - c) Then plot ACT Peak current vs the square root of scan rate.

Q1: What trends do you notice? What do these trends imply?

Summary of Assessment: All the students were able to produce the requested plots and describe the linear correlation between the peak current and square root of scan rate. Most of the students recognized the correlation based on Randles-Ševčík, and a few of them explained the underlying logic (i.e. the diffusion-controlled process is at different time scales for CVs with different scan rate).

2. Make a plot of the normalized CV curves (overlaid over one another) at the four scan rates.
(Hint: Normalized CVs are derived by dividing the currents from the entire CV curve by the square root of scan rate.)

Q2: What differences do you notice between the Non-Normalized CV's versus the Normalized CV's?

Summary of Assessment: All the voltammograms after normalization had same heights (with less than 8% standard deviation) and most of the students identified and reported the scan rate independence of the normalized voltammograms.

3. Make a graph of the CV curves (overlaid over one another) for the ACT in the presence of 4 mM solketal at the four scan rates.
 - a) Plot ACT Peak Current vs scan rate.

Q3: What trends do you notice? What do these trends imply?

4. Open the data for all CVs of ACT-solketal solutions collected at a scan rate of 50 mV s⁻¹.
Obtain the following graphs:

- a) Plot the peak currents vs the concentration of solketal.
- b) Plot the peak current vs the square root of the concentration of solketal.

Q4: What trends do you notice? What does this tell you about the kinetics of this reaction?

Summary of Assessment for 3 and 4: The students recognized that the voltammetric currents became independent of scan rate and depended on the concentration of solketal (substrate). All the students were able to relate the peak current and solketal concentration, but some of them didn't point out the effect of reaction kinetics clearly.

Note1: As directed by one of the reviewers, the equation that shows the effect of the rate constant of catalytic reaction on peak current was added to the student's handout.

$$I_{cat} = nFAC_{cat}(D_{sub}k_{obs}C_{sub})^{1/2}$$

This will help the students to address the relationship between concentration of k_{obs} (and concentration of solketal and) and anodic peak current (Figure B.2–B4)

***Note2:** One of the student groups didn't observe the linear trend between the voltammetric and chronoamperometric currents. The results by this group are presented in Table B.3 and Figure B.7. The students noticed this unexpected trend while they were in the lab. They students stated that the catalytic voltammetric and chronoamperometric currents should increase in proportion to concentration of substrate. The trend of their data doesn't follow the expected trend. After discussing with the instructors, comparing their results with other groups' results, and inspecting the results, the students concluded the 2 mM solution was mislabeled as a 16 mM solution.*

5. Calculate the TOF (h^{-1}) for ACT in the presence of 2, 4, 9 and 16 mM solketal.

All the students were able to calculate the TOF of ACT at different concentrations of solketal. Except for one group (discussed above), all the TOFs increased with increasing solketal concentrations. Statistical analyses of the TOFs shows 8% to 14% standard deviation for different groups at same concentration of ACT and solketal (solutions prepared individually by each group).

6. Make a plot of the normalized CV curves (overlaid over one another) at the four scan rates.

Q5: What differences do you notice between the Non-Normalized CV's versus the Normalized CV's? Explain the difference between the trends in the absence and presence of solketal.

All the students were able to conclude that when the catalytic current does not increase as scan rate increases, a decreasing current trend is observed when the catalytic current is normalized by scan rate. They distinguished the difference between the normalized currents in the absence

and presence of solketal, but they didn't clearly explain the reason for these differences in these trends. This question may be answered more clearly by adding the equation for catalytic current and its related discussion. See section A of student's handout.

Survey

This survey was done from the attendees of "Organic Electrochemistry Short Course by M. Rafiee and S. S. Stahl at University of Wisconsin–Madison.

1. Why did you attend the lab portion of this short course? Did the labs fulfill your expectations?

"Understand new methods"

"Learn electrochemical experiments"

"General interest"

"Applications of electrochemistry on organic synthesis"

"Hands on experience"

"To see what was all needed for setup"

"How do organic chemists think?"

"Ask software questions, wide breadth of experiments, correct misconceptions (not really)"

"To get exposed to more advanced analytical techniques and mechanistic/kinetic questions"

2. Was the lab manual clear? If not, how could it be improved?

Overall, they liked the lab manual and its combination with in-person instruction.

They have asked for more technical techniques, more photos in handout, and a table for trainees to input data.

3. Was the allotted time appropriate for the experiments in the manual?

All answered this question "yes".

4. Was there enough time to ask questions?

All answered this question "yes".

5. Did you feel that the teaching assistants were available and knowledgeable?

All answered this question "yes" and one of them answered: "Lot's of TAs!".

6. Did the data analysis help you better understand what was going on during the experiments?

All answered this question "yes" and one of them answered: "helped visualize it".

7. How likely would you be to recommend this lab to others?

"In 2019, anyone interested in organic chemistry for a career should have baseline experimental understanding of organic electrochemistry, which this lab provides"

"Great exposure!"

"Good for a beginner"

"Recommend to my friends"

8. To what extent do you agree with the following statement? "The lab experiments helped me understand the topics covered in the lecture sessions in a practical way." Please circle one number.

Strongly Disagree 1 2 3 4 5

Strongly Agree

Average of 16 answers was 4.56

To what extent do you agree with the following statement? "I now feel more equipped to execute and troubleshoot an organic electrosynthesis reaction." Please circle one number.

Strongly Disagree 1 2 3 4 5

Strongly Agree

Average of 16 answers was 4.14

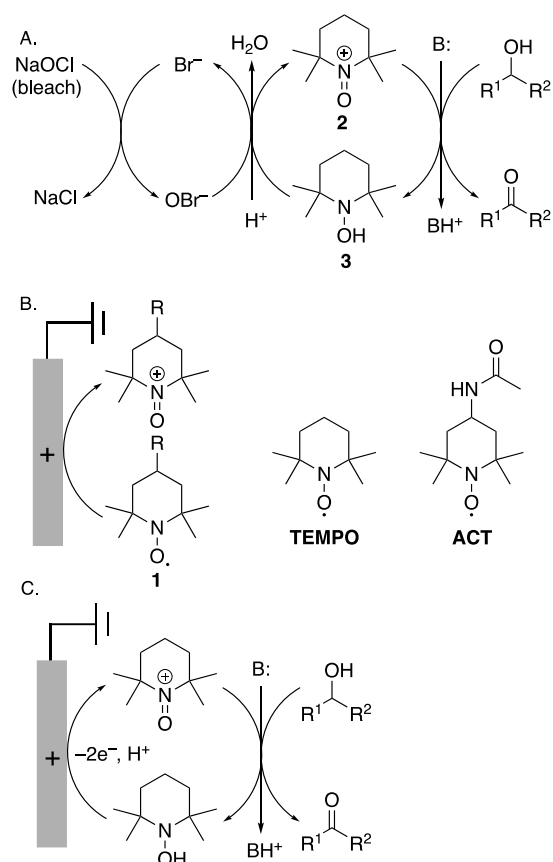
B.10. Student Handouts

Example of the handout prepared for students is provided.

Electrochemical Solketal Oxidation Catalyzed by 4-Acetamido-TEMPO, Deriving TOF and TON by Chronoamperometric Experiments

Introduction

Oxidation reactions of alcohols are among the most important and widely used functional group transformation reactions in organic chemistry. These oxidation reactions are known to be thermodynamically favored, using a variety of oxidants. However, they are kinetically sluggish and require relatively harsh oxidants, such as chromium and manganese oxide. It is known, however, that performing these reactions under catalytic conditions is kinetically favorable and enables the use of milder oxidants, including air (oxygen) and bleach (NaOCl) with minimal or no hazardous side products. The prominent examples of catalysts used for alcohol oxidations are 2,2,6,6-tetramethylpiperidin-N-oxyl (TEMPO) and its derivatives, known as aminoxyl radicals. The Anelli–Montonari oxidation, which employs bleach and TEMPO, is known to be especially effective for alcohol oxidation (**Scheme B.1A**).^{4,5} Aminoxyl radicals (**1**, see **Scheme B.1**) undergo facile redox reactions at electrode surfaces to form oxoammonium species (**2**, see **Scheme B.1**), enabling them to mediate alcohol oxidation under electrochemical conditions (**Scheme B.1B**). The oxoammonium reacts with alcohols to generate the corresponding carbonyl product and reduced catalyst (**2**, see **Scheme B.1**), which is turned over at the electrode surface (**Scheme B.1C**). Electrochemical alcohol oxidation methods using organic aminoxyl mediators have advanced considerably in recent years, and they provide a compelling alternative to the more traditional chemical methods.⁶



Scheme B.1. Anelli–Montonari oxidation. B. electrode reaction and structure of ACT and TEMPO, and C. TEMPO catalyzed electrochemical Alcohol oxidation.

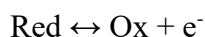
Electroactivity of the aminoxyl radicals not only provides a sustainable route for alcohol oxidation by avoiding the use of any external oxidant, but also offers a unique mechanistic tool for the study of the redox reactions and their coupled chemical reactions by measuring the current flowing through the electrode surface.⁷ In this experiment you will learn about two methods – Cyclic Voltammetry (CV) and Chronoamperometry (CA) – and their application to the study of the efficiency of catalysts for alcohol oxidation.

Cyclic Voltammetry

Cyclic Voltammetry (CV) experiments are among the most widely used electrochemistry techniques today. CV provides both qualitative and quantitative information about electrochemical systems and is well established as a fast and reliable characterization tool. CV provides

considerable information about the thermodynamics of redox processes and the kinetics of heterogeneous electron transfer.

During a CV experiment, the working electrode potential is swept linearly between final and initial values, and the corresponding current is measured. A *cyclic voltammogram* is obtained, showing current vs. potential. The observed current is a measure of the electroactive species that is being transformed at the electrode surface. For example, consider the following reaction:



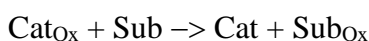
with a formal potential E° (Red is the reduced species, Ox is the oxidized species). If a potential sweep is started sufficiently more negative to E° and swept positively, a current will flow. As the potential of the electrode approaches E° , Red starts oxidizing to Ox, and an anodic current will begin to increase, until an *anodic peak* is reached. The peak is caused by the formation of the diffusion layer near the electrode surface. As oxidation takes place a concentration gradient is created, which leads to an increased flux (mass transfer) to the surface of the electrode. As the swept potential passes E° , the concentration of Red at the surface of the electrode is nearly zero, as Red has consumed to form Ox, and the reaction is mass transfer controlled. The same, but reverse process takes place in the reverse sweep, as a similar concentration gradient is made as reduction takes place. The concentration of Ox molecules at the surface of the electrode is now high, since they were generated in the forward sweep. Therefore, Ox is reduced back to Red once the swept potential begins to approach E° again. A similarly shaped, but inverted, *cathodic peak* will form as the potential is swept in the reverse direction.

The peak height of both the anodic and cathodic peaks, I_p in amperes (A), is best described by the Randles-Ševčík equation (at 25 °C),⁸

$$I_p = 2.69E5 n^{3/2}AD^{1/2}Cv^{1/2}$$

where n is the number of electrons, A is the electrode area (cm^2), D is the diffusion coefficient ($\text{cm}^2 \text{s}^{-1}$), C is the concentration (mol cm^{-3}), and v is the sweep rate of voltammetric experiment (V s^{-1}). Accordingly, the peak height is proportional to the square root of scan rate. Such a dependence on scan rate indicates that the reaction is diffusion-limited (or mass-transfer controlled).^{9,10}

Deriving the kinetic information from voltammetric experiment is possible. One option to derive the kinetic information by cyclic voltammetry is to plot the catalytic peak current, in the presence of various concentrations of substrate, as a function of the square root of substrate concentration. For example, consider the following reactions:



In circumstances where the anodic peak current is limited by the kinetics of the catalytic reaction, there is a linear correlation between the square root of substrate concentration and catalytic current as described here:

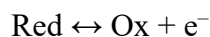
$$I_{\text{cat}} = nFAC_{\text{cat}}(D_{\text{sub}}k_{\text{obs}}C_{\text{sub}})^{1/2}$$

I_{cat} is the anodic catalytic current, C_{cat} and C_{sub} are the bulk concentrations of electroactive catalyst and substrate (mol cm^{-3}), and n , F and A represent the number of transferred electrons in a catalytic cycle, the Faraday constant, and the electrode surface area. D_{sub} denotes the diffusion coefficient of substrate ($\text{cm}^2 \text{s}^{-1}$).¹⁻³ This linear trend can be used to prove that the peak current is controlled by the reaction kinetics. The slopes can be used for comparison of catalytic activities under different conditions and for different substrates or catalysts.

Chronoamperometry

Chronoamperometry (CA) is a potential step method, as opposed to the potential sweep method of cyclic voltammetry. It is also known as bulk electrolysis. More simply, chronoamperometry is the measurement of current vs time at a constant applied potential.

Consider the same reaction as before:



As was stated previously, if the potential is sufficiently beyond E° , the concentration of Red is effectively zero. Therefore, in CA, if the potential is “stepped” immediately to that high E value, then mass transport is entirely diffusion controlled, much like the current that flows in a CV curve after the potential of the electrode is swept past E° . Therefore, the current-time curve that CA produces will reflect the change in the concentration gradient near the surface of the electrode. Accordingly, the current will decay with time, as described the by Cottrell equation:⁹

$$I(t) = nFA\pi^{-1/2}D_O^{1/2}C_O^* t^{-1/2}$$

where $I(t)$ is current, n is the number of electrons transferred in the half reaction, F is Faraday's Constant ($96,485 \text{ C mol}^{-1}$), A is the area of the electrode, D_O is the diffusion coefficient, C_O^* is the initial concentration, and t is time. From chronoamperometry, it is possible to determine the amount of charge that is passed during a given time, which could be used to determine a number of kinetic parameters.^{9,10}

Experimental

Materials

- 4-Acetamido-TEMPO (ACT) (CAS 14691-89-5), $231.30 \text{ g mol}^{-1}$, *oral toxicity*
- 0.2 M NaHCO_3 solution (CAS 497-19-8), 84.01 g mol^{-1} , *eye irritant*
- 0.2 M Na_2CO_3 solution (CAS 144-55-8), $105.99 \text{ g mol}^{-1}$, *eye irritant*
- 0.2 M stock solution of Solketal (1,2-Isopropylidenglycerol) (CAS 100-79-8) $132.16 \text{ g mol}^{-1}$, 1.063 g mL^{-1} , *flammable, eye irritant*

- Six – eight 10 mL volumetric flasks
- Volumetric pipettes
- Pine glass electrolysis cell
- Pine glassy carbon working electrode, 3 mm diam., with o-ring
- Pine Pt wire counter electrode, with o-ring
- Pine 3 M KCl Ag/AgCl reference electrode, with o-ring
- Electrode holder
- Metal clamp
- Polishing pad
- Polishing solution
- Water wash bottle
- Rinse beaker and waste container
- Pine Wavenow XV 100 Potentiostat

Make Solutions

You will be given a 0.2 M stock solution of solketal. You need to prepare the following stock solutions:

ACT (10 mL of 20 mM solution)

NaHCO₃ (100 mL of 0.2 M solution)

Na₂CO₃ (100 mL of 0.2 M solution).

Now, prepare a blank solution. Label a 10 mL volumetric flask. Add 4 mL of 0.2 M NaHCO₃ and 4 mL of 0.2 M Na₂CO₃ to the flask using a volumetric pipette. Then add solketal to

give a concentration of 4 mM in 10 mL. Fill the flask to the mark with DI water and invert the flask until the solution is well mixed.

Prepare a 1.0 mM ACT solution. Label a 10 mL volumetric flask. Add 0.5 mL of the ACT stock solution to the flask by volumetric pipette. Then add 4 mL 0.2 M NaHCO₃ and 4 mL 0.2 M Na₂CO₃ solutions to the flask. Fill the flask to the mark with DI water and invert the flask until the solution is well mixed.

Prepare 1.0 mM ACT solutions with solketal added. Make sure to label all flasks. All solutions should be made in a 10 mL volumetric flask with 4 mL 0.2 M NaHCO₃ and 4 mL 0.2 M Na₂CO₃. Make four ACT – Solketal solutions with the following final concentrations of solketal: 2 mM, 4 mM, 9 mM, and 16 mM. The concentration of ACT in all four flasks should be 1.0 M.

Initial Voltammetric Study

Transfer the entire contents of the ACT-only solution into the voltammetric cell. (Note: The applied potentials will not be sufficiently negative to necessitate sparging the solution with inert gas to remove O₂). Place the electrode holder on the cell and place the polished GC working electrode and platinum wire counter electrode in the large holes in the cap. Remove the reference electrode from the storage solution, rinse the tip of the electrode with DI water, and place the reference electrode in the small hole in the cap (**Figure B.9**). The reference and working electrodes should be placed close together to minimize solution resistance. Adjust the depth of electrode immersed in solution using the o-rings. Attach the alligator clip leads of the Wavenow Pine Potentiostat to the electrodes of the cell.



Figure B.9. Pine Research cell setup for electrochemical analysis.

Always conduct a quick visual check of your cell set-up just before running an experiment! Make sure the electrode connections are not touching and that all electrodes are completely immersed in the solution.

Open the Aftermath software and turn on the potentiostat. You should be able to see the interface as shown in **Figure B.10**. Using File/New archive option, make your own archive and save it in a new folder for your group in the C:Drive > AfterMath Data Files. In the experiment menu, choose CV experiment, and adjust the CV parameters as necessary (Hints: because this is an oxidation reaction first, you should scan in the positive direction. The suggested scan rate for primary data is 100 mV s^{-1} .) Click Perform when you are prepared to run the experiment. **Rename the experiment once the CV is finished**. Once the experiment is finished, a new experiment will appear underneath “CV Parameters” called “CV Experiment (#)”. Right click on “CV Experiment (#)” and select “Rename” in the pop-up window. A good name might be “ACT, 100 mV s^{-1} , 0-1.2 V”, for example.

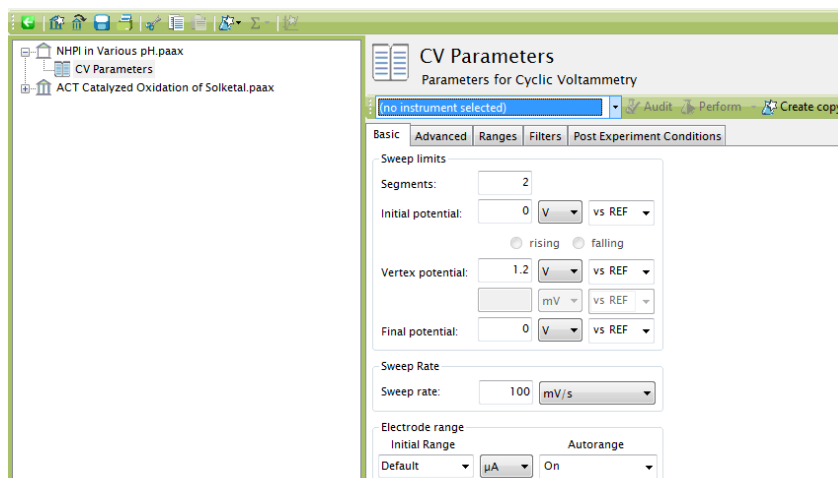


Figure B.10. Aftermath software interface for cyclic voltammetry analysis

After seeing the oxidation and reduction peaks you can now adjust the potential range, ideally between 350 mV less than reduction peak potential and 350 mV more than oxidation peak potential. Return to the “CV Parameters” and adjust the potential window around the peak of interest (**Figure B.11**). Double check that the entered potentials correspond with the correct units. Collect a CV using the adjusted potential window conditions. Always remember to rename the experiment right after you run it!

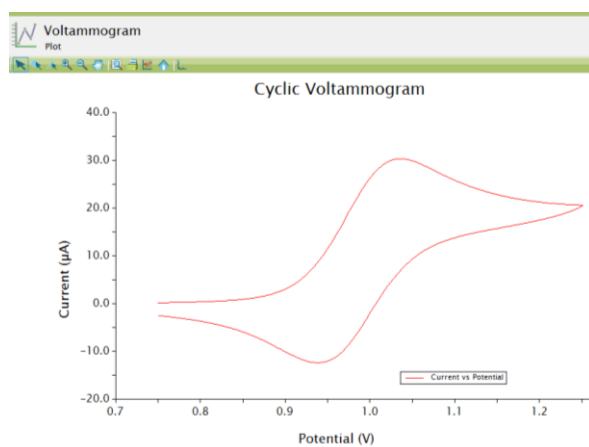


Figure B.11. A CV displayed on Aftermath Software.

Polish the Working Electrode

Since electrochemistry is a surface technique, a clean and uniform surface at the working electrode is required for accurate and reproducible measurements. Therefore, polishing the electrode before running CA experiments is crucial. First, rinse the tip of the working electrode with DI water. For all rinsing steps, make sure the liquid touches the shiny, disc shaped surface of the electrode. Next, put a few drops of the polishing slurry on the polishing pad. Add some water to the polishing pad to wet the surface. Firmly press the tip of the electrode to the polishing pad and move the electrode in a figure eight motion (**Figure B.12**), keeping the electrode perpendicular to the polishing pad, for approximately 20 motions. After polishing, rinse the tip of the electrode with DI water. Allow the electrode to dry before performing your analyses. **Do not dry the electrode surface with absorbent materials to avoid scratching the surface of the electrode!**

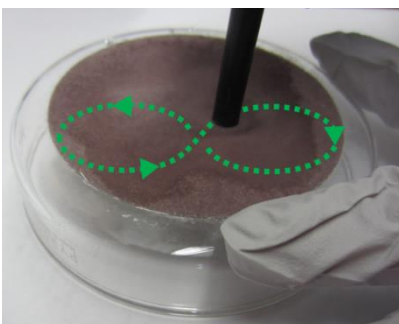


Figure B.12. Polishing the working electrode.

Chronoamperometry and Voltametric Studies of the ACT Solution

After polishing your electrode run your CA experiments (**Figure B.13**). In the experiment menu, choose the CA experiment, and adjust the CA parameters as necessary (Hints: you should run the CA experiment for 20 seconds, and the potential should be 100 – 150 mV more positive to the oxidation peak potential determined from the CVs that were just collected.) Click Perform when you are prepared to run the experiment.

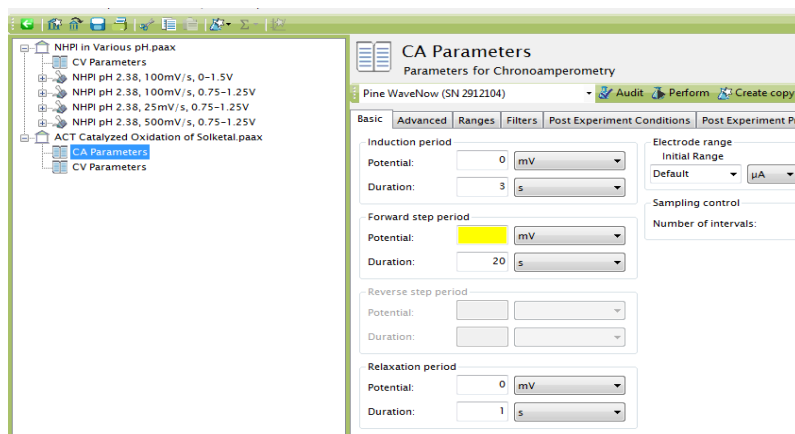


Figure B.13. Aftermath software interface for chronoamperometric analysis.

Make sure to rename your file when the experiment is finished running. (Hint: It may be worth looking at other plots based on this data for your data analysis.)

After your CA experiment, collect CV's at 25, 50, 80, 120 mV s^{-1} , with the same potential range as your initial CV experiment. (Hint: Observe the effect of scan rate on peak current.)

Conduct Chronoamperometric and Voltammetric Studies of ACT Catalyzed Solketal Oxidation

Repeat the same chronoamperometric and voltammetric experiment for all four ACT – Solketal solutions (2, 4, 9, and 16 mM of Solketal). Rinse the cell and electrodes with DI water after each new solution. Make sure to polish the working electrode in between each solution, right before running the CA experiment. Always remember to rename each experiment.

Then, run the CA experiment and one CV experiment at 80 mV s^{-1} for the blank (solketal only) solution.

Study the Effect of Base

Run the CA experiment and one CV experiment at 80 mV s^{-1} for 1.0 mM ACT in the presence of 4 mM of Solketal in a NaCl solution instead of carbonate/bicarbonate buffer (8 mL of 0.2 M NaCl instead of 4 mL 0.2 M NaHCO_3 and 4 mL 0.2 M Na_2CO_3 solutions).

Data Analysis

After collecting all CA and CV data, export your data for later analysis. At the top of the Aftermath software window, click “File > Save Archive”. Then click “File > Export”. Check the box next to your archive name. Click “Export”. This will allow you to export your data to a flash drive, and it can be opened in Excel as a .csv file. (Hint: There may be some analysis you can do in lab or by using the Aftermath software, which should be available for free to use on your personal computer.)

Correlation of Peak Current and Voltammetry Scan Rate

To determine the oxidation (anodic) and reduction (cathodic) peak currents, the baseline current for each peak must first be determined. The baseline current for each peak is usually determined by fitting a line to the plateau current before a peak (**Figure B.14**). The difference between the current at the peak potential and the baseline current is the peak current (I_{cathodic} or I_{anodic}). In this experiment, we will approximate the baseline current. Use the same CV data files to determine the oxidation (anodic) peak currents based on an approximate baseline current (using Excel or the Aftermath software, more info can be found here: <https://pineresearch.com/shop/kb/software/software-help-and-support/using-aftermath/peak-height/>).

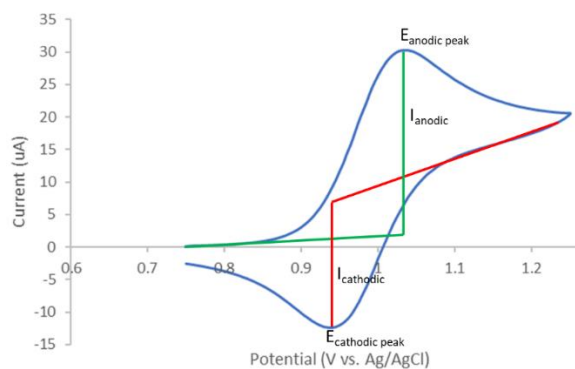


Figure B.14. Determining the oxidation (anodic) and reduction (cathodic) peak current.

Obtain the following graphs for the ACT-only voltammetric data:

- 1) Make a graph of the CV curves (overlaid over one another) at the four scan rates.
- 2) Plot ACT Peak Current vs scan rate.
- 3) Then plot ACT Peak current vs the square root of scan rate.

What trends do you notice? What do these trends imply?

- 4) Make a plot of the normalized CV curves (overlaid over one another) at the four scan rates.
(Hint: Normalized CVs are derived by dividing the currents from the entire CV curve by the square root of scan rate.)

What differences do you notice between the Non-Normalized CV's versus the Normalized CV's?

Normalized CVs of Solketal Oxidation

Open the data for the CVs of the ACT- 4 mM solketal solution at all four scan rates. Obtain the following graphs for these voltammetric data:

- 1) Make a graph of the CV curves (overlaid over one another) at the four scan rates.
- 2) Plot ACT Peak Current vs scan rate.
- 3) Then plot ACT Peak current vs the square root of scan rate.

What trends do you notice? What do these trends imply?

- 4) Make a plot of the normalized CV curves (overlaid over one another) at the four scan rates.

What differences do you notice between the Non-Normalized CV's versus the Normalized CV's?

Explain the difference between the trends in the absence and presence of solketal.

CV Analysis with Differing Solketal Concentrations

Open the data for all CVs of ACT-solketal solutions collected at a scan rate of 50 mV s^{-1} . Obtain the following graphs:

- 1) Plot the peak currents vs the concentration of solketal.
- 2) Plot the peak current vs the square root of the concentration of solketal.

What trends do you notice? What does this tell you about the kinetics of this reaction?

Turnover Frequency Using Differing Solketal Concentration

Calculate the TOF (h^{-1}) of ACT for the ACT catalyzed solketal oxidation using the following equation:

$$\text{TOF} = \frac{(Q_{\text{mM solketal}} - Q_{\text{ACT}}) \times 3600}{(Q_{\text{ACT}} - Q_{\text{blank}}) \times n \times t}$$

TOF = turnover frequency, units of h^{-1}

$Q_{\text{mM solketal}}$ = total charge for reactions with ACT and solketal, units of Coloumb

Q_{blank} = total charge for blank solution (background charge), units of Coloumb

Q_{ACT} = total charge for reaction with ACT (*no* solketal), units of Coloumb

n = number of electrons required for reaction

t = total reaction time, units of seconds

For the ACT catalyzed oxidation of solketal, $n = 2$ electrons and the chronoamperogram reactions ran for 20 seconds. The constant 3600 is included to convert the TOF from s^{-1} to h^{-1} . Calculate the TOF (h^{-1}) for ACT in the presence of 2, 4, 9 and 16 mM solketal.

B.11. References

1. Savéant, J. M.; Vianello, E. *Electrochim. Acta* **1965**, *10*, 905–920.
2. Savéant, J. M. *Elements of Molecular and Biomolecular Electrochemistry; An Electrochemical Approach to Electron Transfer Chemistry*, pp 106-119. John Wiley & Sons, Inc.: New York, 2006.
3. Rafiee, M.; Karimi, B.; Alizadeh, S. *ChemElectroChem* **2014**, *1*, 455–462.
4. Anelli, P. L.; Biffi, C.; Montanari, F.; Quici, S. *J. Org. Chem.* **1987**, *52*, 2559–2562.
5. Iwabuchi, Y. *Chem. Pharm. Bull.* **2013**, *61*, 1197–1213.
6. Nutting, J. E.; Rafiee, M.; Stahl, S. S. *Chem. Rev.* **2018**, *118*, 4834–4885.
7. Rafiee, M.; Konz, Z. M.; Graaf, M. D.; Koolman, H. F.; Stahl, S. S. *ACS Catal.* **2018**, *8*, 6738–6744.

8. Elgrishi, N.; Rountree, K. J.; McCarthy, B. D.; Rountree, E. S.; Eisenhart, T. T.; Dempsey, J. L. *J. Chem. Educ.* **2018**, *95*, 197–206.
9. Wang, J. *Analytical Electrochemistry*, 3rd Edition; John Wiley & Sons, Inc.: Hoboken, NJ, 2006.
10. Pine Research. Voltammetric Methods: Cyclic Voltammetry (CV). <https://pineresearch.com/shop/kb/software/methods-and-techniques/voltammetric-methods/cyclic-voltammetry-cv/>, accessed January 16, 2020.

**Appendix C: Electrochemical Aminoxy-Mediated α -Cyanation of Secondary
Piperidines for Pharmaceutical Building Block Diversification Supporting
Information**

C.1. General Experimental Details

Reagents

Organic solvents were obtained from an LC Technology Solutions Inc. solvent purification system using columns containing molecular sieves under argon and purged for 15-20 min with N₂ gas before use. All commercially available organic compounds were used as received unless otherwise specified. 4-(4-bromophenyl)piperidine (**1b**), 4-(4-methoxyphenyl) piperidine hydrochloride (**1c**), 4-(3-methylphenyl)piperidine hydrochloride (**1d**), 2-(4-piperidinyl)-1,3-benzoxazole (**1f**), 4-hydroxy-4-phenylpiperidine (**1h**), perhydroisoquinoline (**1i**), 6-fluoro-3-(4-piperidinyl)benzoxazole (**1j**), 2-(5-piperidin-4-yl-1,2,4-oxadiazol-3-yl)pyrazine (**1k**), 4-(5-phenyl-1,3,4-oxadiazol-2-yl)piperidine (**1l**), 1-(piperidin-4-ylcarbonyl)piperidine hydrochloride (**1n**), piperidine (**1t**), morpholine (**1u**), 2-(trifluoromethyl)piperidine (**1v**), 4-hydroxypiperidine (**1x**), 4-piperidinopiperidine (**1z**), pyrrolidine (**1ac**), 2,2,6,6-Tetramethylpiperidine 1-oxyl (TEMPO), 9-Azabicyclo[3,3,1]nonan-3-one-9-oxyl (ketoABNO), sodium perchlorate, potassium hexafluorophosphate, tetraethylammonium tetrafluoroborate, tetrabutylammonium tetrafluoroborate, potassium tetrafluoroborate, tetrabutylammonium hexfluorophosphate, hydrochloric acid, p-toluenesulfonic acid monohydrate, methanol-d₄, benzene-d₆, acetonitrile-d₃, dimethyl sulfoxide-d₆, and dioxane were purchased from Millipore Sigma. 4-(piperidin-4-yl)pyridine (**1g**), tert-butyl 3,9-diazaspiro[5.5]undecane-3-carboxylate (**1q**), methyl 2-piperidinecarboxylate (**1w**), 4-trifluoromethyl piperidine (**1y**), and 4-(1-pyrrolidinyl) piperidine (**1aa**) were purchased from Ark Pharm. 4-phenyl piperidine (**1a**) and hexafluoroisopropanol were purchased from Combi-blocks. 2-(piperidin-4-yl)-1,3-benzothiazole (**1o**), and 4-(3-piperidinyl)pyrimidine (**1s**) 2,3,4,5-tetrahydro-1H-2-benzazepine (**1ab**) were purchased from Enamine. 4-Acetamido-2,2,6,6-tetramethylpiperidine 1-oxyl was purchased from TCI. 1-(3,4-dichlorophenyl)-3-azabicyclo[3.1.0]hexane hydrochloride (**1ad**) was purchased from Advanced

ChemBlocks Inc. 4-[3-(2,4-dichlorophenyl)-1H-pyrazol-5-yl]piperidine (**1m**) was purchased from Key Organics / BIONET. 1-benzylpiperidine and ferrocene was purchased from Alfa Aeser. Trimethylsilyl cyanide was purchased from Matrix Scientific. 4-(3-isopropyl-1,2,4-oxadiazol-5-yl)piperidine hydrochloride (**1e**) was purchased from ChemBridge Corporation. 9-Azabicyclononane N-oxyl (ABNO) was received from Merck.

Before being subjected to the reaction conditions, **1c**, **1d**, **1e**, **1p** and **1ad** were converted to the free base (100-300 mg of the salt was dissolved in 1-3 mL of 1 M aqueous sodium hydroxide solution, stirred and extracted 3x with DCM. The organic solution was dried with Na₂SO₄, filtered and concentrated). 2'-chloro-4',5'-dihydrospiro[piperidine-4,7'-thieno[2,3-c]pyran] (**1r**)¹ and 1-(piperidin-4-yl)-3-propyl-1,3-dihydro-2H-benzo[d]imidazol-2-one (**1p**)² were prepared according to literature procedures.

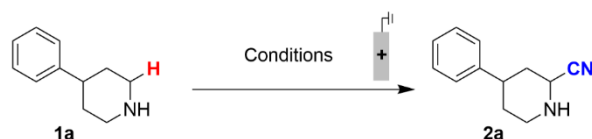
Instruments and techniques

¹H, ¹³C, and ¹⁹F NMR spectra were recorded on Bruker 400 and 500 MHz spectrometers. Chemical shifts are given in parts per million (ppm) relative to residual solvent peaks in the ¹H and ¹³C NMR spectra and relative to CFCl₃ in the ¹⁹F NMR spectra. Coupling constants, J, were calculated in MestReNova to the nearest 0.1 Hz. The following abbreviations (and their combinations) are used to label the multiplicities: s (singlet), d (doublet), t (triplet), q (quartet), quin (quintet), sext (sextet), h (heptet), m (multiplet), br (broad) and app (apparent). Structural assignment was achieved using 1H-1H COSY, HSQC, HMBC and TOCSY analysis where appropriate and the relative stereochemistry was assigned by nOe experiments. High-resolution mass spectra were obtained using a Thermo Q ExactiveTM Plus by the mass spectrometry facility at the University of Wisconsin. Chromatographic purification of products was accomplished by chromatography on Silicycle P60 silica gel (particle size 40-63 μm, 230-400 mesh) using Teledyne Isco Combiflash Rf or Biotage Isolera One flash chromatography systems. Thin-layer

chromatography (TLC) was performed on Silicycle silica gel UV254 pre-coated plates (0.25 mm). Visualization of the developed chromatogram was performed by using UV lamps and KMnO_4 stain.

All cyclic voltammetric, chronoamperometric and chronopotentiometric measurements were performed at room temperature using a Pine WaveNow PGstat. The CV experiments were carried out in a three-electrode cell configuration with a glassy carbon (GC) working electrode (3 mm diameter, unless otherwise stated) and a platinum wire counter electrode. The potentials were measured versus an Ag/AgNO_3 (0.01 M) reference electrode (all electrodes from BASi) and recorded against a ferrocene/ferrocenium reference. The GC working electrode was polished with alumina before each experiment. Bulk electrolysis experiments were performed in custom-built undivided cells made of Teflon, with graphite rod working electrodes, platinum wire counter electrodes and Ag/AgNO_3 (0.01 M) for a reference electrode. The graphite rod working electrode and the platinum wire counter electrode were both sonicated for 1 min in water before being washed with distilled water and then acetone. The graphite rod was then very lightly rubbed down with a Kimwipe before use.

C.2. Reaction Optimization

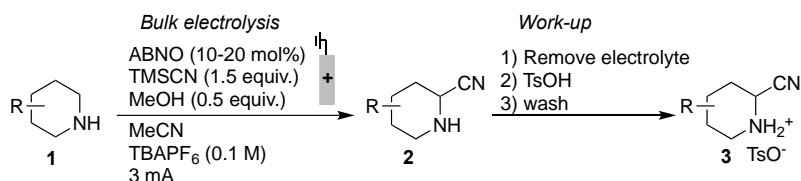


Entry	Catalyst (mol%)	Solvent	Electrolyte	TMSCN equiv.	Additive (equiv.)	Current /mA	Yield/% ^a
1	-	MeCN	NaClO_4	1.5	-	1	19
2	ABNO (20)	MeCN	NaClO_4	1.5	-	1	37
3 ^b	ABNO (20)	MeCN	NaClO_4	1.5	HFIP (1)	0	0
4	ABNO (20)	MeCN	NaClO_4	1	HFIP (1)	1	52
5	ABNO (20)	MeCN	NaClO_4	1.5	HFIP (1)	1	54
6	ABNO (20)	MeCN	NaClO_4	3	HFIP (1)	1	43
7	ABNO (20)	MeCN	KBF_4	1.5	HFIP (1)	1	22
8	ABNO (20)	MeCN	KPF_6	1.5	HFIP (1)	1	53

9	ABNO (20)	MeCN	TBAPF ₆	1.5	HFIP (1)	1	54
10	ABNO (20)	MeCN	TBABF ₄	1.5	HFIP (1)	1	55
11	ABNO (20)	THF	TBABF ₄	1.5	HFIP (1)	1	52
12	ABNO (20)	DCM	TBABF ₄	1.5	HFIP (1)	1	16
13	ABNO (20)	MeOH	TBABF ₄	1.5	HFIP (1)	1	44
14	TEMPO (10)	MeCN	TBABF ₄	1.5	HFIP (1)	1	10
15	ACT (10)	MeCN	TBABF ₄	1.5	HFIP (1)	1	24
16	AZADO (10)	MeCN	TBABF ₄	1.5	HFIP (1)	1	62
17	KetoABNO (10)	MeCN	TBABF ₄	1.5	HFIP (1)	1	81
18	ABNO (10)	MeCN	TBABF ₄	1.5	HFIP (1)	1	57
19	ABNO (10)	MeCN	TBAPF ₆	1.5	HFIP (1)	3	66
20	ABNO (10)	MeCN	TBAPF ₆	1.5	H ₂ O (1)	3	68
21	ABNO (10)	MeCN	TBAPF ₆	1.5	MeOH (1)	3	79
22	ABNO (10)	MeCN	TBAPF ₆	1.5	MeOH (1.5)	3	74
23	ABNO (10)	MeCN	TBAPF₆	1.5	MeOH (0.5)	3	84
24 ^c	ABNO (10)	MeCN	TBAPF ₆	1.5	MeOH (0.5)	3	0
25	ABNO (10)	MeCN	TBAPF ₆	1.5	MeOH (0.5)	3	79 ^d (77) ^e
26	ABNO (10)	MeCN	TBAPF ₆	1.5	MeOH (0.5)	3	72 ^f

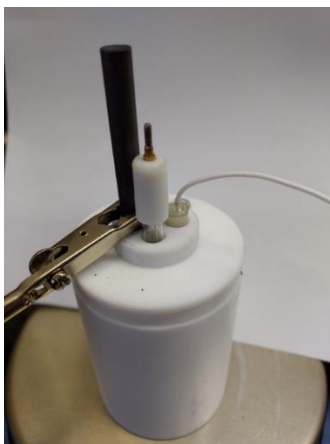
^aNMR (¹H NMR) yields against a mesitylene internal standard. ^bStirred for five days at room temperature. ^cPreformed HBF₄ salt of **1a** was used as the starting material; ^dwith 20 mol% 2,6-Lutidine; ^e with 1 equiv. 2,6-Lutidine; ^fwith 20 mol% pyridine.

C.3. Optimized Procedure for the Electrochemical Cyanation of Secondary Amines



C.3.1. Bulk Electrolysis

Degassed MeCN (2 mL) was added to the secondary amine substrate (1 equiv., 0.3 mmol) in a 1.5-dram vial and stirred vigorously. If necessary, heat and sonication was applied to aid dissolution of the solid. The solution was transferred via pipette to the bulk electrolysis cell containing a stir bar.



In a separate vial was added tetrabutylammonium hexafluorophosphate (0.5 mmol, 193 mg), ABNO (10 mol%, 0.03 mmol, 4.2 mg, or 20 mol% 0.06 mmol, 8.4 mg), and degassed MeCN (3 mL) and stirred until all solids were dissolved. This red solution was transferred in three batches to the bulk electrolysis cell via the substrate-containing vial to ensure complete transfer of the amine.

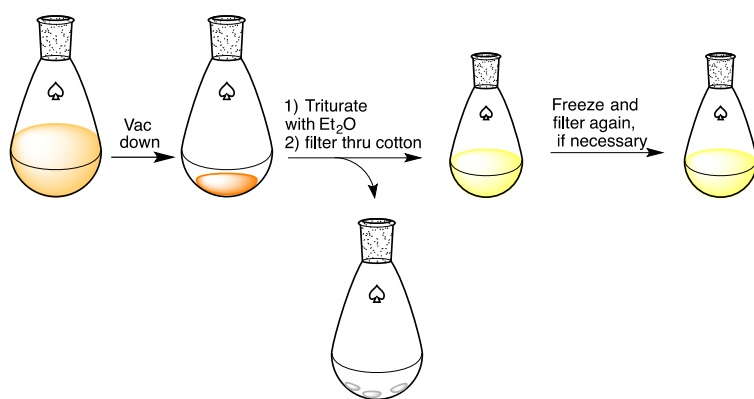
To this solution in the bulk electrolysis cell was first added methanol (0.5 equiv., 0.15 mmol, 6.1 μL) and then TMSCN (1.5 equiv., 0.45 mmol, 56 μL) with stirring. The three electrodes were then inserted into the cell. A cut-off potential was added to the electrolysis method and the value was calculated as follows: 0.5 V was added to the potential that was reached when 3 mA was applied for a 20 s period. 3 mA was then applied until that cut-off potential was reached, normally within 2-2.5 F/mol. The graphite rod was immersed 2 cm into the reaction solution, which gives an electrode surface area of 4.3 cm^2 .

At the end of the reaction, mesitylene (0.33 equiv., 0.1 mmol, 13.6 μL) was added to the cell and stirred, before a sample (50 μL) was removed, diluted with benzene- d_6 (0.4 mL) and analyzed by ^1H NMR. If the ^1H NMR indicated remaining starting material, then further portions of ABNO (5 mol%, 0.015 mmol, 2.1 mg or 10 mol%, 0.03 mmol, 4.2 mg depending on substrate conversion), TMSCN (0.5 equiv., 0.15 mmol, 19 μL) and methanol (0.5 equiv., 0.15 mmol, 6.1

μL) were added and the bulk electrolysis run again. NMR product yield was calculated by comparing the alpha cyanated proton (3.3-4.3 ppm) peak to mesitylene.

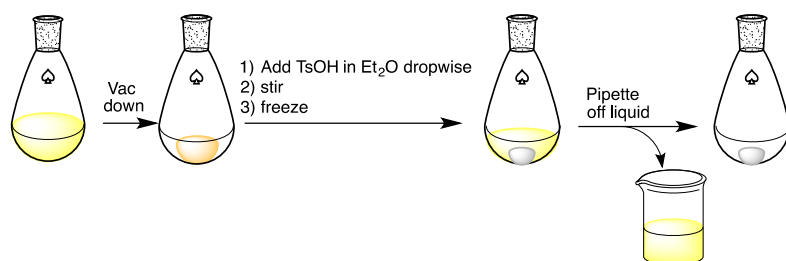
C.3.2. Work-Up

Electrolyte (NBu_4PF_6) removal: The solution was transferred to a round-bottom flask and concentrated under reduced pressure. Diethyl ether (ca. 5 x 4 mL) was used to extract the product from the solid mixture via trituration: a portion of solvent was added to the flask, stirred until the electrolyte crystallized out, and then filtered through a glass pipette filled with cotton wool into a pre-weighed vial and stir bar, and repeated with further portions of Et_2O . To ensure high product purity, it is important at this stage to make sure that all the NBu_4PF_6 salt has been separated from the solution. This can be confirmed by observing the formation of white crystals after cooling the vial down to $-20\text{ }^\circ\text{C}$ in the freezer. If observed, the solution should be filtered an additional time. The separated NBu_4PF_6 can be reused in subsequent reactions after drying under vacuum overnight. (EA Calc: ($\text{C}_{16}\text{H}_{36}\text{F}_6\text{NP}$) C, 49.60; H, 9.37; N, 3.62; F, 29.42. Measured: C, 49.95; H, 9.58; N, 3.70; F, 29.13. Difference: C, 0.35; H, 0.21; N, 0.08; F, 0.29.)



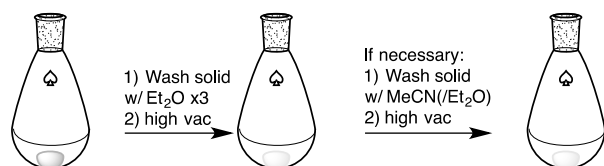
TsOH addition: The resulting solution was evaporated down to a volume of ca 2 mL. To this was added a solution of tosic acid (30 % more than calculated NMR yield) in diethyl ether (2 mL) dropwise with rapid stirring, during which a precipitate formed. Rapid stirring continued for

a further 10-20 min. The mixture was cooled in the freezer and the solid allowed to settle, before the liquid was carefully removed from the solid *via* pipette.

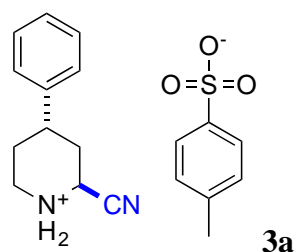


Wash: The solid product was briefly (3-4 mins) dried under vacuum before being washed three times in the following cycle: Et₂O (ca. 2 mL) was added, stirred, cooled in the freezer and then pipetted off. To remove traces of remaining Et₂O in the crystal lattice, MeCN (1 mL) was added, stirred and evaporated. The product was then dried under high vacuum for 3-4 hours.

¹H NMR analysis revealed that some compounds required further purification (indicated next to the characterisation data). Thus, a small quantity (>0.5 mL) of cooled MeCN was added, stirred, cooled in the freezer and carefully pipetted away from the insoluble product. If the product was found to dissolve in MeCN, recrystallization with Et₂O was necessary.



C.3.3. Characterization Data



The general procedure was followed using 20 mol% ABNO, which furnished 92 mg of a white powder (87%) after purification by Et₂O washes only. A literature search did not reveal any previously documented characterization data.

¹H NMR (500 MHz, Methanol-*d*₄) δ 7.72 (d, *J* = 8.2 Hz, 2H), 7.39 – 7.31 (m, 2H), 7.30 – 7.25 (m, 3H), 7.24 (d, *J* = 8.2 Hz, 2H), 5.09 (dd, *J* = 4.7, 2.2 Hz, 1H), 3.60 (dt, *J* = 13.3, 3.6 Hz, 1H), 3.43 (td, *J* = 13.3, 3.2 Hz, 1H), 3.14 (tt, *J* = 12.4, 3.8 Hz, 1H), 2.37 (s, 3H), 2.33 (dd app t, *J* = 14.8, 3.8, 2.2 Hz, 1H), 2.24 (ddd, *J* = 14.8, 12.4, 4.7 Hz, 1H), 2.14 (d app quin., *J* = 14.5, 3.0 Hz, 1H), 1.96 (dtd, *J* = 14.5, 12.7, 4.3 Hz, 1H).

¹³C NMR (126 MHz, Methanol-*d*₄) δ 143.62, 143.42, 141.80, 129.99, 129.87, 128.43, 127.75, 126.95, 115.63, 45.99, 43.46, 37.84, 33.75, 30.46, 21.30.

HRMS (ESI⁺) Calc: [M⁺] (C₁₂H₁₅N₂) 187.1230; measured: 187.1229 = 0.5 ppm difference.

IR (film) ν_{max} /cm⁻¹: 2965, 2735, 2527, 1611, 1496, 1455, 1231, 1144, 1121, 1029, 1006.

C.3.4. Large Scale Reaction

The reaction was performed in a BASi bulk electrolysis cell using an RVC working electrode (as pictured), steel mesh as the counter electrode (separated from the working electrode by rubber O-rings), and Ag/AgNO₃ (0.01 M) as the reference electrode solution. Degassed MeCN (85 mL) was added to 4-phenylpiperidine **1a** (1 equiv, 6.2 mmol, 1g), ABNO (10 mol%, 0.62 mmol, 86.9 mg), and TBAPF₆ (0.5 mol, 3.991g) and stirred vigorously. Sonication was applied to aid dissolution of the solid. To this solution in the bulk electrolysis cell was first added methanol (0.5 equiv., 3.1 mmol, 125.6 μ L) and then TMSCN (1.5 equiv., 9.3 mmol, 1.16 mL) with stirring. The three electrodes were then inserted, and the cell was sealed to prevent solvent evaporation. A current of 15 mA was applied for 2 F/mol (26.1 h). Work-up of the reaction solution was performed similarly to the standard method with a few exceptions: 5 x 20 mL diethyl ether washes were performed during the electrolyte removal, a total of 40 mL diethyl ether was used addition of TsOH (0.075 mM), and 3 x 20 mL diethyl ether and 3 x 15 mL MeCN washes were performed to purify the product, which was formed as a light orange powder (1.6 g, 75% yield).

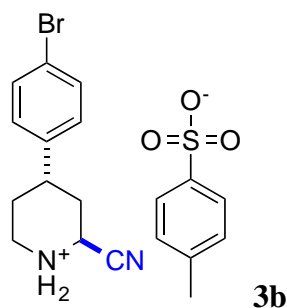


C.3.5. ElectraSyn 2.0 Reaction:

The reaction was performed in an ElectraSyn 2.0 in a 10 mL vial using a graphite SK-50 working electrode and platinum plated counter electrode. Degassed MeCN (5 mL) was added to 4-phenylpiperidine **1a** in the vial containing a stir bar and stirred vigorously. TBAPF₆ hexafluorophosphate (0.5 mmol, 193 mg) and ABNO (10 mol%, 0.03 mmol, 4.2 mg, or 20 mol% 0.06 mmol, 8.4 mg) were added and stirred until all solids were dissolved. To this solution in the cell was first added methanol (0.5 equiv., 0.15 mmol, 6.1 μ L) and then TMSCN (1.5 equiv., 0.45 mmol, 56 μ L) with stirring. The electrodes were then inserted into the cell. A current of 2 mA was applied for 2 F/mol (402 min). This current setting was selected after observing the steady-state current recorded when applying a potential of 200 mV vs. Fc⁺/Fc with the indicated electrodes. A somewhat reduced value (2 mA) was then used for the bulk electrolysis experiment.



At the end of the reaction, mesitylene (0.33 equiv., 0.1 mmol, 13.6 μL) was added to the cell and stirred, before a sample (50 μL) was removed, diluted with benzene- d_6 (0.4 mL) and analyzed by ^1H NMR.



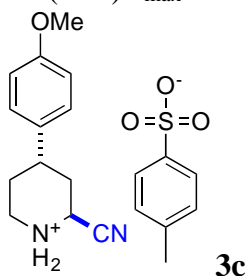
The general procedure was followed using 20 mol% ABNO, which furnished 103 mg of a white powder (81%) after purification by Et₂O washes only. A literature search did not reveal any previously documented characterization data.

^1H NMR (500 MHz, Methanol- d_4) δ 7.72 (d, J = 8.2 Hz, 2H), 7.49 (d, J = 8.5 Hz, 1H), 7.24 (d, J = 8.2 Hz, 2H), 7.20 (d, J = 8.5 Hz, 1H), 5.10 (dd, J = 5.0, 2.4 Hz, 1H), 3.60 (dt, J = 13.3, 3.7 Hz, 1H), 3.42 (td, J = 13.3, 3.3 Hz, 1H), 3.14 (tt, J = 12.4, 3.7 Hz, 1H), 2.37 (s, 3H), 2.35 – 2.29 (m, 1H), 2.26 – 2.18 (m, 1H), 2.17 – 2.08 (m, 1H), 1.99 – 1.87 (m, 1H).

^{13}C NMR (126 MHz, Methanol- d_4) δ 143.38, 142.85, 141.84, 133.03, 129.88, 129.82, 126.95, 122.03, 115.51, 45.88, 43.34, 37.27, 33.41, 30.22, 21.31.

HRMS (ESI⁺) Calc: [M^+] (C₁₂H₁₄BrN₂) 265.0335; measured: 265.0333 = 0.8 ppm difference.

IR (film) $\nu_{\text{max}}/\text{cm}^{-1}$: 2965, 2729, 2522, 1605, 1490, 1231, 1144, 1121, 1029, 1006.



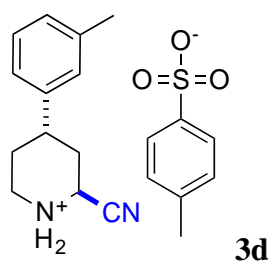
The general procedure was followed using 20 mol% ABNO, which furnished 96 mg of an off-white powder (66%) after purification by 3x Et₂O wash and 1x MeCN wash. A literature search did not reveal any previously documented characterization data.

^1H NMR (500 MHz, Methanol- d_4) δ 7.72 (d, J = 8.2 Hz, 2H), 7.24 (d, J = 8.2 Hz, 2H), 7.18 (d, J = 8.7 Hz, 2H), 6.90 (d, J = 8.7 Hz, 2H), 5.07 (dd, J = 4.8, 2.3 Hz, 1H), 3.77 (s, 3H), 3.58 (dt, J = 13.4, 3.3 Hz, 1H), 3.42 (td, J = 13.4, 3.3 Hz, 1H), 3.09 (tt, J = 12.5, 3.7 Hz, 1H), 2.37 (s, 3H), 2.33 – 2.27 (m, 1H), 2.23 – 2.14 (m, 1H), 2.14 – 2.08 (m, 1H), 1.98 – 1.85 (m, 1H).

^{13}C NMR (126 MHz, Methanol- d_4) δ 160.40, 143.46, 141.77, 135.57, 129.85, 128.72, 126.95, 115.64, 115.31, 55.72, 46.01, 43.50, 37.02, 34.00, 30.67, 21.30.

HRMS (ESI $^+$) Calc: [M^+] ($\text{C}_{13}\text{H}_{17}\text{N}_2\text{O}$) 217.1335; measured: 217.1334 = 0.4 ppm difference.

IR (film) $\nu_{\text{max}}/\text{cm}^{-1}$: 3444, 3363, 3006, 2833, 2729, 2522, 1611, 1513, 1461, 1248, 1207, 1179, 1121, 1035, 1012.



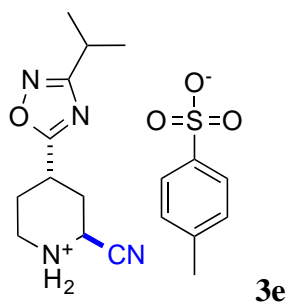
The general procedure was followed using 20 mol% ABNO, which furnished 60 mg of a white powder (54%) after purification by Et₂O washes and 1x MeCN wash. A literature search did not reveal any previously documented characterization data.

^1H NMR (500 MHz, Methanol- d_4) δ 7.72 (d, J = 8.2 Hz, 2H), 7.24-7.21 (m 3H), 7.10-7.08 (m, 2H), 7.05 (d, J = 7.5 Hz, 1H), 5.08 (dd, J = 4.0, 2.1 Hz, 2H), 3.60 (dt, J = 13.3, 3.5 Hz, 1H), 3.43 (td, J = 13.3, 3.2 Hz, 1H), 3.11 (tt, J = 12.4, 3.7 Hz, 1H), 2.37 (s, 3H), 2.34-2.30 (m, 4H), 2.25 – 2.17 (m, 1H), 2.17 – 2.08 (m, 1H), 2.01 – 1.86 (m, 1H).

^{13}C NMR (126 MHz, Methanol- d_4) δ 143.52, 143.48, 141.75, 139.81, 129.89, 129.84, 129.11, 128.42, 126.96, 124.70, 115.59, 45.99, 43.49, 37.77, 33.80, 30.47, 21.45, 21.30.

HRMS (ESI $^+$) Calc: [M^+] ($\text{C}_{13}\text{H}_{17}\text{N}_2$) 201.1386; measured: 201.1385 = 0.5 ppm difference.

IR (film) $\nu_{\text{max}}/\text{cm}^{-1}$: 2971, 2735, 2522, 2130, 1611, 1438, 1225, 1150, 1121, 1029, 1006.



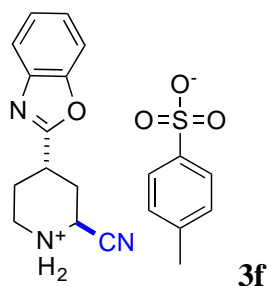
The general procedure was followed using 20 mol% ABNO, which furnished 90 mg of a white powder (77%) after purification by Et₂O washes and 1x MeCN wash. A literature search did not reveal any previously documented characterization data.

¹H NMR (500 MHz, Methanol-*d*₄) δ 7.71 (d, *J* = 8.1 Hz, 2H), 7.24 (d, *J* = 8.1 Hz, 2H), 5.07 (t, *J* = 4.9 Hz, 1H), 3.65 (tt, *J* = 9.6, 4.1 Hz, 1H), 3.54 (dt, *J* = 13.5, 4.8 Hz, 1H), 3.47 (ddd, *J* = 13.5, 9.8, 3.7 Hz, 1H), 3.08 (h, *J* = 6.9 Hz, 1H), 2.64 (dt, *J* = 14.9, 4.0 Hz, 1H), 2.46 (dt, *J* = 9.4, 4.6 Hz, 1H), 2.43 – 2.38 (m, 1H), 2.37 (s, 3H), 2.10 (dtd, *J* = 14.3, 9.8, 4.3 Hz, 1H), 1.33 (d, *J* = 6.9 Hz, 6H).

¹³C NMR (126 MHz, Methanol-*d*₄) δ 179.81, 176.32, 143.42, 141.77, 129.84, 126.94, 115.29, 44.54, 42.28, 30.42, 29.98, 27.95, 26.26, 21.30, 20.71.

HRMS (ESI⁺) Calc: [M⁺] (C₁₁H₁₇N₄O) 221.1397; measured: 221.1393 = 1.8 ppm difference.

IR (film) $\nu_{\max}/\text{cm}^{-1}$: 2977, 2274, 1576, 1461, 1346, 1196, 1121, 1029, 1006.



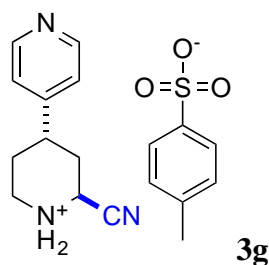
The general procedure was followed using 20 mol% ABNO, which furnished 94 mg of a pale yellow powder (80%) after purification by Et₂O washes only. A literature search did not reveal any previously documented characterization data.

¹H NMR (500 MHz, Methanol-*d*₄) δ 7.76 – 7.67 (m, 3H), 7.64 – 7.57 (m, 1H), 7.45 – 7.35 (m, 2H), 7.22 (d, *J* = 8.2 Hz, 2H), 5.12 (dd, *J* = 6.0, 4.4 Hz, 1H), 3.71 (tt, *J* = 9.1, 4.2 Hz, 1H), 3.60 – 3.45 (m, 2H), 2.70 (dddd, *J* = 14.8, 6.0, 4.2, 1.3 Hz, 1H), 2.58 (ddd, *J* = 14.8, 9.1, 4.4 Hz, 1H), 2.51 – 2.42 (m, 1H), 2.35 (s, 3H), 2.23 (dtd, *J* = 14.8, 9.1, 4.4 Hz, 1H).

¹³C NMR (126 MHz, Methanol-*d*₄) δ 167.05, 152.17, 143.43, 141.88, 141.74, 129.82, 126.94, 126.70, 125.89, 120.72, 115.47, 111.78, 44.54, 42.42, 31.74, 30.16, 26.29, 21.29.

HRMS (ESI⁺) Calc: [M⁺] (C₁₃H₁₄N₃O) 228.1131; measured: 228.1129 = 0.9 ppm difference.

IR (film) $\nu_{\max}/\text{cm}^{-1}$: 2971, 2764, 2522, 1611, 1571, 1450, 1231, 1144, 1115, 1029, 1006.



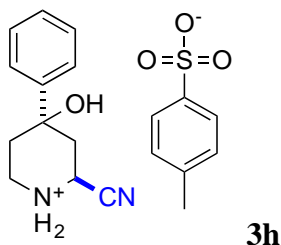
The general procedure was followed using 10 mol% ABNO, which furnished 69 mg of an off-white powder (64%) after purification by Et₂O washes and 1x MeCN washes. A literature search did not reveal any previously documented characterization data.

¹H NMR (500 MHz, Methanol-*d*₄) δ 8.71 – 8.56 (m, 2H), 7.75 – 7.66 (m, 2H), 7.71 (d, *J* = 8.1 Hz, 2H), 7.24 (d, *J* = 8.1 Hz, 2H), 4.73 (dd, *J* = 4.6, 2.3 Hz, 1H), 3.35 (dt, *J* = 13.1, 3.2 Hz, 1H), 3.29 – 3.21 (m, 1H), 3.23 – 3.12 (m, 1H), 2.26 (ddt, *J* = 13.8, 4.1, 2.3 Hz, 1H), 2.15 (td, *J* = 13.5, 13.0, 4.6 Hz, 1H), 2.07 (dt, *J* = 13.5, 2.9 Hz, 1H), 1.84 (qd, *J* = 12.6, 4.4 Hz, 1H).

¹³C NMR (126 MHz, Methanol-*d*₄) δ 144.42, 141.32, 139.66, 127.73, 124.80, 123.53, 116.10, 44.22, 40.83, 36.94, 31.57, 29.18, 27.56, 19.17.

HRMS (ESI⁺) Calc: [M⁺] (C₁₁H₁₄N₃) 188.1182; measured: 188.1182 = <0.1 ppm difference.

IR (film) ν_{max}/cm⁻¹: 2974, 2724, 2107, 1597, 1494, 1420, 1279, 1167, 1116, 1031, 1002, 889, 816, 712, 677, 561.



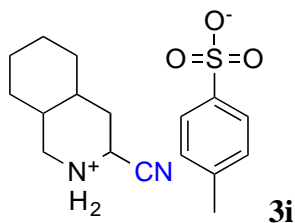
The general procedure was followed using 20 mol% ABNO, which furnished 85 mg of a pale yellow powder (77%) after purification by Et₂O washes only. A literature search did not reveal any previously documented characterization data.

¹H NMR (500 MHz, Methanol-*d*₄) δ 7.71 (d, *J* = 8.2 Hz, 2H), 7.51 – 7.46 (m, 2H), 7.38 (dd, *J* = 8.6, 7.0 Hz, 2H), 7.32 – 7.28 (m, 1H), 7.23 (d, *J* = 8.2 Hz, 2H), 5.02 (dd, *J* = 6.0, 2.0 Hz, 1H), 3.77 (td, *J* = 13.0, 3.1 Hz, 1H), 3.45 (dt, *J* = 13.0, 3.5 Hz, 1H), 2.51 (dd, *J* = 15.2, 5.7 Hz, 1H), 2.37 (s, 3H), 2.33 – 2.19 (m, 2H), 2.02 (dq, *J* = 14.8, 2.8 Hz, 1H).

¹³C NMR (126 MHz, Methanol-*d*₄) δ 147.27, 143.46, 141.75, 129.84, 129.64, 128.77, 126.95, 125.50, 116.43, 69.52, 42.76, 39.82, 37.77, 35.76, 21.30.

HRMS (ESI⁺) Calc: [M⁺] (C₁₂H₁₅N₂O) 203.1179; measured: 203.1176 = 1.5 ppm difference.

IR (film) $\nu_{\max}/\text{cm}^{-1}$: 3330, 3031, 2956, 2852, 2800, 2737, 2668, 2513, 1602, 1498, 1469, 1428, 1205, 1187, 1125, 1154, 1043, 1015.



The general procedure was followed using 10 mol% ABNO, which furnished 45 mg of a white powder (45%) after purification by Et₂O washes and 2x MeCN washes. A literature search did not reveal any previously documented characterization data.

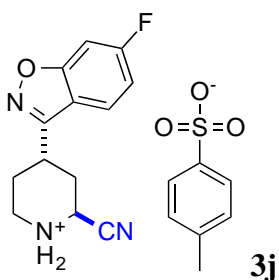
¹H NMR (500 MHz, Methanol-*d*₄) δ 7.73 (d, *J* = 8.1 Hz, 2H), 7.26 (d, *J* = 8.1 Hz, 2H), 3.31 (d, *J* = 4.3 Hz, 1H), 2.93 (t, *J* = 12.5 Hz, 1H), 2.39 (s, 3H), 2.11 (dt, *J* = 14.7, 2.7 Hz, 1H), 1.94 – 1.63 (m, 5H), 1.56 (qt, *J* = 11.5, 3.4 Hz, 1H), 1.49 – 1.27 (m, 3H), 1.24 – 0.98 (m, 2H).

¹³C NMR (126 MHz, Methanol-*d*₄) δ 142.10, 140.30, 128.41, 125.55, 114.47, 46.32, 44.63, 39.34, 39.13, 38.58, 36.05, 32.08, 31.17, 28.65, 25.28, 25.01, 19.89.

¹H NMR (500 MHz, DMSO-*d*₆) δ 7.48 (d, *J* = 8.1 Hz, 2H), 7.12 (d, *J* = 7.8 Hz, 2H), 5.03 (dd, *J* = 5.0, 2.1 Hz, 1H), 3.24 (dd, *J* = 12.8, 3.4 Hz, 1H), 2.67 (t, 1H), 2.29 (s, 3H), 1.99 (dt, *J* = 14.5, 2.6 Hz, 1H), 1.80 – 1.50 (m, 5H), 1.42 – 1.14 (m, 4H), 1.11 – 0.88 (m, 2H).

HRMS (ESI⁺) Calc: [M⁺] (C₁₀H₁₇N₂) 165.1386; measured: 165.1386 = <0.1 ppm difference.

IR (film) $\nu_{\max}/\text{cm}^{-1}$: 2980, 2920, 2851, 2475, 1705, 1586, 1494, 1447, 1347, 1245, 1157, 1113, 1070, 1028, 1000.



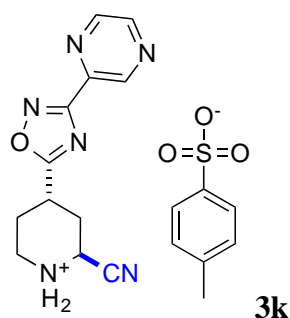
The general procedure was followed using 20 mol% ABNO, which furnished 106 mg of white powder (85%) after purification by Et₂O washes only. A literature search did not reveal any previously documented characterization data.

^1H NMR (500 MHz, Methanol- d_4) δ 7.94 (dd, $J = 8.7, 5.1$ Hz, 1H), 7.73 (d, $J = 8.2$ Hz, 2H), 7.48 (dd, $J = 8.7, 2.2$ Hz, 1H), 7.25 (d, $J = 8.2$ Hz, 2H), 7.23 (dd, $J = 5.1, 2.2$ Hz, 1H), 5.15 (*app t*, $J = 4.9$ Hz, 1H), 3.87 (tt, $J = 9.6, 4.0$ Hz, 1H), 3.66 – 3.49 (m, 2H), 2.68 (dt, $J = 14.8, 4.0$ Hz, 1H), 2.60 (ddd, $J = 14.8, 9.6, 4.4$ Hz, 1H), 2.52 – 2.41 (m, 1H), 2.38 (s, 3H), 2.16 (dtd, $J = 14.2, 9.6, 4.4$ Hz, 1H).

^{13}C NMR (126 MHz, Methanol- d_4) δ 164.63 (d, $J = 250.1$ Hz), 163.98 (d, $J = 13.9$ Hz), 158.66, 142.07, 140.32, 128.42, 125.55, 122.63 (d, $J = 11.2$ Hz), 116.67 (d, $J = 1.4$ Hz), 114.18, 112.71 (d, $J = 25.8$ Hz), 96.83 (d, $J = 27.5$ Hz), 43.61, 41.30, 29.31, 28.28, 26.13, 19.88.

HRMS (ESI $^+$) Calc: $[\text{M}^+]$ ($\text{C}_{13}\text{H}_{13}\text{FN}_3\text{O}$) 246.1037; measured: 246.1034 = 1.2 ppm difference.

IR (film) $\nu_{\text{max}}/\text{cm}^{-1}$: 2965, 2729, 2527, 1617, 1496, 1415, 1231, 1150, 1115, 1029, 1006.



The general procedure was followed using 20 mol% ABNO, which furnished 85 mg of a

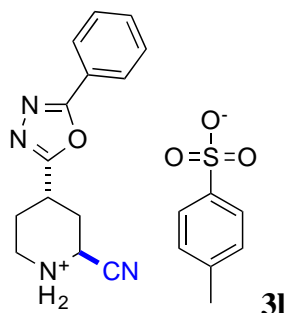
white powder (66%) after purification by Et₂O washes only. A literature search did not reveal any previously documented characterization data.

^1H NMR (500 MHz, Methanol- d_4) δ 9.34 (d, $J = 1.5$ Hz, 1H), 8.88 – 8.75 (m, 2H), 7.71 (d, $J = 8.1$ Hz, 2H), 7.23 (d, $J = 8.1$ Hz, 2H), 5.16 (dd, $J = 5.9, 4.3$ Hz, 1H), 3.85 (tt, $J = 8.8, 4.2$ Hz, 1H), 3.64 – 3.57 (m, 1H), 3.53 (ddd, $J = 13.4, 9.3, 4.0$ Hz, 1H), 2.80 – 2.70 (m, 1H), 2.61 (ddd, $J = 14.9, 9.2, 4.4$ Hz, 1H), 2.54 – 2.44 (m, 1H), 2.36 (s, 3H), 2.24 (dtd, $J = 14.7, 9.1, 4.0$ Hz, 1H).

^{13}C NMR (126 MHz, Methanol- d_4) δ 181.53, 167.65, 148.20, 146.27, 145.30, 143.35, 143.31, 141.80, 129.84, 126.95, 115.31, 44.37, 42.22, 30.50, 29.82, 26.05, 21.30.

HRMS (ESI $^+$) Calc: $[\text{M}^+]$ ($\text{C}_{12}\text{H}_{13}\text{N}_6\text{O}$) 257.1145; measured: 257.1142 = 1.2 ppm difference.

IR (film) $\nu_{\text{max}}/\text{cm}^{-1}$: 2942, 2717, 2498, 1569, 1448, 1362, 1212, 1148, 1119, 1027, 1004.



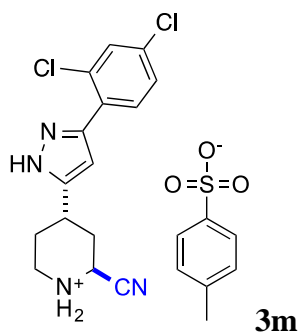
The general procedure was followed using 20 mol% ABNO, which furnished 87 mg of an off-white solid (69%) after purification by Et₂O washes only. A literature search did not reveal any previously documented characterization data.

¹H NMR (500 MHz, Methanol-*d*₄) δ 8.09 – 8.04 (m, 2H), 7.71 (d, *J* = 8.1 Hz, 2H), 7.66 – 7.54 (m, 3H), 7.23 (d, *J* = 8.1 Hz, 2H), 5.10 (dd, *J* = 6.0, 4.4 Hz, 1H), 3.75 (tt, *J* = 8.9, 4.2 Hz, 1H), 3.59 (ddd, *J* = 13.4, 6.2, 4.2 Hz, 1H), 3.52 (ddd, *J* = 13.4, 9.3, 3.7 Hz, 1H), 2.76 – 2.68 (m, 1H), 2.56 (ddd, *J* = 14.8, 9.2, 4.4 Hz, 1H), 2.50 – 2.42 (m, 1H), 2.36 (s, 3H), 2.27 – 2.19 (m, 1H).

¹³C NMR (126 MHz, Methanol-*d*₄) δ 167.72, 166.78, 143.44, 141.75, 133.39, 130.41, 129.83, 127.98, 126.95, 124.67, 115.34, 44.45, 42.31, 29.86, 29.57, 25.98, 21.29.

HRMS (ESI⁺) Calc: [M⁺] (C₁₄H₁₅N₄O) 255.1240; measured: 255.1238 = 0.8 ppm difference.

IR (film) $\nu_{\text{max}}/\text{cm}^{-1}$: 3063, 2637, 2499, 1588, 1571, 1548, 1450, 1254, 1225, 1150, 1115, 1029, 1006.



The general procedure was followed using 20 mol% ABNO, which furnished 81 mg of a light yellow solid (56%) after purification by Et₂O washes and 2x MeCN wash. Note: product could only be purified to 85% purity. A literature search did not reveal any previously documented characterization data.

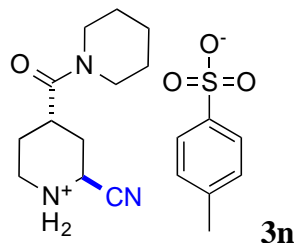
¹H NMR (500 MHz, Methanol-*d*₄) δ 7.71 (d, *J* = 8.0 Hz, 2H), 7.60 (d, *J* = 2.1 Hz, 1H), 7.58 (d, *J* = 8.3 Hz, 1H), 7.42 (dd, *J* = 8.3, 2.1 Hz, 1H), 7.23 (d, *J* = 8.0 Hz, 2H), 6.60 (s, 1H), 5.08 (t, *J* =

4.2 Hz, 1H), 3.57 (dt, $J = 13.3, 4.1$ Hz, 1H), 3.49 – 3.42 (m, 1H), 3.38 (tt, $J = 10.8, 3.8$ Hz, 1H), 2.53 (dtd, $J = 14.7, 3.9, 1.4$ Hz, 1H), 2.36 (s, 3H), 2.36 – 2.22 (m, 2H), 2.08 – 1.97 (m, 1H).

^{13}C NMR (126 MHz, Methanol- d_4) δ 143.45, 141.74, 135.89, 134.14, 132.67, 132.64, 131.11, 131.05, 129.83, 128.63, 128.56, 126.95, 115.64, 104.97, 45.28, 42.94, 32.53, 30.66, 28.85, 21.30.

HRMS (ESI⁺) Calc: [M⁺] (C₁₅H₁₅Cl₂N₄) 321.0668; measured: 321.0664 = 1.2 ppm difference.

IR (film) $\nu_{\text{max}}/\text{cm}^{-1}$: 3219, 3012, 2937, 2504, 2366, 1594, 1478, 1438, 1156, 1035, 1006.



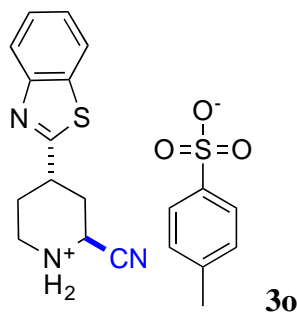
The general procedure was followed using 20 mol% ABNO, which furnished 71 mg of a white powder (61%) after purification by Et₂O washes and 1x MeCN wash. A literature search did not reveal any previously documented characterization data.

^1H NMR (500 MHz, Methanol- d_4) δ 7.71 (d, $J = 8.0$ Hz, 2H), 7.24 (d, $J = 8.0$ Hz, 2H), 5.10 (t, $J = 4.9$ Hz, 1H), 3.64 – 3.49 (m, 4H), 3.48 – 3.38 (m, 2H), 3.28 (dt, $J = 9.0, 4.6$ Hz, 1H), 2.37 (s, 3H), 2.28 (ddd, $J = 14.8, 9.0, 4.6$ Hz, 1H), 2.22 (dt, $J = 15.0, 4.3$ Hz, 1H), 2.09 – 1.99 (m, 1H), 1.89 (dtd, $J = 14.3, 9.4, 4.6$ Hz, 1H), 1.69 (app q, $J = 5.3$ Hz, 2H), 1.67 – 1.59 (m, 2H), 1.58 – 1.51 (m, 2H).

^{13}C NMR (126 MHz, Methanol- d_4) δ 172.21, 143.49, 141.71, 129.82, 126.96, 115.74, 47.86, 44.69, 44.25, 42.44, 33.46, 29.73, 27.79, 26.69, 25.78, 25.41, 21.30.

HRMS (ESI⁺) Calc: [M⁺] (C₁₂H₂₀N₃O) 222.1601; measured: 222.1597 = 1.8 ppm difference.

IR (film) $\nu_{\text{max}}/\text{cm}^{-1}$: 2931, 2856, 2660, 2522, 2043, 1622, 1438, 1231, 1150, 1121, 1029, 1006.



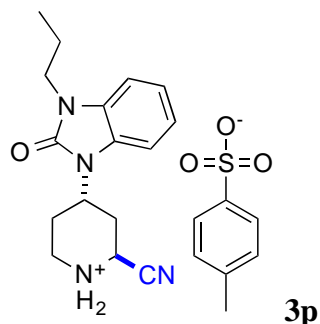
The general procedure was followed using 20 mol% ABNO, followed by the addition of 10 mol% ABNO and 0.5 equiv. TMSCN and the reaction run again. This furnished 67 mg of a pale pink solid (56%) after purification by Et₂O washes and 2x MeCN wash. A literature search did not reveal any previously documented characterization data.

¹H NMR (500 MHz, Acetonitrile-*d*₃) δ 7.99 (d, *J* = 8.1 Hz, 1H), 7.97 (d, *J* = 8.1 Hz, 1H), 7.69 (d, *J* = 8.2 Hz, 2H), 7.53 (ddd, *J* = 8.1, 7.2, 1.2 Hz, 1H), 7.44 (ddd, *J* = 8.1, 7.2, 1.2 Hz, 1H), 7.18 (d, *J* = 8.2 Hz, 2H), 5.06 (app t, *J* = 4.4 Hz, 1H), 3.72 – 3.64 (m, 1H), 3.60 (dt, *J* = 13.4, 4.3 Hz, 1H), 3.43 – 3.35 (m, 1H), 2.67 – 2.58 (m, 2H), 2.39 (dq, *J* = 14.5, 3.7 Hz, 1H), 2.32 (s, 3H), 2.17 (dtd, *J* = 14.5, 10.8, 4.1 Hz, 1H).

¹³C NMR (126 MHz, Acetonitrile-*d*₃) δ 172.72, 153.77, 143.77, 141.30, 135.74, 129.80, 127.33, 126.74, 126.36, 123.67, 123.05, 115.50, 45.05, 42.62, 36.02, 31.50, 28.63, 21.31.

HRMS (ESI⁺) Calc: [M⁺] (C₁₃H₁₄N₃S) 244.0903; measured: 244.0900 = 1.2 ppm difference.

IR (film) ν_{max}/cm⁻¹: 2977, 2729, 2504, 2032, 1594, 1507, 1432, 1219, 1150, 1121, 1029, 1006.



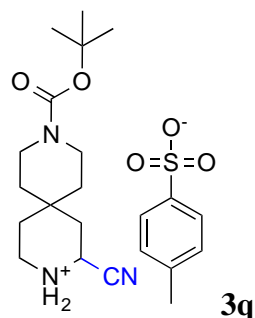
The general procedure was followed using 20 mol% ABNO, which furnished 78 mg of a pale yellow powder (59%) after purification by Et₂O washes and recrystallization with MeCN/Et₂O. A literature search did not reveal any previously documented characterization data.

¹H NMR (500 MHz, Methanol-*d*₄) δ 7.73 (d, *J* = 8.1 Hz, 2H), 7.32 – 7.27 (m, 1H), 7.23 (d, *J* = 8.1 Hz, 2H), 7.12 – 7.03 (m, 3H), 4.75 (dd, *J* = 11.0, 4.8 Hz, 1H), 4.61 (tt, *J* = 12.2, 4.2 Hz, 1H), 3.89 (ddt, *J* = 12.4, 4.9, 2.8 Hz, 1H), 3.80 (ddt, *J* = 12.4, 4.8, 2.6 Hz, 1H), 3.53 – 3.45 (m, 2H), 3.41 (td, *J* = 12.7, 3.0 Hz, 1H), 2.97 – 2.80 (m, 2H), 2.36 (s, 3H), 2.21 – 2.09 (m, 3H), 1.21 (t, *J* = 7.4 Hz, 3H).

¹³C NMR (126 MHz, Methanol-*d*₄) δ 156.12, 143.43, 141.82, 130.35, 129.88, 129.66, 126.97, 122.88, 122.49, 114.55, 110.63, 109.78, 66.89, 59.60, 53.63, 51.03, 27.50, 27.31, 23.14, 21.30, 10.34.

HRMS (ESI⁺) Calc: [M⁺] (C₁₆H₂₁N₄O) 285.1709; measured: 285.1704 = 1.8 ppm difference.

IR (film) $\nu_{\max}/\text{cm}^{-1}$: 3167, 2942, 2660, 2360, 1692, 1484, 1386, 1207, 1156, 1115, 1029, 1006.



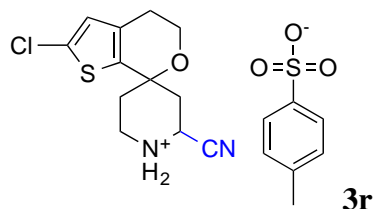
The general procedure was followed using 10 mol% ABNO, which furnished 77 mg of a white powder (58%) after purification by Et₂O washes and 1x MeCN washes. A literature search did not reveal any previously documented characterization data.

¹H NMR (500 MHz, Methanol-*d*₄) δ 7.71 (d, *J* = 8.1 Hz, 2H), 7.24 (d, *J* = 8.1 Hz, 2H), 4.67 (dd, *J* = 12.2, 3.4 Hz, 1H), 3.55 – 3.36 (m, 6H), 3.24 (td, *J* = 13.2, 3.1 Hz, 1H), 2.38 (s, 3H), 2.31 (dd, *J* = 14.3, 2.6 Hz, 1H), 1.93 (dd, *J* = 14.9, 2.6 Hz, 1H), 1.85 (dd, *J* = 14.5, 12.2 Hz, 1H), 1.64 – 1.53 (m, 3H), 1.52 – 1.46 (m, 4H), 1.45 (s, 9H).

¹³C NMR (126 MHz, Methanol-*d*₄) δ 154.24, 141.33, 139.63, 127.71, 127.70, 124.82, 114.37, 79.07, 40.41, 39.08, 36.95, 34.61, 29.64, 29.05, 26.50, 19.17.

HRMS (ESI⁺) Calc: [M⁺] (C₁₅H₂₆N₃O₂) 280.2020; measured: 280.2017 = 1.1 ppm difference.

IR (film) $\nu_{\max}/\text{cm}^{-1}$: 2981, 2940, 2857, 2720, 2110, 1693, 1448, 1408, 1366, 1233, 1149, 1116, 1030, 1003.



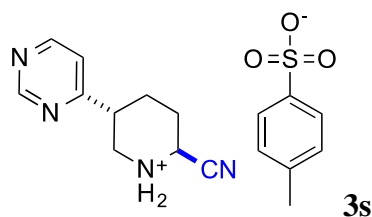
The general procedure was followed using 20 mol% ABNO, which furnished 97 mg of a pale yellow fine powder (74%) after purification by Et₂O washes and 1x MeCN wash. A literature search did not reveal any previously documented characterization data.

¹H NMR (500 MHz, Methanol-*d*₄) δ 7.72 (d, *J* = 8.1 Hz, 2H), 7.24 (d, *J* = 8.1 Hz, 2H), 6.77 (s, 1H), 5.00 (d, *J* = 5.5 Hz, 1H), 4.08 – 3.93 (m, 2H), 3.66 (td, *J* = 13.2, 3.1 Hz, 1H), 3.47 – 3.40 (m, 1H), 2.78 – 2.69 (m, 2H), 2.64 (dt, *J* = 16.3, 4.3 Hz, 1H), 2.37 (s, 3H), 2.27 – 2.22 (m, 1H), 2.20 (dd, *J* = 15.5, 5.8 Hz, 1H), 2.08 (ddd, *J* = 14.8, 13.2, 4.4 Hz, 1H).

^{13}C NMR (126 MHz, Methanol- d_4) δ 143.46, 141.76, 137.75, 136.12, 130.18, 129.85, 127.83, 126.97, 115.82, 70.87, 60.78, 42.44, 39.36, 36.14, 35.80, 26.74, 21.31.

HRMS (ESI⁺) Calc: [M⁺] (C₁₂H₁₄ClN₂OS) 269.0510; measured: 269.0505 = 1.9 ppm difference.

IR (film) $\nu_{\text{max}}/\text{cm}^{-1}$: 2969, 2722, 2641, 2485, 1615, 1449, 1239, 1146, 1120, 1072, 1004.



The general procedure was followed using 20 mol% ABNO, which furnished 58 mg of a white powder (55%) after purification by Et₂O washes and 2x MeCN washes. A literature search did not reveal any previously documented characterization data.

^1H NMR (500 MHz, Methanol- d_4) δ 9.16 (d, J = 1.4 Hz, 1H), 8.76 (d, J = 5.3 Hz, 1H), 7.71 (d, J = 8.2 Hz, 2H), 7.54 (dd, J = 5.3, 1.4 Hz, 1H), 7.24 (d, J = 8.2 Hz, 2H), 4.95 (t, J = 4.4 Hz, 1H), 3.67 (d, J = 6.9 Hz, 2H), 3.36 – 3.32 (m, 1H), 2.37 (s, 3H), 2.31 – 2.16 (m, 3H), 2.13 – 2.01 (m, 1H).

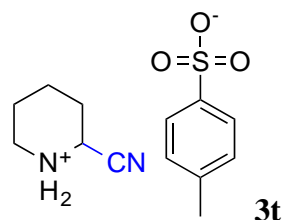
^{13}C NMR (126 MHz, Methanol- d_4) δ 169.85, 159.29, 158.66, 143.47, 141.75, 129.84, 126.95, 121.68, 115.57, 45.79, 45.40, 39.87, 26.46, 26.18, 21.30.

^1H NMR (500 MHz, DMSO- d_6) δ 9.18 (d, J = 1.4 Hz, 1H), 8.79 (d, J = 5.2 Hz, 1H), 7.57 (dd, J = 5.2, 1.4 Hz, 1H), 7.48 (d, J = 8.0 Hz, 2H), 7.11 (d, J = 8.0 Hz, 2H), 5.02 (d, J = 4.1 Hz, 1H), 3.60 (dd, J = 12.8, 3.8 Hz, 1H), 3.27 (dd, J = 12.8, 11.3 Hz, 1H), 3.17 (tt, J = 11.3, 3.8 Hz, 1H), 2.29 (s, 3H), 2.21 – 2.14 (m, 1H), 2.14 – 2.02 (m, 2H), 1.86 – 1.74 (m, 1H).

^{13}C NMR (126 MHz, DMSO- d_6) δ 167.97, 158.33, 157.68, 145.69, 137.62, 128.06, 125.49, 120.31, 115.95, 109.53, 44.01, 43.66, 25.12, 24.98, 20.80.

HRMS (ESI⁺) Calc: [M⁺] (C₁₀H₁₃N₄) 189.1135; measured: 189.1133 = 1.1 ppm difference.

IR (film) $\nu_{\text{max}}/\text{cm}^{-1}$: 2971, 2729, 1576, 1455, 1398, 1207, 1121, 1035, 1012.



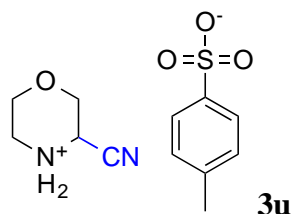
The general procedure was followed using 10 mol% ABNO, which furnished 66 mg of an off-white powder (80%) after purification by Et₂O washes and 1x MeCN washes. A literature search did not reveal any previously documented characterization data of this salt.

¹H NMR (500 MHz, Methanol-*d*₄) δ 7.71 (d, *J* = 8.1 Hz, 2H), 7.24 (d, *J* = 8.1 Hz, 2H), 4.64 (dd, *J* = 8.7, 3.9 Hz, 1H), 3.40 (ddd, *J* = 13.2, 5.9, 3.3 Hz, 1H), 3.20 (ddd, *J* = 12.9, 8.8, 3.8 Hz, 1H), 2.37 (s, 3H), 2.20 (ddd, *J* = 14.8, 7.2, 3.7 Hz, 1H), 2.04 (dtd, *J* = 14.8, 8.9, 3.6 Hz, 1H), 1.94 – 1.66 (m, 4H).

¹³C NMR (126 MHz, Methanol-*d*₄) δ 141.34, 139.57, 127.68, 124.80, 113.93, 43.78, 42.83, 25.72, 20.55, 19.16, 19.09.

HRMS (ESI⁺) Calc: [*M*⁺] (C₆H₁₁N₂) 111.0917; measured: 111.0917 = <0.1 ppm difference.

IR (film) $\nu_{\max}/\text{cm}^{-1}$: 2980, 2766, 2727, 2642, 2550, 2489, 2444, 1677, 1606, 1494, 1454, 1359, 1285, 1222, 1144, 1115, 1029, 1004.



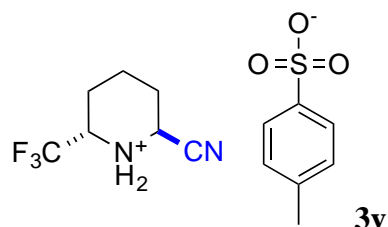
The general procedure was followed using 10 mol% ABNO, which furnished 65 mg of a light orange powder (78%) after purification by Et₂O washes and 2x MeCN washes. A literature search did not reveal any previously documented characterization data of this salt.

¹H NMR (500 MHz, Methanol-*d*₄) δ 7.71 (d, *J* = 8.1 Hz, 2H), 7.24 (d, *J* = 8.1 Hz, 2H), 4.78 (t, *J* = 4.2 Hz, 1H), 4.08 (m, 2H), 3.96 (ddd, *J* = 13.1, 5.6, 3.5 Hz, 1H), 3.89 (ddd, *J* = 13.1, 7.6, 3.2 Hz, 1H), 3.45 (ddd, *J* = 13.3, 7.5, 3.5 Hz, 1H), 3.36 – 3.32 (m, 1H), 2.37 (s, 3H).

¹³C NMR (126 MHz, Methanol-*d*₄) δ 141.27, 139.65, 127.71, 124.80, 112.41, 64.63, 62.87, 42.87, 41.00, 19.16.

HRMS (ESI⁺) Calc: [*M*⁺] (C₅H₉N₂O) 113.0709; measured: 113.0709 = <0.1 ppm difference.

IR (film) $\nu_{\max}/\text{cm}^{-1}$: 2973, 2725, 2669, 2506, 1909, 1694, 1608, 1490, 1450, 1220, 1166, 1109, 1031, 1002.



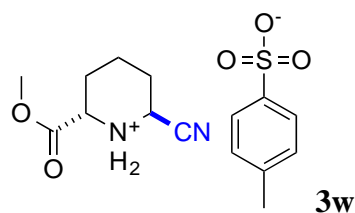
The general procedure was followed using 20 mol% ABNO, which furnished 56 mg of a white powder (54%) after purification by Et₂O washes and 1x MeCN wash. A literature search did not reveal any previously documented characterization data.

¹H NMR (500 MHz, Methanol-*d*₄) δ 7.71 (d, *J* = 8.2 Hz, 2H), 7.24 (d, *J* = 8.2 Hz, 2H), 4.65 – 4.54 (m, 1H), 3.88 – 3.71 (m, 1H), 2.37 (s, 3H), 2.08 – 1.93 (m, 3H), 1.91 – 1.72 (m, 2H), 1.64 – 1.47 (m, 1H).

¹³C NMR (126 MHz, Methanol-*d*₄) δ 143.36, 141.79, 129.82, 126.97, 126.11 (q, *J* = 279.0 Hz), 118.29, 55.52 (q, *J* = 30.5 Hz), 46.63, 27.76, 24.13 (q, *J* = 2.3 Hz), 21.30, 19.83.

HRMS (ESI⁺) Calc: [*M*⁺] (C₇H₁₀F₃N₂) 179.0791; measured: 179.0789 = 1.1 ppm difference.

IR (film) ν_{max}/cm⁻¹: 2977, 2511, 2034, 1615, 1448, 1402, 1264, 1218, 1126, 1138, 1034, 1011.



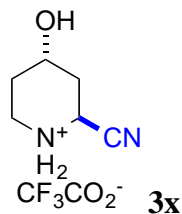
The general procedure was followed using 10 mol% ABNO, which furnished 34 mg of a white powder (36%) after purification by Et₂O washes. A literature search did not reveal any previously documented characterization data.

¹H NMR (500 MHz, Methanol-*d*₄) δ 7.71 (d, *J* = 8.1 Hz, 2H), 7.24 (d, *J* = 8.1 Hz, 2H), 4.98 (t, *J* = 4.3 Hz, 1H), 4.33 (dd, *J* = 10.5, 3.8 Hz, 1H), 3.87 (s, 3H), 2.37 (s, 3H), 2.30 (dq, *J* = 14.8, 4.3 Hz, 1H), 2.14 (dq, *J* = 14.1, 4.2, 1.3 Hz, 1H), 2.02 (ddt, *J* = 14.6, 9.6, 4.8 Hz, 1H), 1.91 (m, 2H), 1.82 (dtd, *J* = 14.7, 9.4, 8.8, 6.1 Hz, 1H).

¹³C NMR (126 MHz, Methanol-*d*₄) δ 167.60, 141.38, 139.52, 127.65, 124.81, 113.46, 53.93, 51.87, 43.23, 24.66, 24.18, 19.15, 17.71.

HRMS (ESI⁺) Calc: [*M*⁺] (C₈H₁₃N₂O₂) 169.0972; measured: 169.0971 = 0.6 ppm difference.

IR (film) $\nu_{\text{max}}/\text{cm}^{-1}$: 2956, 2818, 2768, 2960, 2575, 2511, 2420, 1747, 1598, 1484, 1444, 1360, 1310, 1253, 1219, 1149, 1120, 1035, 1006.



The general procedure was followed using 10 mol% ABNO, which furnished 37 mg of an orange powder (53%) after purification by Et₂O washes. A literature search did not reveal any previously documented characterization data.

¹H NMR (500 MHz, Methanol-*d*₄) δ 4.77 (dd, $J = 10.0, 4.1$ Hz, 1H), 4.15 (tt, $J = 5.4, 2.9$ Hz, 1H), 3.42 (ddd, $J = 12.9, 10.9, 3.6$ Hz, 1H), 3.36 – 3.28 (m, 1H), 2.28 – 2.12 (m, 2H), 2.00 – 1.88 (m, 2H), 1.88 – 1.76 (m, 1H).

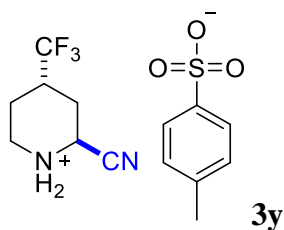
¹⁹F NMR (376 MHz, Methanol-*d*₄) δ -77.77.

¹³C NMR (126 MHz, Methanol-*d*₄) δ 160.80, 160.52, 117.08, 114.76, 114.45, 114.05, 59.51, 40.47, 38.84, 32.88, 29.25, 27.98.

¹H NMR (500 MHz, DMSO-*d*₆) δ 4.57 (dd, $J = 9.1, 3.9$ Hz, 1H), 3.74 (tt, $J = 9.1, 3.0$ Hz, 1H), 3.02 (ddd, $J = 13.1, 9.4, 3.6$ Hz, 1H), 2.99 – 2.91 (m, 1H), 1.97 – 1.85 (m, 1H), 1.83 – 1.70 (m, 1H), 1.66 – 1.52 (m, 1H), 1.45 – 1.27 (m, 1H).

HRMS (ESI⁺) Calc: 127.0866; measured: 127.0865 = 0.8 ppm difference.

IR (film) $\nu_{\text{max}}/\text{cm}^{-1}$: 3493, 2949, 2695, 2486, 1816, 1661, 1477, 1429, 1276, 1177, 1127, 1056.



The general procedure was followed using 10 mol% ABNO, which furnished 57 mg of a white powder (59%) after purification by Et₂O washes and 1x MeCN wash. A literature search did not reveal any previously documented characterization data.

¹H NMR (500 MHz, Methanol-*d*₄) δ 7.69 (d, $J = 8.1$ Hz, 2H), 7.22 (d, $J = 8.1$ Hz, 2H), 5.10 (dd, $J = 4.9, 2.8$ Hz, 1H), 3.58 (dt, $J = 13.6, 3.7$ Hz, 1H), 3.41 – 3.31 (m, 1H), 2.85 (m, 1H), 2.44 (dq,

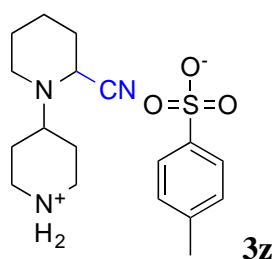
$J = 14.8, 2.9$ Hz, 1H), 2.35 (s, 3H), 2.20 (dp, $J = 14.4, 3.1$ Hz, 1H), 2.05 (ddd, $J = 14.7, 12.5, 4.9$ Hz, 1H), 1.77 (dtd, $J = 14.2, 12.4, 4.4$ Hz, 1H).

^{19}F NMR (376 MHz, Methanol- d_4) δ -75.95.

^{13}C NMR (126 MHz, Methanol- d_4) δ 142.07, 140.31, 128.41, 125.54, 113.60, 43.24, 40.34, 35.19, 34.95, 24.77, 20.89, 19.89.

HRMS (ESI⁺) Calc: 179.0791; measured: 179.0788 = 1.7 ppm difference.

IR (film) $\nu_{\text{max}}/\text{cm}^{-1}$: 3092, 2978, 2628, 2499, 1590, 1495, 1461, 1406, 1362, 1336, 1260, 1223, 1149, 1111, 1064, 1031, 1002.



The general procedure was followed using 10 mol% ABNO, which furnished 29 mg of a

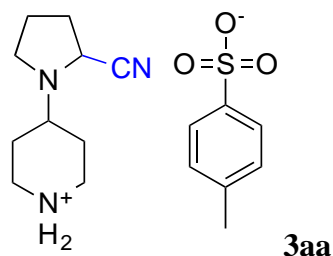
white powder (26%) after purification by Et₂O washes and 1x MeCN washes. A literature search did not reveal any previously documented characterization data.

^1H NMR (500 MHz, Methanol- d_4) δ 7.71 (d, $J = 8.1$ Hz, 2H), 7.24 (d, $J = 8.1$ Hz, 2H), 4.22 (d, $J = 4.0$ Hz, 1H), 3.40 (m, 2H), 3.22 – 2.85 (m, 3H), 2.69 (tt, $J = 10.3, 3.6$ Hz, 1H), 2.46 – 2.37 (m, 4H), 2.22 (dd, $J = 14.7, 4.1$ Hz, 1H), 2.07 (dt, $J = 14.4, 3.2$ Hz, 1H), 1.95 – 1.86 (m, 1H), 1.86 – 1.67 (m, 5H), 1.60 – 1.47 (m, 2H)

^{13}C NMR (126 MHz, Methanol- d_4) δ 141.40, 139.54, 127.67, 124.80, 116.69, 56.22, 48.99, 44.20, 41.91, 41.83, 28.40, 25.24, 25.01, 24.33, 19.66, 19.15.

HRMS (ESI⁺) Calc: [M⁺] (C₁₁H₂₀N₃) 194.1652; measured: 194.1652 = <0.1 ppm difference.

IR (film) $\nu_{\text{max}}/\text{cm}^{-1}$: 2946, 2830, 2745, 2538, 1918, 1625, 1449, 1388, 1330, 1213, 1160, 1117, 1031.



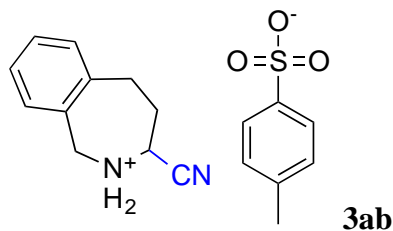
The general procedure was followed using 10 mol% ABNO, which furnished 75 mg of a white powder (71%) after purification by Et₂O washes and 1x MeCN washes. A literature search did not reveal any previously documented characterization data.

¹H NMR (500 MHz, Methanol-*d*₄) δ 7.71 (d, *J* = 8.1 Hz, 2H), 7.25 (d, *J* = 8.1 Hz, 2H), 4.13 (dd, *J* = 7.6, 2.0 Hz, 1H), 3.41 – 3.32 (m, 2H), 3.13 – 3.01 (m, 3H), 2.71 (tt, *J* = 8.4, 3.5 Hz, 1H), 2.53 (dt, *J* = 8.8, 6.9 Hz, 1H), 2.37 (s, 3H), 2.27 – 2.04 (m, 4H), 2.01 – 1.87 (m, 2H), 1.87 – 1.72 (m, 2H).

¹³C NMR (126 MHz, Methanol-*d*₄) δ 141.37, 139.59, 127.70, 124.80, 117.07, 53.70, 50.12, 47.67, 40.66, 40.62, 28.60, 26.79, 26.40, 20.82, 19.16.

HRMS (ESI⁺) Calc: [M⁺] (C₁₀H₁₈N₃) 180.1495; measured: 180.1495 = <0.1 ppm difference.

IR (film) $\nu_{\max}/\text{cm}^{-1}$: 2962, 2822, 2538, 2219, 2161, 1975, 1687, 1628, 1450, 1387, 1323, 1280, 1214, 1162, 1118, 1031, 1004.



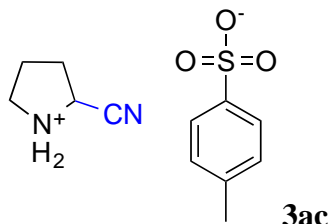
The general procedure was followed using 20 mol% ABNO, which furnished 78 mg of an off-white powder (76%) after purification by Et₂O washes with extended sonication and stirring, followed by recrystallization with MeCN/Et₂O. A literature search did not reveal any previously documented characterization data.

¹H NMR (500 MHz, Methanol-*d*₄) δ 7.70 (d, *J* = 8.2 Hz, 2H), 7.43 – 7.35 (m, 2H), 7.34 – 7.28 (m, 2H), 7.23 (d, *J* = 8.2 Hz, 2H), 4.99 (dd, *J* = 9.2, 3.4 Hz, 1H), 4.53 (d, *J* = 14.6 Hz, 1H), 4.47 (d, *J* = 14.6 Hz, 1H), 3.23 – 3.07 (m, 2H), 2.48 – 2.40 (m, 1H), 2.37 (s, 3H), 2.28 – 2.15 (m, 1H).

¹³C NMR (126 MHz, Methanol-*d*₄) δ 143.51, 142.98, 141.69, 132.60, 131.90, 131.35, 130.86, 129.81, 128.67, 126.96, 116.12, 51.30, 51.03, 32.33, 30.68, 21.30.

HRMS (ESI⁺) Calc: [M⁺] (C₁₁H₁₃N₂) 173.1073; measured: 173.1072 = 0.6 ppm difference.

IR (film) $\nu_{\max}/\text{cm}^{-1}$: 2937, 2614, 2516, 2360, 2026, 1605, 1496, 1467, 1225, 1138, 1115, 1029, 1006.

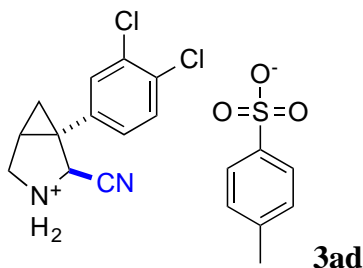


The general procedure was followed using 10 mol% ABNO, which furnished 61 mg of a yellow solid (75%) after purification by Et₂O washes. A literature search did not reveal any previously documented characterization data of this salt.

¹H NMR (500 MHz, Methanol-*d*₄) δ 7.73 (d, *J* = 8.1 Hz, 2H), 7.27 (d, *J* = 8.1 Hz, 2H), 4.73 (t, *J* = 7.5 Hz, 1H), 3.52 – 3.37 (m, 2H), 2.50 (dtd, *J* = 13.4, 7.8, 5.9 Hz, 1H), 2.39 (s, 3H), 2.29 (dq, *J* = 13.2, 7.4 Hz, 1H), 2.26 – 2.06 (m, 2H).

¹³C NMR (126 MHz, Methanol-*d*₄) δ 141.27, 139.73, 127.77, 124.82, 114.28, 45.94, 45.15, 29.06, 22.39, 19.20.

HRMS (ESI⁺) Calc: [*M*⁺] (C₅H₉N₂) 97.0760; measured: 97.0760 = <0.1 ppm difference.



The general procedure was followed using 10 mol% ABNO, which furnished 61 mg of a white powder (48%) after purification by Et₂O washes and 1x MeCN washes. A literature search did not reveal any previously documented characterization data.

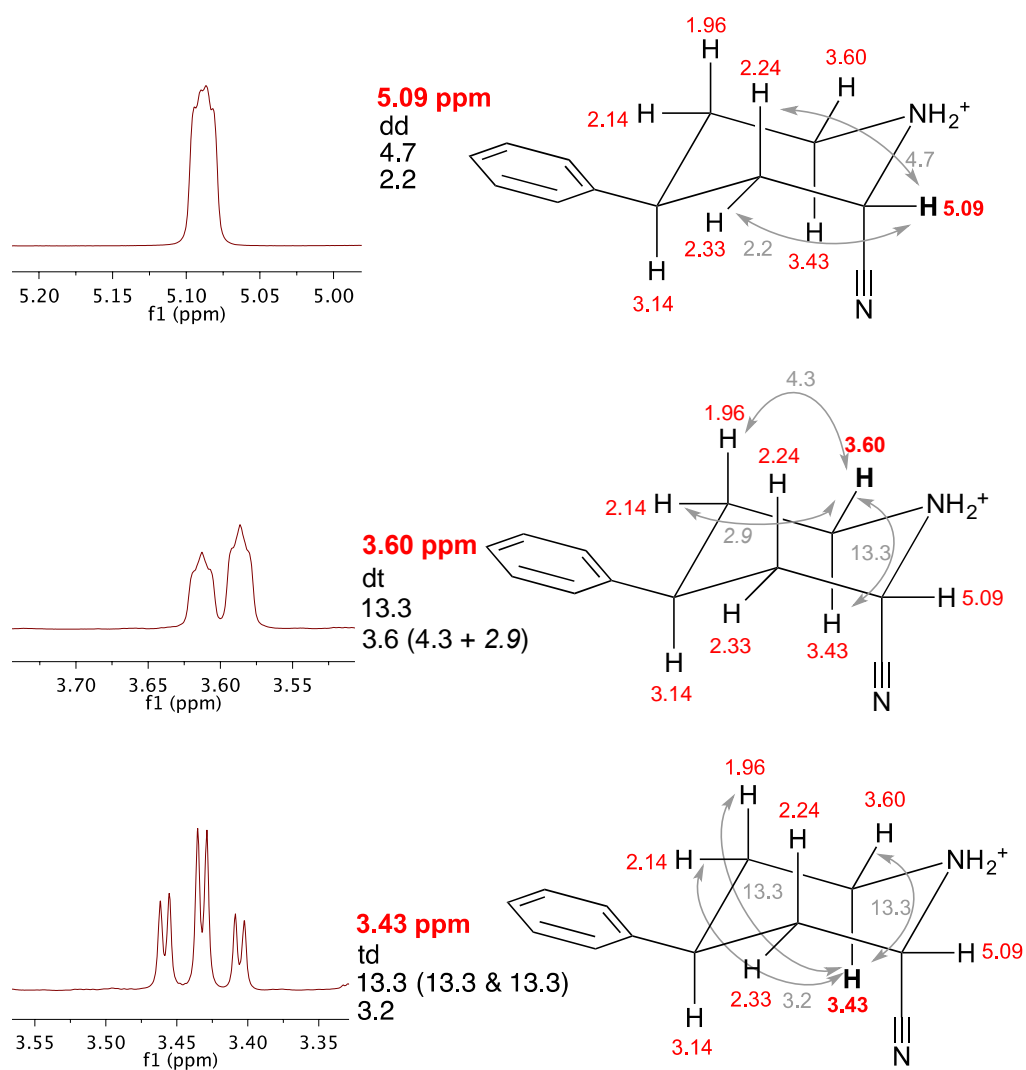
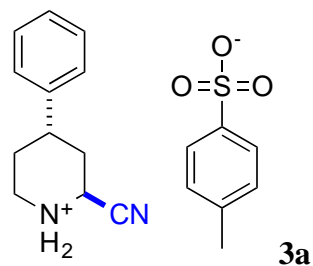
¹H NMR (500 MHz, Methanol-*d*₄) δ 7.71 (d, *J* = 7.9 Hz, 2H), 7.60 – 7.52 (m, 2H), 7.30 (dd, *J* = 8.4, 2.2 Hz, 1H), 7.24 (d, *J* = 7.9 Hz, 2H), 5.00 (s, 1H), 3.93 (d, *J* = 11.8 Hz, 1H), 3.76 (dd, *J* = 11.7, 1.6 Hz, 1H), 2.60 (dd, *J* = 8.8, 4.5 Hz, 1H), 2.37 (s, 3H), 1.45 (ddd, *J* = 8.8, 7.2, 1.6 Hz, 1H), 1.25 (dd, *J* = 7.4, 4.5 Hz, 1H).

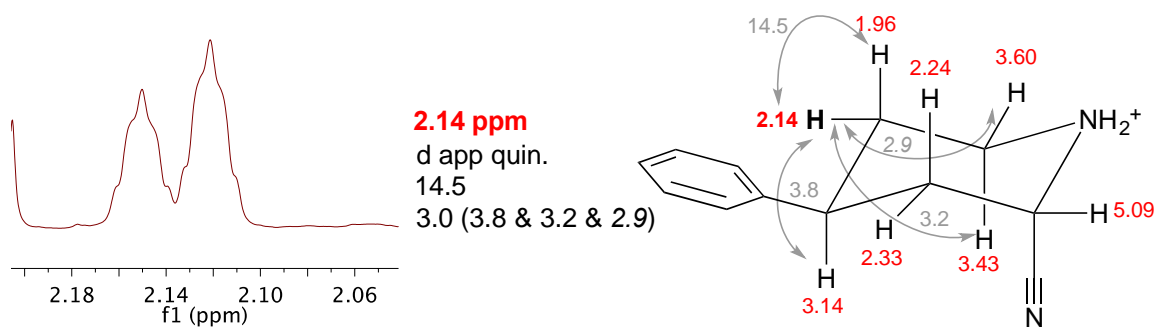
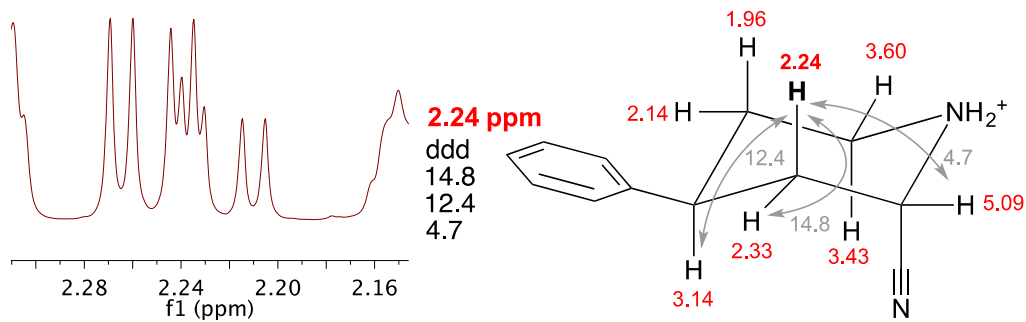
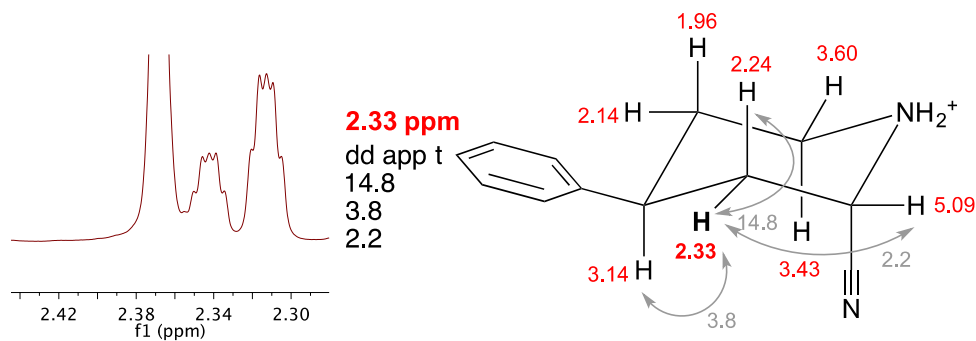
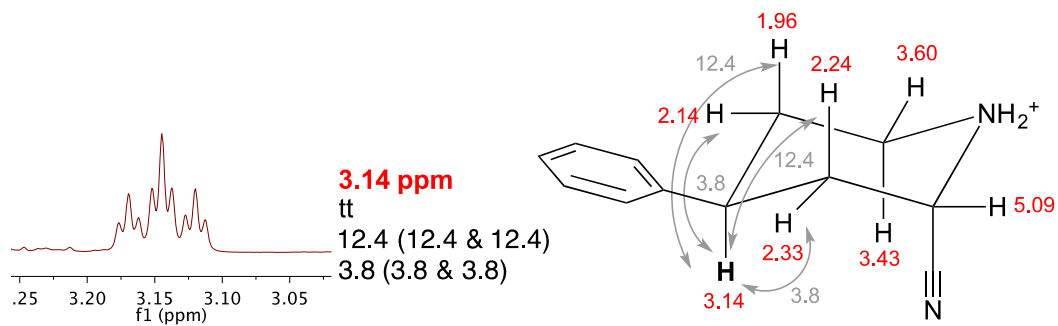
¹³C NMR (126 MHz, Methanol-*d*₄) δ 141.31, 139.58, 136.70, 130.56, 129.97, 129.88, 128.77, 127.68, 126.46, 124.81, 113.93, 49.37, 48.55, 29.97, 26.33, 19.16, 12.96.

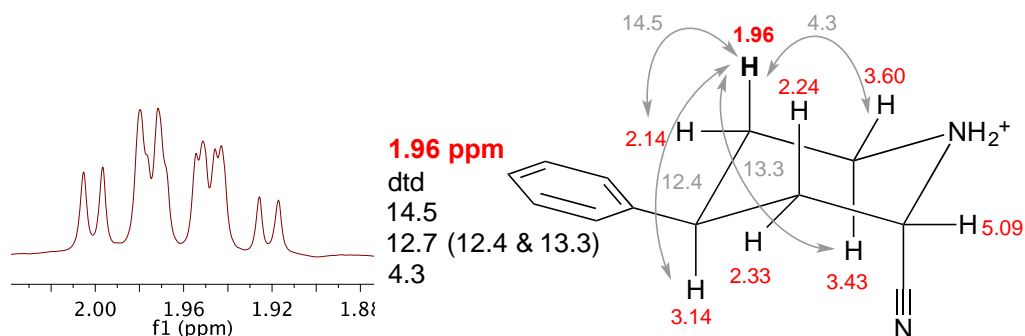
HRMS (ESI⁺) Calc: [*M*⁺] (C₁₂H₁₁N₂Cl₂) 253.0294; measured: 253.0293 = 0.4 ppm difference.

IR (film) $\nu_{\text{max}}/\text{cm}^{-1}$: 2968, 2723, 2667, 2621, 2585, 2532, 2464, 2164, 1937, 1937, 1620, 1555, 1448, 1381, 1226, 1203, 1141, 1032, 1007.

C.3.6. Coupling constant assignments



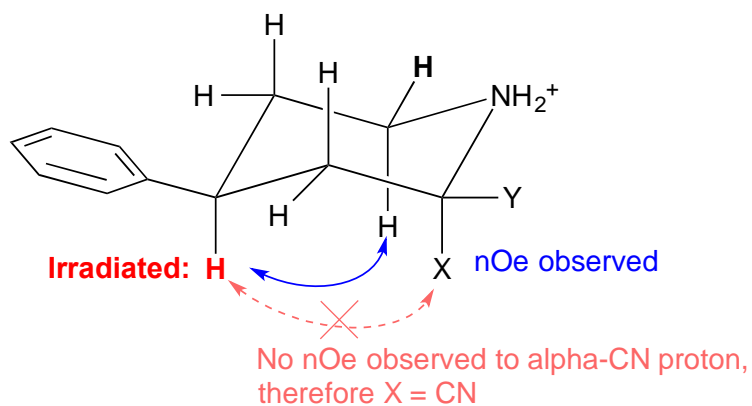




Signals at 2.33 and 2.14 are those of the equatorial protons alpha to the phenyl ring and show apparent splitting patterns that may possibly be due to the proximity of the phenyl ring or longer range couplings that complicates their splitting pattern.

C.3.7. Determination of Stereochemistry

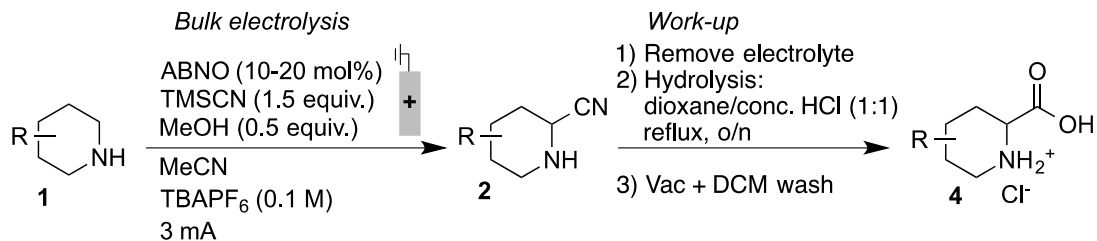
Nuclear Overhauser effect experiments were conducted to establish the relative stereochemistry of the nitrile and substituent of the piperidine ring. Selective irradiation of the benzylic proton, which appears as a tt, revealed an nOe cross peak to the axial proton alpha to nitrogen. However, there was no cross-peak observed to the alpha cyano peak, thereby confirming the nitrile moiety to sit in the axial position, and thus assume an anti-configuration to the substituent in the 4-position.



The coupling constants in the alpha-cyano proton provide additional evidence for it to be in an equatorial position. The couplings to the neighbouring protons are in the range expected of

equatorial-equatorial (~2–6 Hz) and equatorial-axial (~2–6 Hz) couplings and are not in the range expected for a large axial-axial coupling (~10–14 Hz), according to the Karplus relation.³

C.4. Cyanation and Hydrolysis of Secondary Amines



C.4.1. Bulk Electrolysis:

Same procedure as detailed above.

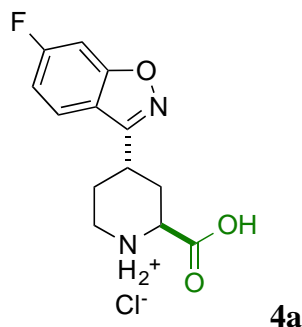
C.4.2. Work-Up

Removal of electrolyte salt: The solution was transferred to a round-bottom flask and concentrated under reduced pressure. Diethyl ether (ca. 5 x 4 mL) was used to extract the product from the solid mixture via trituration: a portion of solvent was added to the flask, stirred until the electrolyte crystallized out and then filtered through a glass pipette filled with cotton wool into a pre-weighed round-bottom flask and stir bar, and repeated with further portions of Et₂O. To generate high product purity, it is important at this stage to make sure that all the NBu₄PF₆ salt has been separated from the solution. This can be confirmed by observing the formation of white crystals after cooling the vial down to -20 °C in the freezer. If observed, the solution should be filtered an additional time. The separated NBu₄PF₆ can be reused in subsequent reactions after drying under vacuum overnight.

Hydrolysis: With the electrolyte salt (TBAPF₆) removed, the solution was concentrated under reduced pressure. To the residue was added dioxane (2 mL) and conc. HCl (2 mL) with stirring. A condenser was fitted onto the round-bottom flask and heated to 95 °C for 12 hours. The solution was allowed to cool and toluene (5 mL) was added, before being concentrated to dryness

under reduced pressure. Further portions of toluene were added and then concentrated if necessary. The solid mixture was washed with DCM (5 x 5 mL) and then dried under high vacuum for 4-5 hours.

C.4.3. Characterization Data



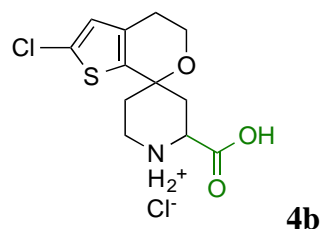
The general hydrolysis procedure was followed using 20 mol% ABNO, which furnished 67 mg of a white crystalline solid (76%) after purification by DCM washes. A literature search did not reveal any previously documented characterization data.

¹H NMR (500 MHz, Methanol-*d*₄) δ 7.90 (dd, *J* = 8.8, 5.1 Hz, 1H), 7.46 (dd, *J* = 8.7, 2.1 Hz, 1H), 7.23 (td, *J* = 9.0, 2.1 Hz, 1H), 4.46 (dd, *J* = 9.4, 4.1 Hz, 1H), 3.82 (app p, *J* = 5.1 Hz, 1H), 3.53 – 3.44 (m, 1H), 3.41 (ddd, *J* = 13.2, 9.4, 3.9 Hz, 1H), 2.64 (dt, *J* = 14.6, 4.8 Hz, 1H), 2.49 (ddd, *J* = 14.4, 9.4, 4.4 Hz, 1H), 2.34 (ddt, *J* = 14.1, 9.4, 4.5 Hz, 1H), 2.27 (dq, *J* = 14.7, 4.9 Hz, 1H).

¹³C NMR (126 MHz, Methanol-*d*₄) δ 170.60, 166.13 (d, *J* = 225.5 Hz), 165.08 (d, *J* = 10.5 Hz), 160.47, 124.04 (d, *J* = 11.3 Hz), 118.40, 114.05 (d, *J* = 25.8 Hz), 98.19 (d, *J* = 27.5 Hz), 54.89, 41.87, 29.82, 29.74, 26.47.

HRMS (ESI⁺) Calc: [*M*⁺] (C₁₃H₁₄FN₂O₃) 265.0983; measured: 265.0979 = 1.5 ppm difference.

IR (film) ν_{max} /cm⁻¹: 3329, 2919, 2758, 2493, 1732, 1611, 1490, 1415, 1357, 1259, 1110.



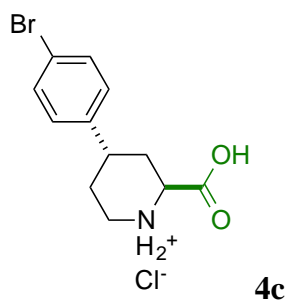
The general hydrolysis procedure was followed using 20 mol% ABNO, which furnished 72 mg of a dark green solid (82%) after purification by DCM washes. A literature search did not reveal any previously documented characterization data.

$^1\text{H NMR}$ (600 MHz, Methanol- d_4) δ 6.77 (s, 1H), 4.28 (dd, $J = 12.9, 3.2$ Hz, 1H), 4.06 – 3.95 (m, 2H), 3.47 – 3.34 (m, 2H), 2.68 (app q, $J = 5.6$ Hz, 2H), 2.62 (dt, $J = 14.5, 2.9$ Hz, 1H), 2.26 (d app q, $J = 14.9, 2.6$ Hz, 1H), 2.08 – 1.96 (m, 2H).

$^{13}\text{C NMR}$ (151 MHz, Methanol- d_4) δ 170.87, 138.42, 135.72, 129.92, 127.72, 72.05, 60.97, 54.30, 40.96, 38.77, 34.95, 26.87.

HRMS (ESI $^+$) Calc: [M^+] ($\text{C}_{12}\text{H}_{15}\text{ClNO}_3\text{S}$) 288.0456; measured: 288.0451 = 1.7 ppm difference.

IR (film) $\nu_{\text{max}}/\text{cm}^{-1}$: 3115, 3029, 2937, 2810, 2337, 1744, 1403, 1259, 1207, 1184, 1075.



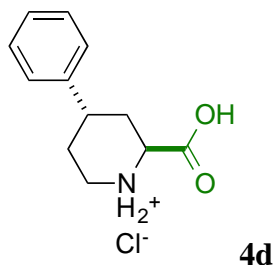
The general hydrolysis procedure was followed using 20 mol% ABNO, which furnished 87 mg of a pale purple powder (91%) after purification by DCM washes. A literature search did not reveal any previously documented characterization data.

$^1\text{H NMR}$ (500 MHz, Methanol- d_4) δ 7.50 (d, $J = 8.4$ Hz, 2H), 7.22 (d, $J = 8.4$ Hz, 2H), 4.48 (dd, $J = 5.4, 3.1$ Hz, 1H), 3.51 – 3.37 (m, 2H), 2.84 (tt, $J = 11.8, 3.6$ Hz, 1H), 2.49 (dq, $J = 14.5, 2.9$ Hz, 1H), 2.20 (ddd, $J = 14.4, 12.1, 5.4$ Hz, 1H), 2.10 – 2.03 (m, 1H), 1.97 (dtd, $J = 14.2, 11.7, 4.7$ Hz, 1H).

$^{13}\text{C NMR}$ (126 MHz, Methanol- d_4) δ 170.26, 143.66, 132.94, 129.72, 121.73, 55.42, 42.73, 37.38, 32.40, 30.18.

HRMS (ESI $^+$) Calc: [M^+] ($\text{C}_{12}\text{H}_{15}\text{BrNO}_2$) 284.0281; measured: 284.0276 = 1.8 ppm difference.

IR (film) $\nu_{\text{max}}/\text{cm}^{-1}$: 3110, 2931, 2793, 1732, 1571, 1450, 1403, 1202, 1000.



The general hydrolysis procedure was followed using 20 mol% ABNO, which furnished 59 mg of a pale brown solid (82%) after purification by DCM washes. The spectroscopic data collected for this compound are consistent, considering the difference in NMR solvents used, with those published in the literature.⁴

¹H NMR (500 MHz, Methanol-*d*₄) δ 7.38 – 7.32 (m, 2H), 7.30 – 7.20 (m, 3H), 4.47 (dd, *J* = 5.2, 3.2 Hz, 1H), 3.54 – 3.37 (m, 2H), 2.84 (tt, *J* = 11.7, 3.6 Hz, 1H), 2.50 (dtd, *J* = 14.5, 3.3, 1.9 Hz, 1H), 2.22 (ddd, *J* = 14.5, 12.1, 5.2 Hz, 1H), 2.13 – 2.04 (m, 1H), 2.00 (dtd, *J* = 14.3, 11.7, 4.5 Hz, 1H).

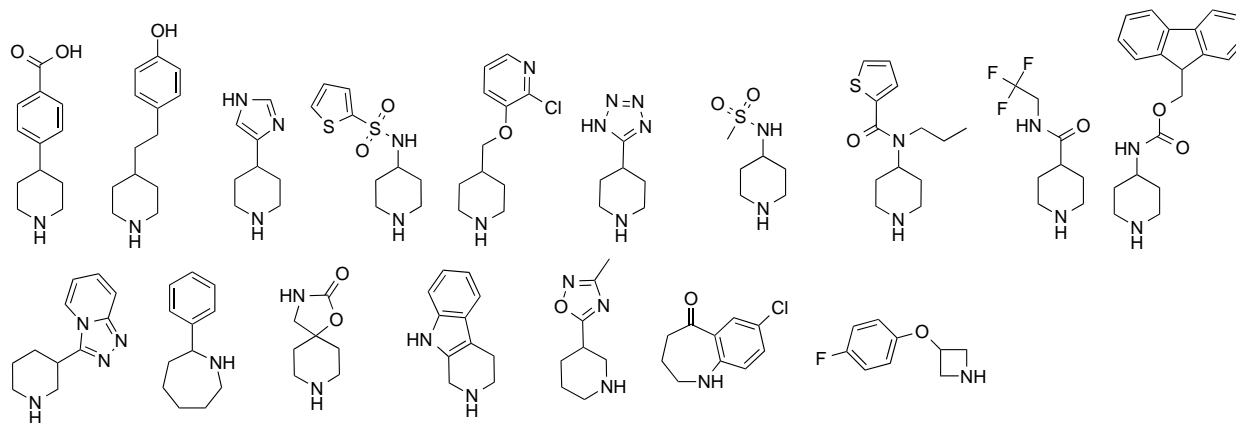
¹³C NMR (126 MHz, Methanol-*d*₄) δ 170.38, 144.35, 129.90, 128.13, 127.64, 55.52, 42.84, 37.87, 32.69, 30.34.

HRMS (ESI⁺) Calc: [M⁺] (C₁₂H₁₆NO₂) 206.1176; measured: 206.1173 = 1.5 ppm difference.

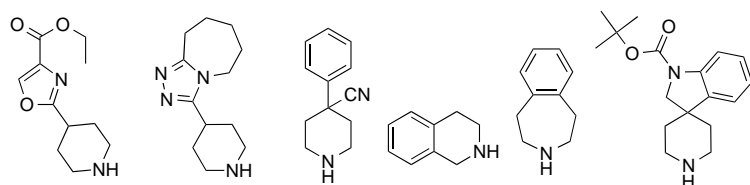
IR (film) ν_{max} /cm⁻¹: 3110, 2925, 2798, 1726, 1576, 1427, 1386, 1248, 1225, 1196, 1161, 1098.

C.5. Unsuccessful Substrates

Each of the following substrates did not undergo successful alpha-cyanation due to their insolubility in the reaction medium.



Alpha-cyanated product was detected in the crude ¹H NMR spectrum obtained from reactions of the following substrates, but pure products were not successfully isolated.



C.6. X-Ray Crystallographic Data

C.6.1. Data Collection for Compound 3e [PhSO₃]

A colorless crystal with approximate dimensions $0.2 \times 0.08 \times 0.04$ mm³ was selected under oil under ambient conditions and attached to the tip of a MiTeGen MicroMount©. The crystal was mounted in a stream of cold nitrogen at 100(1) K and centered in the X-ray beam by using a video camera.

The crystal evaluation and data collection were performed on a Bruker Quazar SMART APEXII diffractometer with Mo K_α ($\lambda = 0.71073$ Å) radiation and the diffractometer to crystal distance of 4.96 cm.⁵

The initial cell constants were obtained from three series of ω scans at different starting angles. Each series consisted of 12 frames collected at intervals of 0.5° in a 6° range about ω with the exposure time of 10 seconds per frame. The reflections were successfully indexed by an automated indexing routine built in the APEXII program suite. The final cell constants were calculated from a set of 9958 strong reflections from the actual data collection.

The data were collected by using the full sphere data collection routine to survey the reciprocal space to the extent of a full sphere to a resolution of 0.70 Å. A total of 80903 data were harvested by collecting 6 sets of frames with 0.5° scans in ω and ϕ with exposure times of 80 sec per frame. These highly redundant datasets were corrected for Lorentz and polarization effects. The absorption correction was based on fitting a function to the empirical transmission surface as sampled by multiple equivalent measurements.⁶

C.6.2. Structure Solution and Refinement

The systematic absences in the diffraction data were uniquely consistent for the space group *Pbca* that yielded chemically reasonable and computationally stable results of refinement.⁷

A successful solution by the direct methods provided most non-hydrogen atoms from the *E*-map. The remaining non-hydrogen atoms were located in an alternating series of least-squares cycles and difference Fourier maps. All non-hydrogen atoms were refined with anisotropic displacement coefficients. All hydrogen except the ammonium H atoms were included in the structure factor calculation at idealized positions and were allowed to ride on the neighboring atoms with relative isotropic displacement coefficients.

Atoms C13 and C14 are disordered over two positions each with the major component occupancy of 54(3)%. The disorder was refined with restraints.

The final least-squares refinement of 264 parameters against 5675 data resulted in residuals *R* (based on F^2 for $I \geq 2\sigma$) and *wR* (based on F^2 for all data) of 0.0478 and 0.1191, respectively. The final difference Fourier map was featureless.

C.6.3. Crystal Data

[C₁₁H₁₇N₄O][C₆H₅O₃S] (*M* = 378.44 g/mol): orthorhombic, space group *Pbca* (no. 61), *a* = 9.204(3) Å, *b* = 10.736(3) Å, *c* = 37.751(9) Å, *V* = 3730.1(17) Å³, *Z* = 8, *T* = 100.0 K, $\mu(\text{MoK}\alpha) = 0.204 \text{ mm}^{-1}$, *D*_{calc} = 1.348 g/cm³, 80903 reflections measured ($6.67^\circ \leq 2\Theta \leq 61.074^\circ$), 5675 unique (*R*_{int} = 0.0572, *R*_{sigma} = 0.0286) which were used in all calculations. The final *R*₁ was 0.0478 ($I > 2\sigma(I)$) and *wR*₂ was 0.1191 (all data).

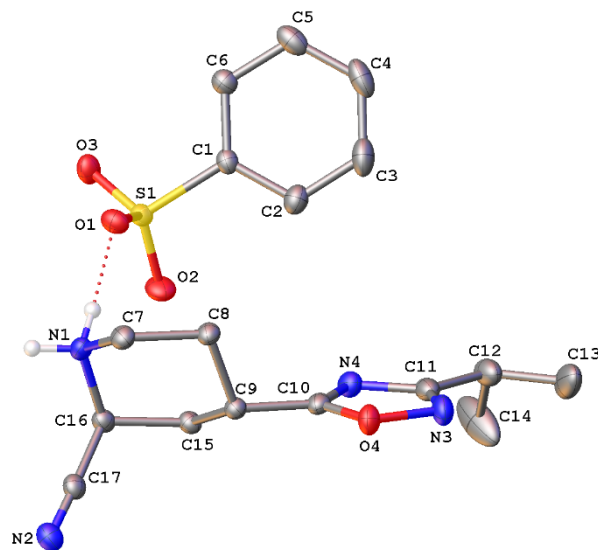


Figure C.1. A molecular drawing of $3e$ [$PhSO_3^-$] shown with 50% probability ellipsoids. All non-ammonium H atoms and minor disorder components are omitted.

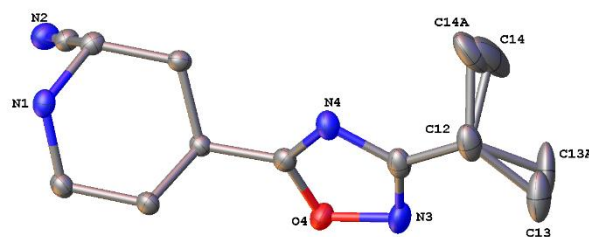


Figure C.2. A molecular drawing of the cation of $3e$ [$PhSO_3^-$] shown with 50% probability ellipsoids. All H atoms are omitted by both disorder components are shown.

Table C.1. Crystal data and structure refinement for $3e$ [$PhSO_3^-$].

Identification code	stahl234
Empirical formula	[C ₁₁ H ₁₇ N ₄ O][C ₆ H ₅ O ₃ S]
Formula weight	378.44
Temperature/K	100.0
Crystal system	orthorhombic
Space group	Pbca
a/Å	9.204(3)

b/Å	10.736(3)
c/Å	37.751(9)
$\alpha/^\circ$	90
$\beta/^\circ$	90
$\gamma/^\circ$	90
Volume/Å ³	3730.1(17)
Z	8
$\rho_{\text{calc}}/\text{g}/\text{cm}^3$	1.348
μ/mm^{-1}	0.204
F(000)	1600.0
Crystal size/mm ³	0.2 × 0.08 × 0.04
Radiation	MoK α ($\lambda = 0.71073$)
2 Θ range for data collection/ $^\circ$	6.67 to 61.074
Index ranges	-13 ≤ h ≤ 12, -15 ≤ k ≤ 15, -53 ≤ l ≤ 53
Reflections collected	80903
Independent reflections	5675 [$R_{\text{int}} = 0.0572$, $R_{\text{sigma}} = 0.0286$]
Data/restraints/parameters	5675/18/264
Goodness-of-fit on F ²	1.093
Final R indexes [$I \geq 2\sigma(I)$]	$R_1 = 0.0478$, $wR_2 = 0.1148$
Final R indexes [all data]	$R_1 = 0.0569$, $wR_2 = 0.1191$
Largest diff. peak/hole / e Å ⁻³	0.58/-0.34

•

Table C.2. Fractional Atomic Coordinates ($\times 10^4$) and Equivalent Isotropic Displacement Parameters ($\text{\AA}^2 \times 10^3$) for $3e$ [$PhSO_3^-$]. U_{eq} is defined as 1/3 of the trace of the orthogonalised U_{ij} tensor.

Atom	<i>x</i>	<i>y</i>	<i>z</i>	$U(eq)$
S1	5401.1(4)	6558.3(3)	6861.9(2)	17.02(9)
O1	4196.0(11)	5809.5(10)	7005.5(3)	21.7(2)
O2	4949.9(14)	7806.1(10)	6767.8(3)	27.6(2)
O3	6668.5(12)	6497.7(11)	7092.2(3)	24.1(2)
C1	5918.4(15)	5801.0(12)	6465.8(4)	17.5(3)
C2	5220.6(18)	6117.3(15)	6152.6(4)	24.5(3)
C3	5584(2)	5482.8(17)	5843.4(4)	32.2(4)
C4	6631(2)	4560.8(16)	5848.4(4)	32.4(4)
C5	7320.1(19)	4244.1(15)	6162.3(4)	28.0(3)
C6	6964.4(16)	4867.6(13)	6474.2(4)	20.5(3)
O4	-453.0(12)	6688(1)	5875.9(3)	23.9(2)
N1	1509.8(14)	6561.0(12)	7187.9(3)	19.4(2)
N2	-1325.6(15)	8515.2(12)	7347.4(4)	25.2(3)
N3	82.8(17)	6883.3(13)	5526.7(3)	27.8(3)
N4	1726.6(14)	7525.4(12)	5930.9(3)	22.9(3)
C7	545.0(16)	5617.7(13)	7014.1(4)	20.2(3)
C8	730.3(16)	5690.3(12)	6614.6(4)	18.7(3)

C9	340.7(15)	7004.0(12)	6482.5(4)	16.2(2)
C10	591.9(16)	7101.6(12)	6093.2(4)	18.9(3)
C11	1355.1(18)	7373.2(14)	5578.6(4)	24.0(3)
C12	2345(2)	7744.9(16)	5282.6(4)	32.2(4)
C13	1641(9)	7406(10)	4924.5(14)	42.3(16)
C14	2714(17)	9125(6)	5305(3)	60(2)
C15	1268.7(15)	7982.0(12)	6672.7(4)	17.2(2)
C16	1176.0(15)	7866.3(13)	7075.4(4)	18.3(3)
C17	-245.5(16)	8229.4(13)	7223.8(4)	19.8(3)
C13A	1590(10)	7867(16)	4928.3(17)	49(2)
C14A	3157(12)	8966(7)	5383(3)	47(2)

.

Table C.3. Anisotropic Displacement Parameters ($\text{\AA}^2 \times 10^3$) for $3e [PhSO_3^-]$. The Anisotropic displacement factor exponent takes the form: $-2\pi^2[h^2a^*U_{11}+2hka^*b^*U_{12}+\dots]$.

Atom	U ₁₁	U ₂₂	U ₃₃	U ₂₃	U ₁₃	U ₁₂
S1	18.39(16)	15.25(15)	17.43(16)	-1.47(11)	0.38(12)	- 0.32(11)
O1	19.3(5)	20.1(5)	25.6(5)	-0.7(4)	5.7(4)	-0.3(4)
O2	37.0(6)	14.8(5)	31.1(6)	-0.5(4)	2.0(5)	2.8(4)
O3	20.3(5)	32.8(6)	19.1(5)	-4.3(4)	-1.8(4)	-2.4(4)

C1	19.3(6)	16.7(6)	16.5(6)	-0.5(5)	1.8(5)	-3.6(5)
C2	27.5(8)	25.4(7)	20.6(7)	3.1(5)	-1.9(6)	-3.2(6)
C3	42.3(10)	37.4(9)	16.9(7)	-0.3(6)	-0.8(7)	-11.4(7)
C4	41(1)	33.5(8)	22.8(7)	-9.6(6)	11.0(7)	-13.3(7)
C5	28.4(8)	23.4(7)	32.2(8)	-5.9(6)	11.3(6)	-4.6(6)
C6	19.7(6)	19.8(6)	22.0(7)	-0.3(5)	2.3(5)	-2.0(5)
O4	28.1(6)	27.4(5)	16.3(5)	-1.0(4)	-1.2(4)	-3.7(4)
N1	18.2(6)	23.8(6)	16.2(5)	1.4(4)	0.1(4)	3.6(5)
N2	27.0(7)	24.6(6)	23.9(6)	-3.1(5)	3.2(5)	-1.5(5)
N3	38.5(8)	29.7(6)	15.3(5)	0.0(5)	1.9(5)	1.5(6)
N4	24.3(6)	24.6(6)	19.7(6)	3.4(5)	2.8(5)	1.9(5)
C7	24.1(7)	16.6(6)	20.0(6)	3.2(5)	1.6(5)	0.2(5)
C8	23.3(7)	14.4(6)	18.3(6)	1.5(5)	-0.3(5)	0.6(5)
C9	17.3(6)	14.9(5)	16.4(6)	1.2(4)	0.6(5)	-0.4(5)
C10	23.1(7)	14.9(6)	18.8(6)	1.4(5)	-1.6(5)	2.6(5)
C11	30.8(8)	21.0(6)	20.3(7)	3.3(5)	4.5(6)	7.3(6)
C12	39.8(10)	32.1(8)	24.6(7)	6.9(6)	11.3(7)	9.9(7)
C13	48(3)	57(4)	21.2(19)	15(2)	10.5(17)	19(3)
C14	91(5)	32(2)	55(4)	10(2)	42(4)	-2(3)
C15	18.9(6)	14.7(5)	18.1(6)	-1.0(5)	1.7(5)	-1.0(5)
C16	17.3(6)	19.1(6)	18.5(6)	-2.1(5)	-0.1(5)	0.1(5)
C17	23.6(7)	17.9(6)	17.8(6)	-2.1(5)	-0.5(5)	-2.1(5)

C13A	44(3)	79(6)	24(2)	24(3)	5(2)	17(4)
C14A	61(4)	28(3)	51(4)	14(2)	27(3)	6(3)

.

Table C.4. Bond Lengths for *3e* [*PhSO₃*].

Atom	Atom	Length/Å	Atom	Atom	Length/Å
S1	O1	1.4732(11)	N3	C11	1.298(2)
S1	O2	1.4468(12)	N4	C10	1.2935(19)
S1	O3	1.4563(12)	N4	C11	1.383(2)
S1	C1	1.7674(14)	C7	C8	1.520(2)
C1	C2	1.388(2)	C8	C9	1.5383(19)
C1	C6	1.390(2)	C9	C10	1.4917(19)
C2	C3	1.392(2)	C9	C15	1.5320(19)
C3	C4	1.381(3)	C11	C12	1.496(2)
C4	C5	1.387(3)	C12	C13	1.543(5)
C5	C6	1.394(2)	C12	C14	1.522(5)
O4	N3	1.4229(17)	C12	C13A	1.513(5)
O4	C10	1.3397(18)	C12	C14A	1.556(6)
N1	C7	1.4981(19)	C15	C16	1.528(2)
N1	C16	1.4962(19)	C16	C17	1.476(2)
N2	C17	1.140(2)			

Table C.5. Bond Angles for *3e* [*PhSO₃⁻*].

Atom	Atom	Atom	Angle/°	Atom	Atom	Atom	Angle/°
O1	S1	C1	105.26(6)	C10	C9	C8	110.35(11)
O2	S1	O1	112.30(7)	C10	C9	C15	109.10(11)
O2	S1	O3	114.69(7)	C15	C9	C8	110.28(11)
O2	S1	C1	107.19(7)	O4	C10	C9	117.95(13)
O3	S1	O1	111.03(7)	N4	C10	O4	113.97(13)
O3	S1	C1	105.59(7)	N4	C10	C9	128.07(13)
C2	C1	S1	118.92(12)	N3	C11	N4	114.57(14)
C2	C1	C6	121.10(13)	N3	C11	C12	123.01(15)
C6	C1	S1	119.92(11)	N4	C11	C12	122.42(16)
C1	C2	C3	118.91(16)	C11	C12	C13	109.6(4)
C4	C3	C2	120.46(16)	C11	C12	C14	110.7(3)
C3	C4	C5	120.42(15)	C11	C12	C13 A	113.8(4)
C4	C5	C6	119.80(16)	C11	C12	C14 A	109.6(4)
C1	C6	C5	119.31(14)	C14	C12	C13	111.8(4)
C10	O4	N3	105.64(12)	C13A	C12	C14 A	111.3(5)
C16	N1	C7	112.78(11)	C16	C15	C9	112.30(11)
C11	N3	O4	103.45(12)	N1	C16	C15	110.32(11)

C10	N4	C11	102.37(13)	C17	C16	N1	108.77(12)
N1	C7	C8	109.47(11)	C17	C16	C15	113.93(12)
C7	C8	C9	110.03(11)	N2	C17	C16	178.07(16)

Table C.6. Hydrogen Bonds for *3e* [*PhSO₃*].

D	H	A	d(D-H)/Å	d(H-A)/Å	d(D-A)/Å	D-H-A/°
N1	H1A	O3 ¹	0.862(16)	1.871(16)	2.7226(17)	169.3(19)
N1	H1B	O1	0.874(16)	1.823(16)	2.6903(17)	171.9(19)

¹-1/2+X,+Y,3/2-Z

Table C.7. Torsion Angles for *3e* [*PhSO₃*].

A	B	C	D	Angle/°	A	B	C	D	Angle/°
S1	C1	C2	C3	-177.25(12)	N4	C11	C12	C13	177.7(4)
S1	C1	C6	C5	177.45(11)	N4	C11	C12	C14	-58.4(8)
O1	S1	C1	C2	88.06(13)	N4	C11	C12	C13A	-162.7(7)
O1	S1	C1	C6	-89.20(12)	N4	C11	C12	C14A	-37.3(5)
O2	S1	C1	C2	-31.69(14)	C7	N1	C16	C15	-56.11(15)
O2	S1	C1	C6	151.05(12)	C7	N1	C16	C17	69.53(14)
O3	S1	C1	C2	-154.40(12)	C7	C8	C9	C10	177.13(12)
O3	S1	C1	C6	28.34(13)	C7	C8	C9	C15	56.53(15)
C1	C2	C3	C4	-0.5(2)	C8	C9	C10	O4	82.98(15)
C2	C1	C6	C5	0.3(2)	C8	C9	C10	N4	-95.72(17)

C2 C3 C4 C5	0.8(3)	C8 C9 C15C16	-53.55(15)
C3 C4 C5 C6	-0.6(2)	C9 C15C16N1	52.67(15)
C4 C5 C6 C1	0.0(2)	C9 C15C16C17	-69.99(15)
C6 C1 C2 C3	0.0(2)	C10O4 N3 C11	0.26(15)
O4 N3 C11N4	0.04(17)	C10N4 C11N3	-0.33(17)
O4 N3 C11C12	-179.98(13)	C10N4 C11C12	179.69(14)
N1 C7 C8 C9	-59.17(15)	C10C9 C15C16	-174.89(11)
N3 O4 C10N4	-0.51(16)	C11N4 C10O4	0.52(16)
N3 O4 C10C9	-179.39(12)	C11N4 C10C9	179.26(13)
N3 C11 C12C13	-2.3(5)	C15C9 C10O4	-155.71(12)
N3 C11 C12C14	121.6(8)	C15C9 C10N4	25.59(19)
N3 C11 C12C13A	17.4(8)	C16N1 C7 C8	59.91(15)
N3 C11 C12C14A	142.7(5)		

Table C.8. Hydrogen Atom Coordinates ($\text{\AA}\times 10^4$) and Isotropic Displacement Parameters ($\text{\AA}^2\times 10^3$) for $3e$ [$PhSO_3$].

Atom	x	y	z	$U(\text{eq})$
H2	4506.69	6756.26	6149.22	29
H3	5109.13	5685.38	5627.55	39
H4	6879.74	4140.96	5635.32	39
H5	8032.75	3603.95	6164.76	34
H6	7431.99	4656.94	6690.45	25
H1A	1450(20)	6497(17)	7415(4)	23

H1B	2403(18)	6392(18)	7126(5)	23
H7A	-480.77	5782.31	7077.72	24
H7B	801	4772.23	7098.19	24
H8A	92.04	5069.24	6499.02	22
H8B	1748.46	5494.74	6550.93	22
H9	-707.93	7169.96	6533.35	19
H12A	3094	7075.46	5258.15	39
H12	3268.16	7260.42	5306.22	39
H13A	1474.7	6504.78	4914.16	64
H13B	2288.98	7653.58	4730.97	64
H13C	711.38	7843.29	4900.87	64
H14A	1823.95	9617.56	5278	89
H14B	3398.3	9341.41	5116.07	89
H14C	3155.41	9304.56	5535.71	89
H15A	2294	7887.64	6598.08	21
H15B	940.53	8823.62	6601.33	21
H16	1930.86	8425.34	7180.42	22
H13D	1097.52	7082.78	4871.03	74
H13E	2308.96	8055.21	4744.54	74
H13F	873.7	8541.03	4939.94	74
H14D	2447.48	9623.17	5433.12	70
H14E	3778.69	9224.08	5185.14	70

H14F 3757.45 8820.67 5593.2 70

Table C.9. Atomic Occupancy for *3e* [*PhSO₃*].

<i>Atom Occupancy</i>	<i>Atom Occupancy</i>	<i>Atom Occupancy</i>
H12A 0.46(3)	H12 0.54(3)	C13 0.54(3)
H13A 0.54(3)	H13B 0.54(3)	H13C 0.54(3)
C14 0.54(3)	H14A 0.54(3)	H14B 0.54(3)
H14C 0.54(3)	C13A 0.46(3)	H13D 0.46(3)
H13E 0.46(3)	H13F 0.46(3)	C14A 0.46(3)
H14D 0.46(3)	H14E 0.46(3)	H14F 0.46(3)

Data Collection for carboxylic acid 4a.

A colorless crystal with approximate dimensions $0.268 \times 0.099 \times 0.042$ mm³ was selected under oil under ambient conditions and attached to the tip of a MiTeGen MicroMount©. The crystal was mounted in a stream of cold nitrogen at 100(1) K and centered in the X-ray beam by using a video camera.

The crystal evaluation and data collection were performed on a Bruker Quazar SMART APEXII diffractometer with Mo K α ($\lambda = 0.71073$ Å) radiation and the diffractometer to crystal distance of 6 cm⁹ for the crystal screening and 5 cm for the data collection.

The initial cell constants were obtained from three series of ω scans at different starting angles. Each series consisted of 15 frames collected at intervals of 0.4° in a 6° range about ω with the exposure time of 10 seconds per frame. The reflections were successfully indexed by an automated indexing routine built in the APEXII program suite. The final cell constants were calculated from a set of 9985 strong reflections from the actual data collection.

The data were collected by using the full sphere data collection routine to survey the reciprocal space to the extent of a full sphere to a resolution of 0.70 Å. A total of 36440 data were harvested by collecting 5 sets of frames with 0.5° scans in ω and ϕ with exposure times of 30 sec per frame. These highly redundant datasets were corrected for Lorentz and polarization effects. The absorption correction was based on fitting a function to the empirical transmission surface as sampled by multiple equivalent measurements.¹⁰

Structure Solution and Refinement

The systematic absences in the diffraction data were uniquely consistent for the space group $P2_1/n$ that yielded chemically reasonable and computationally stable results of refinement.¹¹

A successful solution by the direct methods provided most non-hydrogen atoms from the *E*-map. The remaining non-hydrogen atoms were located in an alternating series of least-squares cycles and difference Fourier maps. All non-hydrogen atoms were refined with anisotropic displacement coefficients. All hydrogen atoms that do not participate in hydrogen bonding were included in the structure factor calculation at idealized positions and were allowed to ride on the neighboring atoms with relative isotropic displacement coefficients.

The asymmetric unit contains 2-carboxy-4-(6-fluoro-1,2-benzoxazol-3-yl)piperidin-1-ium cation, a chloride, a water molecule and half molecule of dioxane. The dioxane molecule occupies a crystallographic inversion center. The carboxylic acid hydrogen is equally disordered over two positions and resides 50% of the time on oxygen O3 and 50% of the time the water molecule oxygen O4, converting the water molecule into a hydronium.

The final least-squares refinement of 235 parameters against 4702 data resulted in residuals *R* (based on F^2 for $I \geq 2\sigma$) and wR (based on F^2 for all data) of 0.0373 and 0.1015, respectively. The final difference Fourier map was featureless.

Summary

Crystal Data for $[\text{C}_{13}\text{H}_{14}\text{FN}_2\text{O}_3]^+\text{Cl}^- \cdot \text{H}_2\text{O} \cdot 1/2\text{C}_4\text{H}_8\text{O}_2$ ($M = 362.78$ g/mol): monoclinic, space group $\text{P}2_1/\text{n}$ (no. 14), $a = 16.188(2)$ Å, $b = 6.4618(8)$ Å, $c = 16.639(2)$ Å, $\beta = 111.357(2)^\circ$, $V = 1621.0(4)$ Å³, $Z = 4$, $T = 99.96$ K, $\mu(\text{MoK}\alpha) = 0.275$ mm⁻¹, $D_{\text{calc}} = 1.487$ g/cm³, 36440 reflections measured ($3.006^\circ \leq 2\Theta \leq 60.104^\circ$), 4702 unique ($R_{\text{int}} = 0.0366$, $R_{\text{sigma}} = 0.0223$) which were used in all calculations. The final R_1 was 0.0373 ($I > 2\sigma(I)$) and wR_2 was 0.1020 (all data).

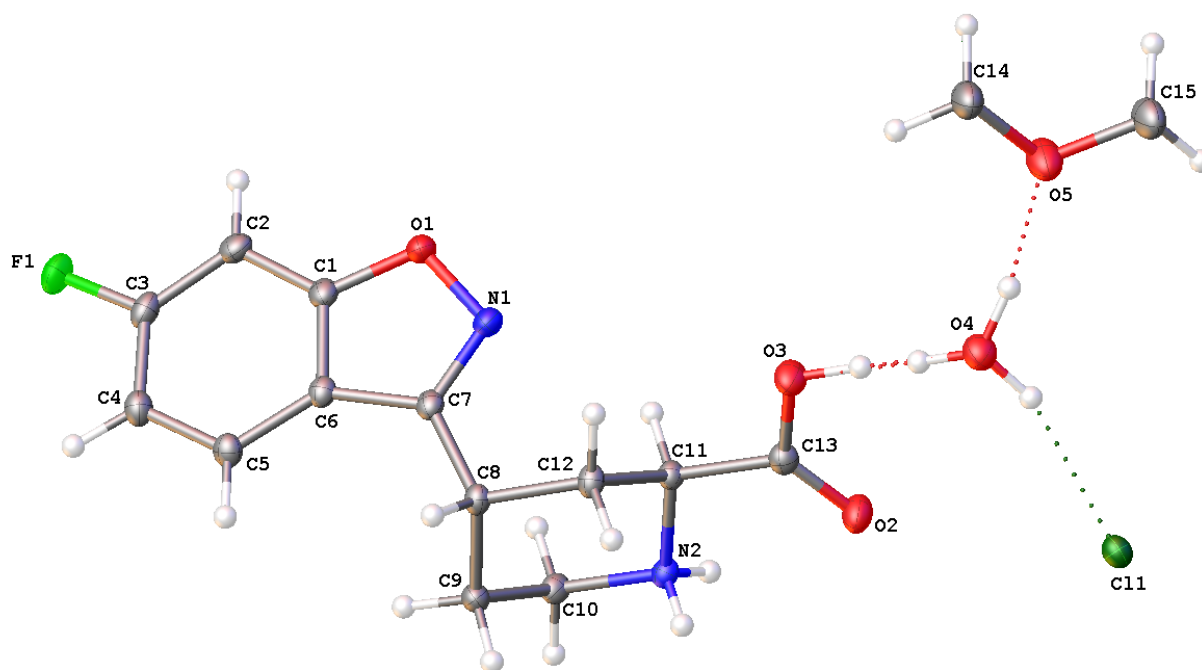


Figure C.3. A molecular drawing of the asymmetric unit of **4a** shown with 50% probability ellipsoids. The H atoms at O3 and O4 pointing toward each other are 50% occupied.

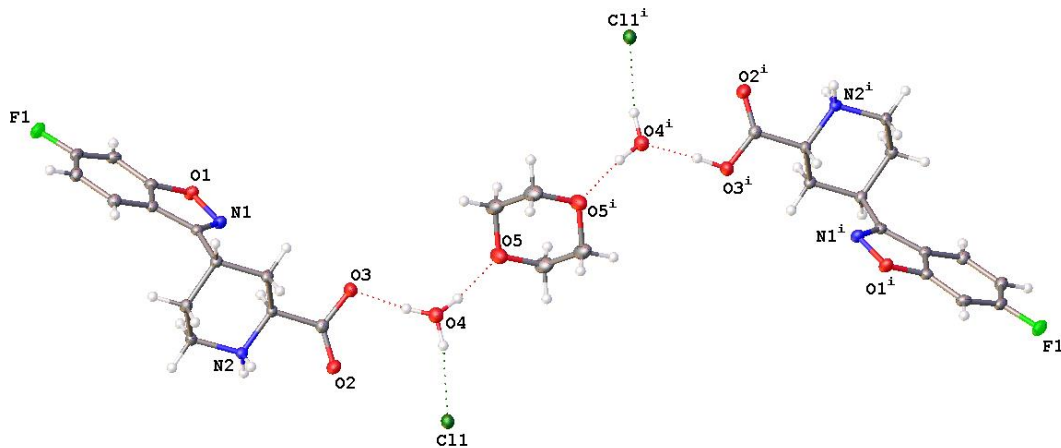


Figure C.4. A molecular drawing of **4a** shown with 50% probability ellipsoids. Symmetry code: i $1-x, -1-y, 1-z$.

Crystal data and structure refinement for 4a

Identification code	stahl235
Empirical formula	$[\text{C}_{13}\text{H}_{14}\text{FN}_2\text{O}_3]^+\text{Cl}^- \cdot \text{H}_2\text{O} \cdot 1/2\text{C}_4\text{H}_8\text{O}_2$
Formula weight	362.78
Temperature/K	99.96
Crystal system	monoclinic
Space group	$P2_1/n$
$a/\text{\AA}$	16.188(2)
$b/\text{\AA}$	6.4618(8)
$c/\text{\AA}$	16.639(2)
$\alpha/^\circ$	90
$\beta/^\circ$	111.357(2)
$\gamma/^\circ$	90
Volume/ \AA^3	1621.0(4)
Z	4
$\rho_{\text{calc}}/\text{g/cm}^3$	1.487
μ/mm^{-1}	0.275
F(000)	760.0
Crystal size/ mm^3	$0.268 \times 0.099 \times 0.042$
Radiation	$\text{MoK}\alpha$ ($\lambda = 0.71073$)
2Θ range for data collection/ $^\circ$	3.006 to 60.104

Index ranges	$-22 \leq h \leq 22, -9 \leq k \leq 9, -23 \leq l \leq 23$
Reflections collected	36440
Independent reflections	4702 [$R_{\text{int}} = 0.0366, R_{\text{sigma}} = 0.0223$]
Data/restraints/parameters	4702/0/235
Goodness-of-fit on F^2	1.040
Final R indexes [$I \geq 2\sigma(I)$]	$R_1 = 0.0373, wR_2 = 0.0986$
Final R indexes [all data]	$R_1 = 0.0422, wR_2 = 0.1020$
Largest diff. peak/hole / $e \text{ \AA}^{-3}$	0.51/-0.22

Table C.10. Fractional Atomic Coordinates ($\times 10^4$) and Equivalent Isotropic Displacement Parameters ($\text{\AA}^2 \times 10^3$) for 4a. U_{eq} is defined as 1/3 of the trace of the orthogonalised U_{ij} tensor.

Atom	<i>x</i>	<i>y</i>	<i>z</i>	$U(\text{eq})$
Cl1	1877.0(2)	-2115.2(4)	6076.8(2)	17.17(8)
F1	7742.6(5)	15288.0(12)	8880.1(5)	24.49(17)
O1	6226.9(6)	9369.5(14)	7303.1(6)	19.34(18)
O2	3013.4(6)	2755.0(15)	6757.7(7)	24.1(2)
O3	4390.5(6)	2089.0(15)	6797.2(7)	22.9(2)
N1	5773.0(7)	7728.7(16)	7544.0(7)	18.0(2)
N2	3512.5(6)	6237.4(15)	7727.2(7)	13.85(18)
C1	6562.0(7)	10645.5(18)	7994.3(8)	16.2(2)
C2	7037.6(8)	12457(2)	8021.7(8)	18.6(2)
C3	7299.6(8)	13474.6(18)	8803.7(8)	18.3(2)
C4	7137.2(8)	12771.1(18)	9528.2(8)	18.4(2)

C5	6661.1(8)	10957.3(18)	9473.8(7)	16.8(2)
C6	6359.8(7)	9897.0(17)	8684.8(7)	14.7(2)
C7	5850.4(7)	8048.2(17)	8344.3(7)	14.8(2)
C8	5415.2(7)	6634.1(17)	8791.7(7)	14.7(2)
C9	4681.4(8)	7785.0(18)	9000.5(7)	16.1(2)
C10	3876.3(8)	8219.0(17)	8191.1(8)	15.8(2)
C11	4192.0(7)	5132.4(17)	7474.5(7)	13.5(2)
C12	5018.6(7)	4676.3(17)	8274.1(7)	15.1(2)
C13	3792.7(8)	3190.8(18)	6974.4(8)	16.5(2)
O4	3730.9(7)	-1237.1(16)	5980.6(6)	23.7(2)
O5	4523.3(7)	-3165.9(18)	4991.0(7)	31.6(2)
C14	5478.7(9)	-3183(2)	5328.6(9)	28.3(3)
C15	4187.1(9)	-4696(3)	4328.2(9)	29.6(3)

Table C.11. Anisotropic Displacement Parameters ($\text{\AA}^2 \times 10^3$) for 4a The Anisotropic displacement factor exponent takes the form: $-2\pi^2[h^2a^{*2}U_{11}+2hka^*b^*U_{12}+\dots]$.

Atom	U_{11}	U_{22}	U_{33}	U_{23}	U_{13}	U_{12}
Cl1	18.62(14)	16.65(14)	14.99(13)	-0.87(9)	4.62(10)	1.06(9)
F1	23.3(4)	18.6(3)	31.0(4)	-1.6(3)	9.2(3)	-7.9(3)
O1	19.4(4)	22.3(4)	18.9(4)	-4.6(3)	10.1(3)	-5.8(3)
O2	17.8(4)	23.6(4)	29.5(5)	-8.4(4)	7.0(4)	-3.4(3)
O3	20.1(4)	21.0(4)	29.0(5)	-8.0(4)	10.5(4)	-1.2(3)
N1	16.0(5)	19.7(5)	20.0(5)	-3.0(4)	8.6(4)	-3.9(4)

N2	11.7(4)	13.4(4)	15.2(4)	0.8(3)	3.5(4)	0.3(3)
C1	12.1(5)	18.2(5)	18.3(5)	-2.1(4)	5.4(4)	0.1(4)
C2	13.7(5)	21.9(5)	21.1(6)	1.2(4)	7.5(4)	-0.8(4)
C3	13.1(5)	14.7(5)	25.3(6)	0.5(4)	4.6(4)	-1.5(4)
C4	17.0(5)	16.8(5)	18.7(5)	-2.2(4)	3.3(4)	-0.9(4)
C5	15.9(5)	17.0(5)	14.9(5)	0.7(4)	2.6(4)	0.2(4)
C6	11.7(5)	13.9(5)	17.0(5)	-0.1(4)	3.4(4)	0.9(4)
C7	11.1(5)	15.7(5)	16.8(5)	-1.7(4)	4.0(4)	0.6(4)
C8	13.2(5)	14.4(5)	14.3(5)	-0.5(4)	2.6(4)	-0.7(4)
C9	16.0(5)	17.5(5)	15.4(5)	-2.7(4)	6.4(4)	-1.9(4)
C10	15.4(5)	12.5(5)	20.0(5)	-1.5(4)	7.2(4)	0.1(4)
C11	12.8(5)	12.1(5)	15.0(5)	-1.2(4)	4.2(4)	0.2(4)
C12	12.8(5)	12.9(5)	16.3(5)	0.2(4)	1.6(4)	0.8(4)
C13	17.5(5)	15.8(5)	15.6(5)	0.3(4)	5.1(4)	-0.4(4)
O4	22.1(5)	24.1(5)	25.0(5)	-5.2(4)	8.8(4)	-0.7(4)
O5	21.6(5)	37.7(6)	33.6(6)	-12.9(4)	7.8(4)	1.3(4)
C14	20.7(6)	37.6(8)	25.2(6)	-9.8(6)	6.8(5)	-5.5(5)
C15	20.7(6)	41.1(8)	22.7(6)	-7.8(6)	2.7(5)	-2.2(6)

Table C.12. Bond Lengths for 4a.

Atom	Atom	Length/Å	Atom	Atom	Length/Å
F1	C3	1.3554(14)	C4	C5	1.3875(17)
O1	N1	1.4281(13)	C5	C6	1.4017(16)

O1	C1	1.3573(14)	C6	C7	1.4449(15)
O2	C13	1.2121(15)	C7	C8	1.5058(16)
O3	C13	1.3185(15)	C8	C9	1.5444(16)
N1	C7	1.3077(15)	C8	C12	1.5335(16)
N2	C10	1.5004(15)	C9	C10	1.5208(17)
N2	C11	1.4945(15)	C11	C12	1.5332(15)
C1	C2	1.3927(17)	C11	C13	1.5141(16)
C1	C6	1.3911(16)	O5	C14	1.4405(17)
C2	C3	1.3795(18)	O5	C15	1.4328(17)
C3	C4	1.4000(18)	C14	C15 ¹	1.507(2)

¹1-X,-1-Y,1-Z

Table C.13. Bond Angles for 4a.

Atom Atom Atom Angle/°				Atom Atom Atom Angle/°			
C1	O1	N1	107.51(9)	C6	C7	C8	127.65(10)
C7	N1	O1	107.48(9)	C7	C8	C9	110.83(9)
C11	N2	C10	111.17(9)	C7	C8	C12	113.49(9)
O1	C1	C2	125.73(11)	C12	C8	C9	108.94(9)
O1	C1	C6	110.30(10)	C10	C9	C8	111.77(9)
C6	C1	C2	123.97(11)	N2	C10	C9	110.33(9)
C3	C2	C1	114.08(11)	N2	C11	C12	110.30(9)
F1	C3	C2	118.10(11)	N2	C11	C13	109.86(9)
F1	C3	C4	117.31(11)	C13	C11	C12	112.37(9)

C2	C3	C4	124.59(11)	C11	C12	C8	112.54(9)
C5	C4	C3	119.49(11)	O2	C13	O3	125.25(11)
C4	C5	C6	118.00(11)	O2	C13	C11	123.08(11)
C1	C6	C5	119.83(11)	O3	C13	C11	111.66(10)
C1	C6	C7	103.65(10)	C15	O5	C14	110.34(11)
C5	C6	C7	136.52(11)	O5	C14	C15 ¹	109.95(12)
N1	C7	C6	111.04(10)	O5	C15	C14 ¹	110.64(11)
N1	C7	C8	121.27(10)				

¹1-X,-1-Y,1-Z

Table C.14. Hydrogen Bonds for 4a.

D	H	A	d(D-H)/Å	d(H-A)/Å	d(D-A)/Å	D-H-A/°
N2	H2A	C11 ¹	0.837(17)	2.331(17)	3.1567(11)	169.3(15)
N2	H2B	C11 ²	0.856(17)	2.379(18)	3.2230(11)	168.8(15)
O4	H4AA	C11	0.89(2)	2.26(2)	3.1151(12)	160.3(18)
O4	H4AB	O5	0.92(2)	1.82(2)	2.7292(15)	167.5(19)
O3	H3	O4	0.92(5)	1.65(5)	2.5591(14)	171(4)
O4	H4B	O3	0.86(5)	1.70(5)	2.5591(14)	171(5)

¹1/2-X,1/2+Y,3/2-Z; ²+X,1+Y,+Z

Table C.15. Torsion Angles for 4a.

A	B	C	D	Angle/°	A	B	C	D	Angle/°
F1	C3	C4	C5	177.92(10)	C3	C4	C5	C6	-0.02(17)
O1	N1	C7	C6	-0.31(13)	C4	C5	C6	C1	1.69(17)

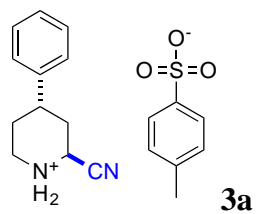
O1N1 C7 C8 177.70(9)	C4 C5 C6 C7 -178.85(12)
O1C1 C2 C3 179.69(11)	C5 C6 C7 N1 -178.68(13)
O1C1 C6 C5 178.56(10)	C5 C6 C7 C8 3.5(2)
O1C1 C6 C7 -1.07(12)	C6 C1 C2 C3 0.07(17)
N1O1 C1 C2 -178.74(11)	C6 C7 C8 C9 63.71(14)
N1O1 C1 C6 0.92(12)	C6 C7 C8 C12 -173.33(10)
N1C7 C8 C9 -113.94(12)	C7 C8 C9 C10 71.37(12)
N1C7 C8 C129.02(15)	C7 C8 C12C11 -70.64(12)
N2C11C12C8 -55.98(12)	C8 C9 C10N2 57.68(12)
N2C11C13O2 6.08(16)	C9 C8 C12C11 53.36(12)
N2C11C13O3 -175.14(10)	C10N2 C11C12 58.06(12)
C1O1 N1 C7 -0.36(12)	C10N2 C11C13 -177.53(9)
C1C2 C3 F1 -177.99(10)	C11N2 C10C9 -59.35(12)
C1C2 C3 C4 1.73(18)	C12C8 C9 C10 -54.18(12)
C1C6 C7 N1 0.85(13)	C12C11C13O2 129.28(12)
C1C6 C7 C8 -177.00(11)	C12C11C13O3 -51.94(13)
C2C1 C6 C5 -1.77(18)	C13C11C12C8 -178.94(9)
C2C1 C6 C7 178.60(11)	C14O5 C15C14 ¹ 58.11(17)
C2C3 C4 C5 -1.80(19)	C15O5 C14C15 ¹ -57.70(17)

¹1-X,-1-Y,1-Z

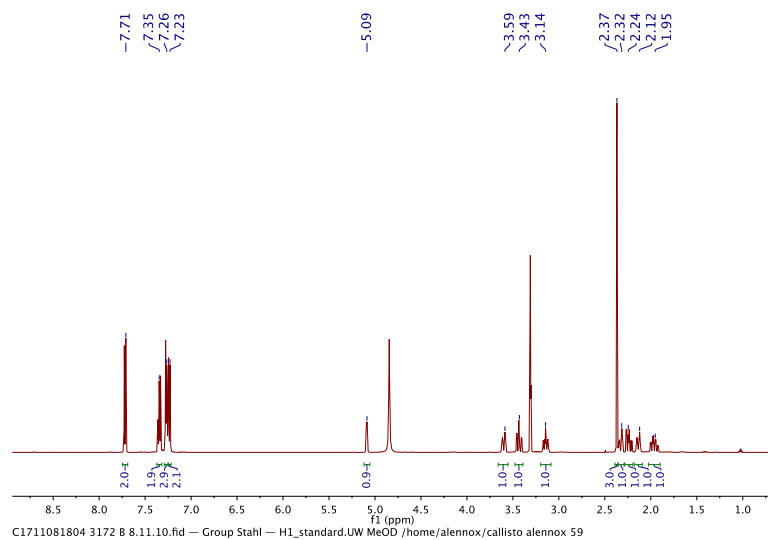
Table C.16. Hydrogen Atom Coordinates ($\text{\AA}\times 10^4$) and Isotropic Displacement Parameters ($\text{\AA}^2\times 10^3$) for 4a.

Atom	x	y	z	U(eq)
H2A	3356(11)	5460(30)	8048(11)	17
H2B	3043(11)	6510(30)	7291(11)	17
H2	7169.89	12948.94	7544.09	22
H4	7351.36	13529.67	10053	22
H5	6542.86	10449.25	9956.91	20
H8	5878.14	6192.66	9350.48	18
H9A	4498.45	6937.91	9402.88	19
H9B	4920.81	9109.57	9291.14	19
H10A	3414.01	8921.07	8350.08	19
H10B	4046.76	9150.8	7805.13	19
H11	4370.84	6064.17	7086.25	16
H12A	5471.71	4008.1	8091.05	18
H12B	4859.92	3691.54	8650.48	18
H4AA	3163(15)	-1550(30)	5870(13)	35
H4AB	3921(13)	-1860(30)	5582(13)	35
H14A	5703.72	-2149.62	5797.21	34
H14B	5700.39	-2805.86	4866.6	34
H15A	4377.39	-4359.37	3841.35	36
H15B	3530.66	-4686.2	4109.75	36
H3	4120(30)	990(80)	6460(30)	44
H4B	3910(30)	-50(80)	6220(30)	44

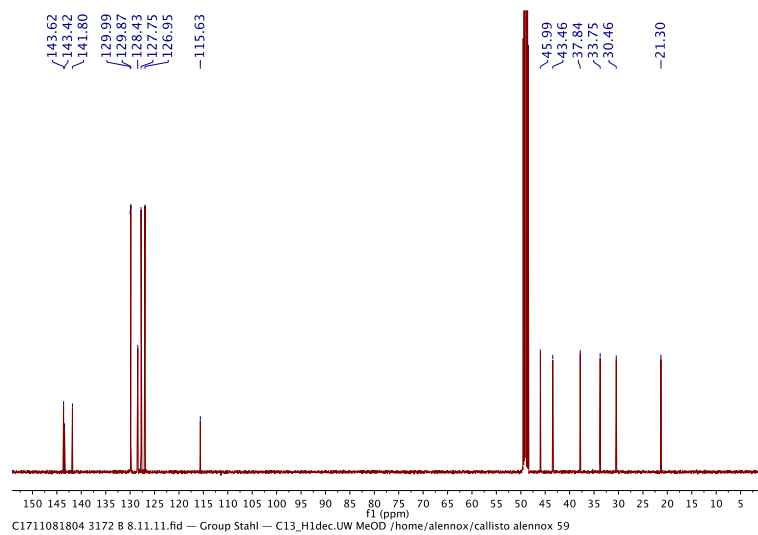
Spectra

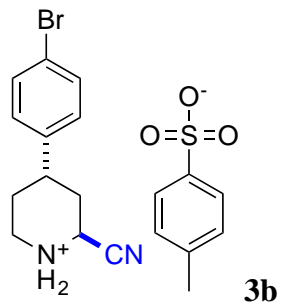


^1H NMR (500 MHz, Methanol- d_4):

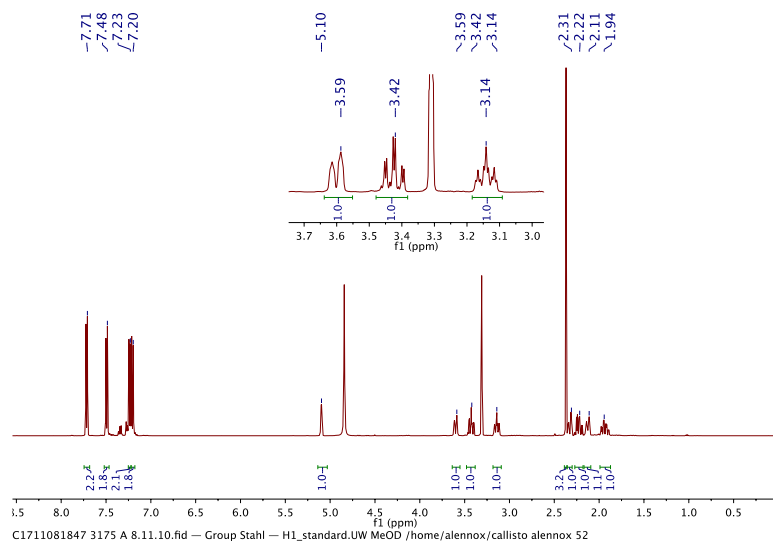


^{13}C NMR (126 MHz, Methanol- d_4):

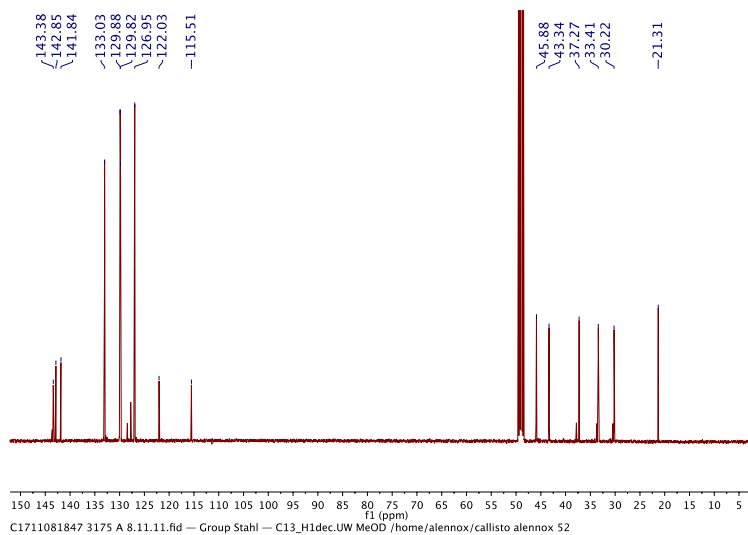


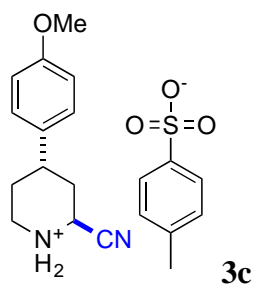


^1H NMR (500 MHz, Methanol- d_4):

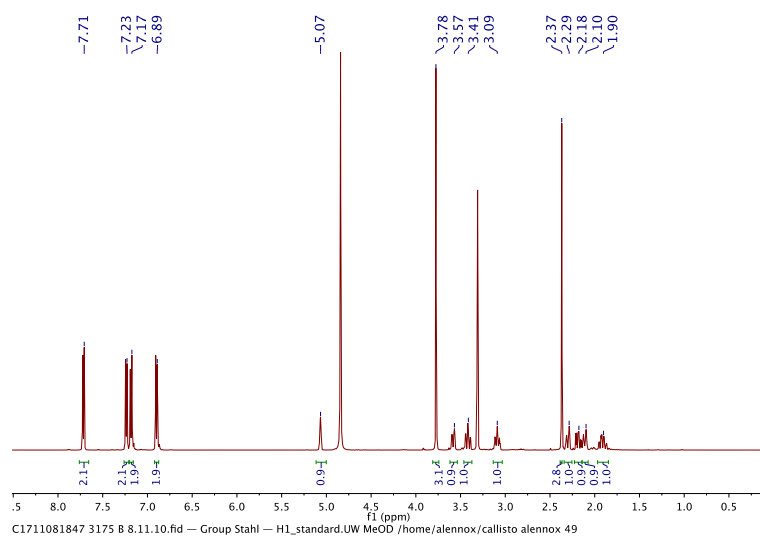


^{13}C NMR (126 MHz, Methanol- d_4):

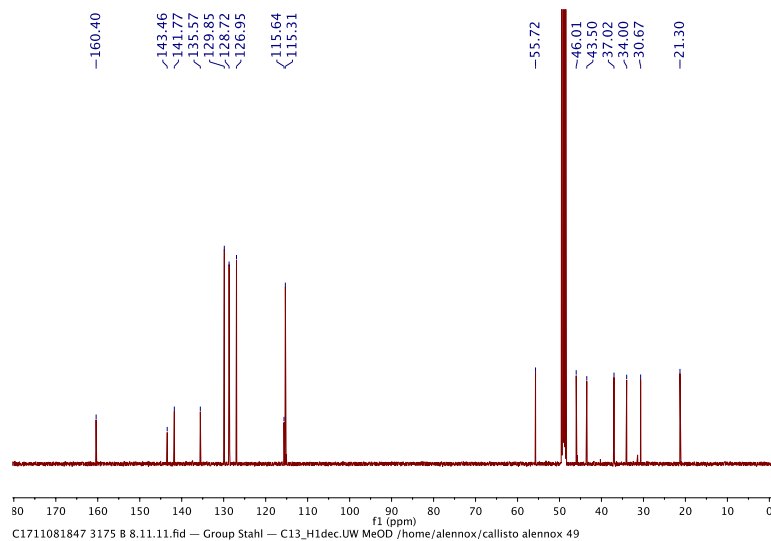


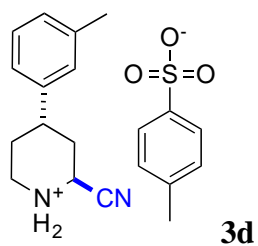


^1H NMR (500 MHz, Methanol- d_4):

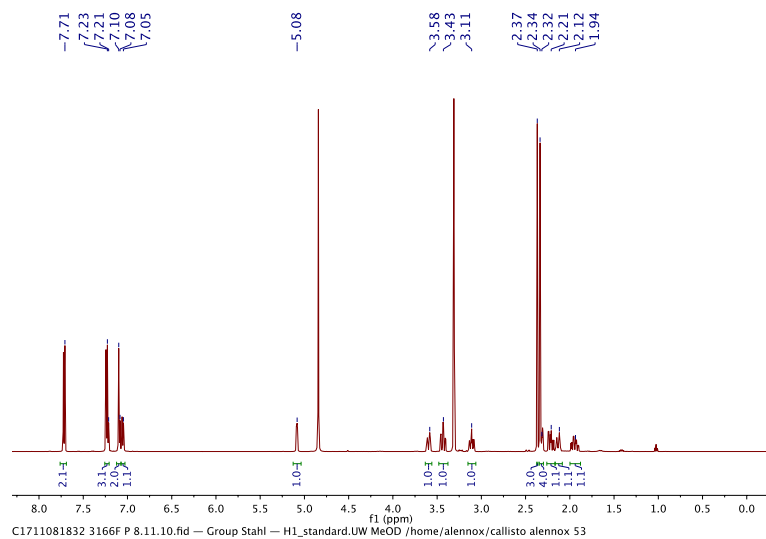


^{13}C NMR (126 MHz, Methanol- d_4):

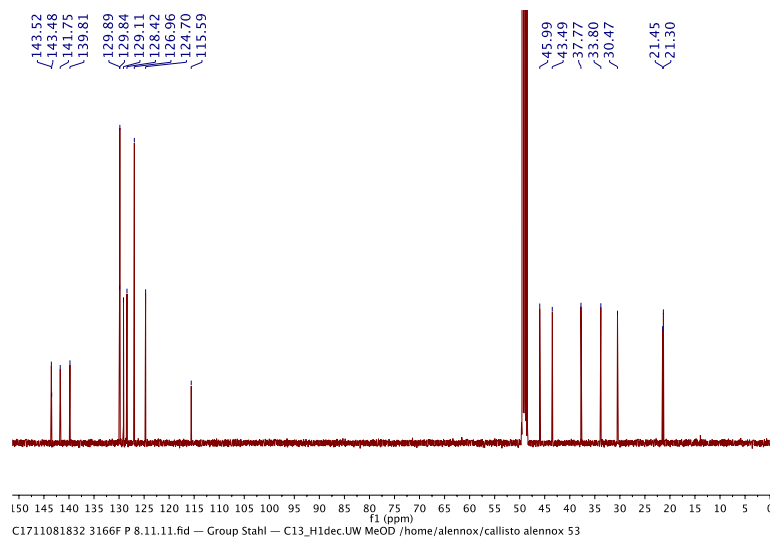


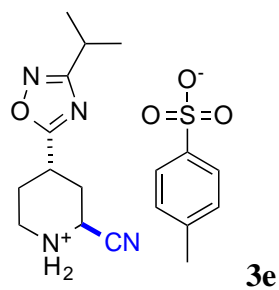


$^1\text{H NMR}$ (500 MHz, Methanol- d_4):

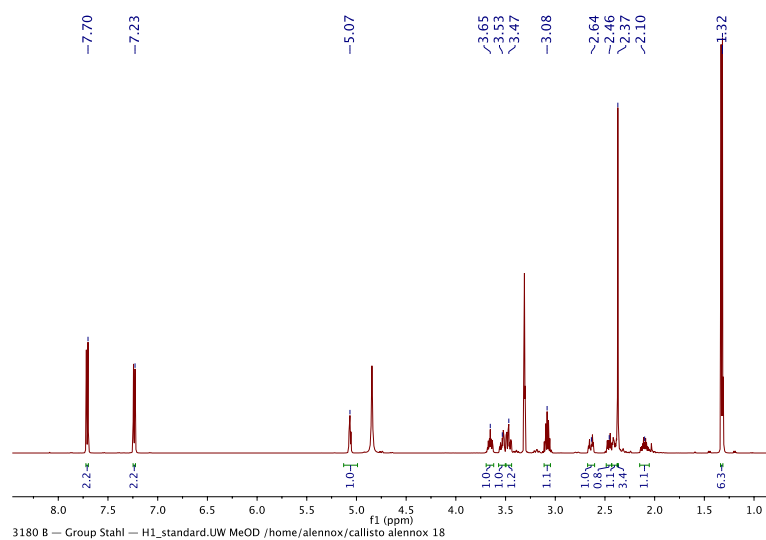


$^{13}\text{C NMR}$ (126 MHz, Methanol- d_4):

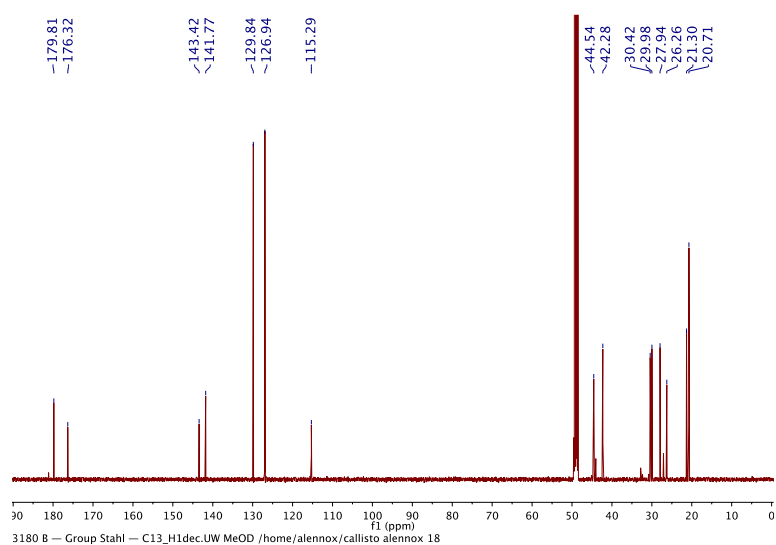


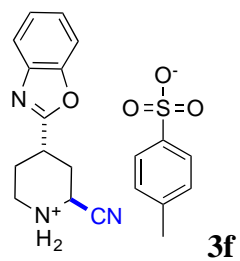


^1H NMR (500 MHz, Methanol- d_4):

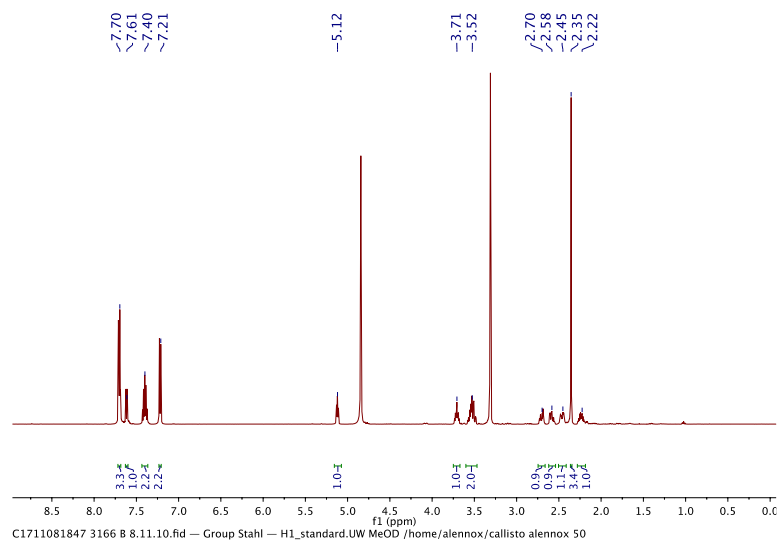


^{13}C NMR (126 MHz, Methanol- d_4):

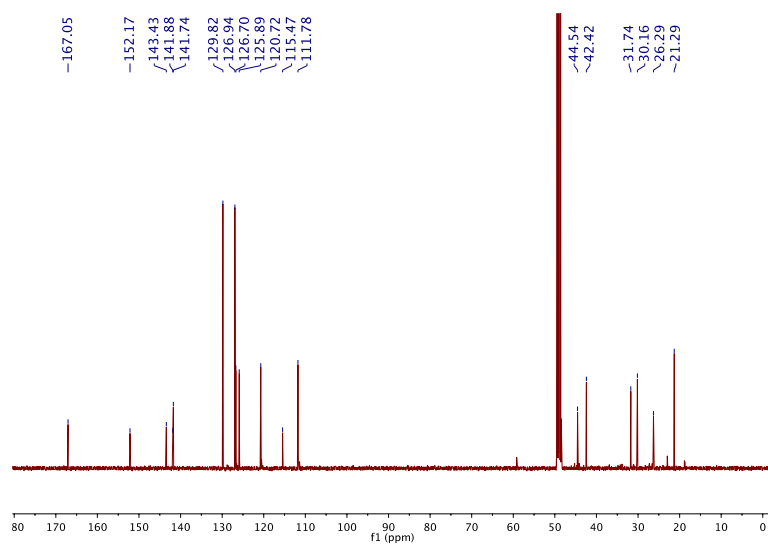


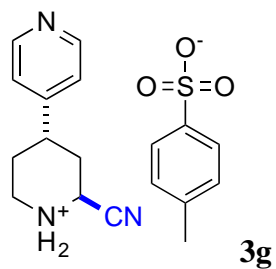


^1H NMR (500 MHz, Methanol- d_4):

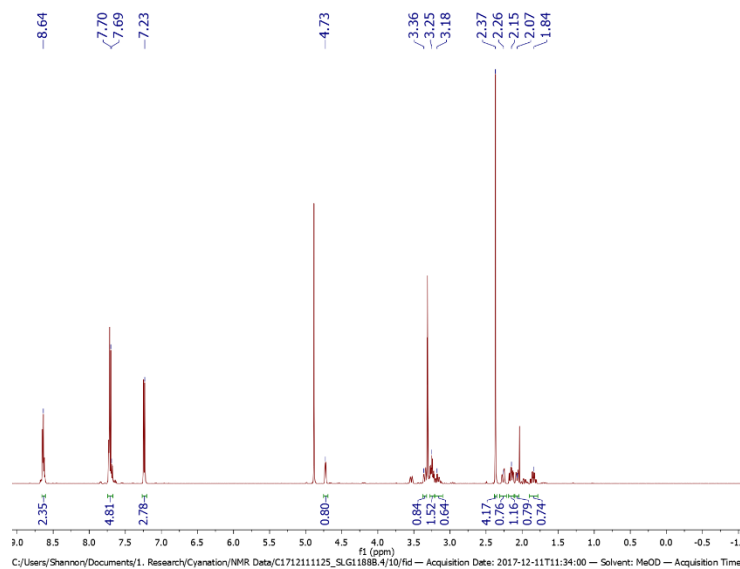


^{13}C NMR (126 MHz, Methanol- d_4):

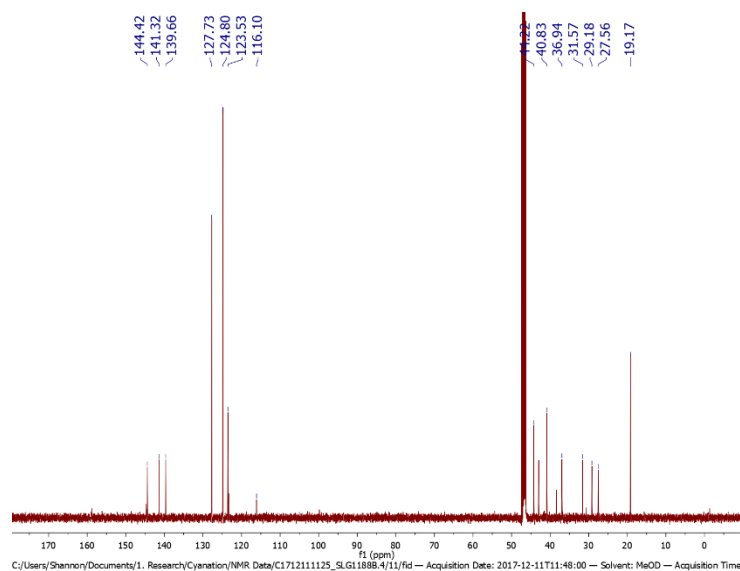


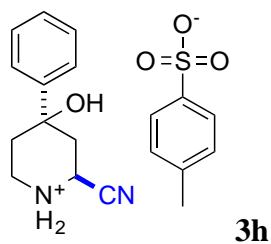


^1H NMR (500 MHz, Methanol- d_4):

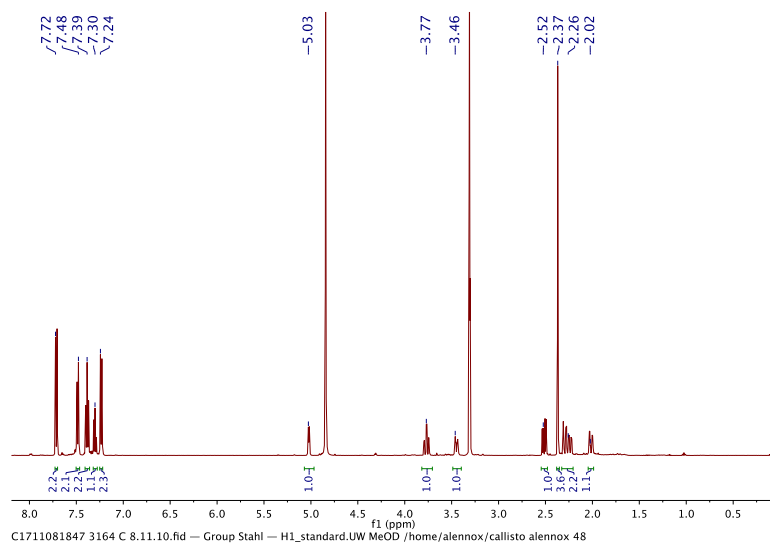


^{13}C NMR (126 MHz, Methanol- d_4):

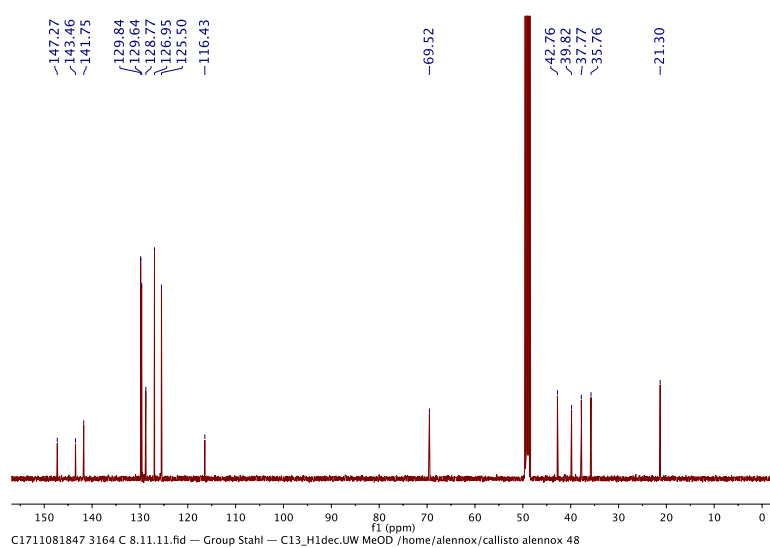


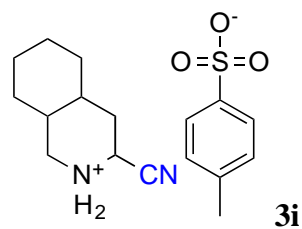


^1H NMR (500 MHz, Methanol- d_4):

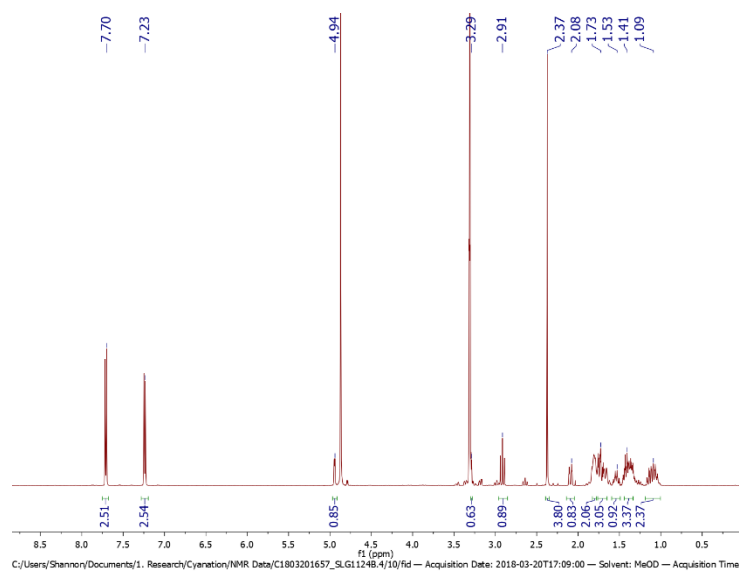


^{13}C NMR (126 MHz, Methanol- d_4):

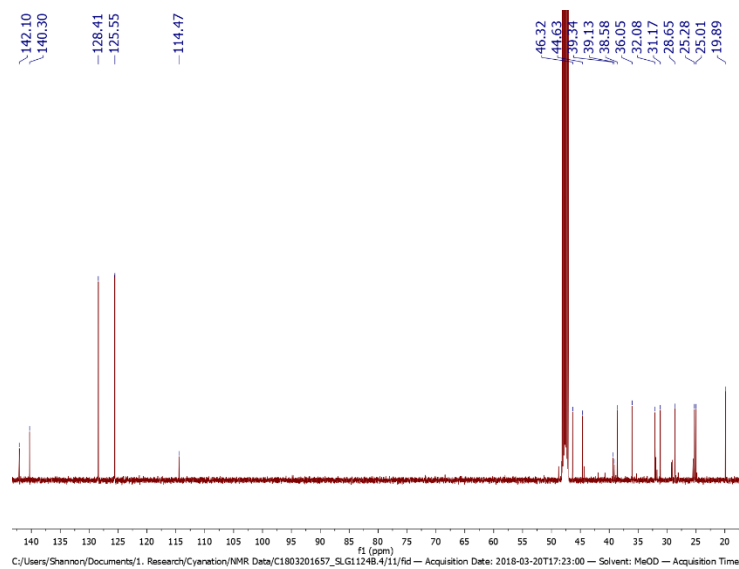


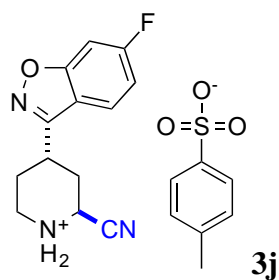


$^1\text{H NMR}$ (500 MHz, Methanol- d_4):

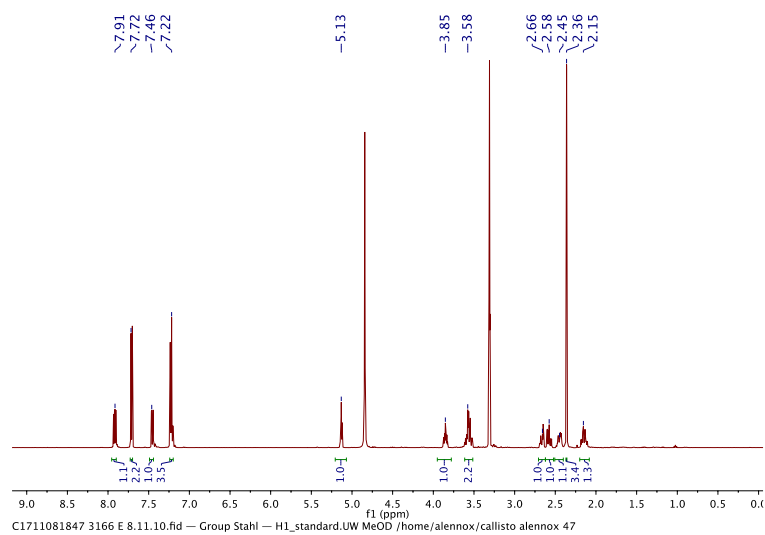


$^{13}\text{C NMR}$ (126 MHz, Methanol- d_4):

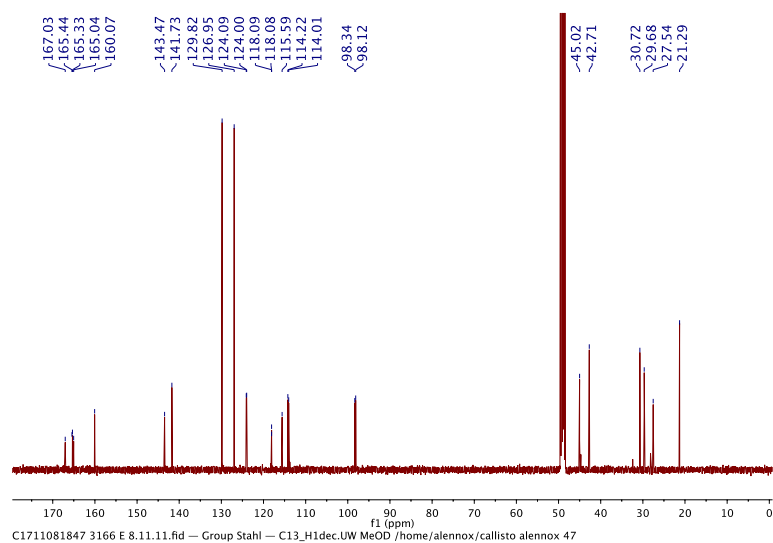


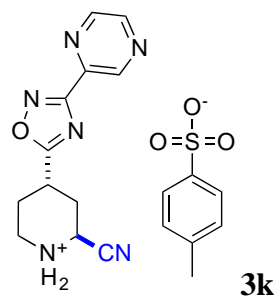


^1H NMR (500 MHz, Methanol- d_4):

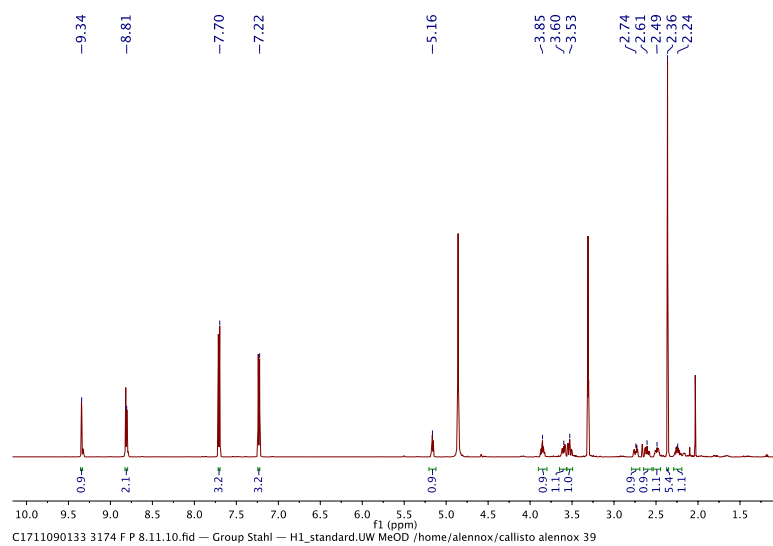


^{13}C NMR (126 MHz, Methanol- d_4):

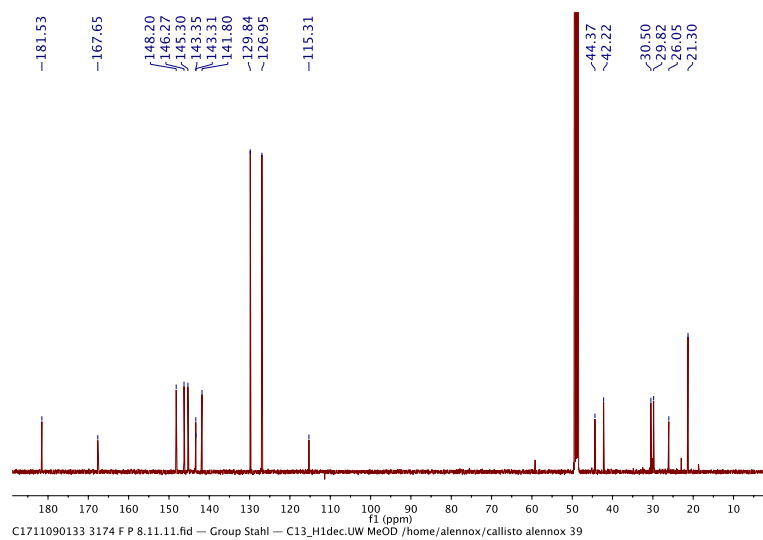


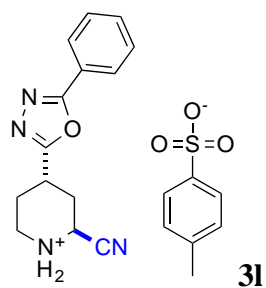


$^1\text{H NMR}$ (500 MHz, Methanol- d_4):

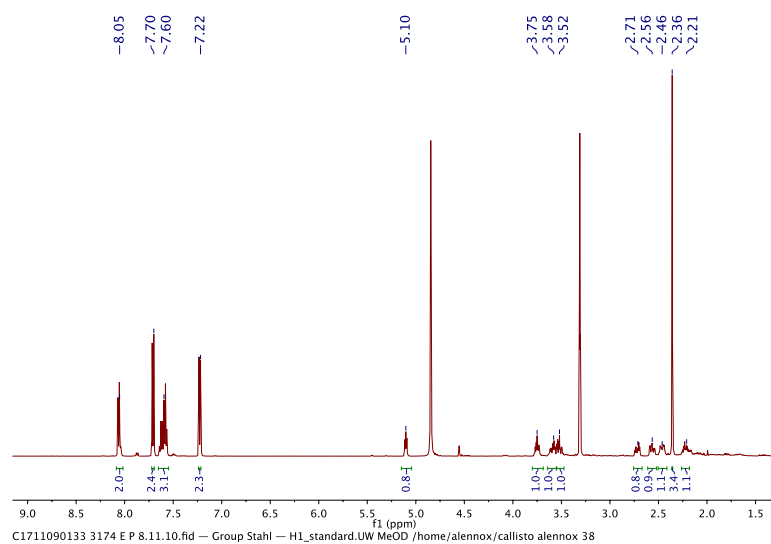


$^{13}\text{C NMR}$ (126 MHz, Methanol- d_4):

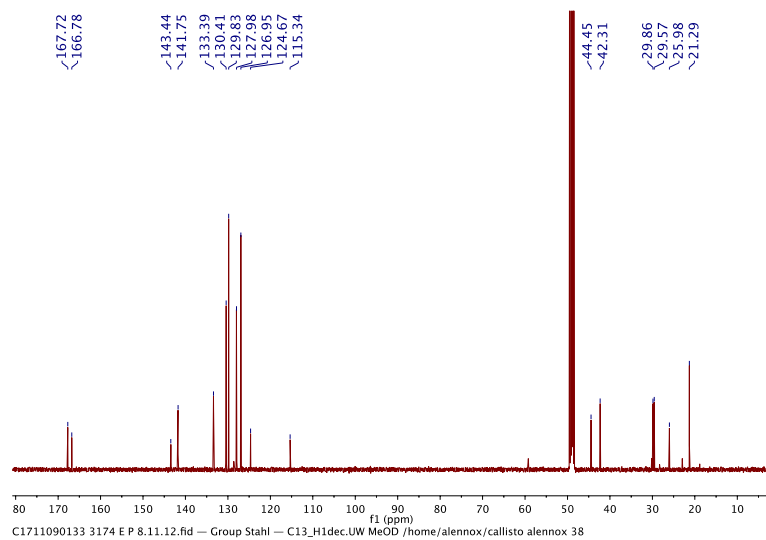


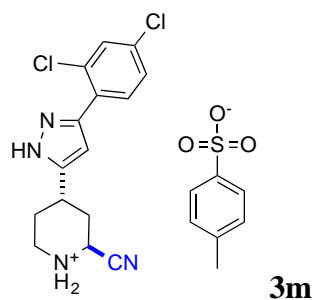


^1H NMR (500 MHz, Methanol- d_4):

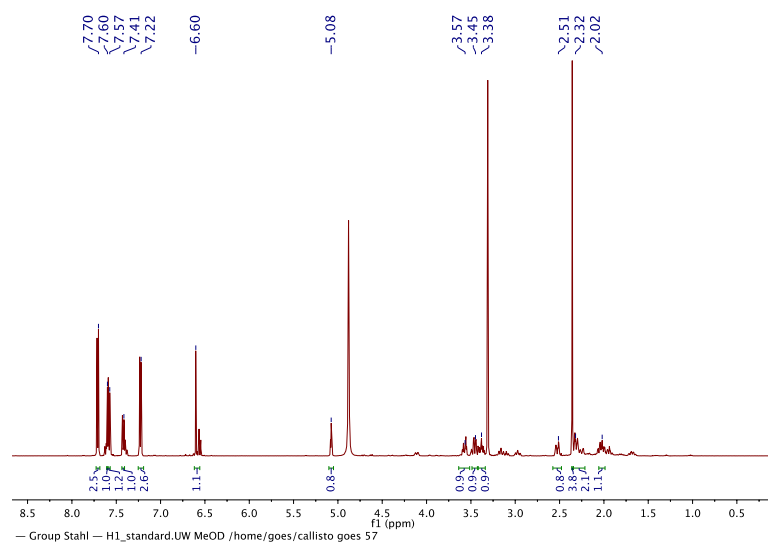


^{13}C NMR (126 MHz, Methanol- d_4):

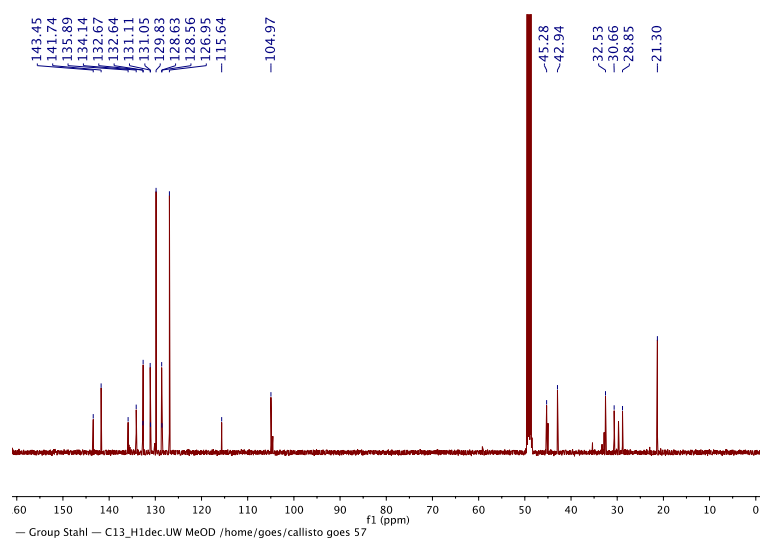


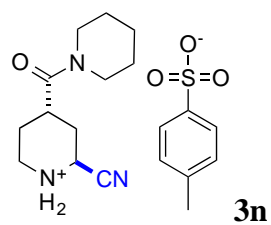


^1H NMR (500 MHz, Methanol- d_4):

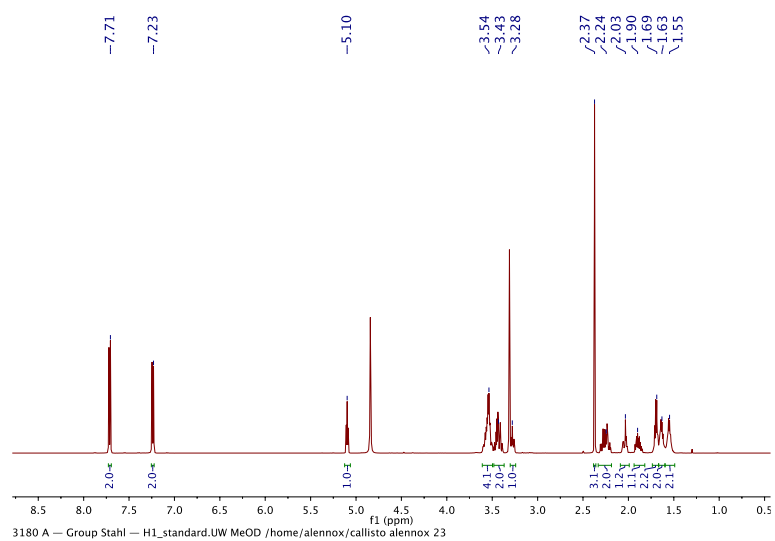


^{13}C NMR (126 MHz, Methanol- d_4):

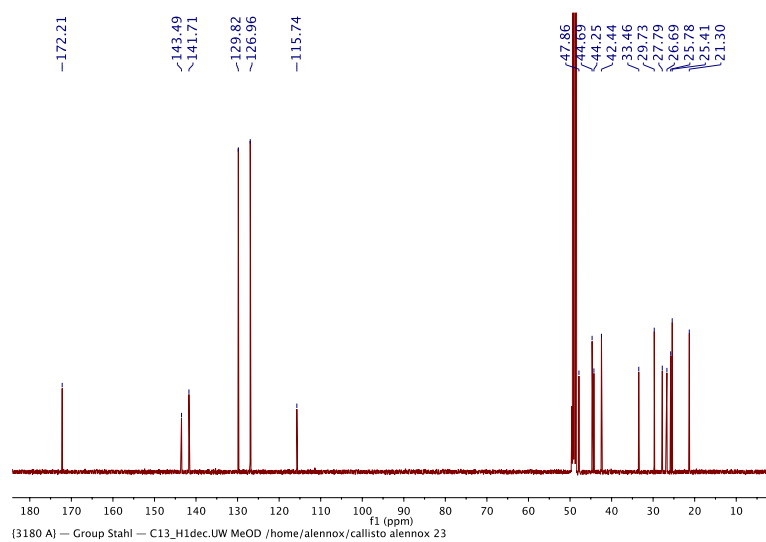


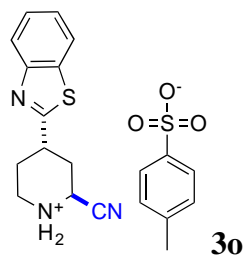


^1H NMR (500 MHz, Methanol- d_4):

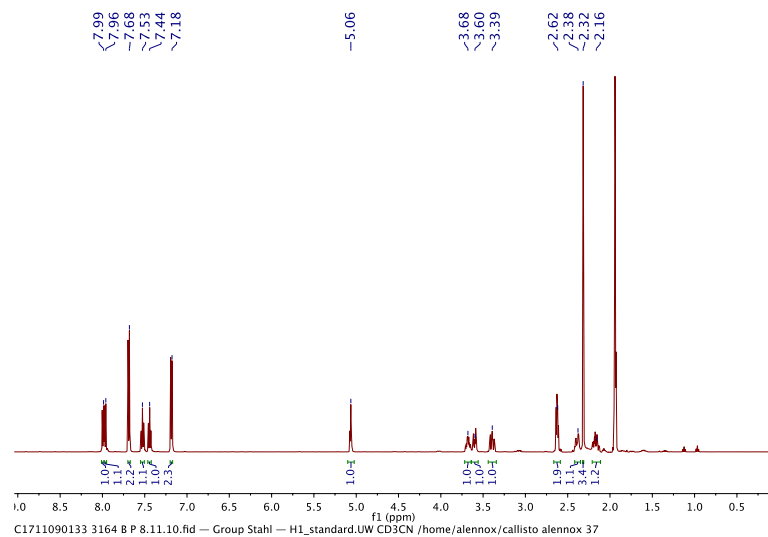


^{13}C NMR (126 MHz, Methanol- d_4):

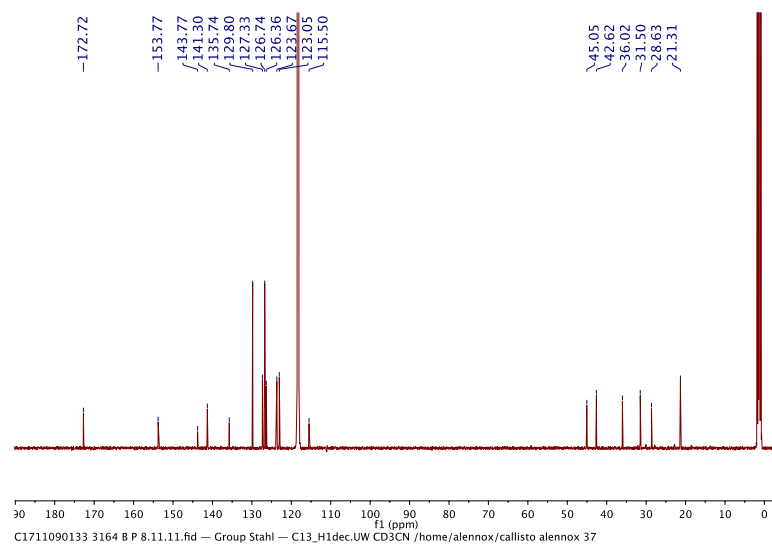


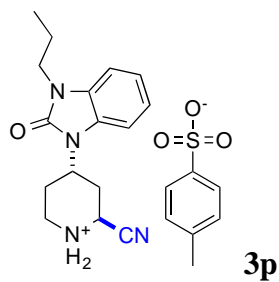


$^1\text{H NMR}$ (500 MHz, Acetonitrile- d_3):

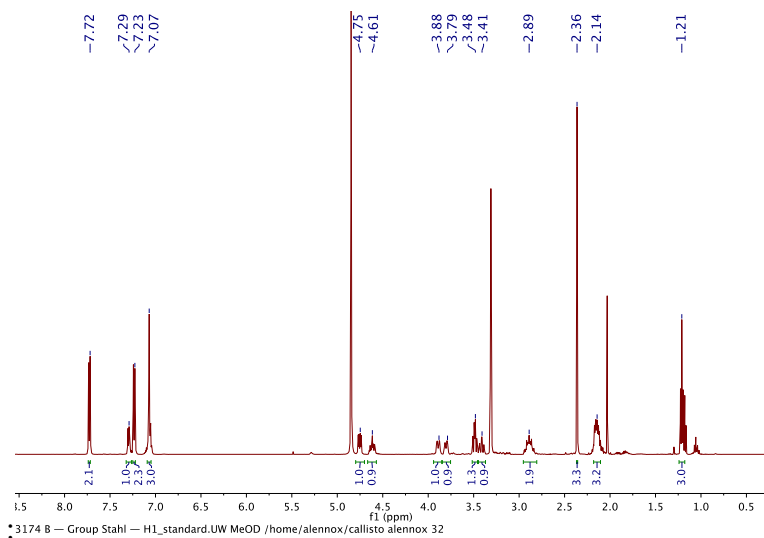


$^{13}\text{C NMR}$ (126 MHz, Acetonitrile- d_3):

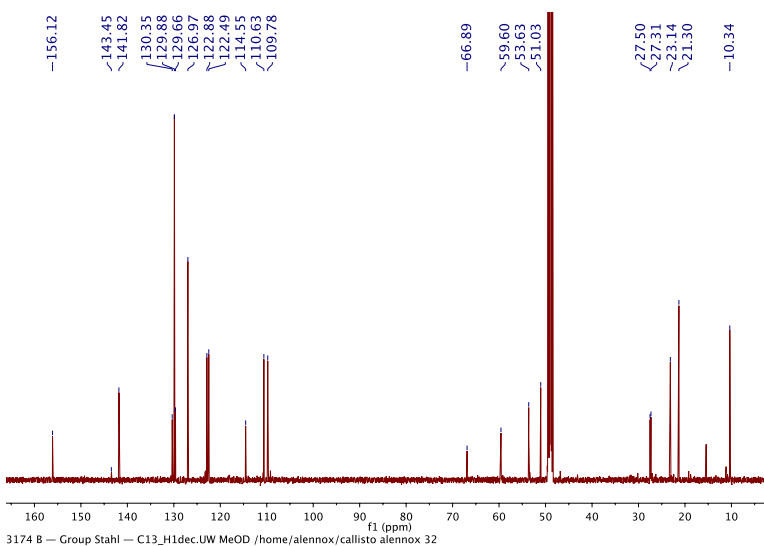


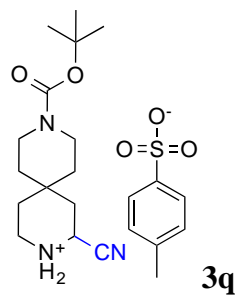


¹H NMR (500 MHz, Methanol-*d*₄)

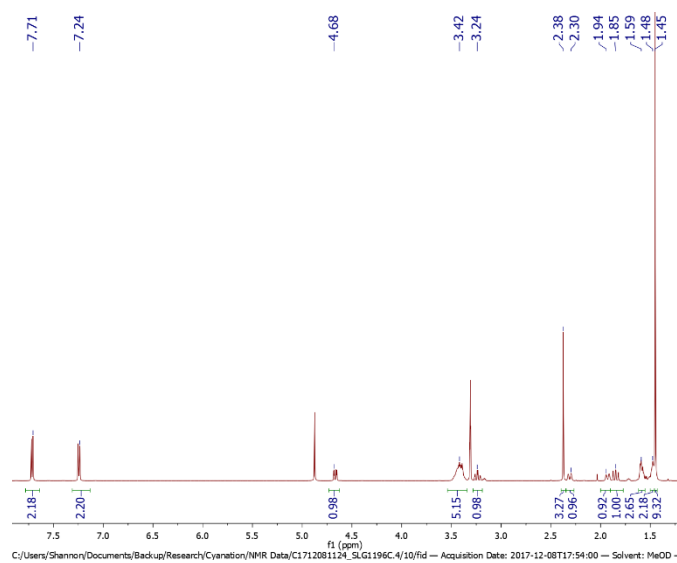


¹³C NMR (126 MHz, Methanol-*d*₄):

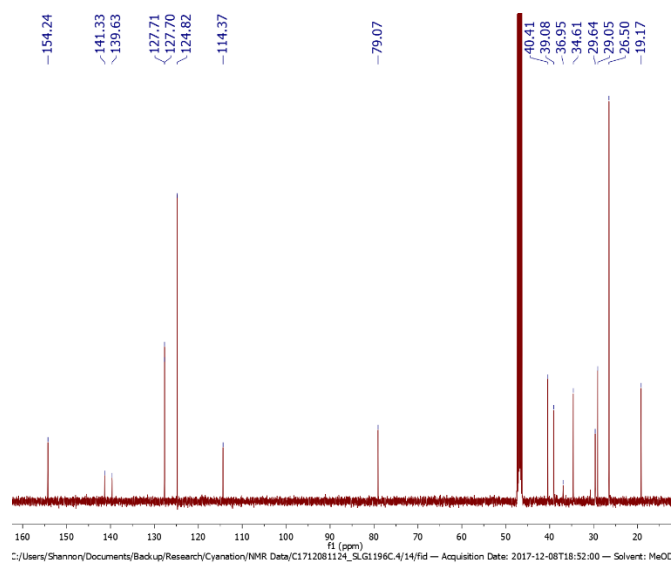


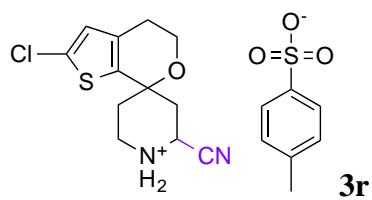


^1H NMR (500 MHz, Methanol- d_4):

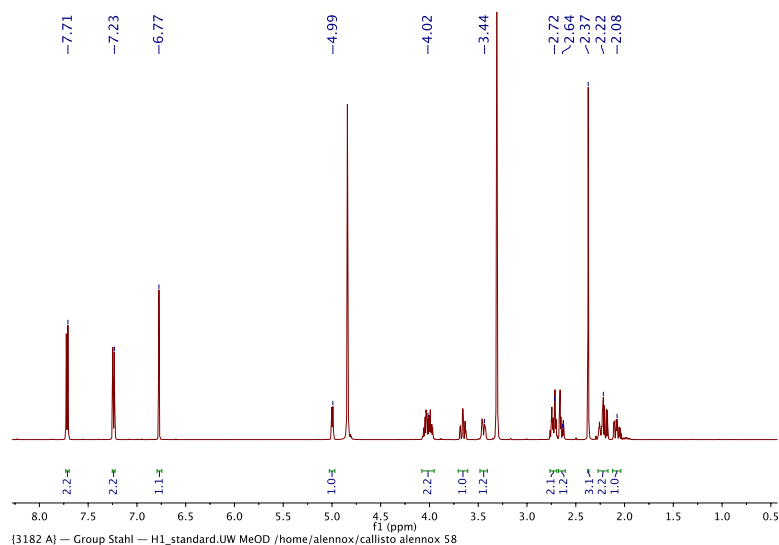


^{13}C NMR (126 MHz, Methanol- d_4):

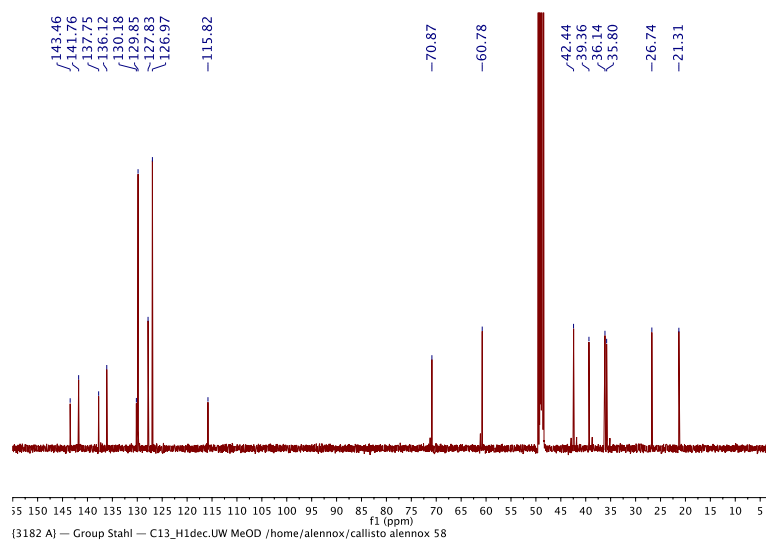


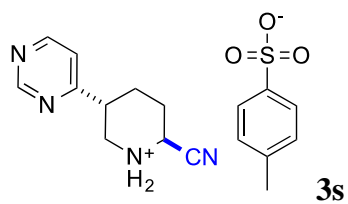


^1H NMR (500 MHz, Methanol- d_4):

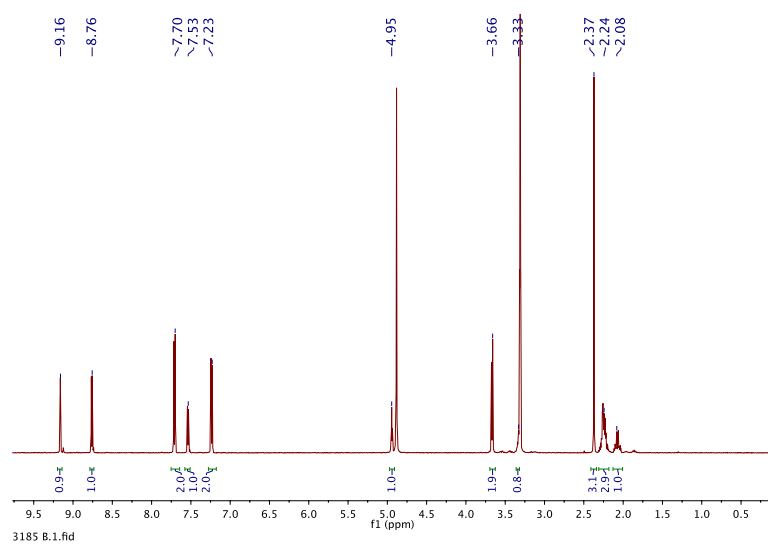


^{13}C NMR (126 MHz, Methanol- d_4):

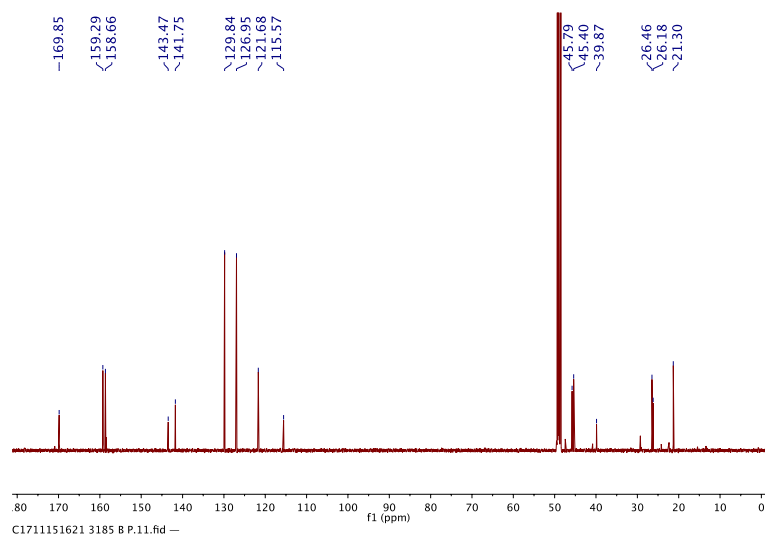


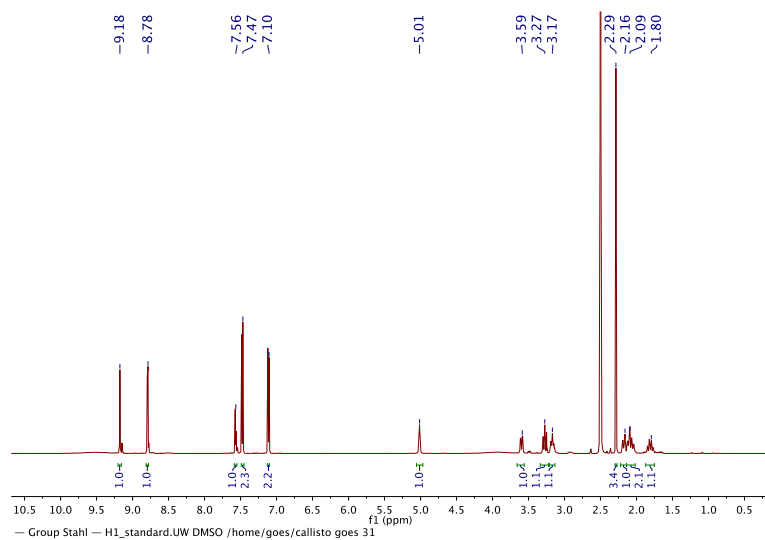
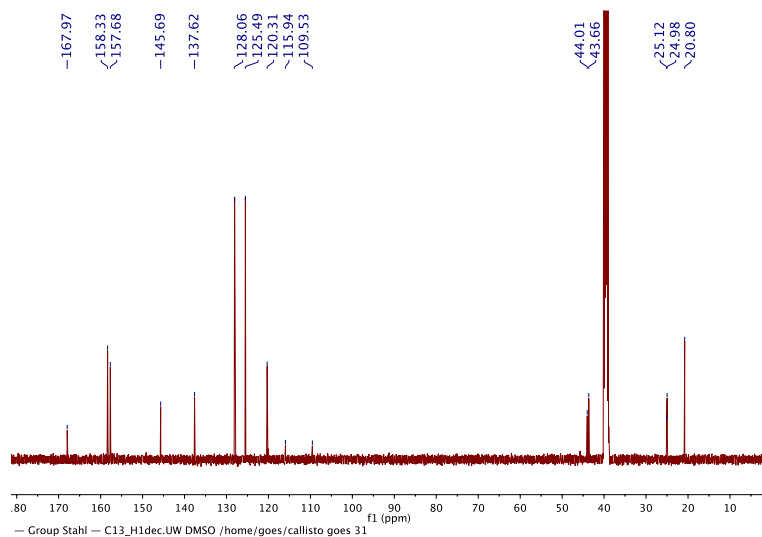


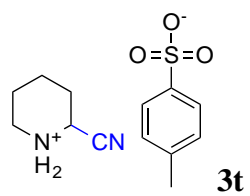
$^1\text{H NMR}$ (500 MHz, Methanol- d_4):



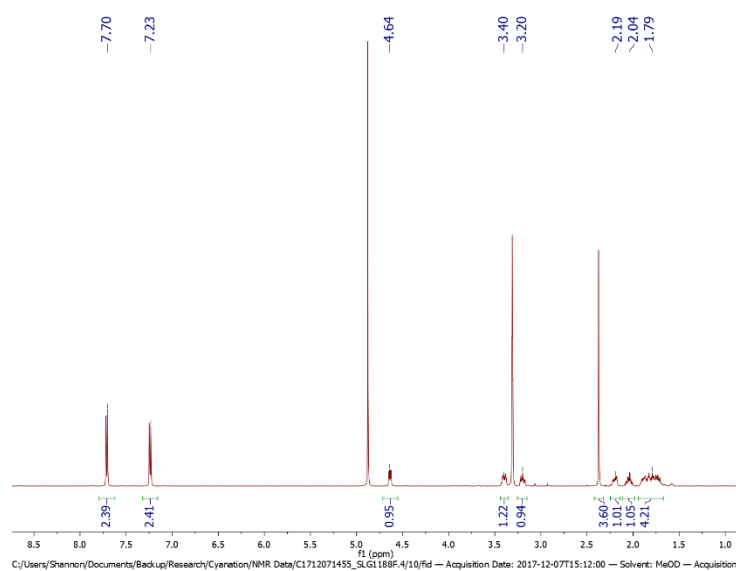
$^{13}\text{C NMR}$ (126 MHz, Methanol- d_4):



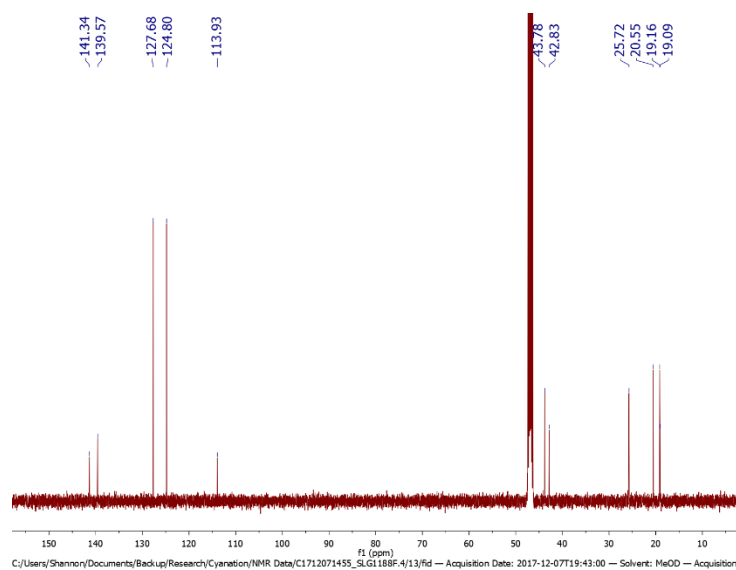
^1H NMR (500 MHz, $\text{DMSO-}d_6$): **^{13}C NMR (126 MHz, $\text{DMSO-}d_6$):**

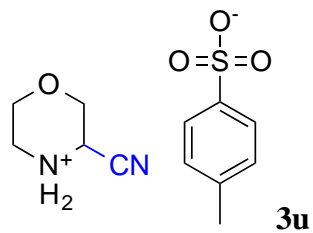


^1H NMR (500 MHz, Methanol- d_4):

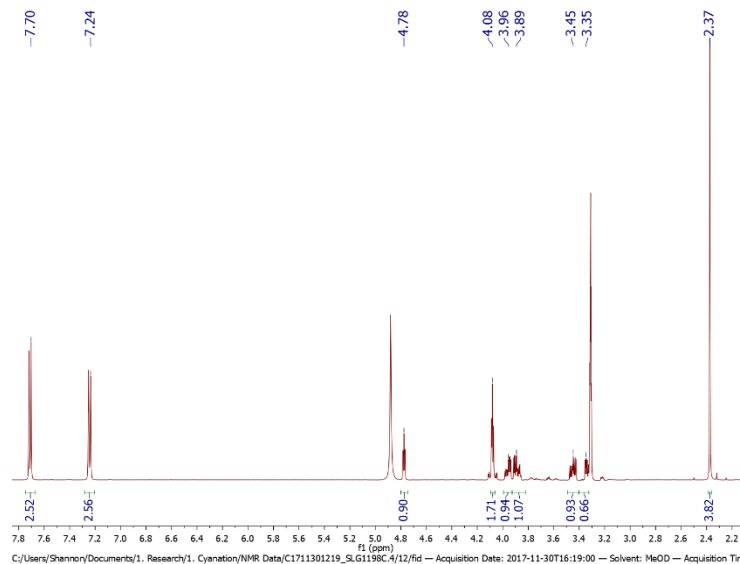


^{13}C NMR (126 MHz, Methanol- d_4):

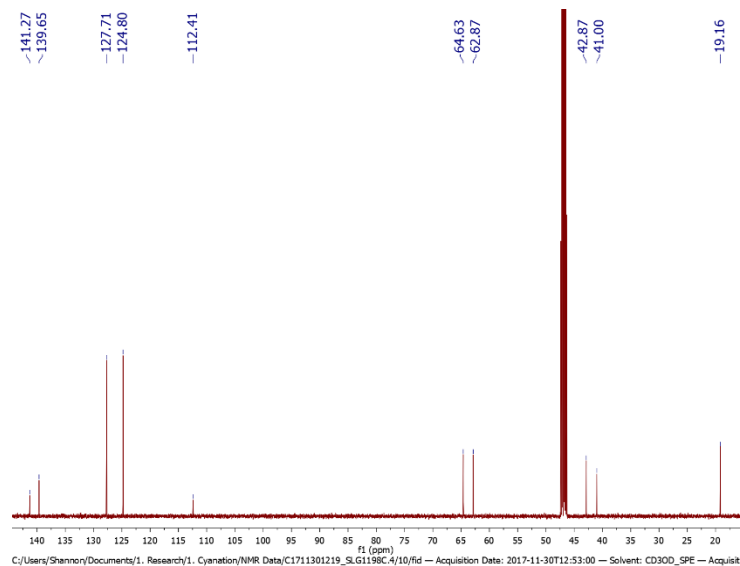


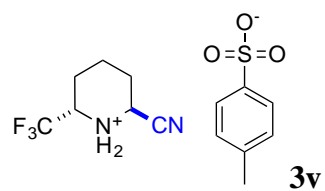


^1H NMR (500 MHz, Methanol- d_4):

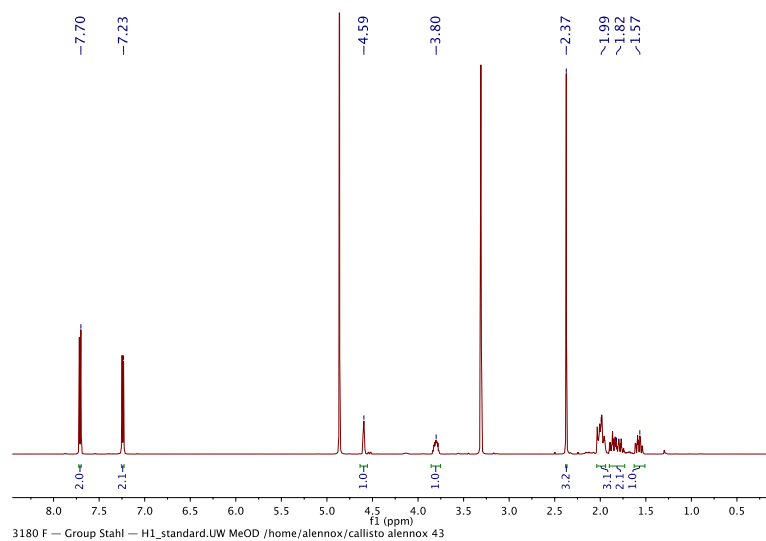


^{13}C NMR (126 MHz, Methanol- d_4):

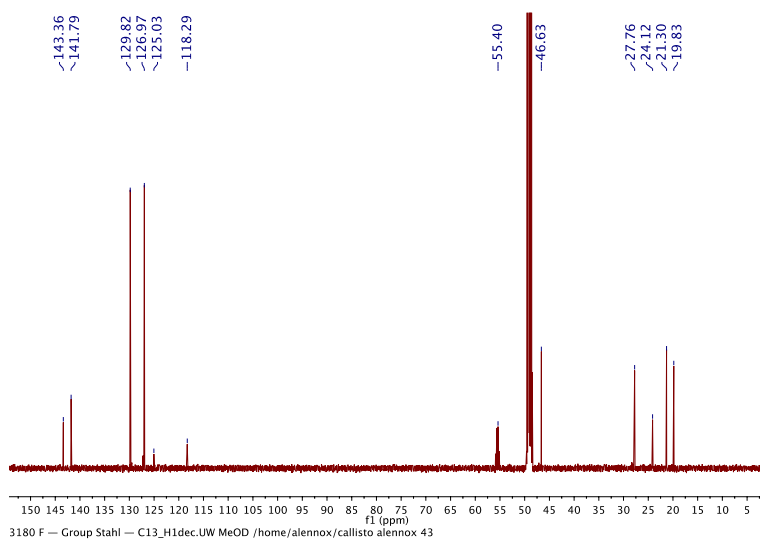


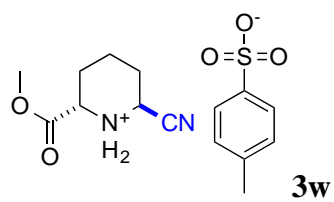


^1H NMR (500 MHz, Methanol- d_4):

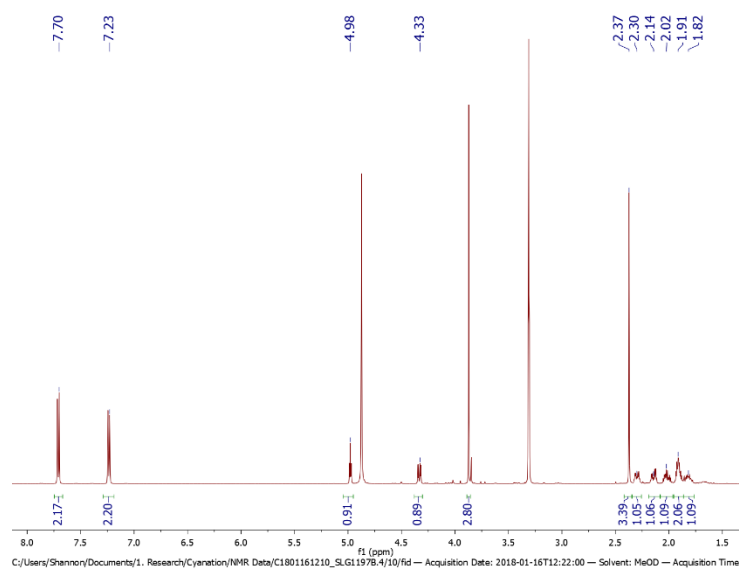


^{13}C NMR (126 MHz, Methanol- d_4):

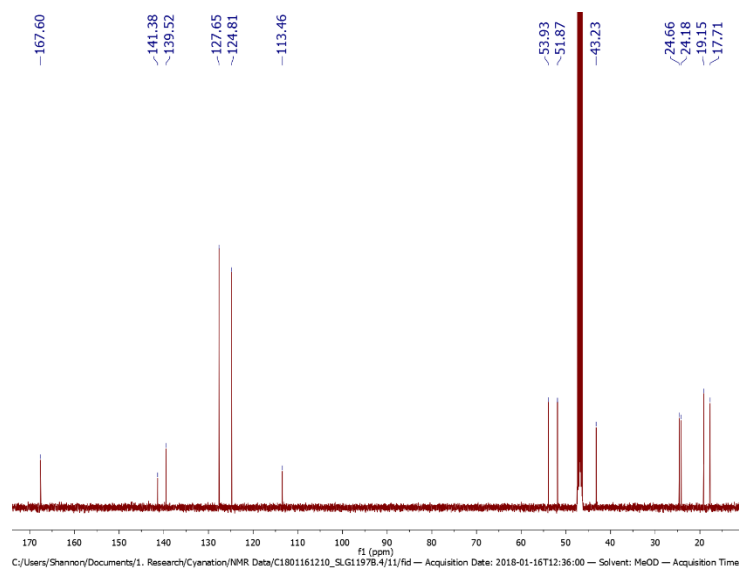


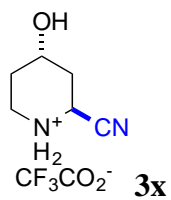


¹H NMR (500 MHz, Methanol-*d*₄):

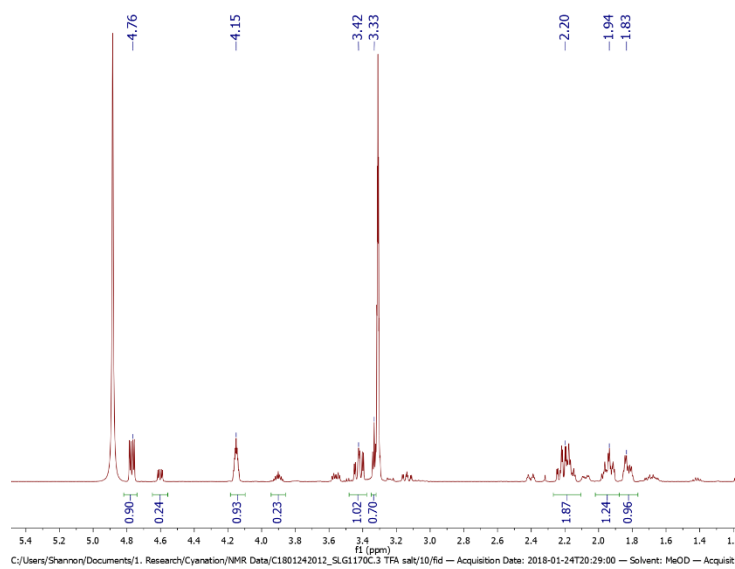


¹³C NMR (126 MHz, Methanol-*d*₄):

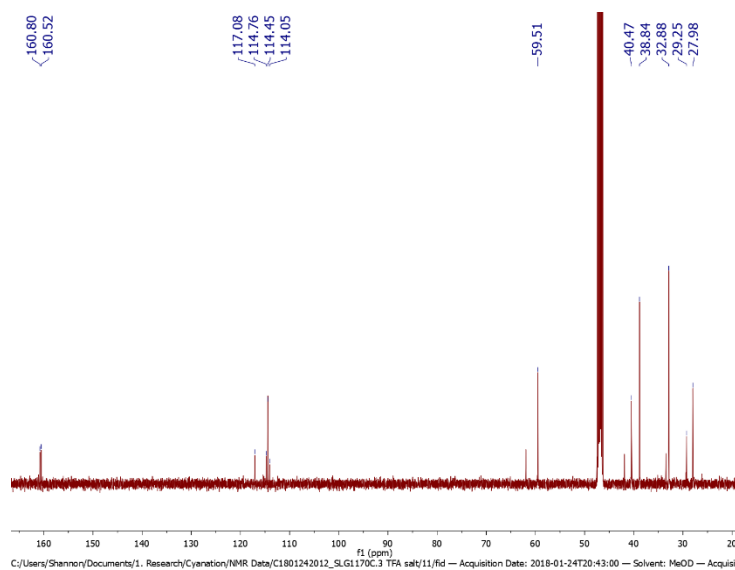


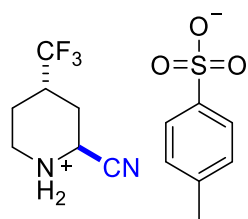


^1H NMR (500 MHz, Methanol- d_4):

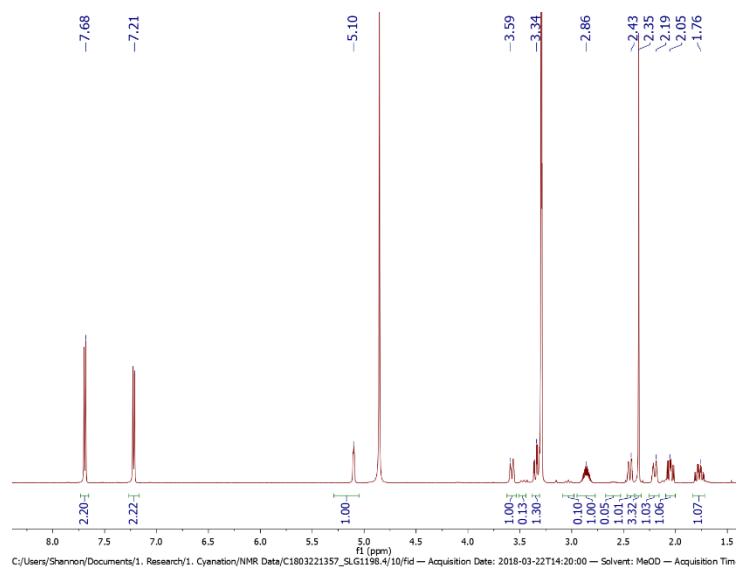


^{13}C NMR (126 MHz, Methanol- d_4):

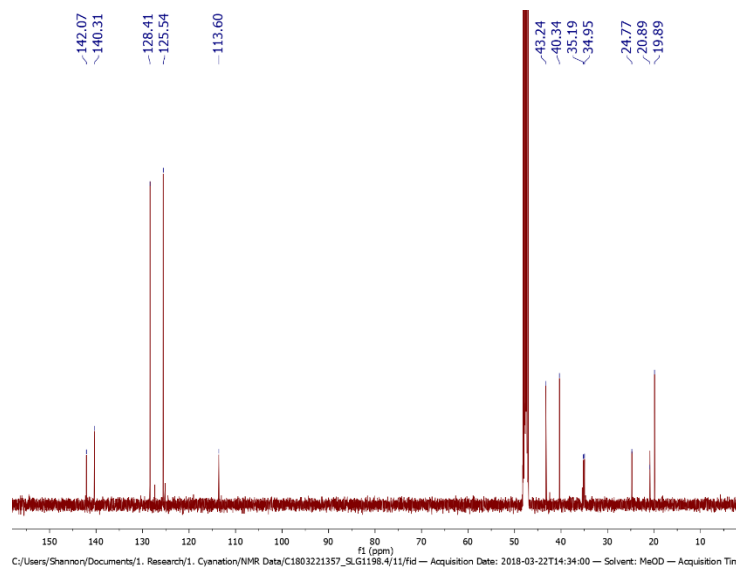


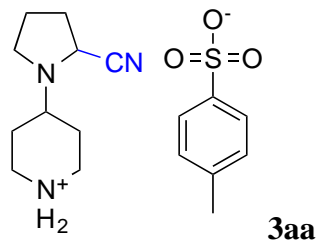


^1H NMR (500 MHz, Methanol- d_4):

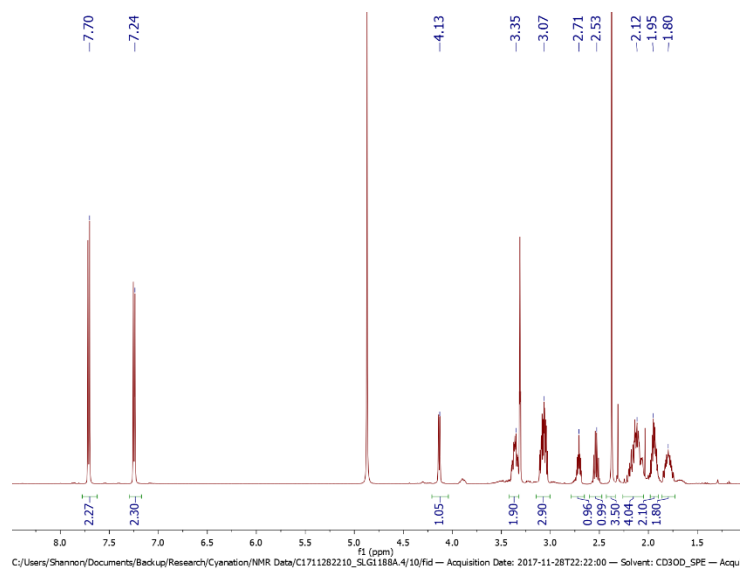


^{13}C NMR (500 MHz, Methanol- d_4):

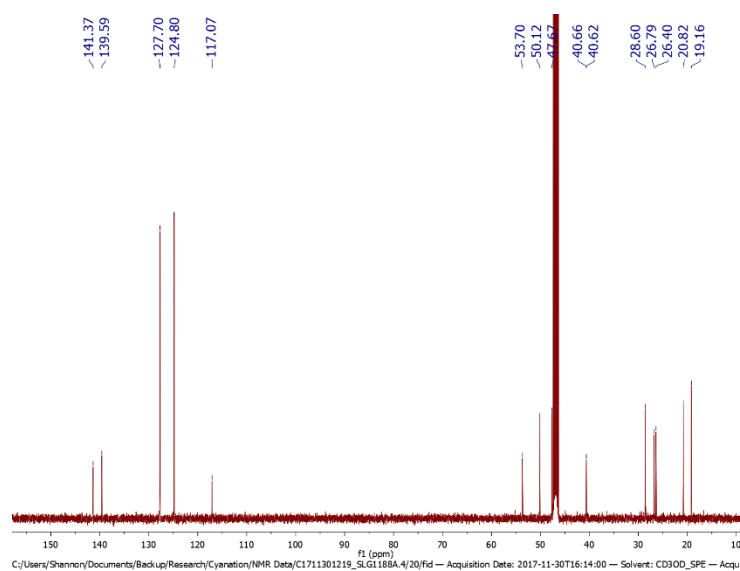


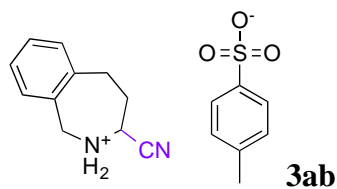


^1H NMR (500 MHz, Methanol- d_4):

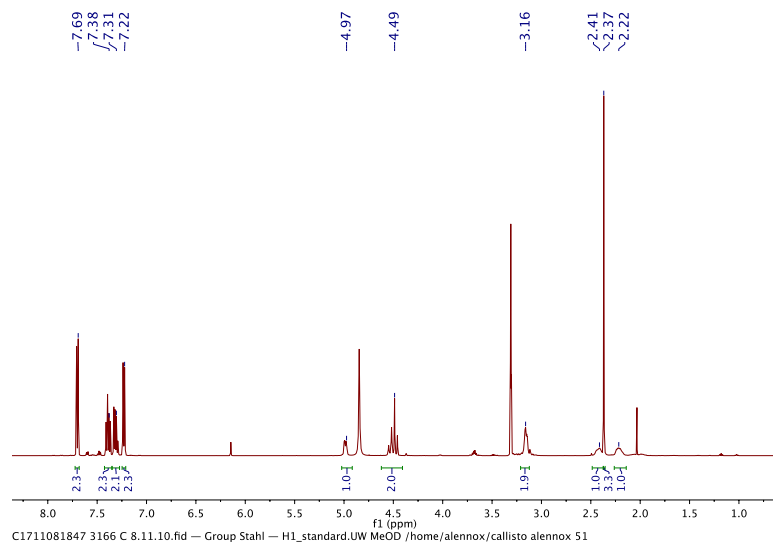


^{13}C NMR (126 MHz, Methanol- d_4):

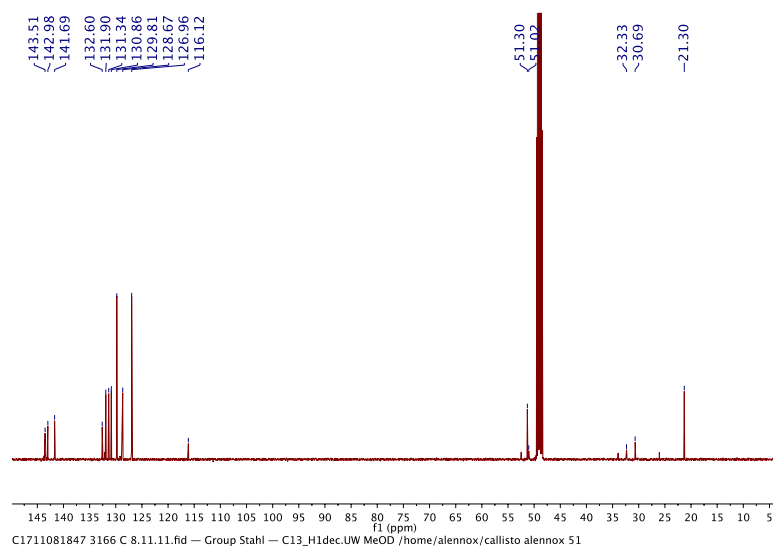


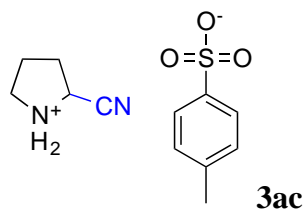


^1H NMR (500 MHz, Methanol- d_4):

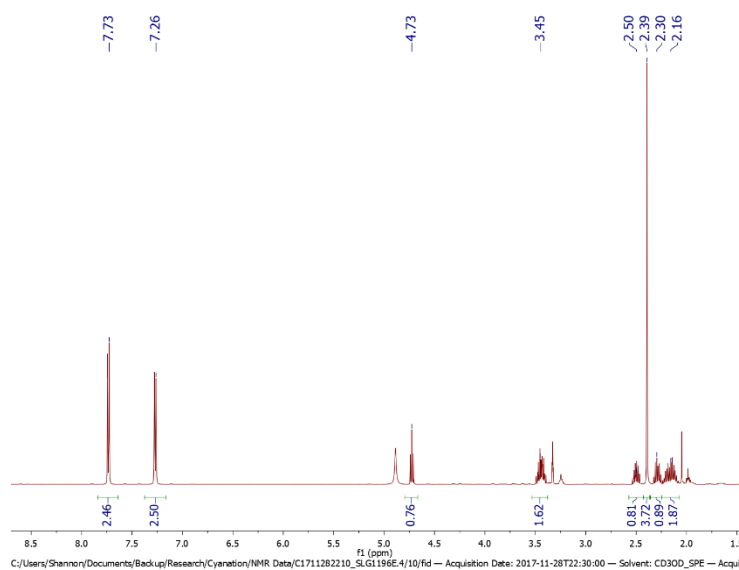


^{13}C NMR (126 MHz, Methanol- d_4):

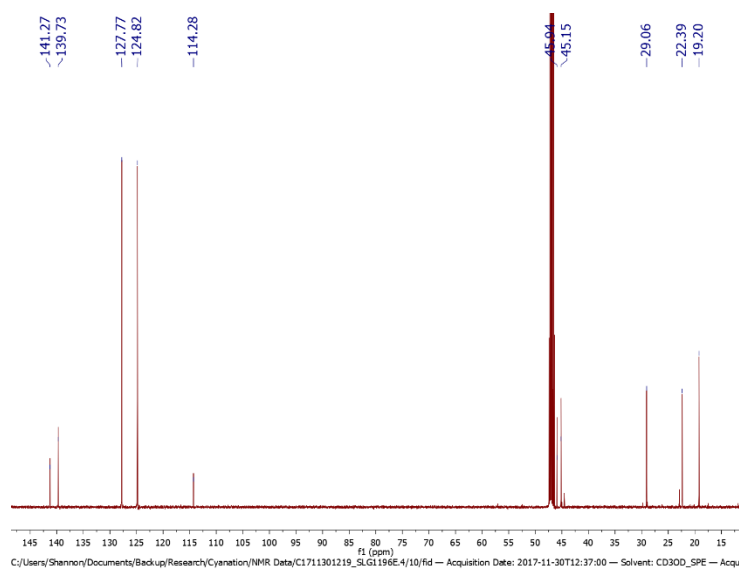


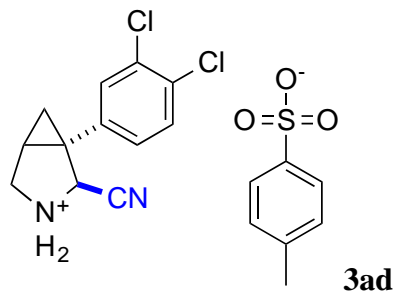


^1H NMR (500 MHz, Methanol- d_4):

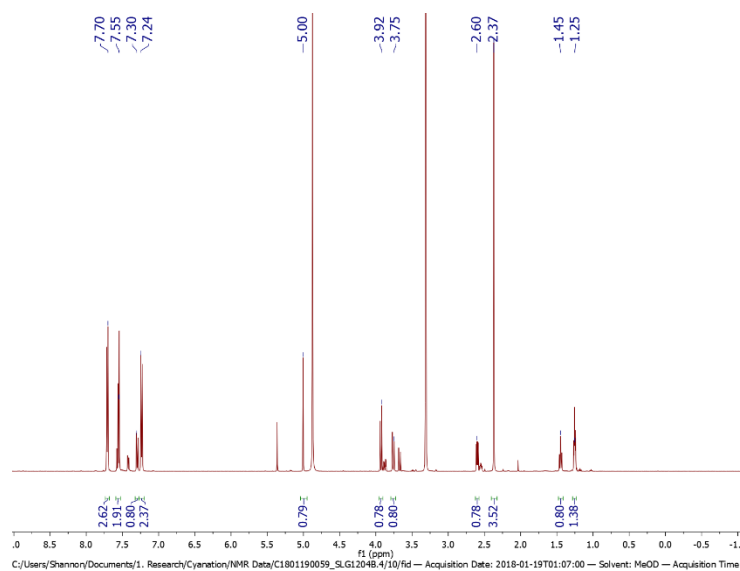


^{13}C NMR (126 MHz, Methanol- d_4):

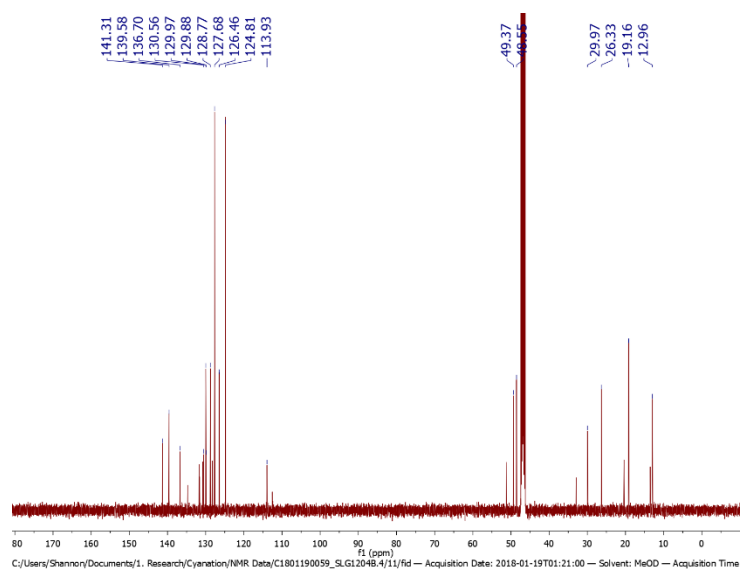




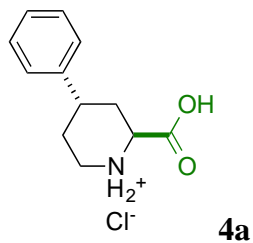
$^1\text{H NMR}$ (500 MHz, Methanol- d_4):



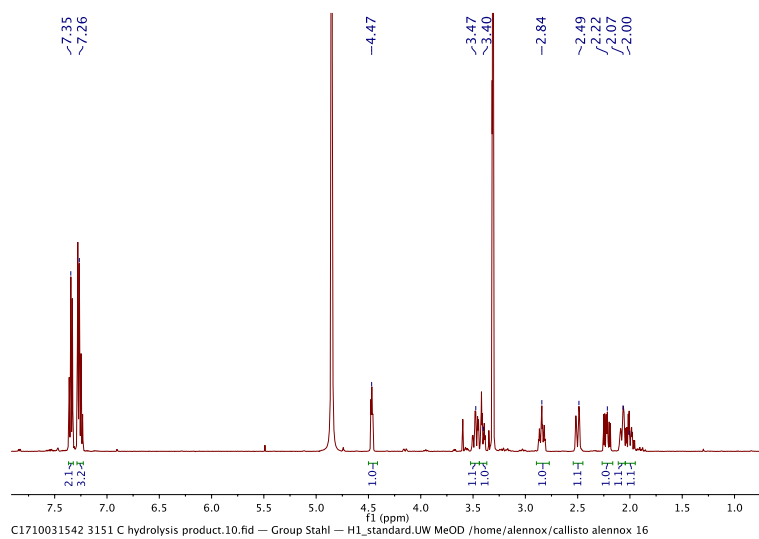
$^{13}\text{C NMR}$ (126 MHz, Methanol- d_4):



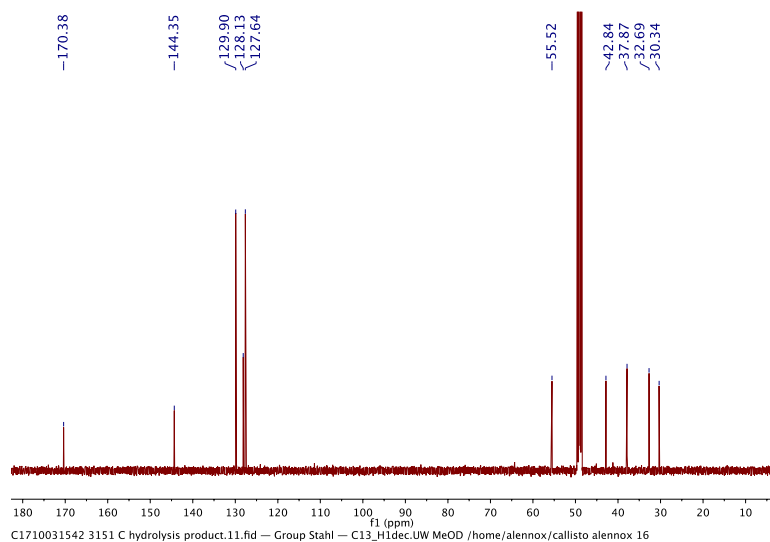
Hydrolysis products

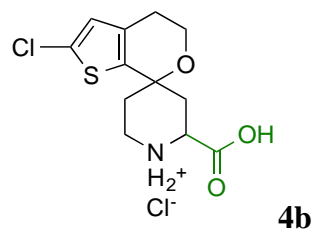


^1H NMR (500 MHz, Methanol- d_4):

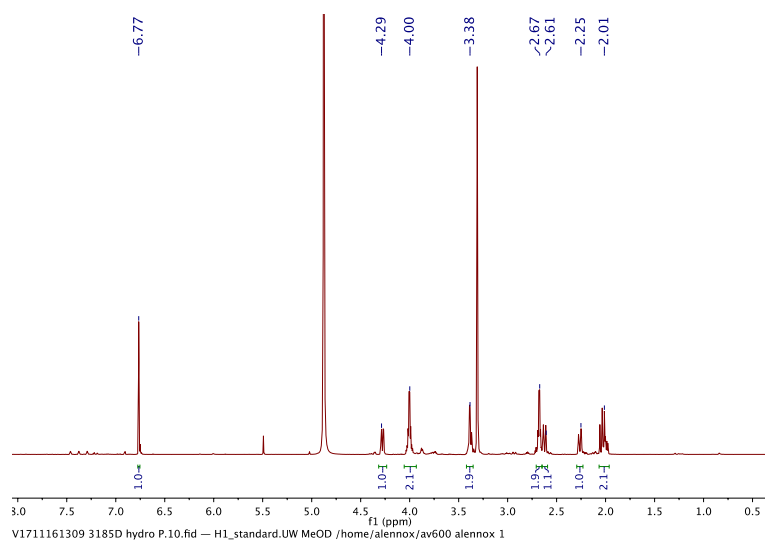


^{13}C NMR (126 MHz, Methanol- d_4):

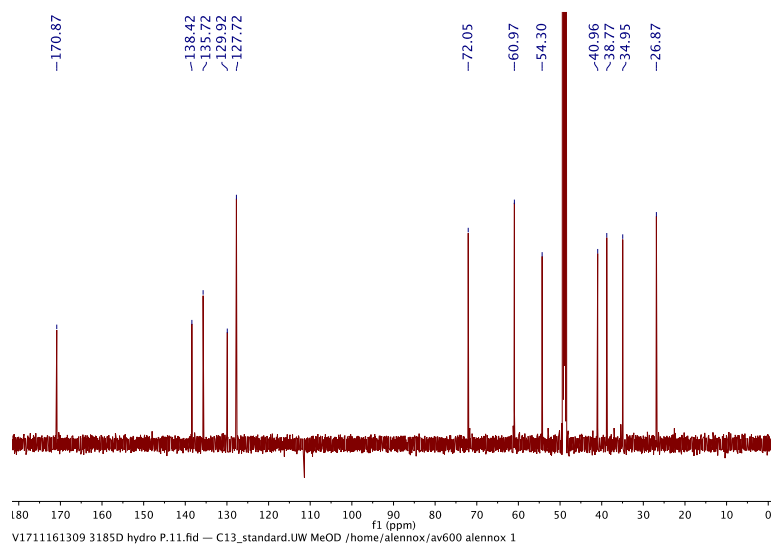


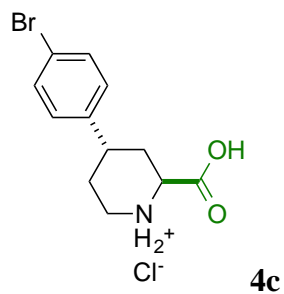


$^1\text{H NMR}$ (500 MHz, Methanol- d_4):

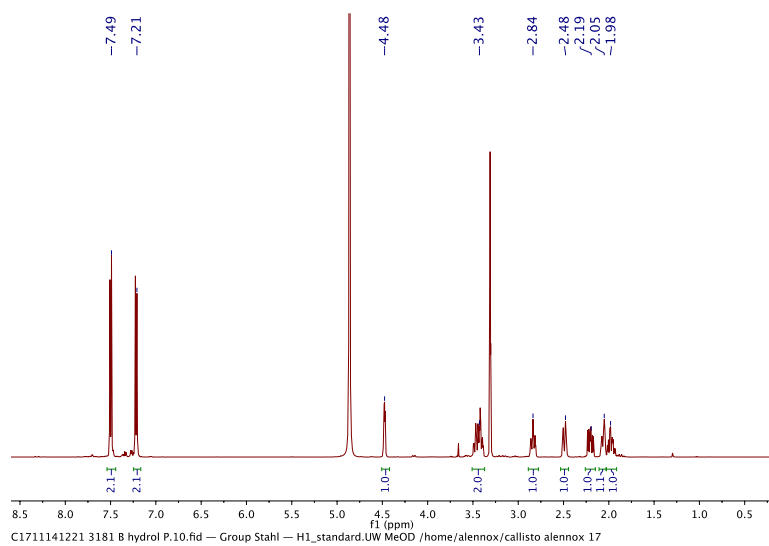


$^{13}\text{C NMR}$ (126 MHz, Methanol- d_4):

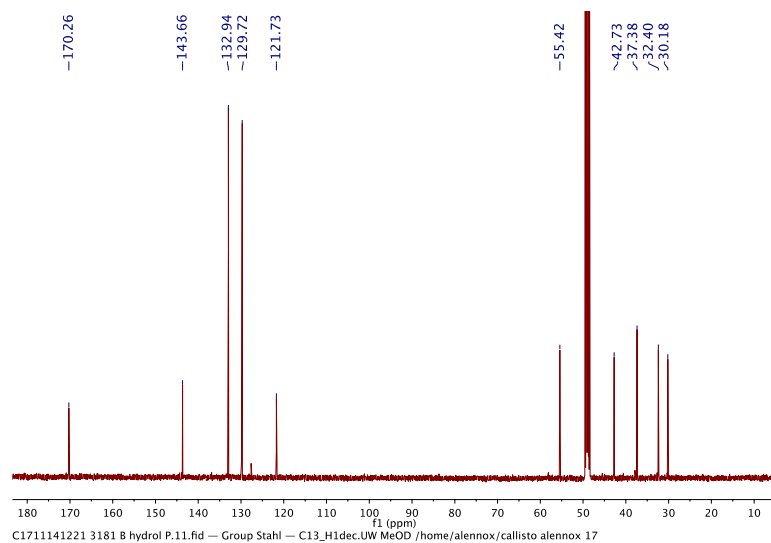


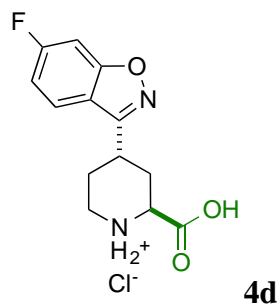


^1H NMR (500 MHz, Methanol- d_4):

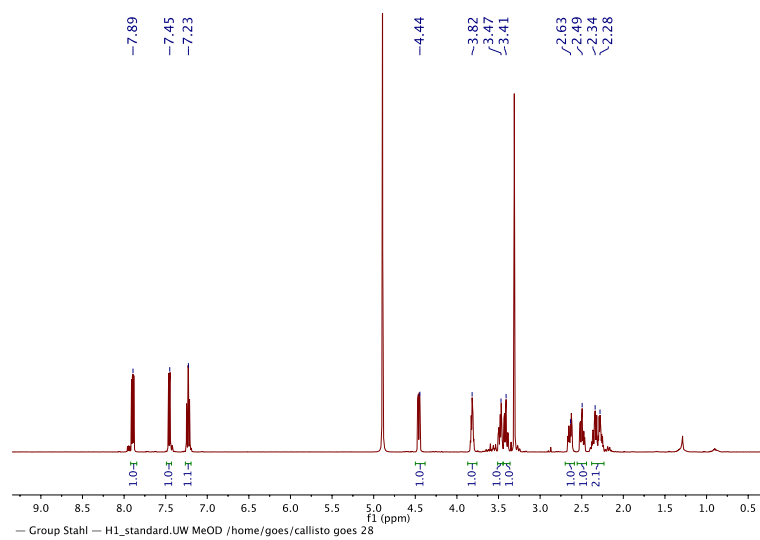


^{13}C NMR (126 MHz, Methanol- d_4):

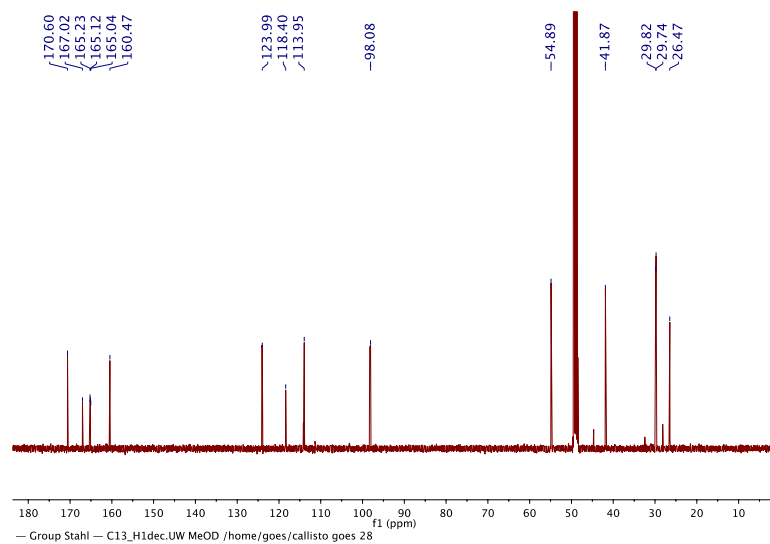




^1H NMR (500 MHz, Methanol- d_4):



^{13}C NMR (126 MHz, Methanol- d_4):



C.7. Reference

1. DeBaillie, A.C.; Jones, C.D.; Magnus, N. A.; Mateos, C.; Torrado, A.; Wepsiec, J.P.; Tokala, R.; Raje, P. *Org. Process Res. Dev.*, **2015**, *19*, 1568–1575.
2. Kodo, T.; Fukaya, T.; Koyama, K.; Masumoto, S.; Yashi, F. European Patent, 1,719,761, February 18, 2018.
3. Minch, M. J. *Concepts Magn. Reson.*, **1994**, *6*, 41–56.
4. Keenan, T.P.; Yaeger, D.; Holt, D. A. *Tetrahedron: Asymmetry*, **1999**, *10*, 4331–4341.
5. Bruker-AXS (**2016**). *APEX3*. Version 2016.5-0. Madison, Wisconsin, USA
6. Krause, L.; Herbst-Irmer, R.; Sheldrick, G. M.; Stalke, D. *J. Appl. Cryst.* **2015**, *48*, 3-10.
7. a) Sheldrick, G. M. (2013b). XPREP. Version 2013/1. Georg-August-Universität Göttingen, Göttingen, Germany; b) Sheldrick, G. M. (2013a). The SHELX homepage, <http://shelx.uni-ac.gwdg.de/SHELX/>; c) Sheldrick, G. M. *Acta Cryst. A*, **2015**, *71*, 3-8; d) Sheldrick, G. M. *Acta Cryst. C*, **2015**, *71*, 3-8; e) Dolomanov, O. V.; Bourhis, L. J.; Gildea, R. J.; Howard, J. A. K.; Puschmann, H. *J. Appl. Crystallogr.* **2009**, *42*, 339-341; e) Guzei, I. A. (2007-2013). Programs Gn. University of Wisconsin-Madison, Madison, Wisconsin, USA.

**Appendix D: Fundamental Studies of N-Oxyl Radicals: Assessment of
Stability, Bond Strength, and Time-Delayed Alcohol Oxidation Supporting
Information**

D.1. General Information

Reagents

All commercially available chemicals were used without further purification. MAN was prepared following a reported method.¹

Instruments and Techniques

All buffer solution pH was measured by Orion Star benchtop pH Meter. All buffer solutions used for CV were tested each day they were used for data collection.

Nuclear magnetic resonance (NMR) spectra were obtained using an internal solvent lock on a Bruker Avance-400 spectrometer. For ¹H spectra, chemical shifts were referenced to the center line of the residual solvent signals (MeCN-*d*₃: δ1.94; D₂O-*d*₃: δ4.79). NMR yield (%) was determined using 1,3,5-trimethoxy benzene as internal standard.

Electrochemical reactions were acquired using a Pine WaveDriver 40 DC Bipotentiostat/Galvanostat or WaveNow XV potentiostat. Reaction run under N₂ atmosphere were performed in a purge box using a wireless WaveNow XV potentiostat. All reactions were referenced by 3.0 M KCl Ag/AgCl reference electrode (BASi). 5-15 mL glass cell with Teflon cell tops (BASi) were fitted with a 3.0 mm glassy carbon working electrode (BASi), handmade Pt wire counter electrode, and Ag/AgCl reference electrode. Handmade cells were used for bulk electrolysis (**Figure D.1**). A piece of glass tube with a fine porosity E frit on the bottom were used to separate the handmade Pt wire counter electrode from the graphite rod (graphitestore) or 11 μm carbon fiber microelectrode (BASi) working electrodes and Ag/AgCl reference. Radical decay was monitored using an RDE set-up (BASi) fitted with 3.0 mM glassy carbon electrode (BASi), Pt wire counter electrode (BASi), and Ag/AgCl reference electrode.

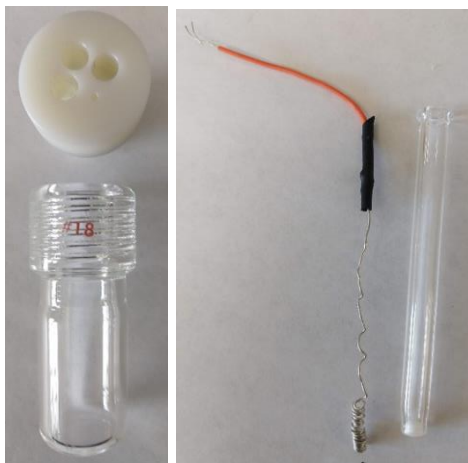


Figure D.1. Divided bulk electrolysis cell.

D.2. CV of HAT Mediators

Buffers

The following buffers were prepared by adding 0.1 M of the acid (or base component) and titrating with NaOH (or HCl) to the desired pH: pH 3 (0.1 M sodium citrate/citric acid), pH 5 (0.1 M sodium acetate/acetic acid, pH 7 (0.1 M monosodium/disodium phosphate), pH 9.5-10.5 (0.1 M carbonic acid/sodium bicarbonate). pH 1 solution was prepared by adding 0.1 M HCl to water.

Collected CVs

Pine Aftermath software was used to calculate the peak current and peak potential (**Figure D.2**) from collected CVs (**Figure D.2-D.9**).

CVs collection of each mediator at pH 5 were repeated three different times on different days to determine the standard deviation and error for the reported $E_{1/2}$.

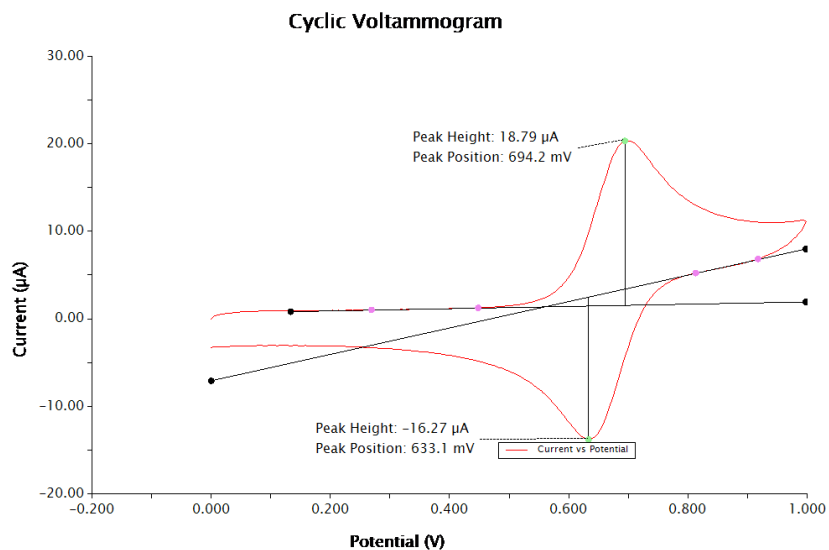


Figure D.2. Example of CV analyzed using Pine Aftermath software.

CVs of VA, DVA, MAN, CyAN, DAN, NHPI, NHSI, and HOBt were collected at 20 mV/s, 50 mV/s, and 100 mV/s.

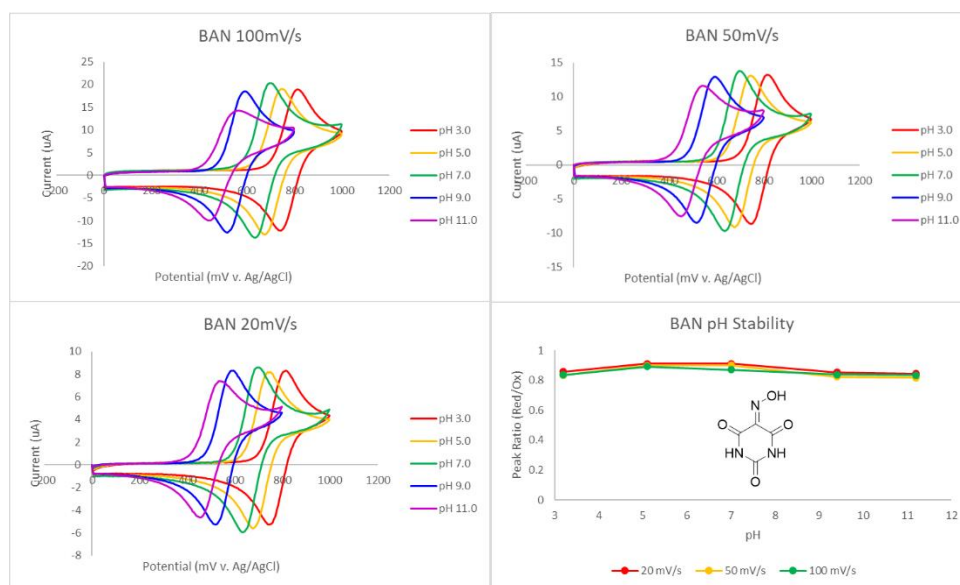


Figure D.3. 1 mM VA; 20, 50, or 100mV/s; glassy carbon working electrode, Pt wire counter electrode, 3 M KCl Ag/AgCl reference electrode; 0.1 M buffer: pH 3 (0.1 M sodium citrate/citric acid), pH 5 (0.1 M sodium acetate/acetic acid), pH 7 (0.1 M monosodium/disodium phosphate), pH 9.5-10.5 (0.1 M carbonic acid/sodium bicarbonate), and pH 1 solution (0.1 M HCl to water).

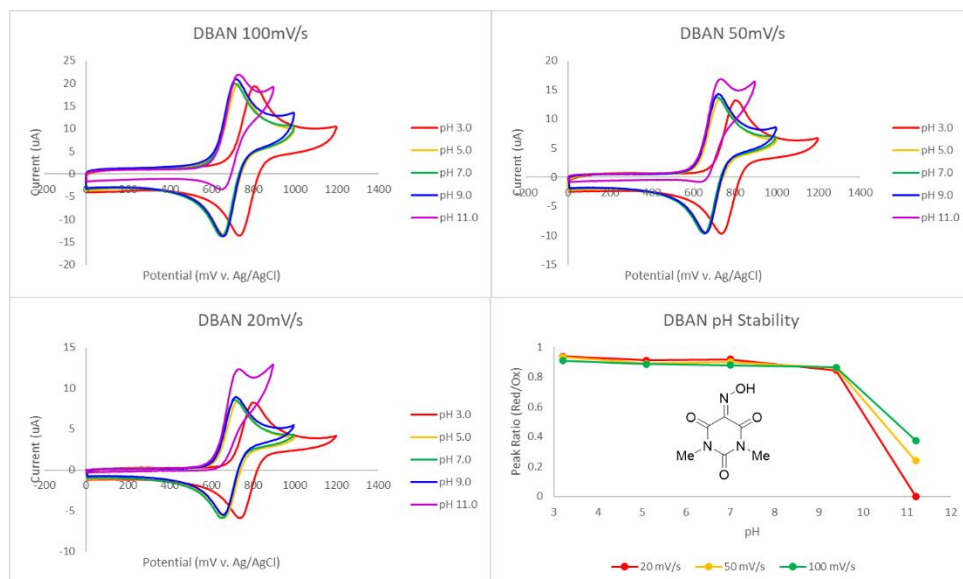


Figure D.4. 1 mM DVA; 20, 50, or 100mV/s; glassy carbon working electrode, Pt wire counter electrode, 3 M KCl Ag/AgCl reference electrode; 0.1 M buffer: pH 3 (0.1 M sodium citrate/citric acid), pH 5 (0.1 M sodium acetate/acetic acid), pH 7 (0.1 M monosodium/disodium phosphate), pH 9.5-10.5 (0.1 M carbonic acid/sodium bicarbonate), and pH 1 solution (0.1 M HCl to water).

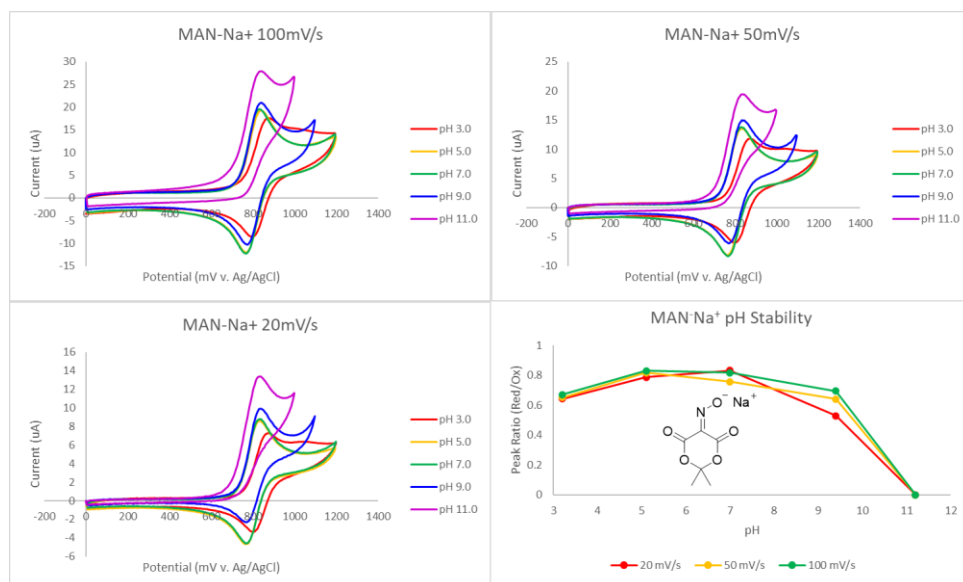


Figure D.5. 1 mM MAN; 20, 50, or 100mV/s; glassy carbon working electrode, Pt wire counter electrode, 3 M KCl Ag/AgCl reference electrode; 0.1 M buffer: pH 3 (0.1 M sodium citrate/citric acid), pH 5 (0.1 M sodium acetate/acetic acid), pH 7 (0.1 M monosodium/disodium phosphate), pH 9.5-10.5 (0.1 M carbonic acid/sodium bicarbonate), and pH 1 solution (0.1 M HCl to water).

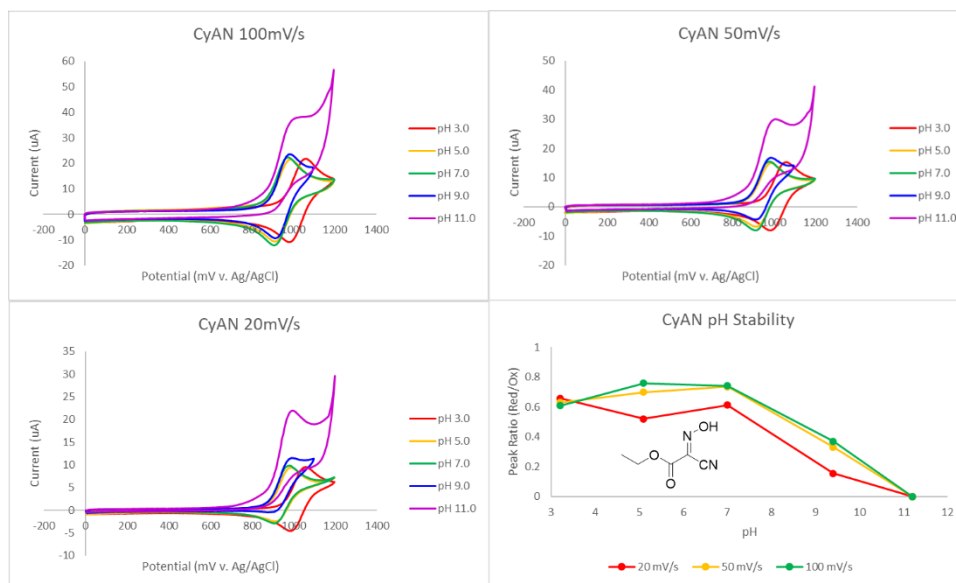


Figure D.6. 1 mM CyAN; 20, 50, or 100mV/s; glassy carbon working electrode, Pt wire counter electrode, 3 M KCl Ag/AgCl reference electrode; 0.1 M buffer: pH 3 (0.1 M sodium citrate/citric acid), pH 5 (0.1 M sodium acetate/acetic acid, pH 7 (0.1 M monosodium/disodium phosphate), pH 9.5-10.5 (0.1 M carbonic acid/sodium bicarbonate), and pH 1 solution (0.1 M HCl to water).

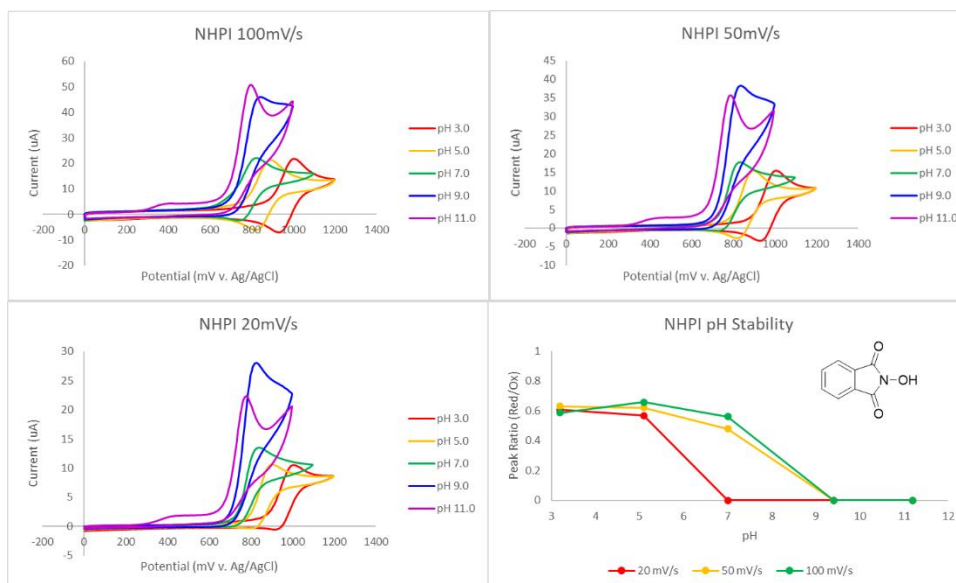


Figure D.7. 1 mM NHPI; 20, 50, or 100mV/s; glassy carbon working electrode, Pt wire counter electrode, 3 M KCl Ag/AgCl reference electrode; 0.1 M buffer: pH 3 (0.1 M sodium citrate/citric acid), pH 5 (0.1 M sodium acetate/acetic acid, pH 7 (0.1 M monosodium/disodium phosphate), pH 9.5-10.5 (0.1 M carbonic acid/sodium bicarbonate), and pH 1 solution (0.1 M HCl to water).

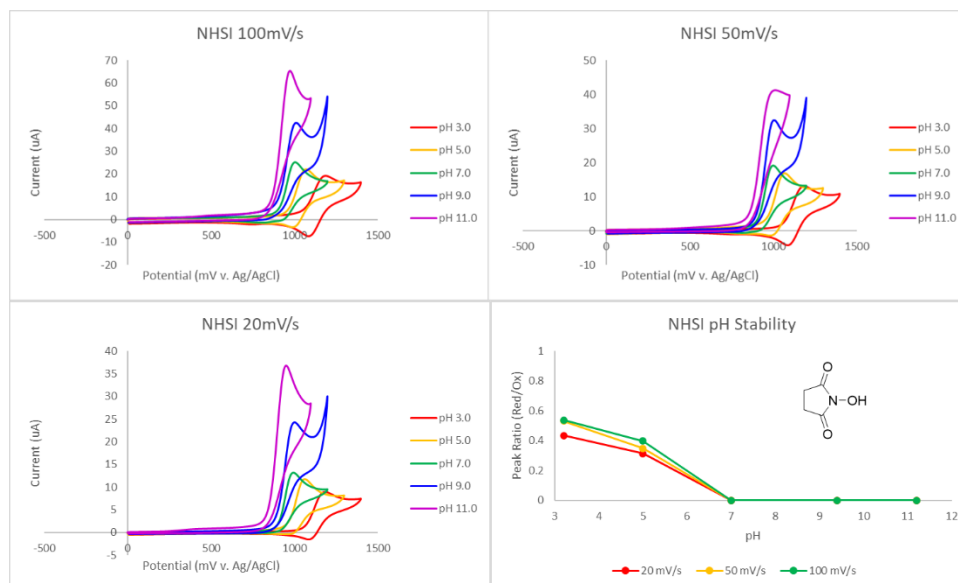


Figure D.8. 1 mM NHI; 20, 50, or 100mV/s; glassy carbon working electrode, Pt wire counter electrode, 3 M KCl Ag/AgCl reference electrode; 0.1 M buffer: pH 3 (0.1 M sodium citrate/citric acid), pH 5 (0.1 M sodium acetate/acetic acid), pH 7 (0.1 M monosodium/disodium phosphate), pH 9.5-10.5 (0.1 M carbonic acid/sodium bicarbonate), and pH 1 solution (0.1 M HCl to water).

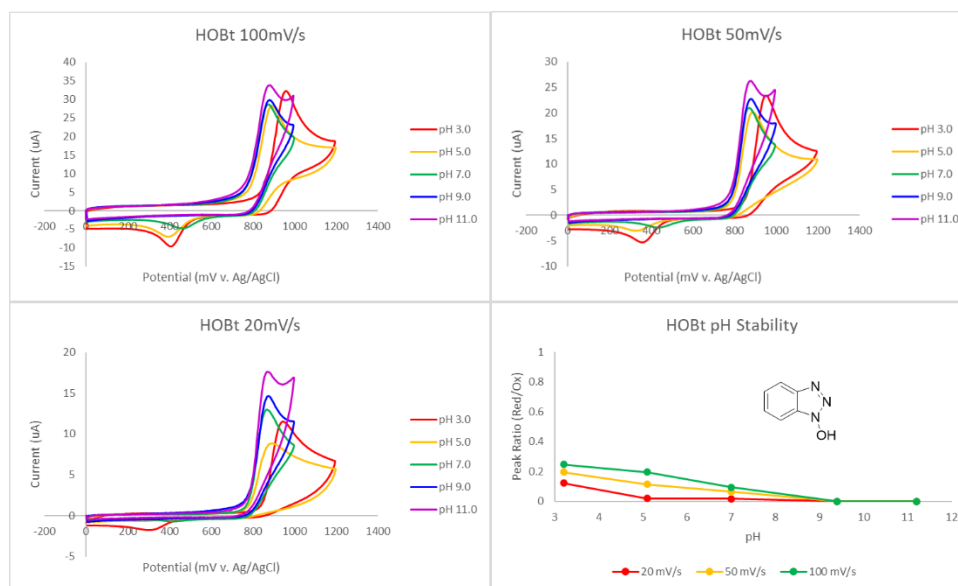


Figure D.9. 1 mM HOBt; 20, 50, or 100mV/s; glassy carbon working electrode, Pt wire counter electrode, 3 M KCl Ag/AgCl reference electrode; 0.1 M buffer: pH 3 (0.1 M sodium citrate/citric acid), pH 5 (0.1 M sodium acetate/acetic acid), pH 7 (0.1 M monosodium/disodium phosphate), pH 9.5-10.5 (0.1 M carbonic acid/sodium bicarbonate), and pH 1 solution (0.1 M HCl to water).

Collected DPV

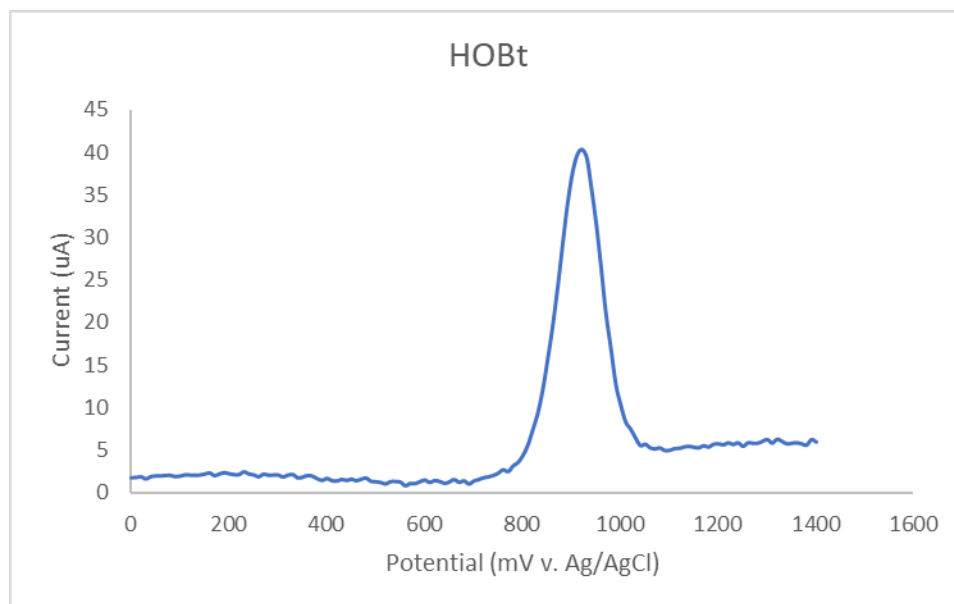


Figure D.10. 1 mM HOBt; glassy carbon working electrode, Pt wire counter electrode, 3 M KCl Ag/AgCl reference electrode; 0.1 M buffer: pH 3 (0.1 M sodium citrate/citric acid); pulse height: 100 mV, width: 0.01 s, period: 0.1 s, increment: 10 mV; pre- and post-pulse width: 0.003 s.

D.3. pK_a Analysis by NMR

A 1 mM solution DVA, MAN, CyAN, NHPI, NHSI, and HOBt in D₂O was titrated with DCl or NaOD. 1 mM BnOH was added as internal standard. The pH was recorded and corrected for D₂O. The sample analyzed by ¹H NMR, referenced to BnOH (4.60 ppm) and analyzed using the multistart function in MATLAB to determine the equivalence point. The results are summarized in (Figure D.11-D.15).

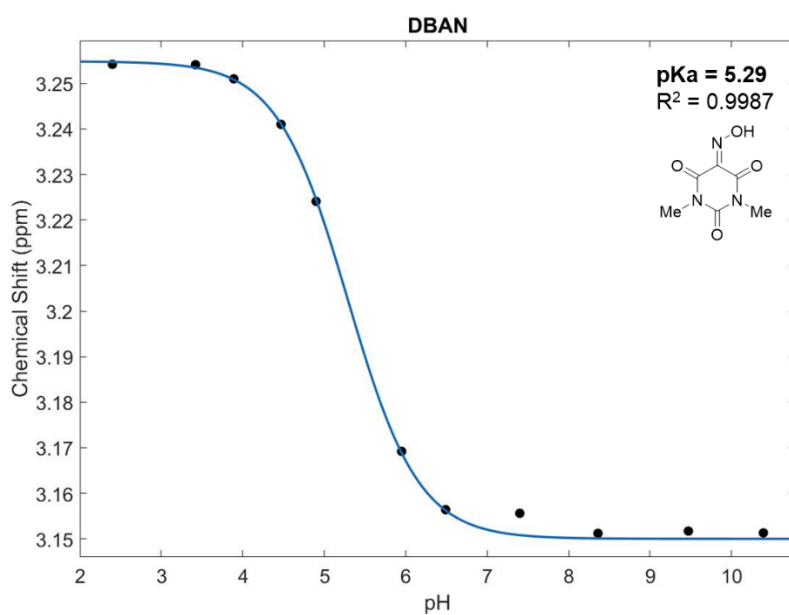
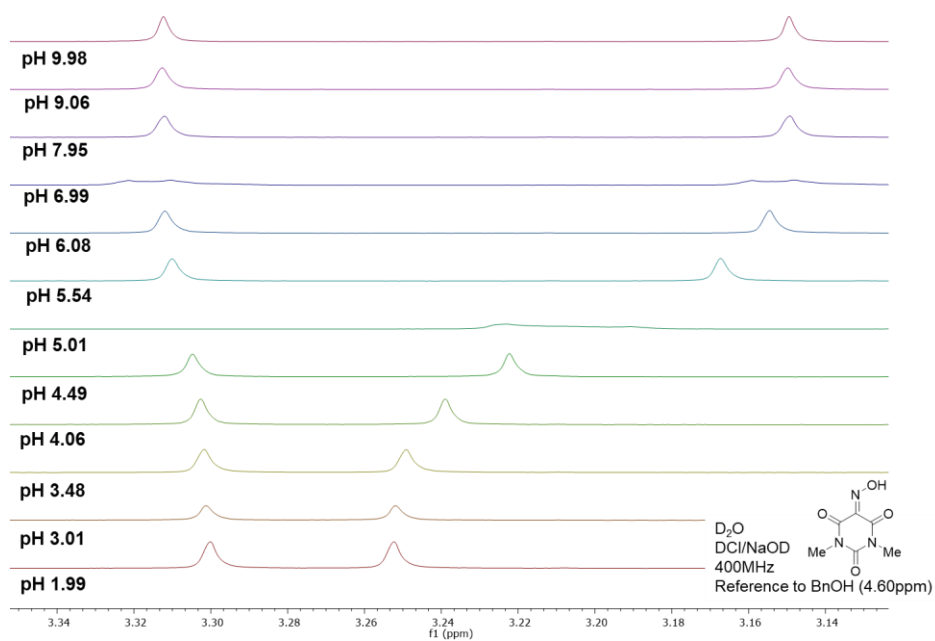


Figure D.11. 1 mM DVA in D_2O titrated from pH 2-10 using DCl or NaOD and analysis in R.

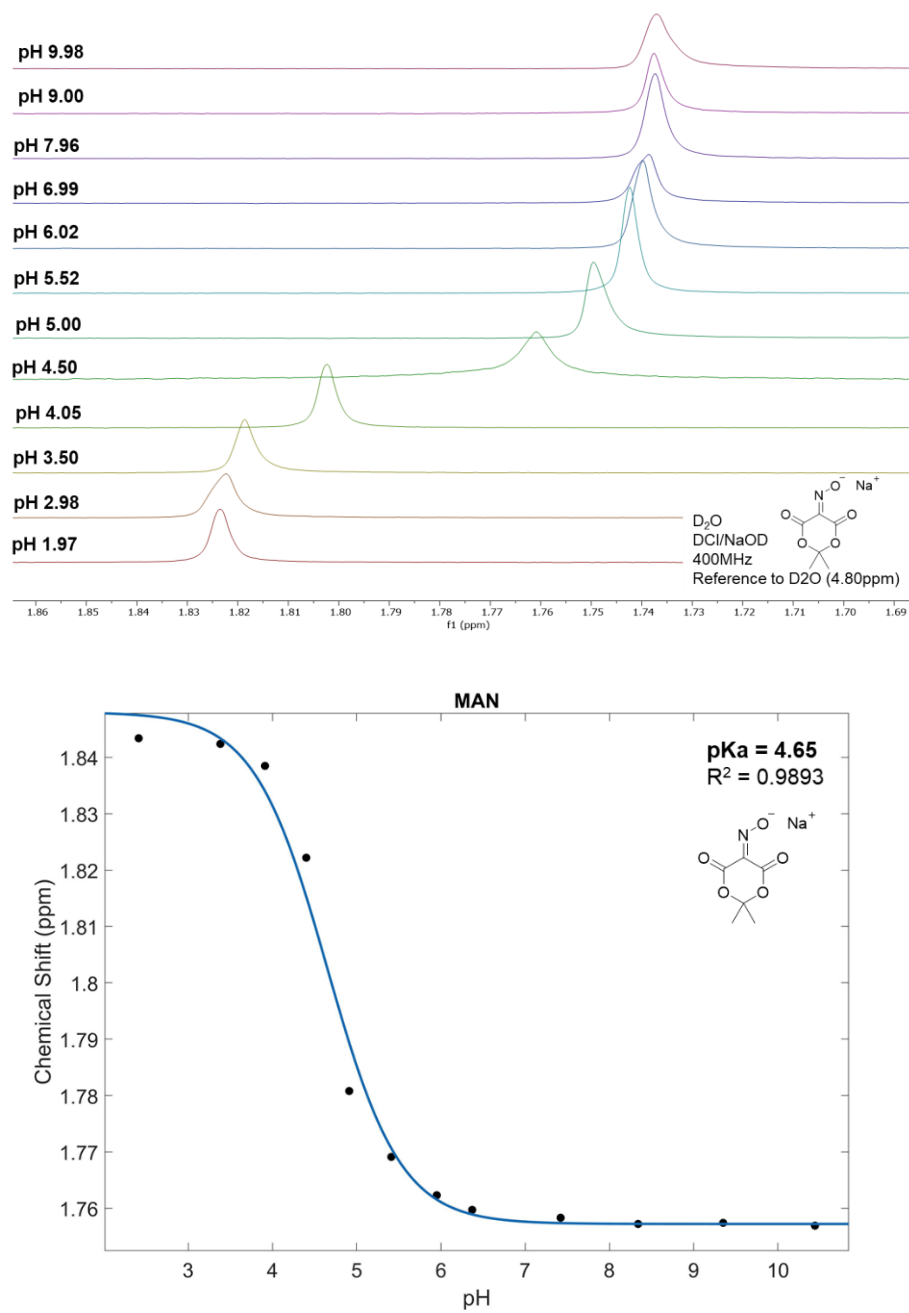


Figure D.12. 1 mM MAN in D_2O titrated from pH 2-10 using DCl or NaOD and analysis in R.

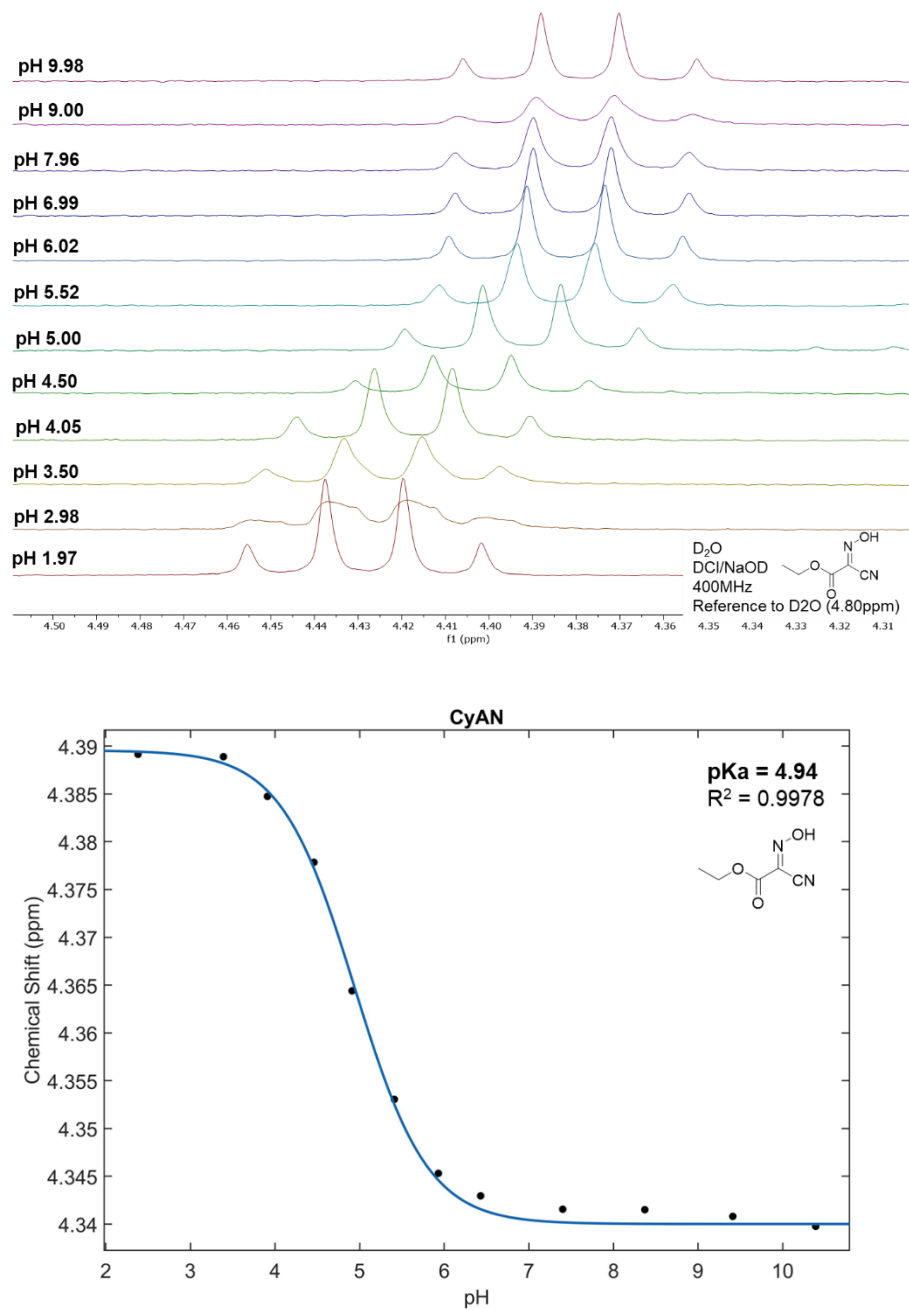


Figure D.13. 1 mM CyAN in D_2O titrated from pH 2-10 using DCl or NaOD and analysis in R.

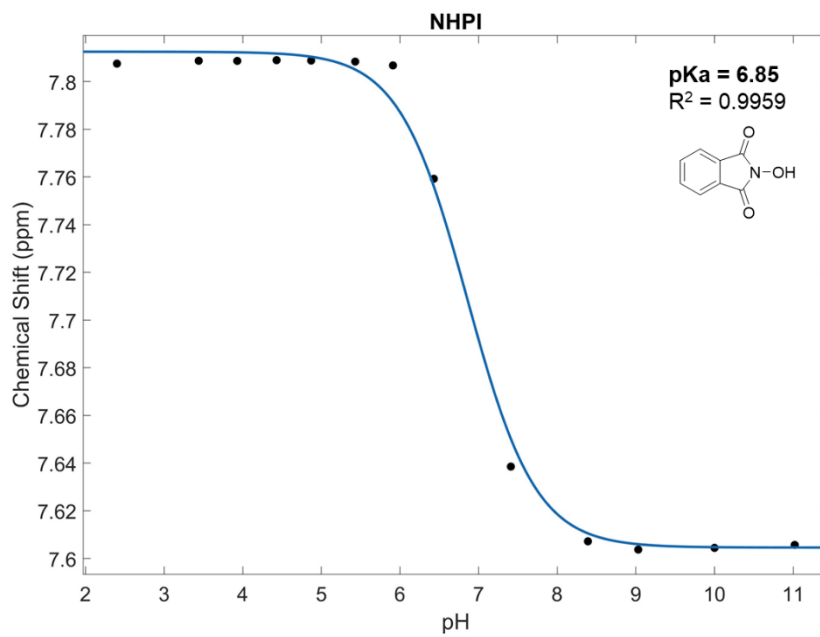
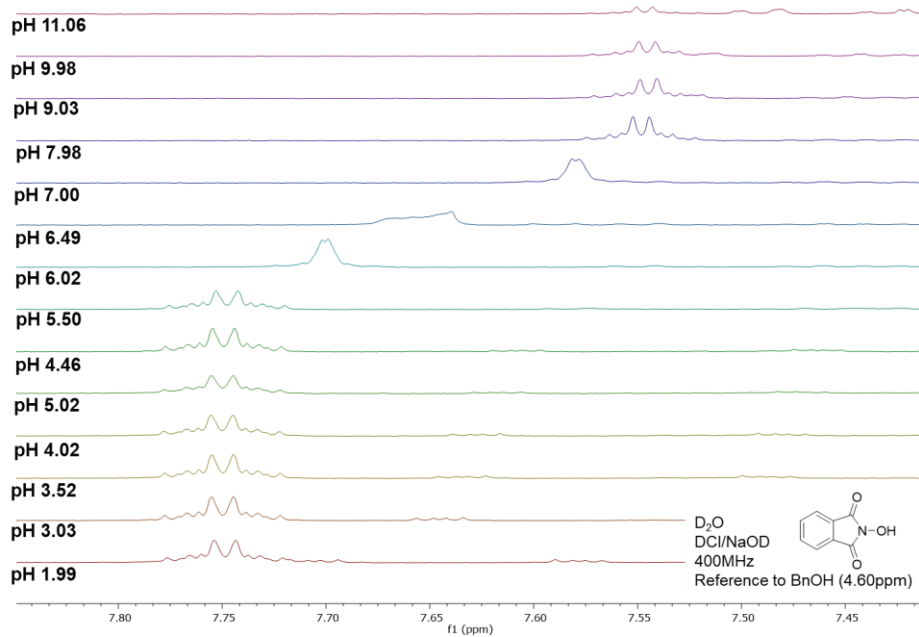


Figure D.14. 1 mM NHPI in D_2O titrated from pH 2-10 using DCl or NaOD and analysis in R.

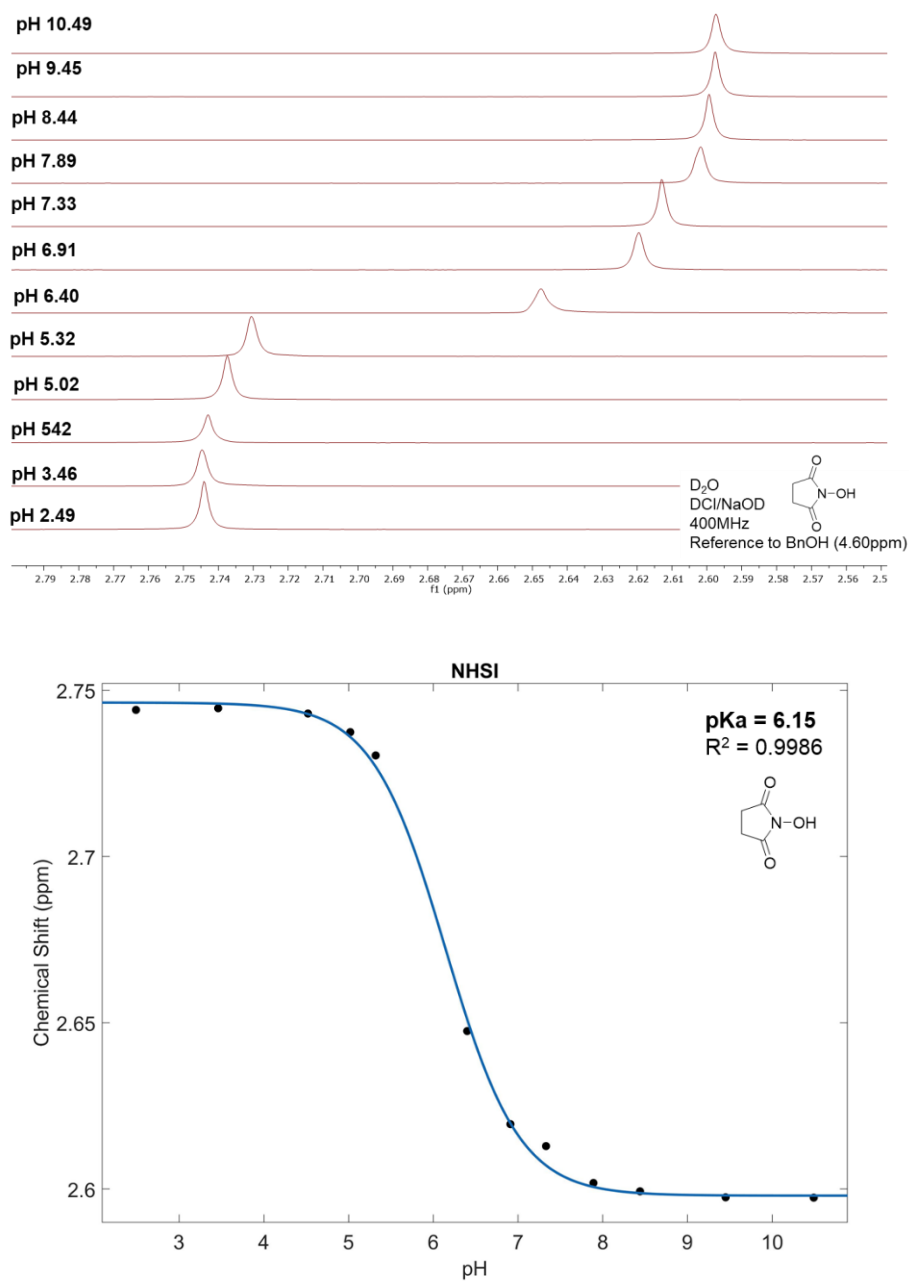


Figure D.15. 1 mM NHSI in D_2O titrated from pH 2-10 using DCl or NaOD and analysis in R.

D.4. Bulk Electrolysis

The radical pool bulk electrolysis experiments were conducted by bulk electrolysis of a 10 mM mediator solution in 1:1 MeCN: 0.1 M HCl (aq). Constant current electrolysis using the graphite working electrode was conducted for 5-10 minutes. Immediately after electrolysis, an

LSV was collected in the same cell using a carbon fiber microelectrode. Bulk electrolysis was continued until monitoring showed that maximum oxidation current corresponding to maximum radical generation was achieved.

Radical Degradation Experiments

After bulk electrolysis was used to generate a maximum amount of radical, the mediator solution was transferred to an RDE cell with a rotation rate of 1000 rpm. Collection of LSV data using this RDE set-up occurred 1.5 minutes after the pool was achieved by bulk electrolysis

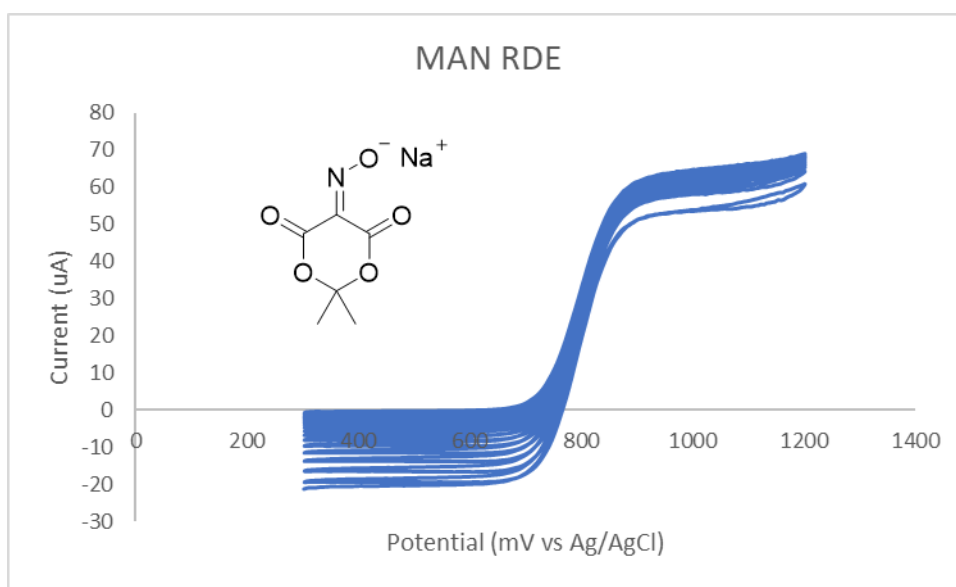


Figure D.16. An example of radical degradation data collected by LSV; 3.0 mm glassy carbon working electrode, Pt wire counter electrode, Ag/AgCl reference electrode; 1000 rpm; 20 mV/s.

Oxidation of 4-methoxy- α -methylbenzyl alcohol

After bulk electrolysis was used to generate a maximum amount of radical, the mediator solution was transferred to a cell containing pre-weighed substrate. The reaction was stirred no radical could be detected by microelectrode LSV analysis. 1,3,5-trimethoxybenzene was added as internal standard and an NMR sample of the crude mixture was prepared in MeCN- d_3 . No aldol condensation products were observed under the conditions used for this study.

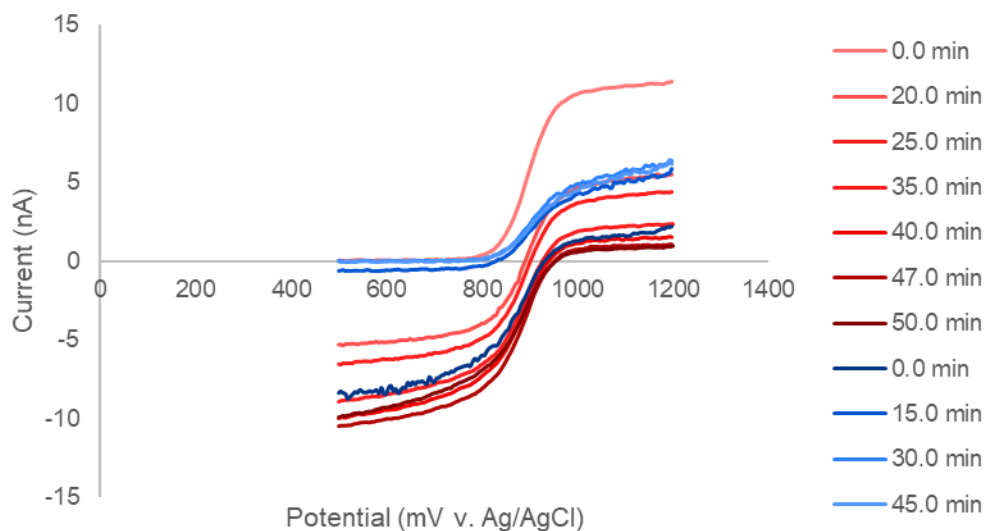


Figure D.17. An example of LSV monitoring during radical pooling (red traces) and after addition of substrate (blue traces). 10 mM VA; 1:1 MeCN: 0.1 M HCl (aq); 20 mV/s; graphite rod (working electrode: generation), carbon fiber microelectrode (working electrode: monitoring), Pt wire counter electrode; Ag/AgCl reference; divided cell.

D.5. References

1. a) Matsui, H.; Zukerman, E. J. *J. Phys. Chem. A* **1997**, *101*, 3936–3941. b) Briehl, H.; Lukosck, A.; Wentrup, C. *J. Org. Chem.* **1984**, *49*, 2772–2779.

**Appendix E: Electrochemical Oxidative Stabilization in Mild Aqueous
Conditions Enhances Lignin Monomer Production During Biomass
Depolymerization**

E.1. Chemicals and Materials

All commercial chemicals were purchased and used as received without further purification unless otherwise noted. Violuric acid monohydrate (26351-19-9, >97.0%), 1,4-dioxane (123-91-1, > 99.0%), sodium hydroxide (1310-73-2, > 97.0%, pellet), sodium bicarbonate (144-55-8, > 99.7%), ethyl acetate (141-78-6, □ 99.8%), formic acid (64-18-6, □ 95.0%), and magnesium sulfate (7487-88-9, > 99.5%) were purchased from Sigma Aldrich. Potassium chloride electrolyte solution (7447-40-7, 3 mol/L) was purchased from Mettler Toledo. Glacial acetic acid (64-19-7, 99.99%), sodium formate (141-53-7, 99.52%, white crystals) and hydrochloric acid (7647-01-0, 37.10%) were purchased from Chem Impex International. NE-19 (*Populus nigra charkowiensis* × *P. nigra caudina*) poplar was harvested on 2011-07-01 and obtained from the Great Lakes Bioenergy Research Center in Madison, WI. The biomass was then coarsely ground (e.g., 2-4 mm Wiley-milled) and washed in a Soxhlet extractor with subsequent 24 h ethanol and toluene wash, with an additional 1,4-dioxane wash applied as noted in the text.

NMR spectra were acquired on a Bruker Biospin Avance 500 MHz spectrometer fitted with a 5 mm TCI (triple resonance; ^1H , ^{13}C , ^{15}N) gradient cryoprobe with inverse geometry (proton coils closest to the sample). HSQC experiments were carried out using the following parameters: acquired from 10 to 0 ppm in F2 (^1H) with 1000 data points (acquisition time 100 ms), 200 to 0 ppm in F1 (^{13}C) with 400 increments (F1 acquisition time 8 ms) of 72 scans with 500 ms interscan delay; the d24 delay was set to 0.89 ms ($1/8J$, $J = 145$ Hz). The total acquisition time was 5 h.

Solid State NMR (ssNMR) spectra were obtained with Bruker Avance-500 MHz NMR spectrometer with a 1.2 mm magic-angle spinning ssNMR probe and chemical shifts are reported in parts per million (ppm). 2D NMR spectra were obtained with a Bruker Avance 600 MHz NMR spectrometer equipped with a TCI-F cryoprobe and chemical shifts are reported in parts per million

(ppm). Experiments were carried out using the following parameters: acquired from -155 to 341 ppm (^{13}C) with 10 kHz MAS frequency and acquisition time 0.03 s with 4264 scans and a 3 s relaxation delay.

HPLC/UV analysis on lignin-derived monomers was obtained on a Shimadzu Prominence HPLC system equipped with SPD-M20A diode array detector and a Restek Ultra C18 column (150 mm x 4.6 mm ID – 3-micron particle size) at 35 °C. Solvent A was 0.1% formic acid in Millipure water and solvent B was HPLC grade acetonitrile for the HPLC separations (flow rate 2 mL/min). Monomer yields were calculated based on a 1,4-dimethoxybenzene internal standard.

E.2. Experimental

E.2.1. Flow Reaction Set-Up

One end of a 1" x 2 1/8" or 1/2" x 10 1/8" diameter borosilicate glass tube was plugged with glass wool. The tube is partially filled with 4 mm glass beads (Fisher Scientific) to a height of approximately 3 cm (for 1/2" diameter tube) or 1 cm (for 1" diameter tube). 1 g of washed poplar biomass is added to the tube and packed by tapping the tube lightly on the table. The rest of the tube is filled with glass beads, and the end is plugged with glass wool. Both ends of the tube are fitted with ultra-Torr fittings, and the reactor suspended vertically. The inlet and outlet tubes are attached to the fittings, and a temperature probe is inserted into the top of the reactor through the ultra-Torr fittings at a T-joint.

Typically, a 0.2 M acetic acid/sodium acetate buffer solution (pH 4.5) was prepared for the anodic and cathodic reservoirs by adding 0.2 M acetic acid to water and titrating to pH 4.5 using NaOH. For reaction optimization using different buffer systems, 0.2 M phosphoric acid/monosodium phosphate buffer (pH 7) was prepared using a similar method. A 0.2 M HCl solution (pH 1) was also prepared for optimization. The anodic and cathodic reservoirs were filled

with 600 ml buffer. 50 wt% (10 mM) violuric acid monohydrate was added to the anodic reservoir and dissolved.

Once the reactor, flow cell, and reservoirs were prepared, all the components were assembled around a Masterflex L/S peristaltic pump (Model 77800-60) fitted with three Masterflex L/S Easy-Load 3 pump heads. **Anodic:** One end of a Masterflex C-flex tube was inserted into the anodic reservoir, passed through the pump head, and attached to the anodic inlet of the flow cell (**Figure E.1**). Another tube connects the anodic outlet of the flow cell to the inlet of the reactor. The reactor outlet is connected to the small reservoir fitted with an 11 μm glassy carbon microelectrode (BASi), Pt wire counter electrode, and 3.0 M KCl Ag/AgCl reference electrode (BASi). The outlet tube of the small reservoir was passed through the pump head and connected to the anodic reservoir. **Cathodic:** One end of a Masterflex C-flex tube was inserted into the cathodic reservoir, passed through the pump head, and attached to the cathodic inlet of the flow cell. Another tube connects the cathodic outlet of the flow cell to the cathodic reservoir.

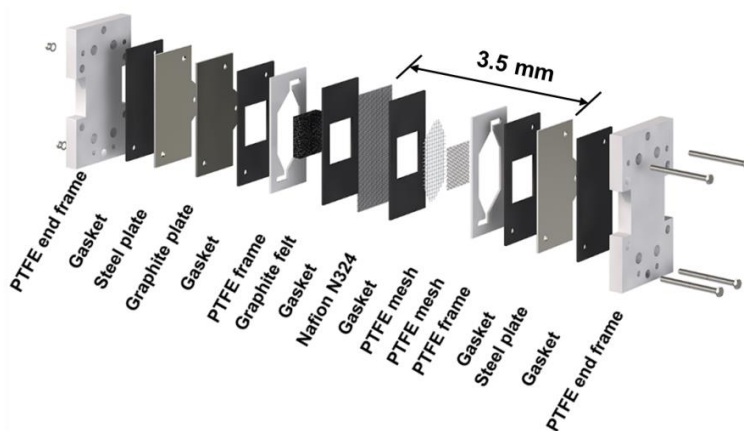


Figure E.1. Graphic illustration of the components of the divided flow cell reactor. Interelectrode distance between anode and cathode is 3.5 mm.

Solution is pumped through the flow reactor system at a rate of 3 mL/min. The temperature probe and heat tape (HTS/Amptek Model ASR-051-020D-MP) were connected to the Parr 4848

reaction controller and set to an output of 17.5 to achieve 43-45 °C in the reactor. The heat tape was wrapped around the lower half of the reactor.

Two parallel reactions can be conducted using this set-up, as shown in **Figure E.2**.

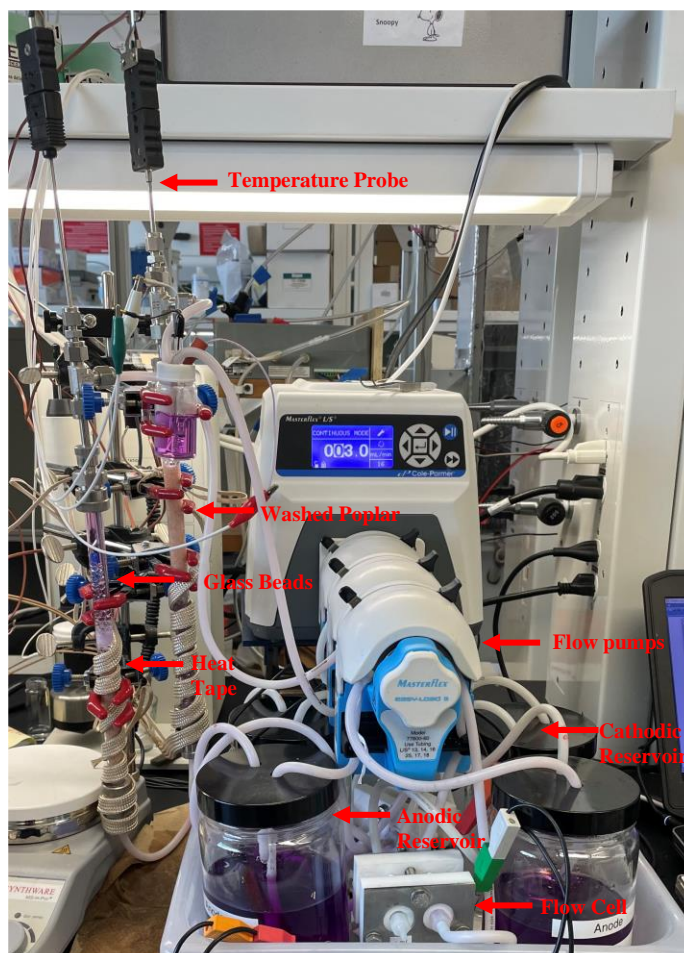


Figure E.2. Flow reaction set up with three flow pumps, two columns, pair of anodic and cathodic reservoirs and two flow cells.

A Pine WaveNow potentiostat was used to apply 1.5 V to the flow cell for 72 h once the temperature reached steady state. A CH Instruments 600E potentiostat/galvanostat was used to monitor the concentration of violuric acid (VA) and violuric acid *N*-oxyl radical (VANO) in the small reservoir at the microelectrode. Linear sweep voltammograms (0.4 – 1.0 V, 20 mV/s) were collected every 30 minutes for the duration of the reaction.

After the reaction was finished, the reactor was allowed to cool to room temperature and the biomass and cell were washed with approximately 600 mL of DI water. The glass tube containing biomass was disconnected from the reactor. The biomass was separated from the glass beads and wool and transferred to a pre-weighed glass vial. The biomass was dried on a rotary evaporator at room temperature overnight.

The dried biomass was ground for 2 min (2x1 min grinding) at 30 Hz using a Retsch MM301 mixer mill with corrosion-resistant stainless-steel screw-top grinding jars (50 ml) containing a single stainless steel ball bearing (30 mm). Ground biomass was used for 2D gel-NMR HSQC analysis¹ and mild-acidolysis fractionation.

E.2.2. Mild-Acidolysis Fractionation²

1 g ground biomass was suspended in a dioxane/water mixture (9/1 v/v) containing 0.2 M HCl. The suspension was refluxed and stirred for 45 min. The cooled mixture was gravity filtered through Whatman filter paper (18.5 cm) to separate insoluble polysaccharides from lignin. The insoluble polysaccharides were analyzed by ssNMR. The residue was washed three times with 15 mL of dioxane/water mixture. The pH of the resulting solution was adjusted to 3-4 by saturated aqueous NaHCO₃ solution. Then, the solution was concentrated by rotary-evaporation (45 °C), taking care to stop before any insoluble lignin appeared. Lignin was precipitated by pouring the concentrated solution into 40 mL of cold water. The precipitated lignin was isolated by centrifugation (30 min at 1200 g, 4°C), washed with 40 mL of deionized water. The washed lignin was dried by lyophilization and analyzed by 2D HSQC or depolymerized to monomers.

E.2.3. Formic Acid Depolymerization³

50 mg of oxidized lignin was added to a 15 mL thick-walled pressure tube. 37 mg NaCO₂H and 5 mL formic acid were added to the tube. The reaction was stirred behind a blast shield at 110° C for 24 h. After the reaction was cooled to room temperature, the reaction was

transferred to a round bottom flask and concentrated using a rotary evaporator until the mixture is thick. Do not rotovap to dryness. The mixture was then transferred to a separatory funnel and extracted 3x with 15 mL ethyl acetate and 1x with brine. The organic layer was dried over magnesium sulfate and analyzed by UPLC.

Safety note: Heating formic acid above its boiling point causes pressure build-up during the reaction, and extra care must be taken when opening the pressure tube after the reaction has cooled. This depolymerization reaction should not be scaled-up due to these safety considerations.

E.2.4. Preliminary Radical Pool Batch Reaction

A 28 mM solution of VA and 0.5 M NaCl in 5 mL 0.1 M acetic acid/acetate buffer (pH 4.5) was prepared and heated to 70 °C. The divided cell was fitted with an RVC working electrode, Pt wire counter electrode, and 3.0 M KCl Ag/AgCl reference electrode. The solution was electrolyzed at 50 mA for 25 minutes under stirring. The solution was then transferred to a stirred tank of 500mg (5% w/v) poplar biomass and allowed to react for 62 h. After the reaction, the sample was dried using a rotary evaporator at room temperature and ground with mortar and pestle in liquid N₂. The resulting sample was analyzed by ss NMR.

E.3. Analysis

E.3.1. 2D Gel-NMR HSQC

30-50 mg milled biomass is added to a 5 mm diameter NMR tube. The biomass is distributed off the bottom of the tube (approximately 1" up the sides). A 4:1 mixture of DMSO-*d*₆:pyridine-*d*₅ was added. The tube was capped and sonicated until a homogeneous gel formed (1-2 h). The central DMSO solvent peak was used as internal reference (δ H 2.50 ppm). Integrations are reported relative to the signal arising from methoxy functional groups in biomass.

E.3.2. 2D HSQC

30-50 mg milled biomass is added to a 5 mm diameter NMR tube. A 4:1 mixture of DMSO-*d*₆:pyridine-*d*₅ was added.

E.3.3. ssNMR

The insoluble polysaccharides obtained from mild-acidolysis fractionation were ground (with mortar and pestle or spatula) and added to a 4.0 mm silicon nitride thin wall rotor.

E.4. References

1. Kim, H.; Ralph, J. *RSC Adv.* **2014**, *4*, 7549.
2. Rafiee, M.; Alherech, M.; Karlen, S. D.; Stahl, S. S. *J. Am. Chem. Soc.* **2019**, *141*, 15266-15276.
3. Rahimi, A.; Ulbrich, A.; Coon, J.; Stahl, S. S. *Nature* **2014**, *515*, 249-252.